Integrated modelling of climate and land use change impacts on groundwater flooding risk in a Chalk catchment

Benjamin Rabb

Cardiff University

February 2011

ProQuest LLC
789 East Eisenhower Parkway
P.O. Box 1346
Ann Arbor, MI 48106-1346

DECLARATION

This work has not previously been accepted in substance for any degree and is not concurrently submitted in candidature for any degree.

Signed ..... (candidate)
Date 2/3/11

STATEMENT 1

This thesis is being submitted in partial fulfilment of the requirements for the degree of PhD.

Signed ..... (candidate)
Date 2/3/11

STATEMENT 2

This thesis is the result of my own independent work/investigation, except where otherwise sated.

Other sources are acknowledged by explicit references.

Signed ..... (candidate)
Date 2/3/11

STATEMENT 3

I hereby give consent for my thesis, if accepted, to be available for photocopying and for inter-library loan, and for the title and summary to be made available to outside organisations.

Signed ..... (candidate)
Date 2/3/11

STATEMENT 4

I hereby give consent for my thesis, if accepted, to be available for photocopying and for inter-library loans **after expiry of a bar on access previously approved by the Graduate Development Committee**.

Signed ..... (candidate)
Date .....

No Bar

2/3/11

Summary

In Chalk lowland catchments, groundwater emerging from an aquifer can inundate regions for up to several months, resulting in a hazard distinct in aetiology and impact from fluvial or coastal flooding. It is estimated that 1.7 million properties are at risk from groundwater flooding in England, of which 382,407 are located on Chalk. From 2010 *The Flood and Water Management Act* has given the Environment Agency and local authorities in the United Kingdom a statutory requirement to manage flooding from groundwater.

A robust, long-term groundwater flood risk assessment methodology was developed using the Pang/Lambourn catchment in West Berkshire as a case study. A recharge model based on a soil moisture budget was built in GIS and tested against observations. The timing and mechanism of flow in the vadose zone was also assessed using cross-correlation analysis between rainfall and borehole responses for a better understanding of recharge processes. Regional MODFLOW models were developed for saturated groundwater flow using input from the recharge model. This integrated model was then coupled with a Global Climate Model using a stochastic weather generator to downscale output to the catchment. An ensemble of high and low climate change scenarios suggests there will be between a 5.5% and 27% reduction in recharge over the coming century and mean groundwater levels will lower by up to 3.8%. Land use modification characterised by afforestation and urbanisation resulted in nuanced changes in the spatial distribution of recharge as well as a further mean reduction of 6.8% on top of the climate change impacts.

Groundwater flood hazard maps were developed and integrated with a social vulnerability index to identify 1.7 km^2 of the Pang/Lambourn at high risk. In the Pang catchment this represents around 1400 properties. Climate and land use change scenarios suggest however that the risk of groundwater flooding in the catchment will decrease considerably (25-98%) over the next century. This reduction in risk is likely to make mitigation through targeted land use modification unnecessary.

Acknowledgements

I would firstly like to thank my supervisors and advisors Yuesuo Yang, TC Hales and Huw Davies for their invaluable support throughout the project.

My sincere thanks also to those who have provided assistance throughout my time at Cardiff; Luca Traverso for groundwater modelling guidance, Andy Gray and Alessia Tobaga for help in the field, Alun Rogers for being a GIS guru and Tim Jones for lending me the van.

I am also grateful to Rosa Tyson at the Environment Agency for providing data and bestowing her local knowledge of the Berkshire Downs. Thanks also to members of the Compton Parish Council, particularly Kathy Howells and Ian Hinckling for sharing their experiences of flooding in the area.

Finally I would like to thank my family and friends for their enduring encouragement and support.

The project would not have been possible without the data and resources kindly provided by the Environment Agency of England and Wales, British Geology Survey, Ordnance Survey, Cranfield University and the Centre for Ecology and Hydrology*.

Contents

List of figures and tables

Figures

Tables

Abbreviations and parameters

Symbol	*Description*	*Units*
A	Cross sectional area	$[L^2]$
A	Flood frequency change factor	
ACF	Autocorrelation Function	
Aet	Actual Evapotranspiration	$[LT^{-1}]$
ARIMA	Autoregressive Integrated Moving Average	
B	Number of households with lowest level below ground	
BFI	Base Flow Index	
B_h	Percentage of households with a basement	[%]
C	Root constant	[L]
C	Specific moisture capacity	$[L^{-1}]$
CAI	Composite Additive Index	
CCF	Cross Correlation Function	
C_h	Number of cars or vans per household	
CHB	Constant Head Boundary	
d	Order of the Integration	
D	Wilting point	[L]
DD	Dry-dry day precipitation transition sate	
DEFRA	Department for Environment Food and Rural Affairs	
dh/dl	Hydraulic gradient	[-]
DPSIR	Driver Pressure State Impact Response	
DTM	Digital Terrain Model	
DW	Dry-wet day precipitation transition sate	
EA	Environment Agency	
E_a	Number of economically active	
EARWIG	Environment Agency Rainfall and Weather Impacts Generator	
ER	Effective Rainfall	$[LT^{-1}]$
E_r	Proportion of elderly residents	[%]
ERT	Electrical Resistivity Tomography	
ET	Evapotranspiration	$[LT^{-1}]$
EU	European Union	
E_y	Number of residents aged 75 and over	
$f\Delta$	Percentage change in flood frequency	[%]
FC	Field Capacity	[L]
$f\alpha$	Frequency of flood in the baseline	
$f\beta$	Frequency of flood in the climate change scenario	
GCM	Global Climate Model	
GEM	Groundwater Emergence Map	
GHB	General Head Boundary	

GIS	Geographical Information Systems	
GUI	Graphical User Interface	
H	Households	
h2020	High climate scenario, 2020 time slice	
h2050	High climate scenario, 2050 time slice	
h2080	High climate scenario, 2080 time slice	
H_r	Households in rented accommodation.	
HRU	Hydro Response Unit	
H_s	Households suffering from a limiting long-term illness	
H_{sp}	Number of single parent households with dependent children	
IDW	Inverse Distance Weighted	
Int	Interception	$[LT^{-1}]$
I_v	Interception parameter	[%]
K	Saturated hydraulic conductivity	$[LT^{-1}]$
$K(S_d)$	Correlated cokriging variable	
Ku	Unsaturated hydraulic conductivity	
Kv	Riverbed conductance	$[L^3T^{-1}]$
L	Lag function	
L	Vertical Leakage	$[T^{-1}]$
l2020	Low climate scenario, 2020 time slice	
l2050	Low climate scenario, 2050 time slice	
l2080	Low climate scenario, 2080 time slice	
luh2020	Land use (and high climate) change scenario	
LOCAR	Lowland Catchment Research Programme	
mAOD	Meters Above Ordnance Datum	
MORECS	Meteorological Office Rainfall and Evaporation Calculation System	
N_c	Non-car ownership	[%]
N_h	Non-home ownership	[%]
NSRP	Neyman-Scott Rectangular Pulses	
OA	Output Area	
O_b	Households with over 1 person per room	
ONS	Office of National Statistics	
O_v	Overcrowding	[%]
p	Order of the autoregressive model	
P	Precipitation	$[LT^{-1}]$
PCG	Preconditioned Conjugate Gradient	
Pet	Potential Evapotranspiration	$[LT^{-1}]$
P_t	Mean daily precipitation	[L]
P_{in}	Precipitation after interception	$[LT^{-1}]$
P_{iro}	Precipitation after interception and runoff	$[LT^{-1}]$

q	Order of the moving average model	
Q	Groundwater flow	$[L^3T^{-1}]$
Qg	Discharge from groundwater	$[L^3T^{-1}]$
Qr	Discharge from rivers	$[L^3T^{-1}]$
Qs	Discharge from springs	$[L^3T^{-1}]$
R	Recharge	$[LT^{-1}]$
R_d	Direct recharge	$[LT^{-1}]$
Ri	Mean daily temperature range	[°C]
R_{id}	Indirect recharge	$[LT^{-1}]$
RMS	Root Mean Square	
Ro	Surface runoff	$[LT^{-1}]$
Ro_b	Runoff parameter for bare earth	[%]
Ro_i	Runoff parameter for impervious	[%]
Ro_v	Runoff parameter for vegetation	[%]
Ro_w	Runoff parameter for open water	[%]
R_s	All residents living in the OA.	
S	Storage coefficient	[-]
S_b	Surface runoff over bare earth	$[LT^{-1}]$
SES	Socio-Economic Scenario	
SFVI	Social Flood Vulnerability Index	
SGFVI	Social Groundwater Flood Vulnerability Index	
S_i	Surface runoff over impermeable surfaces	$[LT^{-1}]$
S_i	Proportion of long term sick	[%]
SMD	Soil Moisture Deficit	[L]
S_p	Proportion of single parent households	[%]
Ss	Specific Storage	$[L^{-1}]$
S_v	Surface runoff over vegetation	$[LT^{-1}]$
S_w	Surface runoff over open water	$[LT^{-1}]$
T	Transmissivity	$[L^2T^{-1}]$
Ti	Mean daily temperature	[°C]
UK	United Kingdom	
UKCIP	United Kingdom Climate Impacts Programme	
U_n	Unemployment	[%]
U_r	Number of unemployed	
VMF	Visual MODFLOW	
W	Sources and/or sinks	$[L^3T^{-1}]$
WD	Wet-dry day precipitation transition sate	
WG	Weather Generator	
WW	Wet-wet day precipitation transition sate	

$X(S_t)$	Correlated cokriging variable	
$Y(S_v)$	Correlated cokriging variable	
$Z(S_t)$	Primary (known) cokriging variable	
ZFP	Zero Flux Plane	[L]
α	Cost of flooding	[£/m^2]
β	Average time for rain cells after the storm origin	[T]
β	Cost of land use modification	[£/m^2]
β	Hortonian fraction	[%]
ε_t	Random error	
η	Average rain cell duration	[T]
λ	Local vulnerability determined by GWFSVI	
λ	Average time between subsequent storm origins	[T]
$\lambda^1, \lambda^2, \lambda^3, \lambda^4$	Cokriging weighting factors	
ν	Average number of cells per storm	
ξ	Average cell intensity	[LT^{-1}]
$\rho 1, \ldots\ldots, \rho_p$	Parameters of autoregression model	
Ψ_b	Bare earth portion of cell	[%]
Ψ_i	Impervious portion of cell	[%]
Ψ_v	Vegetated surface area of cell	[%]
Ψ_w	Open water portion of cell	[%]
ΔS	Change in water storage	[LT^{-1}]
ΔS_d	Change in other storage	[LT^{-1}]
ΔS_{gw}	Change in groundwater storage	[LT^{-1}]
ΔSMD	Change in Soil Moisture Deficit	[L]
ΔS_{sw}	Change in surface water storage	[LT^{-1}]
$\varnothing_b$	Bare earth surface area of cell	[L^2]
$\varnothing_i$	Impervious surface area of cell	[L^2]
$\varnothing_v$	Vegetated surface area of cell	[L^2]
$\varnothing_w$	Open water surface area of cell	[L^2]

Chapter 1 Introduction

Damage from flooding in the United Kingdom (UK) is greater than from any other natural hazard (Culshaw et al., 2006). Catchments dominated by aquifers provide an interesting problem as groundwater can play a dramatic role in mediating the flood risk. The result is a hazard distinct both in aetiology and impact from fluvial or coastal flooding. The mechanisms associated with groundwater flooding are poorly understood and risks often lie away from delineated flood plains. Most surface water floods peak on a time-scale of hours to days, and generally decline over similar periods of time. However, when an aquifer is the source of a flood, high water can persist for up to several months (Green et al., 2006; Younger, 2007).

Groundwater flooding is defined as a "type of flooding that can be caused by the emergence of water originating from sub-surface permeable strata. The water may emerge from either point or diffuse locations" (DEFRA, 2006a; DEFRA, 2006b). Another common term is 'clear water flooding', which reflects the lack of sediment associated with groundwater. In an attempt to distinguish groundwater from other types of flooding the Department for Environment, Food and Rural Affairs (DEFRA) exclude flooding events downstream of the perennial head. (DEFRA, 2006a) Others however, do not make sure a distinction (Jacobs, 2004). It is estimated that 1.7 million properties are at risk from groundwater flooding in England. 382,407 of these are located on the major Chalk aquifers of southern UK (Jacobs, 2004). Only in the wake of major floods that affected the Chalk catchments of northern France, Belgium, and Southern UK in the winter of 2000-2001 was the term 'groundwater flooding' coined. In England during this time, between 2000 and 3000 properties were flooded by groundwater (DEFRA, 2006b; Jacobs, 2006). Although groundwater was not a major contributor to losses during the extensive flooding in 2007, some areas were affected and remained a serious threat for many months afterwards (Finch et al., 2007; Pitt, 2008).

Management of groundwater flooding has been since become a requirement as part of the European Union (EU) Floods Directive (2007/60/EC). More recently the Environment Agency (EA) and local authorities in the UK have been given a statutory requirement to manage flooding from groundwater (Great Britain, *Flood and Water Management Act 2010*). Although groundwater flooding has been

identified as an important and underrated hazard in the UK (Bloomfield and McKenzie, 2005; Fuller, 2003; Morris et al., 2005) and elsewhere (Kreibich et al., 2009; Mul et al., 2003; USGS, 2006; Zhou, 2007) there is still much work to be done in meeting the requirements of both (Cobby et al., 2009). The focus has largely been on hazard mapping (Morris et al., 2007) and short term (seasonal) predictions of risk using statistical analysis (Bradford and Croker, 2007; Najib et al., 2007), for example regression in conjunction with local warning systems (Adams et al., 2010). It has been suggested however that a robust analysis of risk in the long term is required (Cobby et al., 2009) particularly given the predicted changes in climate and accompanying modifications to land use practices (Jackson et al., 2006).

The Driver Pressure State Impact Response framework (DPSIR) is widely used for describing the interactions between society and the environment initially developed by the Organisation of Economic Co-operation and Development (OECD, 1993). It has been used to structure a wide range of environmental problems ranging from the threat of climate change in general terms (Vescovi et al., 2009) to the impact upon biodiversity (Omann et al., 2009), hurricane risk (Jessamy and Turner, 2003) and flood risk (Carter et al., 2009; Mokrech et al., 2008; O'connell et al., 2004; O'connell et al., 2007). The components of the model (Figure 1.1) include drivers, which are exogenous to the region, for example climate and socio-economic change and government policies. Pressures quantify the drivers within a specific region, for example the day to day weather experienced as a function of climate change or crop prices influencing land use practices. The state represents the environmental (or societal) systems that are affected by the pressure variables. In the case of groundwater flooding, this would include the groundwater system i.e. soil-water interaction, recharge processes and groundwater flow. A change in the state of the system therefore might have an impact on individuals, communities and society in this case the risk of groundwater flooding. Finally societal adaptation response would aim to minimise negative impacts or maximise positive impacts by acting on each of the previous four stages (Holman et al., 2008).

Environmental hazards such as groundwater flooding are problems at the interface between natural physical processes and human socio-economic activities (Smith, 2003). In addition to the DPSIR framework, groundwater flooding can also be viewed in a hazard and risk context (Eakin and Luers, 2006), where

$$risk = hazard \times vulnerability \quad (1.1)$$

Here, the physical processes contributing to the groundwater flooding hazard interact with socio-economic variables, e.g. land use changes and building on flood plains to produce a degree of risk. Similarly to the DPSIR approach, this has been synthesised into the "pressure and release" model (Wisner et al., 2006). On the one hand, the model emphasises the socio-political, cultural and economic factors that together explain differential exposure to hazards and capacities to recuperate from past impacts and adapt to future threats (i.e. vulnerability). On the other, the model shows the hazard acting on the population 'in the middle.'

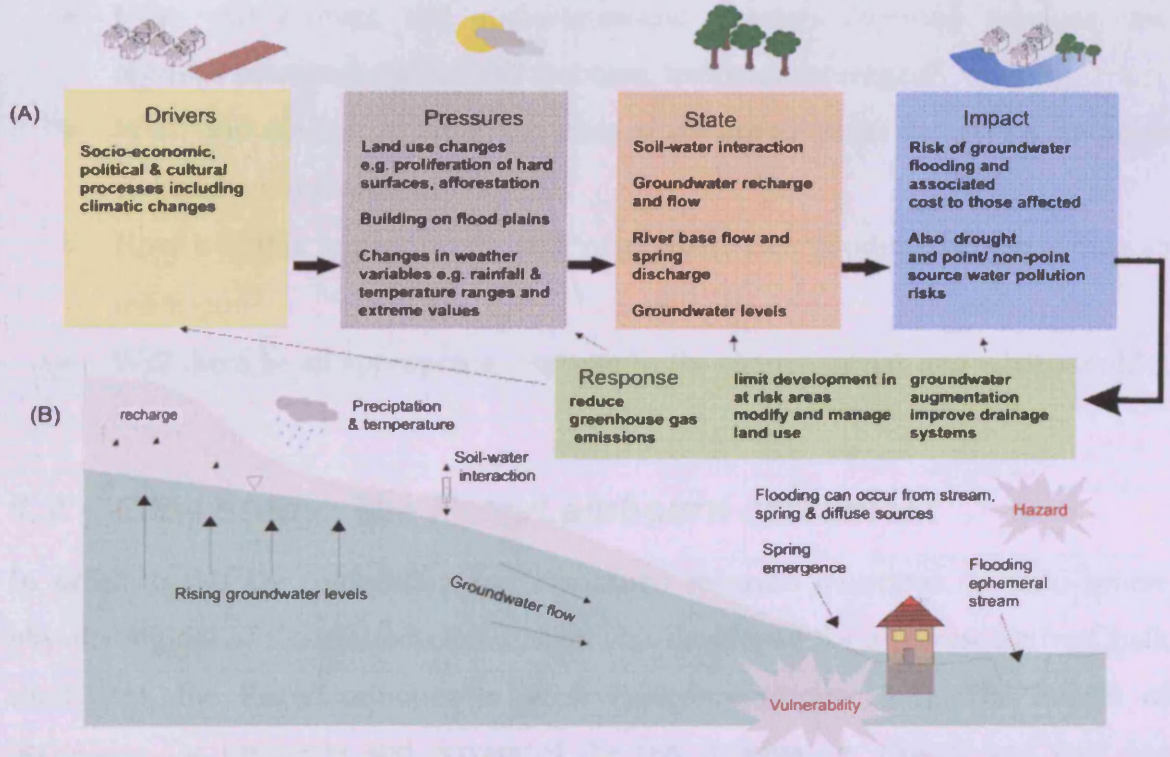

Figure 1.1 (A) DPSIR model summarising the interaction between socio-economic and environment factors to produce groundwater flooding risk. (B) Schematic of the major hazard and vulnerability processes contributing to groundwater flooding risk.

Whether groundwater flooding is viewed in the context of the DPSIR or risk framework, the need for integrated physical and socio-economic modelling is clear. Physically based approaches, often used to help manage water resources (Yusoff et al., 2002) provide an ideal method of investigating changes in future groundwater levels and therefore groundwater flooding risk. They offer a robust representation of surface water/groundwater interaction across an entire region and are ideal for modelling the impact of both climate and land use change on the system (Finch, 2001). As hazards and vulnerability are spatially distributed, risk is inherently a

spatial phenomenon. Geographical Information Systems (GIS) therefore provide an ideal platform for integrating the elements of a risk model covering the transition from drivers to pressures, state, impacts and responses to groundwater flooding.

1.1 Aims

The aim of this thesis is to test the hypothesis that "...global changes in climate and socio-economic systems are likely to have an impact on groundwater recharge and flooding risk within Chalk catchments of the UK...." This can be broken down into a series of research questions linked to the DPSIR framework:

- How will climate and socio-economic changes (drivers) translate into regional pressures e.g. rainfall amounts, temperature ranges?
- What will the impact be on the state of the groundwater system i.e. recharge rate and groundwater levels?
- How will this impact on the risk of groundwater flooding to those living in the region?
- Will there be an appropriate response to the change in risk and what should it be?

1.2 Case study: The Pang/Lambourn catchment

In order to test the hypothesis and associated research questions, a multi-sphere physical model of the groundwater system was developed for a representative Chalk catchment; the Pang/Lambourn in West Berkshire (Figure 1.2). The impact of perturbing the pressures and drivers of the risk process i.e. climate and land use change, can then be assessed. Although the methodology was developed using a specific site, it is equally applicable to Chalk catchments throughout the UK and beyond. The catchment is one of three study sites that are part of the ongoing Natural Environment Research Council funded LOCAR (Lowland Catchment Research) project (Adams B., 2003; Wheater and Peach, 2004). As such, the region has been subject to extensive recent data collection since circa 2001. In addition, during the 1970s, the Chalk aquifer was subject to a large investigation as part of the Thames groundwater scheme. The purpose of the project was to augment the flow of the Thames in times of draught by pumping groundwater into its tributaries including both the Pang and Lambourn (Owen, 1981; Owen et al., 1982). The result has been a legacy of plentiful, good quality data. A further reason for choosing the

Pang/Lambourn is that the region has been subjected to extensive groundwater flooding events in the past, particularly in 2000-2001 (Finch et al., 2004).

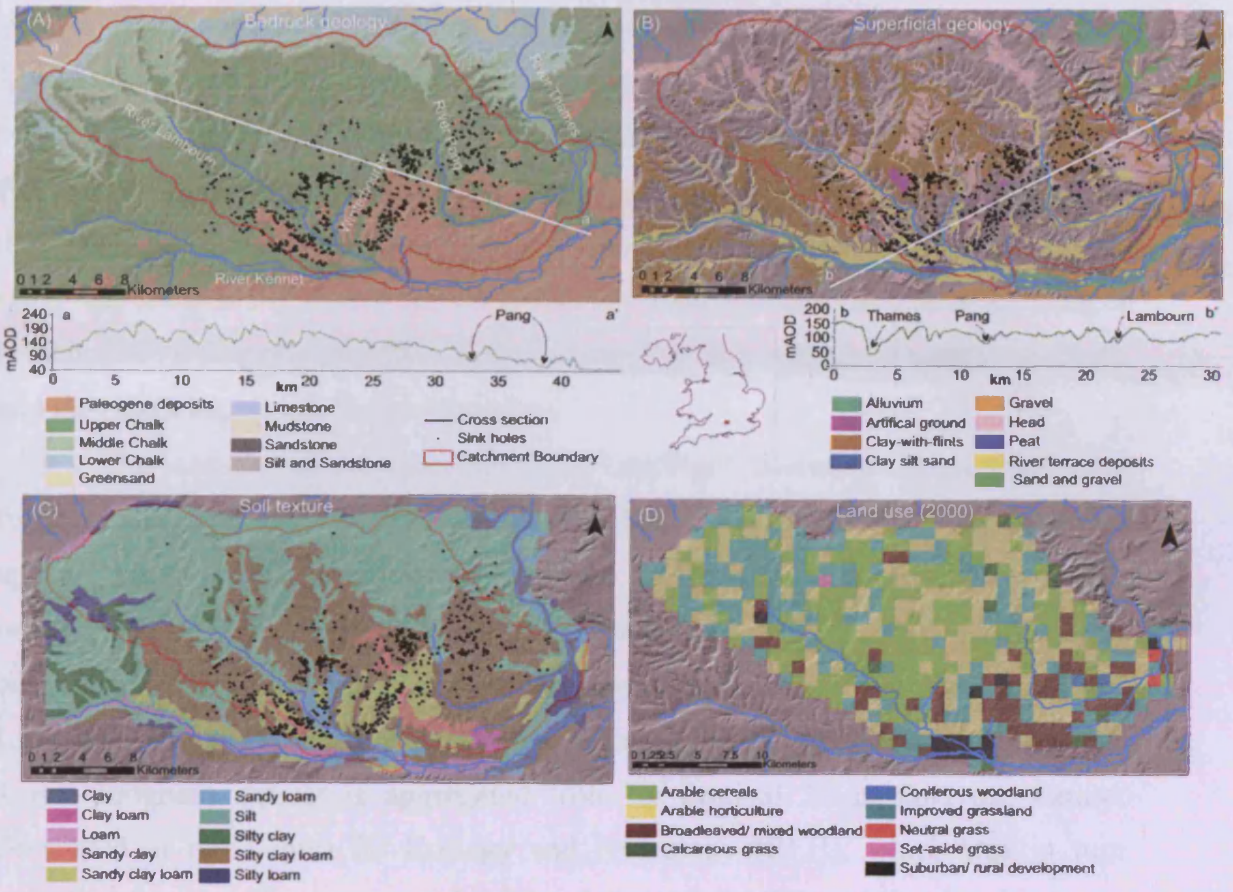

Figure 1.2 (A) Bedrock geology of the Pang/Lambourn, location of known sink holes, major rivers and location of cross section a-a'. (B) Superficial geology and location of cross section b-b'. Both the cross sections are ten times vertically exaggerated. (C) Soil texture interpreted from soil map of England and Wales. (D) Dominant land use in 2000, 1km resolution.

Although datasets specific to modelling procedures are detailed later in the thesis Figure 1.2 details the location of the site in central south England and some key descriptive datasets. The catchment drains approximately 400 km^2 (234 km^2, Lambourn and 170 km^2 Pang) and is located on the north-western side of the Thames Basin. The Lambourn catchment lies almost exclusively on fine-grained Upper Chalk and less permeable Middle Chalk. The upper reaches of the Pang comprises similar geology, although its lower reaches pass though younger and less permeable Palaeogene deposits made up of the Reading beds and London Clay (Figure 1.2A). Karstic features (sink holes) are clustered around the interface between the Chalk and Palaeogene deposits, which could provide a focus for runoff recharge and bypass flow.

Cross sections of the Digital Terrain Model (DTM) reflect a low lying, gently rolling topography, typical of a Chalk lowland catchment (Figure 1.2A & B). Clay-with-flints and superficial head deposits are widespread on the summits of the Upper Chalk ridges, and also further down the slopes. River terrace deposits occur along perennial and ephemeral river course as well as dry valleys (Figure 1.2B). The soil type and texture is associated both with the underlying bedrock and superficial deposits. For example, the Hornbeam soils in the central eastern region of the Pang (silty clay loam in Figure 1.2C) have previously been identified as a recharge hotspot (Finch, 2001). The origin of the soil was deemed to be a mixture of weathered Chalk and the overlying Lower Eocene deposits.

The land use of the combined Pang/Lambourn catchment is predominantly rural, agricultural land and grassland. 1 km dominant land use data suggests that approximately 28% is improved grassland, 29% arable cereals, 28% arable horticulture, 10% broadleaved woodland. A little over 2% represents significantly built up areas, which tend to be concentrated towards the confluence of the Lambourn with the river Kennet and Pang with the river Thames (Figure 1.2D). The 1 km dominant dataset is aggregated from an original 25 m land use dataset developed at the Centre for Ecology and Hydrology (CEH), which was in turn classified from satellite images and validated through field observations.

1.3 Thesis structure

The thesis is structured around a number of specific objectives broken down into chapters. The order of the work reflects the transition of water through the hydrological cycle from the atmosphere, through the soil and vadose zone, into the groundwater system and back out again as discharge along streams and springs. Once this system model is established, the drivers and pressures (climate and land use) are perturbed and the impact on future groundwater flooding risk is assessed. The cost/benefit of a possible mitigating response to the risk is then looked at. GIS is used throughout to integrate data and information from the different modelling spheres (Figure 1.3). More specifically each chapter addresses the following issues:

Chapter 2

- Develop and test a GIS based transient, distributed recharge model using the Pang/Lambourn catchment as a case study.

Chapter 3

- Use time series analysis to determine the timing of water table response to rainfall events at a variety of sites in the Pang/Lambourn in order to gain an insight into the vadose (unsaturated) zone processes of the Chalk.

Chapter 4

- Develop saturated groundwater flow models for the Pang/Lambourn, with an emphasis on simulating extreme (high) groundwater flow conditions using recharge input from the model developed in Chapters 2 & 3.

Chapter 5

- Interface the recharge model with downscaled output from a Global Climate Model (GCM) using an ensemble of possible climate change scenarios and a land use change scenario. Assess the impact of these recharge scenarios on the groundwater system by interfacing them with the groundwater model developed in Chapter 4.

Chapter 6

- Assess the current risk of groundwater flooding in the Pang/Lambourn catchment by integrating hazard maps and socio-economic vulnerability data and determine how this risk may alter under scenarios of climate and land use change. Investigate targeted land use modification as a risk mitigation tool.

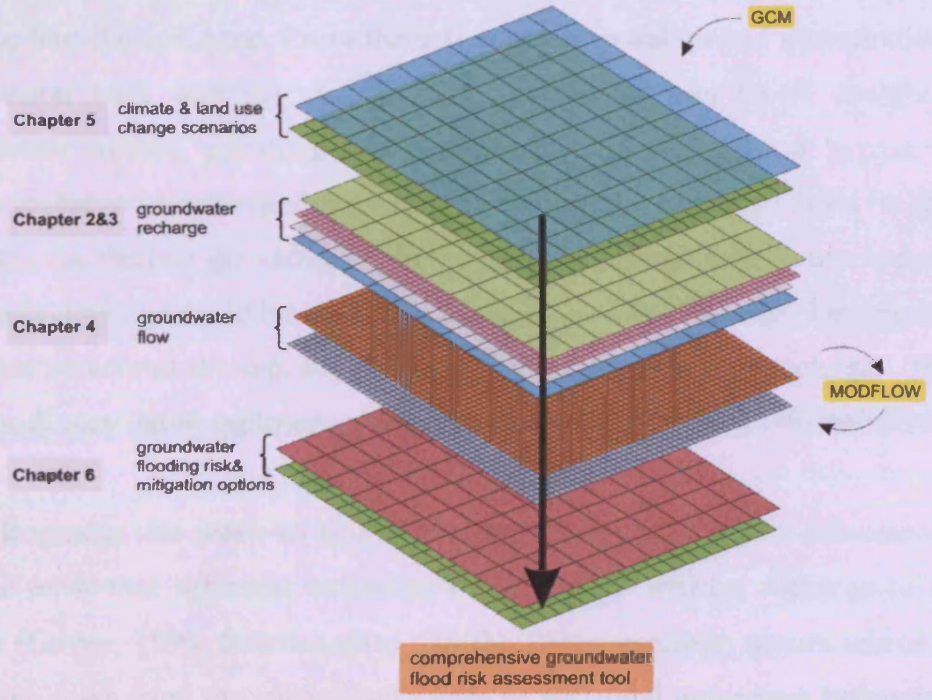

Figure 1.3 Thesis structure illustrated using a GIS gridded data structure and major interfaces with a Global Climate Model (GCM) and groundwater model (MODFLOW).

Chapter 2 GIS-based groundwater recharge model

2.1 Introduction

Climatic variability is propagated into aquifers via the surface and near-surface hydrological systems. Changes in the climate and surface-water hydrology will potentially have an impact on the amount of water entering the groundwater system (Scibek et al., 2007). This in turn has obvious consequences for groundwater flood risk (Cobby et al., 2009). By accurately calculating these fluxes across a catchment, the groundwater system can be modelled more effectively and the implications of change quantified. This chapter discusses a novel methodology for providing distributed transient groundwater recharge calculations directly within a GIS.

Groundwater recharge is the proportion of surface water which reaches the permanent water table by downward percolation or directly in riparian zones (Rushton and Ward, 1979). The hydrological processes typical of a temperate, groundwater dominated catchment are summarised in Figure 2.1. Precipitation (usually rainfall in the UK) may be intercepted before reaching the ground, a portion of which will be lost back to the atmosphere through the process of evapotranspiration (Lerner, 1990). The rest will eventually reach the ground via through-fall and stem-flow, at which point water may runoff over the surface or infiltrate into the soil zone. From the soil zone, evaporation and transpiration act to return water back into the atmosphere. Some water may travel straight to the groundwater surface, particularly at riparian zones and is termed bypass flow or 'bypass recharge'. Discharge back to the surface can be relatively rapid (in the order of weeks) via shallow groundwater flow occurring through drift or perched aquifers. Man-made drainage could be seen as part of this interflow process. The remainder of water that percolates through the soil zone is termed 'infiltration recharge'. Interflow and runoff may later infiltrate and is termed 'runoff recharge' (Heathcote et al., 2004).

Recharge can reach an aquifer directly or indirectly. Many sub-categories of recharge exist that represent examples of direct and indirect recharge to varying degrees (Lerner, 1990; Scanlon et al., 2002). Direct recharge occurs where rainfall percolates down from the surface with little or no lateral movement before reaching the groundwater table. This is comparable to infiltration and bypass recharge

summarised in Figure 2.1. In the temperate, humid climatic system typical of the UK, direct recharge usually dominates (Church, 2005) and so is the main focus of this research. Indirect recharge occurs when significant lateral movement of water occurs either on the surface (runoff-recharge) or in the vadose zone. Dissolution, karstic features in Chalk aquifers (e.g. swallow holes) could be the focus of runoff recharge (Figure 2.1). Such features tend to cluster around the periphery of low permeable confining layers (Maurice et al., 2006). An anthropogenic example would be leakage from drainage networks, which would clearly be of more consequence in urban areas (Thomas and Tellam, 2006). Groundwater augmentation schemes and irrigation could have an impact on indirect recharge outside an urban setting (Lerner, 1990). Leakage from stream beds, particularly where a river is in hydraulic continuity with an underlying aquifer can be important processes too (Jackson and Rushton, 1987).

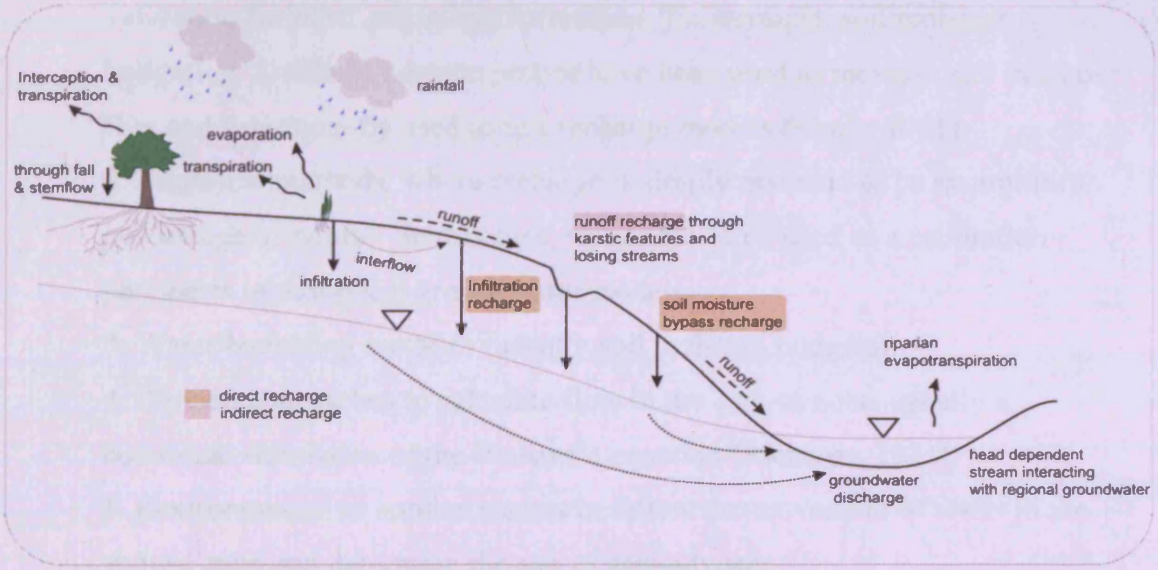

Figure 2.1 A schematic of the major surface and groundwater flow processes in a groundwater dominated Chalk catchment characteristic of a temperate humid environment e.g. the UK.

A second major distinction is between potential and actual recharge (Lerner, 1990; Scanlon et al., 2002). Potential recharge *could* reach the groundwater surface, whereas actual recharge is the water that *does*. A distinction would be rainfall that percolates into the soil column but returns to the atmosphere through evapotranspiration instead of continuing to groundwater. Indeed, not all the water travelling down from the base of the soil zone or river bed would become recharge. If for example it meets a low permeability layer it may be diverted as interflow (Figure 2.1). Depending on the method used to estimate recharge, a certain volume

of rainfall could be accounted for as recharge. However, because the rainfall flux was not observed reaching the groundwater surface, it is defined as potential recharge.

2.1.1 Recharge estimation

Recharge estimation techniques can be broadly categorised into localised field measurements and models of recharge over a larger area, typically a catchment. Often the field data is used to develop and ultimately test a regional water balance model. Lerner (1990) describes 5 major methods that have been used for estimating direct, potential recharge:

1. Localised direct measurement using lysimeters (~10 m^2), which could be extrapolated over a wider area if there are a limited number of surface and soil conditions in the catchment. Measurements could also be used as validation for other modelling techniques, for example. soil moisture budgeting. Similarly neutron probes have been used to measure soil moisture flux and subsequently used to test recharge models (Finch, 2001).

2. Empirical methods, where recharge is simply assumed to be an arbitrary percentage of rainfall. In this case, values are often used as a calibration parameter in numerical groundwater models.

3. Water budgeting methods (usually soil moisture budgets).

4. Darcian approaches to calculate flow in the vadose zone, usually a numerical simulation of the Richard's equation (Richards, 1931).

5. Environmental or applied tracers to follow the movement of water in the vadose zone and determine the age of groundwater.

The choice of technique chosen to estimate recharge is based on the physical characteristics of the area of interest as well as the proposed purpose and scale of the study. A small scale study, where precision is very important would require a different strategy to a large, homogenous catchment. Likewise, the preferred technique is dependent on the zone of interest. For example, Scanlon et al. (2002) define techniques by hydrologic zone where there is a continuum from potential to actual recharge estimation from the surface to the permanent groundwater table. Surface water and vadose zone approaches usually provide estimates of potential recharge, whereas groundwater techniques generally provide information on actual recharge, e.g. rainfall-borehole response studies.

The methods described above are not mutually exclusive and often an iterative combination of monitoring and modelling provide the most robust recharge estimates. A pilot groundwater study might firstly involve a rough estimate of recharge based on empirical formula. As more information is gathered from field lysimeters, tracer tests, observation borehole logging etc., a more comprehensive conceptual model of recharge pathways will be formulated. These could then be represented by a lumped or distributed water (usually soil moisture) budget model allowing for parsimony as more data is collated. Similarly, unlike Darcian recharge techniques; a soil moisture model does not say anything about flow in the vadose zone between the soil store and permanent groundwater table. In turn, a numerical simulation of the Richards equation does not explicitly model the flux from climate to soil store (potential recharge). As such, both should not be viewed as mutually exclusive, but complimentary on the continuum from estimating potential through to actual recharge. Darcian unsaturated flux models could ultimately be used in conjunction with a soil moisture budget to account for vertical flow from the soil zone to the groundwater table.

Any groundwater modelling process, including recharge usually requires the formulation of a water balance model. This process is made possible through the division of recharge into sub-processes and categories. Recharge makes up a portion of the change in storage of water (ΔS),

$$P = Ro + ET + \Delta S \tag{2.1}$$

where P is precipitation [LT^{-1}], Ro the surface runoff [LT^{-1}] and ET the total actual evapotranspiration [LT^{-1}]. This simple water balance can be expanded into its constituent subcomponents, allowing direct (R_d) and indirect (R_{id}) groundwater recharge [LT^{-1}] to become the focus,

$$R_d + R_{id} = P - Int - Ro - ET - \Delta S_{gw} - \Delta S_{sw} - \Delta S_d \tag{2.2}$$

where Int is interception [LT^{-1}], Ro is runoff [LT^{-1}] and ΔS_{gw}, ΔS_{sw} , ΔS_d are the change in groundwater, surface water, and other e.g. (drainage) storage respectively [LT^{-1}]. The number of subcomponents is limited only by the desired complexity of the conceptual representation and ability to measure the variables. Variables such as interception for example, could be further divided into calculations of leaf drip, trunk evaporation, trunk storage and stem flow (Finch, 2001). Likewise, runoff could be further divided into near-surface interflow, deeper interflow and surface runoff (Heathcote et al., 2004).

The most common way of estimating recharge is by measuring, modelling or discounting all the other variables in the equation, otherwise known as the 'residual' method (Anuraga et al., 2006; Church, 2005; Dripps and Bradbury, 2007; Szilagyi et al., 2005). In the case of Equation 2.2, this would be the variables to the right hand side. The major benefit of this approach is flexibility. The variables to be calculated in order to provide an estimate of recharge can be as detailed as necessary or possible given the data and resources available. The range of spatial and temporal scales the method can be applied to is also large; ranging from a single monitoring station over a day, to entire continents over decades. The accuracy of the recharge estimate however depends on the accuracy with which the other components in the water balance are measured. This is particularly the case when recharge rates are relatively small, for example in arid areas or during dry periods. However, by measuring key parameters accurately, for example rainfall and store volumes, the recharge values can be constrained effectively. Methods for measuring or estimating various components of the water budget are summarised in Scanlon et al. (2002) and Lerner (1990).

2.1.2 Soil moisture balance techniques

The most popular water balance for potential, direct recharge estimation in temperate environments is a soil moisture model (Finch, 2001; Ragab et al., 1997; Rushton et al., 2006; Rushton and Ward, 1979). The soil moisture balance technique calculates the relative proportions of precipitation that are stored in the soil, returned to the atmosphere or percolate down towards the aquifer system. Precipitation increases the amount of water stored in the soil and evapotranspiration depletes it. During wet periods, the soil can be at its maximum moisture capacity. This is termed Field Capacity (*FC*), which is the amount of water retained by the soil after it has been allowed to drain fully under gravity. During this time sufficient moisture is available to meet all the demands of the plants (Younger, 2007). If *FC* has been established, any further precipitation is termed hydrological excess and is routed to the groundwater as recharge. Where precipitation is less than evapotranspiration, moisture levels can fall below *FC* and a Soil Moisture Deficit (*SMD*) can develop. If *SMD* is greater than zero, the soil store must usually be filled before recharge can begin again. Determining the magnitude of the *SMD* is important because it controls whether water will enter the groundwater system or be transpired by vegetation. In

the UK *FC* values are usually assumed to be zero in the month of April following the wet, cooler winter months (Younger, 2007).

Penman (Penman, 1949a; Penman, 1949b) and Grindley (Grindley, 1967; Grindley, 1969) originally proposed the soil moisture budget technique as a method of calculating recharge when *SMD* is equal to zero. Within a soil column, the mass of water is conserved such that recharge (R, [LT^{-1}]) is given by,

$$R = P - (Int + Ro + Aet) \qquad \textbf{if SMD} = 0 \tag{2.3}$$

where P [LT^{-1}] is precipitation, *Int* is interception [LT^{-1}], *Ro* is runoff [LT^{-1}] and *Aet* is actual evapotranspiration [LT^{-1}]. If the *SMD* is above zero i.e. the soil is not at *FC*, the excess water left after *Int*, *Ro* and *Aet* goes to the soil store (ΔSMD). P can be directly measured using weather station records. In turn *Ro* and *Int* can be estimated as a fraction of P using standard, calibrated parameters (Batelaan and De Smedt, 2007; Finch, 2000). The most difficult aspect to quantify is *Aet,* because the flux is dependent on the prevailing weather conditions, soil moisture and land use type. Most commonly, a value of potential evapotranspiration (*Pet*) is initially determined. This is defined as 'the rate at which evapotranspiration would occur, given the ambient conditions of atmospheric temperature, humidity and solar radiation, if there were no limit to the supply of water to the soil surface and/or to plants' (Younger, 2007). The UK Meteorological Office uses the Penman-Monteith formula (Monteith, 1965) to estimate *Pet* at 40 km resolution as part of the MORECS system (UK Meteorological Office Rainfall and Evaporation Calculation System). Usually *Pet* is calculated for 'short well watered grass' (Thompson et al., 1981)

The Penman-Grindley approach provides a budgeting procedure which controls the rate of *Aet* relative to *Pet* through the root constant (C) and wilting point (D). Plant roots take water up at the potential rate until a critical *SMD* threshold is reached (i.e. the root constant) at which point, the rate of evapotranspiration falls to a fraction of the potential rate. The maximum available water for plant uptake is the difference between the soil moisture content at *FC* and D. Both the C and D are proportional to the rooting depth of the surface vegetation. For example an oak tree would have a much larger value of C and D than a wheat crop. The value of C and D is indirectly related to soil properties by influencing the type of vegetation that can grow.

These relationships can be seen more clearly in the development of a *SMD* in Figure 2.2. Initially the soil is at *FC*, but a *SMD* develops as *Aet* exceeds *P*. At this stage *Aet* proceeds at the potential rate given that there is plentiful supply of moisture available to the plants (Figure 2.2a). As the *SMD* develops to a value greater than *C*, *Aet* proceeds at a reduced rate. Conceptually, this is because there is less water available to the plants (Figure 2.2b). At this stage, if *P* was greater than the *Pet* then *Aet* would continue at the potential rate. Finally, the *SMD* reaches *D* and the plant wilts. The *SMD* cannot develop beyond this point and *Aet* continues equal to *P*, until *P* begins to increase again (Figure 2.2c). It is useful to envisage this process usually occurring from spring through summer in the UK (Rushton and Ward, 1979). Initially the *SMD* recovers from *D* as more water enters the system than exits (Figure 2.2d). As the *SMD* recovers to below *C*, *Aet* returns to the potential rate (Figure 2.2e). However, because the value of *P* is greater then *Pet* the *SMD* continues to diminish, until the soil is once again at *FC* (Figure 2.2f). Formally, the Penman-Grindley method states that *Aet* is derived from *Pet* depending on antecedent conditions,

$$Aet = Pet \qquad \textbf{when SMD} < \textbf{C or P} \geq \textbf{Pet} \qquad (2.4)$$

$$Aet = P + F(Pet - P) \qquad \textbf{when D} > \textbf{SMD} \geq \textbf{C and P} < \textbf{Pet} \qquad (2.5)$$

$$Aet = P \qquad \textbf{when SMD} = \textbf{D and P} < \textbf{Pet} \qquad (2.6)$$

where *P* is precipitation (after runoff and interception) and *F* is an empirical constant of 10% in the UK (Lerner, 1990). The values of *C* and *D* appropriate for common vegetation types in the UK can be seen in Appendix 1.1 and vary monthly over an annual cycle for agricultural crops but typically remain constant for forests and grassland. Thus vegetation type and harvest patterns affect the *Aet* of a catchment. The date of harvest for crops is important in determining when transpiration proceeds at a limited rate. When the crop is harvested, the value of *D* diminishes which limits the magnitude of the *SMD* and allows more water to be routed as recharge. As the crop grows, the value of *C* and *D* increases, which simulates the improved ability of the vegetation to extract water from the soil via evapotranspiration. According the Penman-Grindley model, transpiration in woodland is not limited by *C* and *D* seasonal reduction (Lerner, 1990).

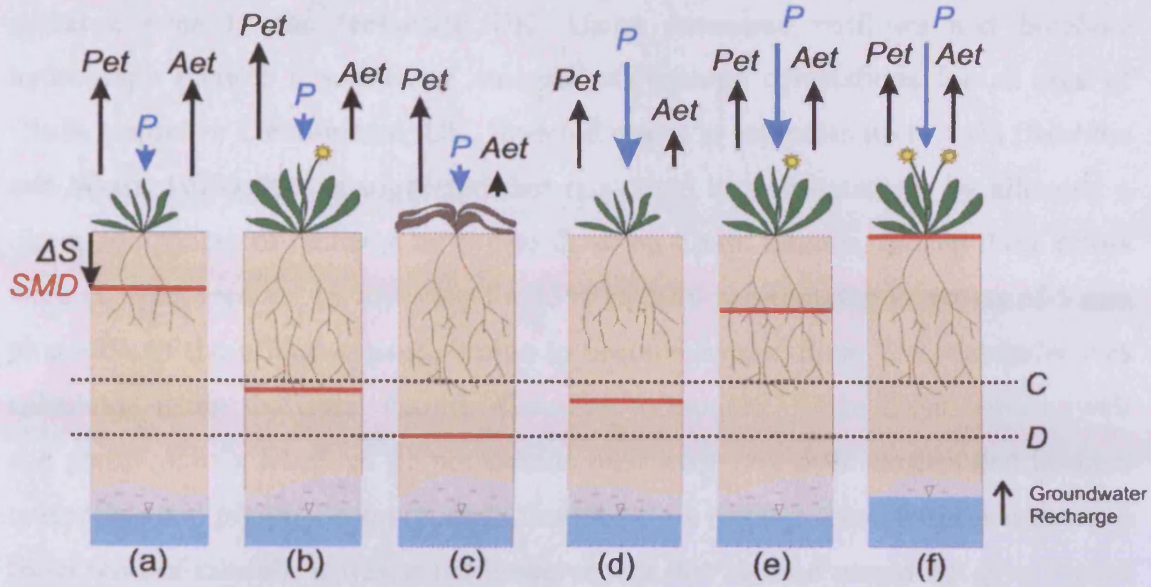

Figure 2.2 (a)-(f) The development of a Soil Moisture Deficit (*SMD*) from Field Capacity (*FC*), through root constant (*C*) to wilting point (*D*) and back to *FC* including the impact of SMD on the relationship between precipitation (*P*), potential (*Pet*) and actual (*Aet*) evapotranspiration.

Other models reflect different approaches towards how soil moisture interacts with the root system. For example, Finch (2001) proposed a soil moisture model consisting of four layers. This was to incorporate the process of evaporation directly from the uppermost soil horizons and the capillary rise of water in response to the development of lower soil water potentials in the layers above. Such techniques can explicitly incorporate soil texture and their hydrological properties into the model. Field studies have suggested for example that a clay horizon near the surface will retain water longer for relatively rapid evaporation back into the atmosphere. For this reason some models determine parameters similar to *C* and *D* based on crop type *and* soil texture (Rushton, 2003). It has been suggested however that the difference between models is less important than the accuracy of *P*, *Pet*, irrigation and cropping data (Lerner, 1990). Indeed it has even been suggested that complex distributed models offer limited benefits for recharge estimates at the catchment scale (Bradford et al., 2002). It makes sense therefore to begin with a relatively simple model and increase complexity only when necessary. This saves data collection resources and often reduces the need to estimate unknown variables e.g. the properties of numerous soil horizons over a catchment scale.

A challenge to all recharge models is parameterising every possible hydrological pathway. Adopting the Penman and Grindley (Grindley, 1967; Grindley, 1969; Penman, 1949a; Penman, 1949b) approach tends to underestimate

recharge even in the temperate UK. Using measured outflows and borehole hydrograph records a sensitivity analysis of recharge calculations for an area of Chalk aquifer in Lincolnshire, UK, revealed errors in estimates up to 15% (Rushton and Ward, 1979). It was suggested that this could be accounted for by allowing a direct component of recharge as bypass flow via Chalk fissures. Indeed these errors were compensated for by allowing for 15% of daily precipitation in excess of 5 mm plus 15% of the effective precipitation to become bypass flow. The remainder was calculated using the usual Penman-Grindley technique. Unlike clays, which swell and shrink, Chalk fractures do not change their geometry over seasons and hence a reasonable and pragmatic approach to describe flow through these fissures is to use a fixed ratio of rainfall. It was noted however that this method would not give correct daily recharge, but would be acceptable in calculating monthly inputs to a regional groundwater flow model (Younger, 2007). It is now common for soil moisture models to incorporate this bypass flow component in Chalk areas (Bradford et al., 2002; Ragab et al., 1997). Finch (2001) however suggested that detailed analysis of the soil moisture data and hydrographs from boreholes showed no evidence of bypass flow occurring in the Pang catchment. Evidence for rapid response bypass flow mechanisms in the Pang and Lambourn are discussed in more detail in Chapter 3.

Soil moisture balance recharge models have been tested directly against borehole hydrograph responses (Lerner, 1990) and stream baseflows (Bradford et al., 2002). There are many factors however that could influence the relationship between potential recharge, groundwater heads and ultimately baseflow, that are independent of the recharge model e.g. perched groundwater tables, preferential flow paths, regional flow patterns, unknown catchment-wide abstractions, a deep water table and a mobile groundwater catchment divide. If combined with a saturated groundwater flow model, e.g. MODFLOW, less accurate estimations could be compensated for by parameterisation bias in a saturated flow model, masking inadequacies in the recharge model itself. A practically infinite number of combinations of hydraulic conductivities and recharge rates that span a wide range could all match the target head distribution for a flow model calibration. Consequently, inadequate control of recharge rates can lead to a situation of non-uniqueness of flow model solutions. A soil moisture balance provides potential recharge estimations based primarily on moisture levels in the soil. It is therefore appropriate for the *SMD* to be compared

with field observations as it plays a direct role in whether recharge takes place or not in the model (Finch, 2001).

In order to reconcile the observed and modelled *SMD* (and therefore recharge) observations, it may be necessary to adapt and calibrate the model. A soil moisture model does not explicitly describe how recharge occurs (Lerner, 1990). It may for example, be dominated by fissures, root channels or topographic depressions. As such, many models need empirical adjustments to allow them match field conditions and better represent the physical processes. The introduction of bypass flow by Rushton and Ward (1979) is an example of such an adjustment. Other examples of model adjustments away from the original Penman-Grindley approach include the introduction of multiple soil horizons (Finch, 2001; Rushton et al., 2006). There has also been an attempt to compare various models with different levels of complexity (Ragab et al., 1997). In this instance, more simple models were found to be adequate and weather input data was more important. In others, the sensitivity of the model to uncertainties in the input data has been explicitly assessed. For example, Bogena, Kunkel et al. (2005) performed a Monte Carlo sensitivity analysis of land use, soil and rainfall input data on soil moisture recharge model. In this case, rainfall was found to be the most important parameter. Other adjustments available include allowing for crop ripening and removal. This can be done by altering the *Aet-Pet* relationship, e.g. by reducing C at harvest time to simulate the removal of transpiring plants. Such changes can be specific to the catchment and modelling goals and so can not necessarily be universally adopted. For this reason it is often best to begin with a simple model representation and build in changes based on local data.

2.1.3 GIS, recharge modelling and WetSpass

GIS allows disparate information about geology, land use, soil properties, topography, hydrology, climate etc. to be integrated, queried and analysed, providing an ideal platform to develop conceptual models of groundwater recharge (Walker et al., 2006) as well as modelling the processes themselves. Usually, GIS process modelling is limited to recharge using a form of the soil moisture balance approach (Dripps and Bradbury, 2007; Szilagyi et al., 2005; Thomas A. et al., 2006; Wendland et al., 2003). Efforts have been made to integrate saturated flow models, e.g. MODFLOW (Harbaugh et al., 2000) with models of surface hydrology, for example Hydrological Simulation Program Fortran (HSPF) (Bicknell et al., 1993) and Soil

and Water Assessment Tool (SWAT) (Arnold et al., 1994). The result has ultimately been holistic catchment models such as System Hydrologique European (SHE) (Abbott et al., 1986), which has been used to model lowland catchments in the UK (Thompson et al., 2004). SHE is made up of many sub-models which aim to be physically realistic, which in theory means that the model should not require calibration. However, aside from the cost of the software, the data requirements to set up such a model are prohibitive. Other examples of distributed recharge models exist, although they are usually bespoke codes that are unavailable for use (Finch, 2001; Heathcote et al., 2004; Scibek et al., 2007).

WetSpass (Water and Energy Transfer between Soil, Plants and Atmosphere under quasi Steady State) offers a more accessible GIS based recharge modelling technique (Batelaan and De Smedt, 2001; Batelaan and De Smedt, 2007; Paul, 2006). It is based on a spatially distributed soil moisture balance model simulating long-term average (6 monthly or annual) recharge as a function of land cover, soil texture, topography and hydrometeorological parameters. A catchment is divided into a 2D raster grid, defining the dominant hydrological characteristics. Every raster cell is further subdivided into a vegetated, bare soil, open water and impervious surface fraction, for which individual water balances are calculated. This allows for sub-cell heterogeneity, which would be important especially if the only available data was coarse scale. The fractions change seasonally, allowing changes in vegetation cover to be modelled. The recharge values are input into a steady state MODFLOW model and resulting long term average groundwater table data is input back into WetSpass.

Parameter definition in the WetSpass is on the basis of literature values from interception and runoff studies primarily in Belgium and the Netherlands (Batelaan and De Smedt, 2007). The model results correspond well with point measurements of water balance fluxes in the field. It was also validated against baseflow estimates in 17 sub-catchments of the Dijle, Demer and Nete catchments in northeast Belgium. WetSpass was developed for estimating long term average recharge under humid temporal conditions, which is equally applicable to the UK. Indeed, a report from the Crop Protection Agency provides a convincing justification for climate comparability between western continental Europe and UK (CPA, 2002). Parameters developed to estimate long term interception and runoff will be equally suitable for monthly or daily calculations (Batelaan 2008, personal communication). Indeed, daily or sub-daily calculations are the focus of most recharge modelling studies (Finch, 2001).

These methods can often be very data intensive (Heathcote et al., 2004), which may preclude the use of distributed calculations for running large numbers of (climate/land use) change scenarios (Herrera-Pantoja and Hiscock, 2008). Other studies have successfully focused on monthly models, which are more efficient (Vandewiele, Xu et al. 1992; Xu and Singh 1998; Jiang, Chen et al. 2007). If monthly recharge models can be shown to adequately reproduce past soil moisture budgets at the local scale, it would be a great advantage given the ensemble methods favoured by climate impact studies.

2.2 Aims and objectives

The aim of this chapter is to develop a catchment scale recharge model for the Pang/Lambourn that can later be used to assess the impact of climate and land use change on the system. This can be broken down in a number of specific objectives:

- Develop a GIS based transient model of direct, potential recharge based on the soil moisture balance technique, using the Pang/Lambourn catchment as a case study.
- Test the model against observations of local soil moisture.
- Use the model to assess the current spatial and temporal patterns of recharge in the Pang/Lambourn.
- Optimise the spatial and temporal resolution of the calculations to allow for efficient climate and land use change impact assessment. This will include a temporal sensitivity analysis to determine the suitability of monthly calculations. In addition the model will be developed at 1 km resolution.

2.3 Methods

2.3.1 GIS-DIRT model framework

GIS-DIRT stands for **G**eographical **I**nformation **S**ystems based **D**istributed **R**echarge **T**ransient model. Using this method, the Pang/Lambourn catchment was represented by a regular raster grid and calculations of water flux are made within each cell providing a 2D representation of the interface between surface and subsurface hydrology (Figure 2.3). A water balance was performed for the vegetated, bare, impervious and open water portions of each grid square. These proportions varied throughout the year allowing spatial and temporal land use changes to be

incorporated into the model, for example vegetation die off in winter, growth in the spring or long term or permanent changes. This method of subdividing the raster grids allowed sub cell heterogeneity to be modelled, so a coarse grid resolution (1 km) could be used to maximise computational efficiency, whilst maintaining an adequate level of detail. Recharge flux (R, [LT^{-1}]) was calculated for each raster cell at each time step

$$R = P - \phi_v(Int + S_v) + \phi_b(S_b) + \phi_i(S_i) + \phi_w(S_w) + ET \quad (2.7)$$

where P is precipitation [LT^{-1}], $\emptyset_v$ is the vegetated surface area of the grid cell [L^2], $\emptyset_b$ is the bare earth portion [L^2], $\emptyset_i$ is the impervious portion [L^2], $\emptyset_w$ is the open water portion [L^2]. Int_v is interception as a proportion of precipitation [LT^{-1}]. S_v, S_b, S_i and S_w are surface runoff fluxes as a proportion of precipitation [LT^{-1}] for the vegetated, bare earth, impervious and open water portions of the grid square. ET is evapotranspiration as a proportion of precipitation [LT^{-1}] for the whole grid square.

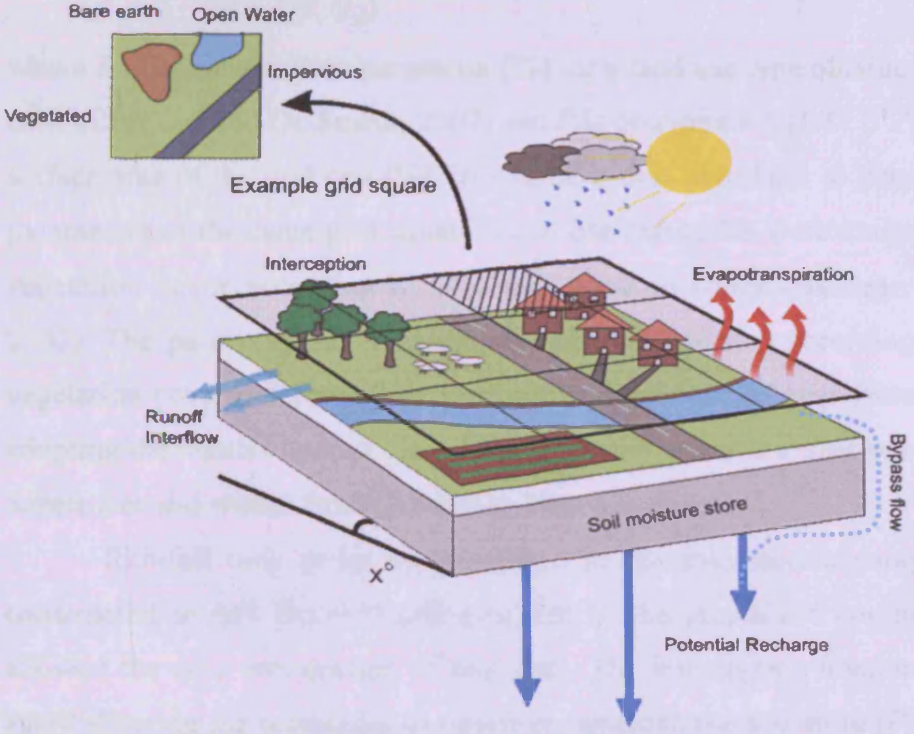

Figure 2.3 Schematic diagram showing the GIS-DIRT model framework which calculates distributed potential recharge.

Output from GIS-DIRT could then be interfaced with a model of the vadose zone and saturated groundwater flow model (Chapter 4). In addition, the framework allows output from a stochastic weather generator to be interfaced with the recharge model and land use to be interactively modified (Chapter 5). The method was implemented in the common GIS program ArcGIS™ in order to maintain flexibility

ad transferability. The use of raster datasets allows the interactive manipulation of the parameters e.g. land use, as well as transferability to other catchments. There was an emphasis on the ability of the modelling methodology to take advantage of increasingly available spatial datasets representing soil properties, land use, topography and meteorological conditions. The following sub-sections detail the calculation of individual fluxes within the recharge model.

2.3.2 Interception

Interception is reasonably consistent for a given annual precipitation rate and land use (Roberts, 1983). This assumption is equally applicable to monthly (and daily) estimates. It was therefore parameterised as a constant fraction of precipitation depending on vegetation type in long term lumped models (Dolman and Nonhebel, 1988). The amount of water that does not reach the ground surface (*Int*, [LT^{-1}])

$$Int = P\Psi_v(I_v) \tag{2.8}$$

where I_v is an interception parameter [%] for a land use type obtained from a look-up table (Batelaan and De Smedt, 2007) and P is precipitation [LT^{-1}]. Ψ_v is the vegetated surface area of the grid cell [%].This value is also used later to determine the runoff parameters of the same grid square. Land use categories were assigned a percentage vegetation cover according to WetSpass look-up tables (Batelaan and De Smedt, 2007). The percentage interception values were adjusted according to the seasonal vegetation cover determined by the land use and time of year (summer/winter). By adopting the regular hydrological calendar in this study, summer represented April to September and winter from October to March inclusive.

Rainfall time series were applied to the interception parameters via code constructed in MS Excel™ and executed in the ArcGIS™ command line, which allowed the easy introduction of new data. The interception fraction (*Int*) was taken away allowing the remainder to runoff or replenish the soil store (P_{in}). Appendix 1.2 shows an example of code that allows rainfall time series to be applied to summer/winter interception raster datasets. The syntax was broken down into component columns in MS Excel™ allowing alternative rainfall time series to be simply pasted in. If necessary the rainfall component could be a replaced by a link to a distributed rainfall dataset at each time step. The flexibility of the scripting procedure was vital for the model's application as a tool for investigating the impact of climate change. Similarly, land use changes could be simulated relatively easily

by assigning different interception parameters. In lieu of interception field data, the model's ability to recreate *SMD*s (and later groundwater levels) was used as a proxy validation of the interception parameters used.

2.3.3 Runoff

Runoff parameters were a function of topographic, soil and land use properties. Surface runoff (*Ro*, [LT^{-1}]) as a proportion of rainfall after interception (P_{in}, [LT^{-1}]) was calculated for the vegetated, bare, impervious and open water fractions of a cell and based on characteristic values from the literature (Chow et al., 1988; Pilgrim and Cordery, 1992,; Smedema and Rycroft, 1988; USDA-NRCS, 1972)

$$Ro = P_{in}((\Psi_v Ro_v + \Psi_b Ro_b + \Psi_i Ro_i + \Psi_w Ro_w)\beta) \quad (2.9)$$

where β is a Hortonian fraction [%], Ψ_v is the vegetated portion of the grid cell [%], Ψ_b is the bare earth portion [%], Ψ_i is the impervious portion [%], Ψ_w is the open water portion [%]. Ro_v, Ro_b, Ro_i and Ro_w are runoff parameters [%] for the vegetated, bare, impervious and open water portions of the raster grid respectively.

These runoff parameters in turn were a function of a Hydrological Response Unit (HRU) Identification code (ID). In order to assign the HRU IDs the land use dataset (Figure 1.2D) was reclassified and assigned a vegetation ID (see Appendix 1.3 for an example lookup table). Secondly the DTM was converted to a percentage slope grid and then aggregated to 1 km resolution to coincide with the land use data. The median slope angle within each 1 km grid was used in the aggregation process in GIS. The grid was then reclassified into 4 ID classes; 1 = <0.5%, 2 = 0.5 – 5%, 3 = 5-10%, 4 = >10%. Thirdly, the soils were then converted to soil texture categories and assigned an ID. This was done by referring to the description of the soil characteristics in the legend for the soil map of England and Wales. The full descriptions for each soil association and ID look up table can be found in Appendix 1.4. Individual HRUs were identified by combining land use, slope and soil IDs (Batelaan and De Smedt, 2007), such that

$$HRU = (soilID \times 100) + (landuseID \times 10) + (slopeID) \quad (2.10)$$

Coefficients were assigned from a look up table (Batelaan and De Smedt, 2007) according to the resulting HRU IDs. For example, a soil texture may have an ID of 3, the land use may have an ID of 2 and slope 1. The HRU ID therefore becomes '321', which has a runoff parameter associated with it. The HRU ID used to determine Ro_v

is based on the slope, vegetation and soil texture. S_b is based on slope and soil texture. Ro_i is based on slope and Ro_w is always 100%.

The original land use grid was reclassified according to the percentage vegetation cover expected in summer and winter. The coefficients were adjusted accordingly, for example if a HRU is 20% vegetation in winter, the runoff coefficient is reduced to 20% of the original value. HRU IDs were determined for the bare-earth and impervious portion of the raster cells in a similar fashion. The vegetated, bare earth and impervious fractions were summed to determine the overall potential runoff coefficient for each grid square over summer and winter. The actual runoff coefficient was mediated by seasonal rainfall intensity quantified by a Hortonian fraction (β). The potential runoff coefficients were multiplied by this fraction to simulate seasonal rainfall intensity characteristics. The resulting value was taken away from 1 in order to give the amount of rainfall that could potentially go to recharge rather than fraction lost to runoff. Vegetation cover changes seasonally, so a winter and summer distributed runoff coefficient dataset was produced to reflect this. Rainfall following interception (P_{int}) distributed time series were applied to the runoff datasets, which effectively act like filters and influence the amount of water available to restore a *SMD* or recharge the groundwater.

2.3.4 Evapotranspiration and recharge

Evapotranspiration calculations were based on a modified Penman-Grindley (Grindley, 1967; Grindley, 1969; Penman, 1949a; Penman, 1949b) approach allowing for 15% bypass flow (Rushton and Ward, 1979). The model relied on distributed *C* and *D* datasets to mediate the divergence of *Aet* from *Pet*. These were developed by reclassifying the land use dataset (Figure 1.2D) according to corresponding *C* and *D* values available from the literature (Lerner, 1990; Younger, 2007). A unique distribution of *C* and *D* was developed for each month of the year, depending on the growing and dying back characteristics of the vegetation. Where cropping (harvesting) dates was unknown, the mean for all cropping scenarios was used e.g. for arable cereals and horticultural land use. The land use classes in the Pang/Lambourn and their associated monthly *C* and *D* values can be seen in Appendix 1.5.

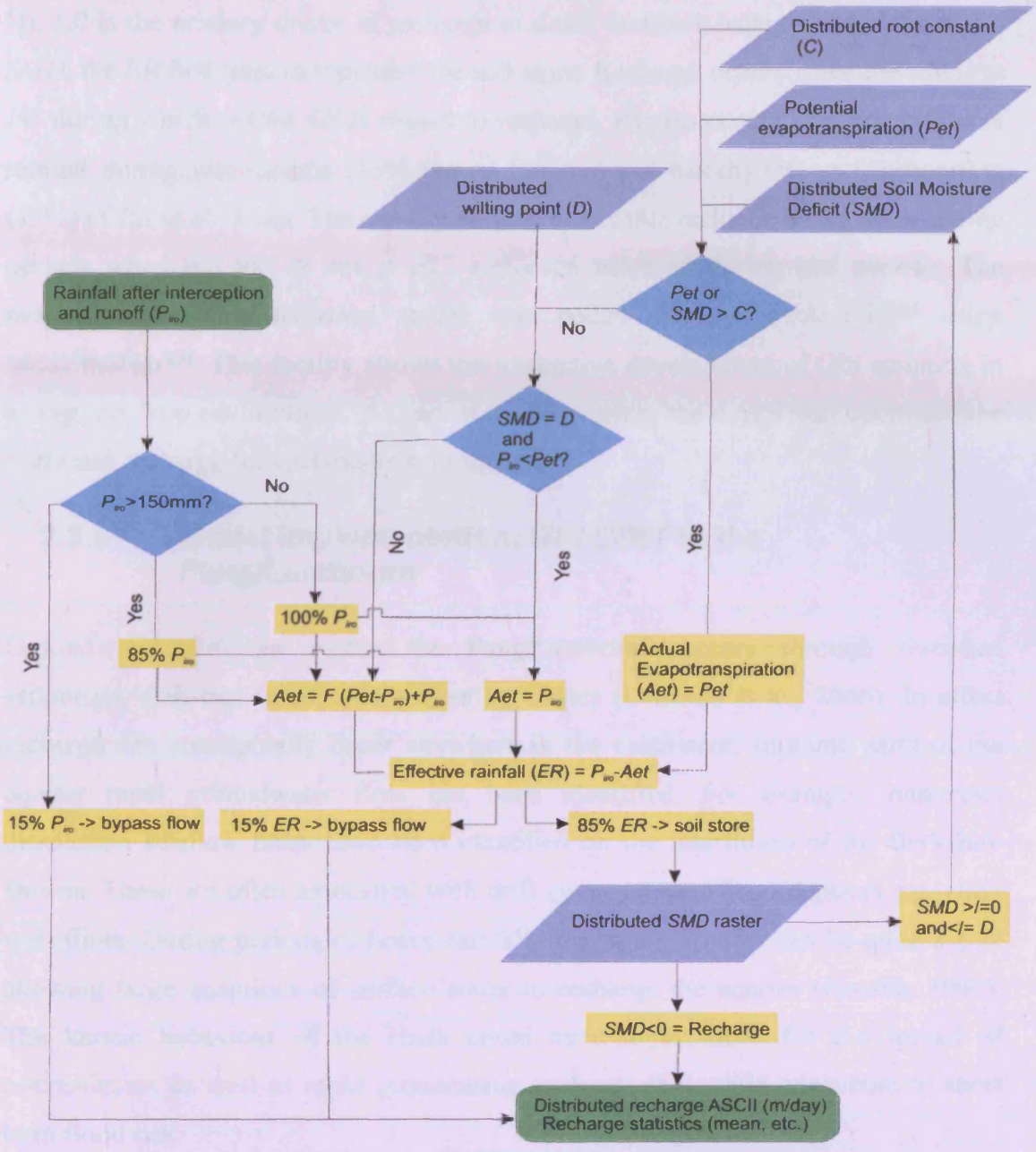

Figure 2.4 Schematic flow diagram representing the key processes of GIS-DIRT after interception and runoff has been calculated and taken away from the precipitation input.

The inputs, processes and output of the model are summarised in Figure 2.4 and can be run for monthly, daily or weekly time steps. A simulation usually begins in April, during which time the soil is assumed to be at *FC* (Younger, 2007). Precipitation after interception and runoff (P_{iro}) and MORECs *Pet* provided the key inputs. The output at each time step provides distributed values of soil moisture, which become a key input in the subsequent calculation of *Aet* and *SMD*. Excessively high *SMD*s are mediated by *D*. If there is any rainfall left after interception, runoff and evapotranspiration, it is termed effective rainfall (*ER*, [LT

[1]). *ER* is the primary driver of recharge in a soil moisture balance and if there is a *SMD*, the *ER* first goes to replenish the soil store. Recharge occurs when the soil is at *FC* during which period *ER* is routed to recharge. Bypass occurs as a proportion of rainfall during wet months (15% above 150 mm per month) and as a proportion (15%) of *ER* at all times. The consequence of this is that recharge could occur during periods when the soil is not at *FC*, and even more so during wet periods. The evapotranspiration calculation model was coded directly in ArcGIS™ using Modelbuilder™. This facility allows the interactive development of GIS scripting in a drag and drop environment. As part of the processing, the model also calculated the *SMD* and recharge for each raster grid square.

2.3.5 Model implementation: GIS-DIRT in the Pang/Lambourn

Groundwater recharge within the Pang/Lambourn occurs through river-bed sediments, drift-free interfluves and valley slopes (Griffiths et al., 2006). In effect recharge can conceptually occur anywhere in the catchment. In some parts of the aquifer rapid groundwater flow has been identified. For example, numerous dissolution swallow holes have been identified on the interfluves of the Berkshire Downs. These are often associated with drift cover or superficial deposits e.g. clay-with-flints. During periods of heavy rainfall, the swallow holes can be quite active allowing large quantities of surface water to recharge the aquifer (Goudie, 1990). The karstic behaviour of the chalk could have implications for the spread of contaminants as well as rapid groundwater recharge that could contribute to short term flood risk.

The characteristics and components of recharge in the Pang Lambourn are summarised in Figure 2.5A and how they translate into the GIS-DIRT distributed soil moisture balance model is shown in Figure 2.5B. In GIS-DIRT these processes may be simplified or grouped together, particularly whilst using a coarse model grid. For example, runoff and interflow are treated as one in the identification of surface runoff. In addition, leaf drip and steam flow are represented by a single interception parameter and runoff recharge is not distinguished from direct recharge. Rapid flow through karstic features is accommodated by a bypass flow component. An important characteristic of GIS-DIRT is that recharge can occur anywhere in the domain and makes no assumption about recharge free zones.

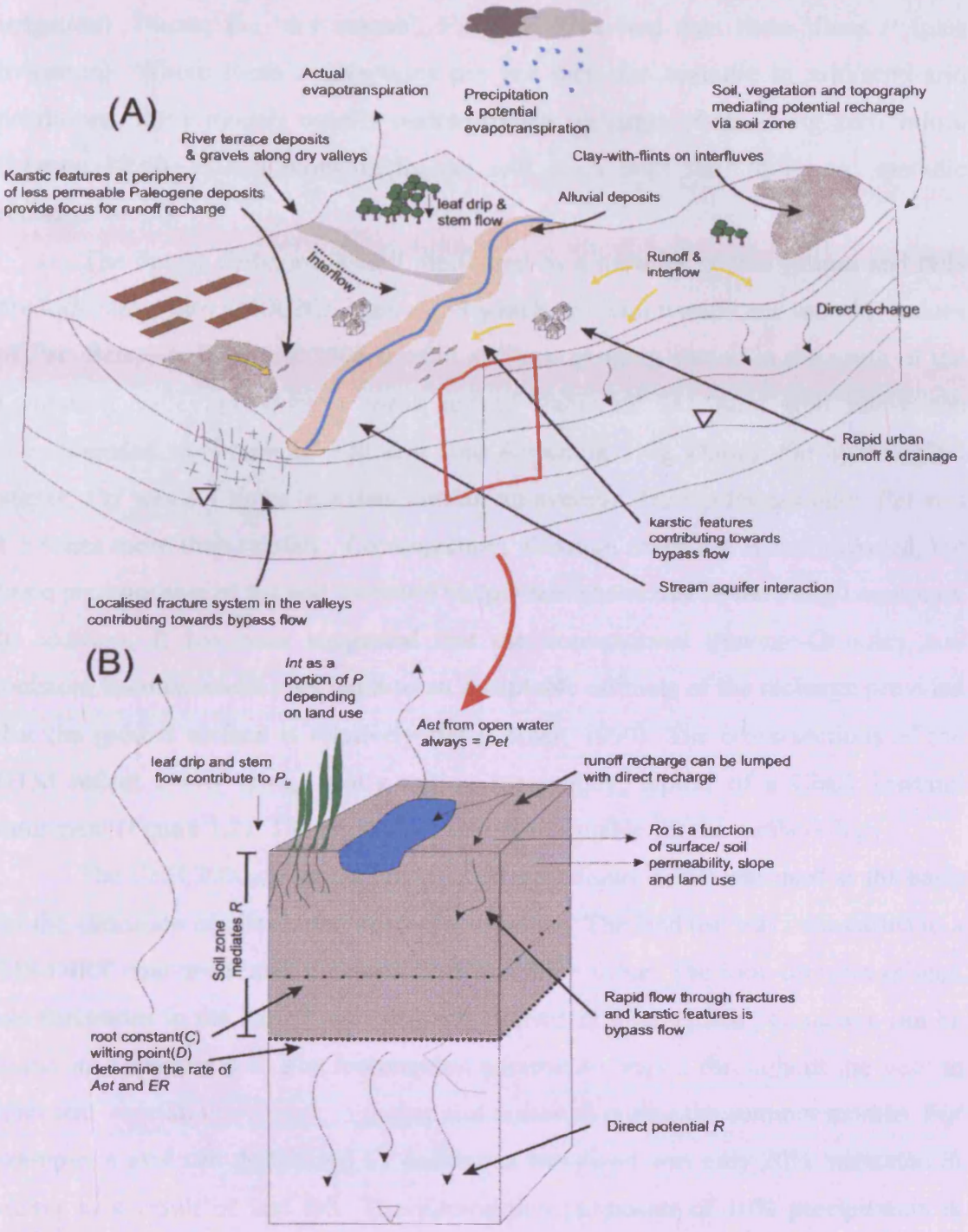

Figure 2.5 Characteristics and components of recharge across a typical section of the Pang or Lambourn (A) and the associated major conceptual components of GIS-DIRT (B).

Soil moisture balance models such as GIS-DIRT were originally developed for humid/temperate climates such as the UK, and work best for seasonal patterns of recharge. The following heuristic determines whether soil moisture budgeting is applicable to a given area; over the whole year, precipitation (plus irrigation) should be above 500mm. During the 'wet season', *Pet* should be less than 1.5 times *P* (plus

irrigation). During the 'dry season', *Pet* should be less than three times *P* (plus irrigation). Where these assumptions are not met, for example in arid/semi-arid conditions, these models usually underestimate recharge, often giving zero values (Lerner, 1990). A soil moisture budget will often miss short duration, sporadic recharge events.

The Pang/Lambourn is well monitored by a network of rain gauges and falls predominantly into MORECS square 159 which provides weekly and monthly values of *Pet*. Between 1978 and 2006 rainfall at Shaw gauging station in the south of the Lambourn valley provides a mean annual value of 741 mm, well above the recommended minimum of 500 mm (see Appendix 1.6). During the hydrological winter, *Pet* was 3.1 times less than rainfall on average. During the summer, *Pet* was 1.5 times more than rainfall. Consequently, although irrigation is not included, the basic prerequisites of the soil moisture budget have been met in the Pang/Lambourn. In addition, It has been suggested that the conventional Penman-Grindley soil moisture balance model only leads to an acceptable estimate of the recharge provided that the ground surface is relatively flat (Lerner, 1990). The cross sections of the DTM reflect a low lying, gently rolling topography, typical of a Chalk lowland catchment (Figure 1.2). The region was therefore suitable for the methodology.

The CEH 2000 dominant land use dataset (Figure 1.2D) was used as the basis for the allocation of distributed interception values. The land use was reclassified to a GIS-DIRT equivalent and allocated an interception value. The look-up table of land use categories in the Pang/Lambourn and equivalent interception parameters can be found in Appendix 1.7. The interception parameters varied throughout the year to represent vegetation die back in winter and regrowth during the summer months. For example, a grid cell dominated by deciduous woodland was only 20% vegetated in winter as a result of leaf fall. The interception parameter of 10% precipitation is reduced accordingly to 2% (i.e. a reduction of 80%). Interception parameters as a function of the proportion vegetation cover for each land use category in the Pang/Lambourn can also be found in Appendix 1.7. The percentages were converted to a fraction of 1, so that when a value of rainfall is multiplied by the resulting raster, the remaining value became P_{in}. Figure 2.6 shows the final distributed interception parameters for the Pang/Lambourn during winter and summer. In winter, the value catchment wide tends towards 1 as a result of vegetation die back and harvesting

operations. Perennial grassland and coniferous woodland tend to maintain a larger interception proportion into winter.

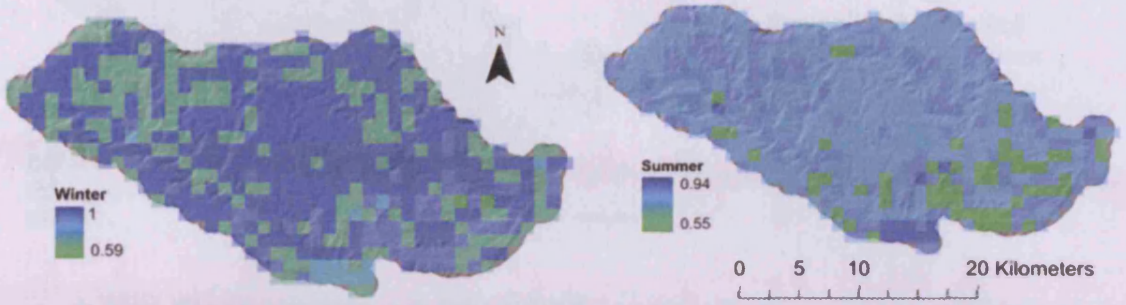

Figure 2.6 Distributed winter and summer interception parameters based on the CEH 2000 dominant land use dataset [% rainfall not intercepted].

Runoff parameters were assigned based on HRU IDs in which a 10 m resolution DTM (Figure 1.2) provided the basis for the slope. Appendix 1.8 shows a schematic of how the DTM was converted into 1 km slope classifications. In addition, the digitised national soil data map was clipped to the study site and converted to a raster grid (1 km resolution). In the resampling process, values were taken from the spatial median of the cell. Appendix 1.9 illustrates the process of conversion from digitised soil map (Figure 1.2C) to distributed soil texture raster. The coefficients represented the proportion of P_{in} that doesn't runoff in the vegetated, bare, open water and impervious portion of the cells, for both summer and winter season (Figure 2.7). A coefficient of 0.98 for example means that only 2% of P_{in} will runoff.

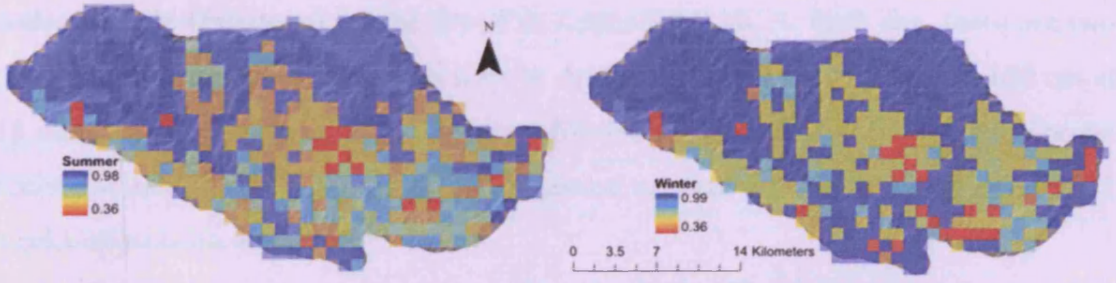

Figure 2.7 Summer and winter distributed run-off parameters. Values represent the proportion of rainfall that does not runoff [%]

Finally, the other major parameters used as input into the model (Figure 2.4) are C and D. These values are assigned based on the original land use raster (Figure 1.2) and Penman-Grindley lookup table (Hiscock, 2005; Lerner, 1990). An example of the resulting distributed C datasets for the month of April can be seen in Figure 2.8. Eleven other monthly distributed C raster datasets were compiled and twelve corresponding D datasets.

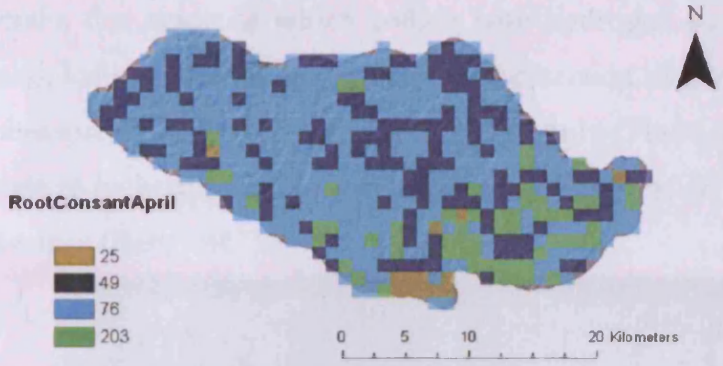

Figure 2.8 Distributed root constant (*C*) values for April [mm].

2.3.6 Field testing of GIS-DIRT

Neutron probe and soil moisture profile probe data was used to reconstruct past mean monthly (and daily) *SMDs* at six existing LOCAR monitoring sites representing different land use, soil type and topographic settings across the Pang/Lambourn. These were then compared with *SMD* output from the corresponding grid square of the model. The observed *SMD*s could then be used to calibrate and test the model at the local scale. The location of these soil moisture data collection sites in relation to the model grid can be seen in Figure 2.9, in addition to a summary table of local characteristics. For example, Warren Farm on the Upper Chalk is situated on silty clay 'Carstens' soil overlain by grassland. Grimsby Wood on the other hand, as the name suggests, is characterised by deciduous woodland and a more clay rich soil, possibly due to the location above the London Clay formation. The distribution of profile probes and neutron probe access points at a typical soil moisture data collection site (Frilsham) can be found in Appendix 1.10. At each site, there are two profile probes monitoring soil moisture at depths of 10, 20, 30, 40, 60 and 100 cm at 15 minute intervals. In addition to the profile probes, there are up to 4 neutron probe access points, where readings of soil moisture content are taken manually every 2 weeks up to circa 4 m depth.

When power is applied to a soil moisture profile probe, it generates a 100 MHz electromagnetic signal about 100 mm into the soil. The water content of the soil surrounding the probe dominates its permittivity – a measure of a material's response to polarisation in an electromagnetic field e.g. water has a permittivity of about 81 compared to soil of 4 and air, 1. The permittivity results in a stable voltage output that acts as a sensitive measure of soil moisture content (Delta-TDevices, 2004). Appendix 1.11 details how the voltage output of the probe was calibrated locally against the water content readings from a neutron probe. A neutron probe

emits fast neutrons which collide with hydrogen nuclei present in the surrounding soil, losing much of their energy. The detection of slow returning neutrons provides a measure of hydrogen and therefore moisture (Finch, 2001). The calibration of count rate to moisture content was using generic calibration curves determined by local soil texture (Bell, 1987).

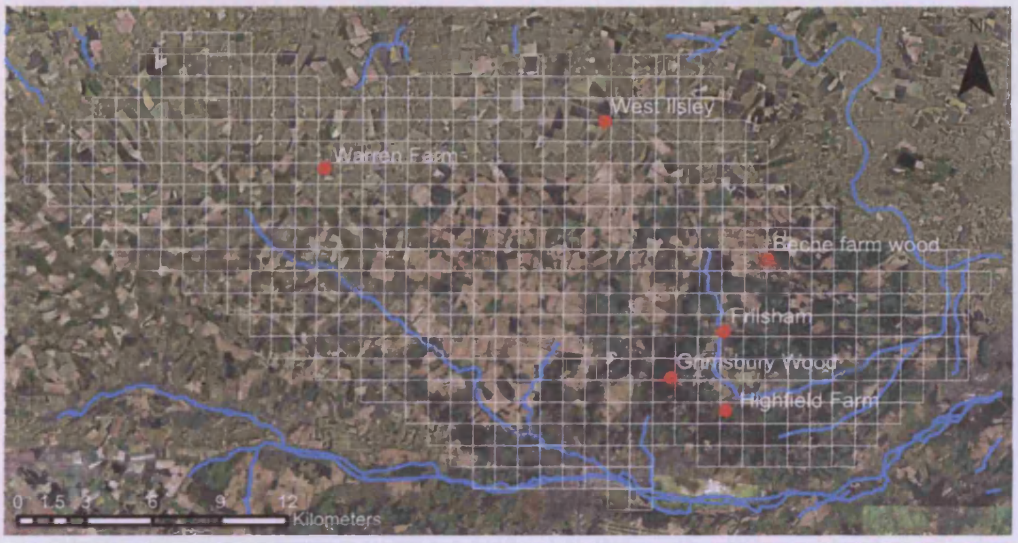

Site	Elevation mAOD	Slope (degrees)	Soil type	Soil texture	Land use	Geology
Warren Farm	63	5-10	Carstens	Silty Clay	Improved grassland	Upper Chalk
West Ilsey	91	5-10	Andover	Silt	Improved grassland	Upper Chalk
Beche Farm Wood	143	0.5-5	Hornbeam	Silty clay loam	Deciduous/ mixed woodland	Upper Chalk/ Clay with flints
Frilsham	102	0.5-5	Frilsham	Silty clay loam	Arable horticulture	Upper Chalk/ river terrace deposits
Grimsbury Wood	108	5-10	Wickham	Sandy clay loam	Deciduous/ mixed woodland	Palaeogene deposits (London Clay)

Figure 2.9 Location of soil moisture data collection sites in the Pang/Lambourn, corresponding model grid cells and site characteristics summary table.

The field values of soil moisture, expressed as a percentage of volume, must first be converted to *SMD*s in order to allow comparison with model output. To do this, the values of the maximum Zero Flux Plane (*ZFP*) and *FC* were estimated (Figure 2.10). The *ZFP* is the depth to which *SMD*s permeate, indicated by a transition from seasonal fluctuations in moisture content to a more consistent pattern. In effect it is the maximum depth to which the root zone or atmospheric conditions permit evapotranspiration flux back to the surface (zero metre depth in riparian areas).

The soil moisture probes or neutron probes were used to determine the moisture content (% volume) in each horizon up to the *ZFP*. *FC* is the maximum soil moisture content of each horizon, up to the *ZFP* (discounting periods immediately after heavy rainfall, at which time the soil may be above *FC*). The *FC* equivalent depth (mm) was calculated by accounting for the depth of each horizon e.g. a 100 mm horizon with a *FC* of 10% moisture is equivalent to 10 mm. For each time step the *SMD* was calculated as the equivalent depth of water below *FC* in mm at each of these horizons. These values were summed to give a *SMD* value for the entire profile for each observation.

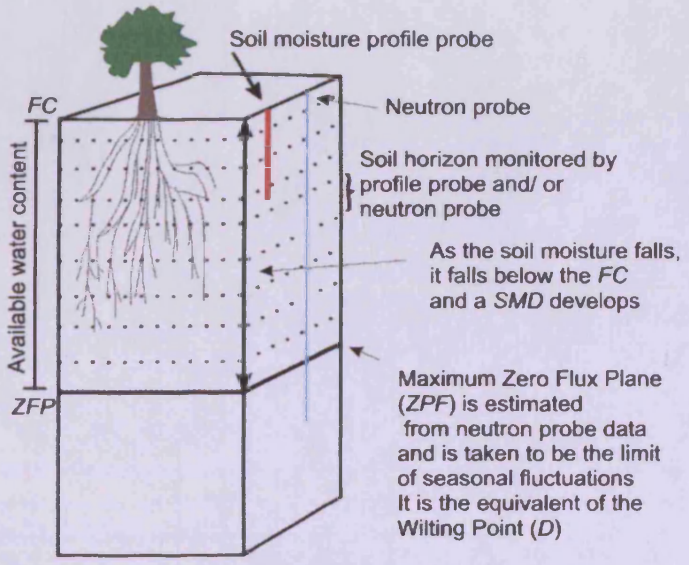

Figure 2.10 Schematic illustrating the key concepts in the conversion of soil moisture field data from neutron or soil moisture probes to *SMD*s

The biweekly neutron probe data were ultimately used to provide monthly *SMD* because the profile probe data used to generate daily *SMD*s is limited to 1 m depth. According to the neutron probe data at Frilsham (Figure 2.11) the horizons between 1 and 2 m exhibit the largest seasonal moisture fluctuations (60% annually). Not taking these horizons into consideration could lead to an underestimation of *FC* and *SMD*. Using neutron probe data ensures data coverage over greater depths however at the expense of temporal resolution. The monthly mean of biweekly *SMD* values were the basis for calibration and validation of the model. Spearman's rank correlations and visual fitting of observed to modelled fluctuation trends provided the basis of comparison.

2.3.7 Temporal sensitivity analysis

It has been suggested that soil moisture budgeting for periods greater than 10 days can lead to errors (Howard and Lloyd, 1979). To test this, a temporal sensitivity analysis was performed by running the recharge model at daily and weekly time steps, in addition to the original monthly. Daily and weekly recharge values were summed to provide monthly values for comparison. Daily values of *Pet* were not available and so weekly MORECS data is used both for daily and weekly calculations. Weekly *Pet* values were equally distributed throughout 7 days for the daily model. For example, a weekly *Pet* value of 55 mm would be represented by 7 consecutive days of 7.9 mm. Daily rainfall data was not available at the Shaw gauging station and so rainfall at Chievely was used for both daily and weekly model runs. Cheively lies circa 6 km north of Shaw (for relative locations see Appendix 1.6). Daily rainfall was aggregated to weekly by summation. The bypass flow limit was also scaled appropriately for the weekly and daily models. The daily rainfall rate over which 15% goes straight to recharge is scaled back from 150 mm to 5 mm (assuming a 30 day month). Likewise, the weekly (7 day) threshold is scaled to 35 mm. Appendix 1.12 summarises the input datasets and times span of the monthly, weekly and daily recharge models. Aside from the input weather data and bypass flow limit, GIS-DIRT remained unchanged.

2.4 Results

2.4.1 Observed Soil Moisture Deficits

Biweekly neutron probe data provided by CEH was the basis for determining field *SMD* for the soil column at each of the field monitoring sites. Figure 2.11 illustrates a sample 2 year period at Frilsham indicating that seasonal fluctuations in soil moisture continued down to a depth between 2 m and 2.3 m. In this case, the maximum *ZPF* is therefore estimated to be 2 m. *FC* for each horizon is determined visually by estimating the maximum mean moisture content. In this example, The *FC* for most horizons is around 20 to 30% moisture content. An exception is the horizon between 180 and 200 cm, where *FC* is as high as 65% moisture. This is likely to correspond to a moisture retaining, perhaps clay rich layer in the soil column.

Appendix 1.13 summarises an attempt at constructing daily *SMD* values from the shallow profile probe (a) data at Frilsham. Because the maximum *ZPF* is below

the profile probe maximum depth, the 100 cm value was assumed to be constant down to 2 m. To illustrate, the *FC* for the horizon 100-200 mm is plotted on the graph as a dashed line. The *FC* of the entire column up to the *ZFP* is a sum of the individual horizon values, in this case 259 mm. Here, a maximum *SMD* of 80 mm occurred during autumn 2003. This is in comparison to a maximum of 130 mm during the same period for monthly values calculated using neutron probe data (Figure 2.12).

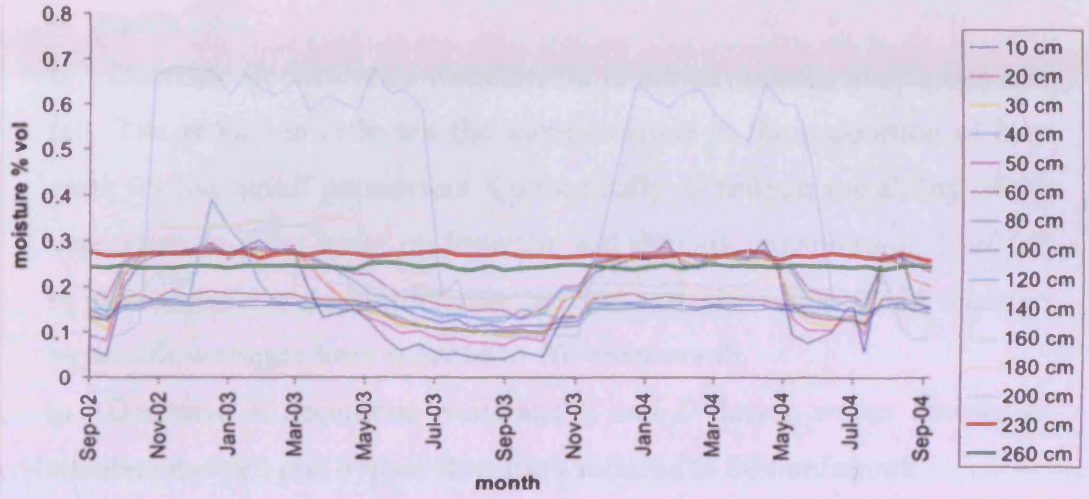

Figure 2.11 Observed soil moisture (% vol) at 10-20 cm intervals up to 2.6 m from calibrated neutron probe '1' at Frilsham between 19/09/02 and 24/09/04. The highlighted profiles at 230 and 260 cm represent the extent of the *ZFP*.

2.4.2 GIS-DIRT calibration against observed *SMD*

The basis of the recharge model calibration is a comparison between modelled *SMD* and observed *SMD*. A systematic series of parameter perturbations were applied to the model in order to improve the 'goodness of fit' and correlation between observed and modelled values. The following summarises the series of changes:

a. Using distributed rainfall instead of a lumped value. Monthly rainfall was interpolated using the Inverse Distance Weighted (IDW) method (Shepard, 1968) across 6 rain gauges (see Appendix 1.6 for gauge locations). In addition, the winter season was extended by 2 months by substituting the April and September *C* and *D* values for March and October values respectively. This was to simulate the relatively early decrease and late arrival of the observed seasonal *SMD* in some areas.

b. Maintained extension of the winter season by 2 months for *C*, *D* (as above). Reverted back to lumped rainfall (at Shaw gauging station).

c. As original parameters plus arable horticulture land use was adjusted to October harvest (rather than a mean of all possible harvest months). Values of *C* and *D* decrease during the harvest month to simulate loss of vegetation.

d. No runoff i.e. following interception, the rainfall went to the soil store or bypass flow.

e. No runoff or interception i.e. all rainfall went straight to the soil store or bypass flow.

f. Decrease in deciduous woodland *C* in winter months to simulate leaf fall. The reduction reflected the same increase in the proportion of bare earth for the runoff parameters. Conceptually, *C* reflects the ability of the vegetation to draw water up from the soil through transpiration. Leaf fall in the winter should restrict this process and so reduce *C*. In addition bypass flow trigger limit reduced to 100 mm/month.

g. Decrease in deciduous woodland C and *D* during winter months to simulate leaf fall and bypass flow limit reduced to 80 mm/month.

h. As **g** but bypass flow limit increased back to 100 mm/month.

The impact changes (**a-h**) had on modelled *SMD* between 2003 and 2005 at the Frilsham and Beche farm monitoring sites are summarised in Figure 2.12. Using distributed rainfall had little impact on the development of seasonal *SMD*s or recharge rates (compare **a** and **b**). Similarly, extending the winter *C* and *D* season did not delay the onset of the *SMD* at either Beche farm or Frilsham comparable with observed values (**a** and **b**). Reducing runoff/interception had the desired effect of delaying the onset and hastening the decrease in *SMD* (see **d** and **e**). This inevitably led to an increase in recharge rates. It was however inappropriate to discount interception and runoff processes altogether. Adjusting *C* and *D* locally to simulate horticultural harvest in October led to an marked improvement in the modelled seasonality of *SMD* development at Frilsham (**c,g** and **h**). A similar improvement was seen at Beche farm where *C* and *D* were modified to simulate woodland leaf fall in the winter season (**g**).

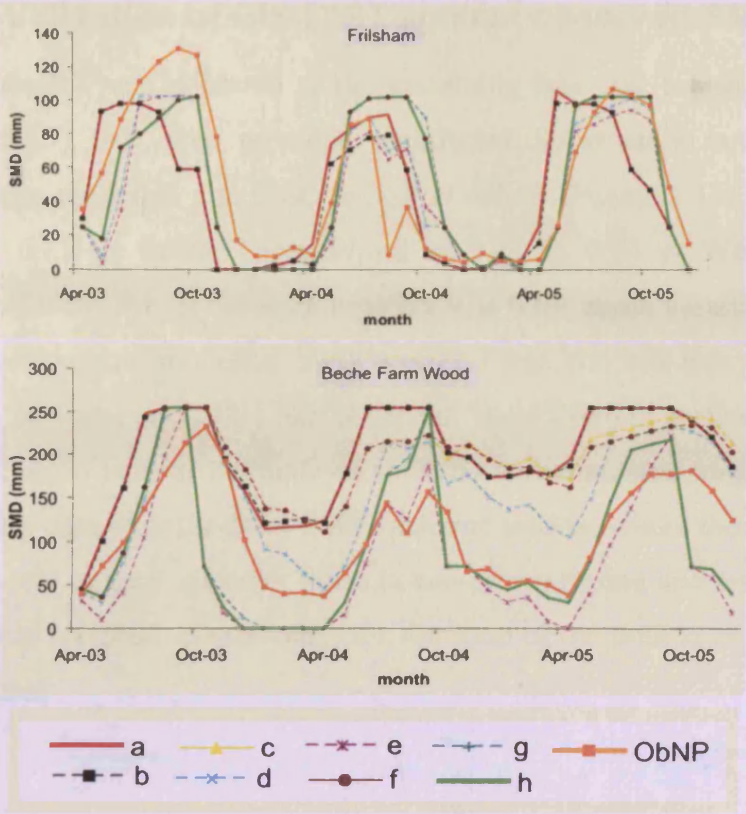

Figure 2.12 Calibration of *SMD* at Beche Farm Wood and Frilsham through the changes a-h in comparison to observed *SMD* calculated from neutron probe data (ObNP).

Reducing the bypass flow limit had little impact on *SMD* development (**g** and **h**). Recharge rates however increased as the limit was reduced (the impact of the changes **a-h** on recharge are shown Appendix 1.14). Reducing the bypass flow limit to 80 mm led to an unrealistically large number proportion of 'wet' months. The frequency of 100 mm rainfall occurring in a month is comparable to 5 mm daily events over the calibration period. In summary, the result of this calibration procedure is that some fundamental changes were made to the parameters of the model:

- Horticultural land use adjusted to October harvest (*C* & *D*).
- Decrease in woodland *C* and *D* in winter months to simulate leaf fall.
- Decrease bypass flow limit to 100 mm/month.

Spearman's rank correlations for observed against the final, calibrated modelled *SMD* (**h**) are 0.67 and 0.72 at Beche farm and Frilsham respectively. Assuming a $p<0.01$, the correlations are significant. These changes were taken into the full 28 year transient model and provide the basis of the validation at other sites. The correlation coefficients for the other calibration conditions (**a-g**) can be found in Appendix 1.14.

2.4.3 Validation of GIS-DIRT against observed *SMD*

The recharge model was validated at the remaining four soil moisture monitoring sites (Figure 2.13). All sites provided significant Spearman's rank correlations ($p<0.01$) between modelled and observed *SMD* values (Figure 2.13). These ranged from between 0.67 at Beche Farm Wood and up to 0.94 at West Ilsley. The correlation coefficient for all the sites together was 0.69, again significant ($p<0.01$). The mean and maximum modelled *SMD* was 72.7 mm and 254 mm respectively in comparison to 74.4 mm and 232.1 mm observed. West Ilsley in particular provided a good match between natural fluctuations in *SMD* and simulated values. There was however missing data over the 2004-2005 recharge season, where the *SMD* could be expected to be low or zero. At other times however, the timing and magnitude of the *SMD* was closely matched. Importantly, the duration of the time at or close to *FC* is well reconstructed.

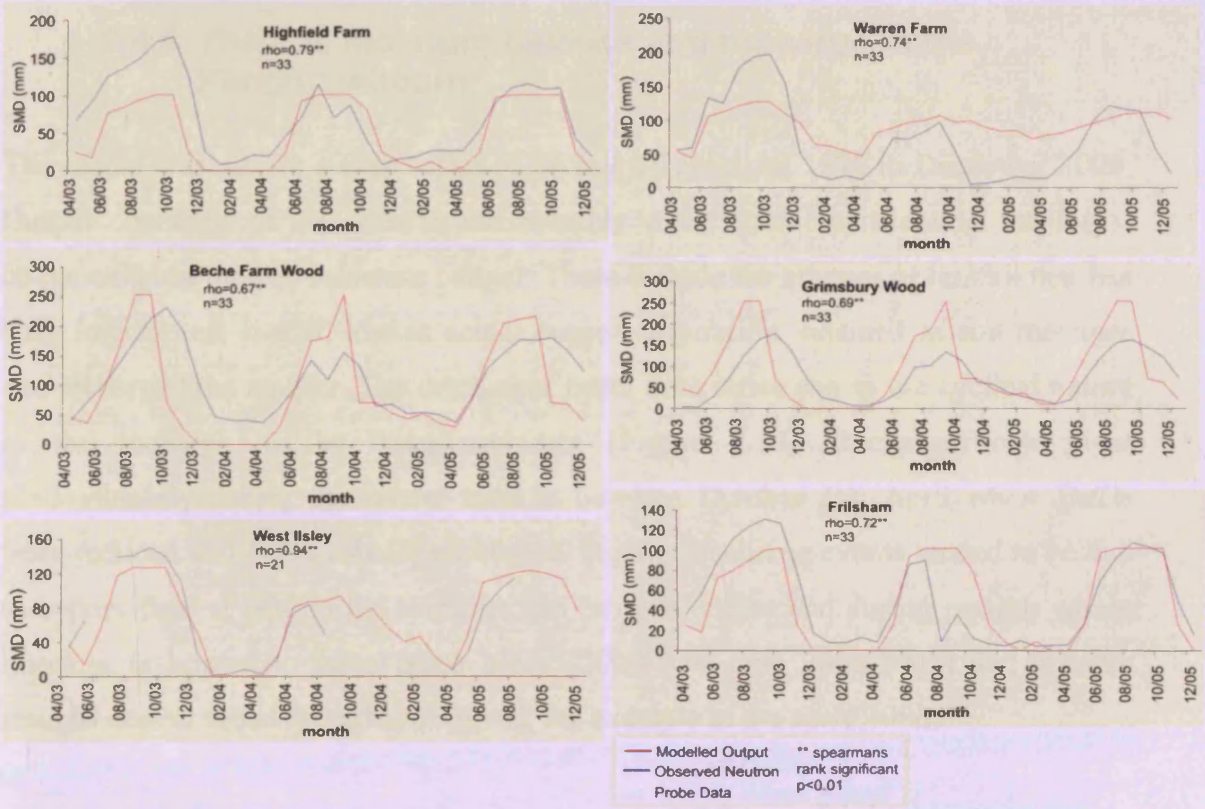

Figure 2.13 Monthly modelled SMD in comparison to observations at all six field sites and Spearman's rank correlation coefficients.

SMD at Warren Farm, which exhibits similar site characteristics to West Ilsley (Figure 2.9), was not modelled as well according to both the correlation coefficient and visual fit. Observed maximum *SMD*s were also considerably higher than at West Ilsley (maximum 200 mm in comparison to 140 mm). The key

difference at the Warren Farm site is a higher clay content in the soil, which could have increased the amount of rainfall running off and prevent *SMD*s from reducing. The impact was that *FC* is not simulated and recharge here would be via bypass flow only. In addition, despite the modifications to the *C* and *D* values of deciduous woodland during model calibration (Figure 2.12), correlation coefficients at Beche Farm Wood and Grimsby Wood were also lower than other sites, albeit significant (Figure 2.13). The modelled values in these cases tended to overestimate the *SMD* during winter. With the exception of the 2004-2005 season, the winter *SMD* reduction was also too early. Observed *FC* was not approached at Beche Farm Wood perhaps due to the deep active rooting system associated with the trees. Any recharge is therefore likely to be via bypass flow. At Grimsbury Wood, *SMD*s tended to be smaller and *FC* approached, suggesting a difference between the two sites in canopy density, rooting depth or density.

2.4.4 The soil moisture balance and recharge in the Pang/Lambourn

The model was run for a time series of 28 years from April 1978 to December 2006. Output consisted of 345 distributed monthly raster grids representing the major components of the soil moisture budget. These include the amount of rainfall that has been intercepted, runoff, lost as actual evapotranspiration, retained as soil moisture and recharged the aquifer. The catchment mean time series shows the cyclical nature of the recharge in the Pang/Lambourn (Figure 2.14). Recharge took place predominantly during the winter months between October and April when *SMD*s were reduced and *FC* is usually simulated. Summer recharge events tended to be due to bypass flow. Peaks in the recharge can be seen before and during periods where flooding is known to have taken place (2000-2001 and 2002-2003) and relative troughs appear when droughts occurred, for example in the early 1990s.

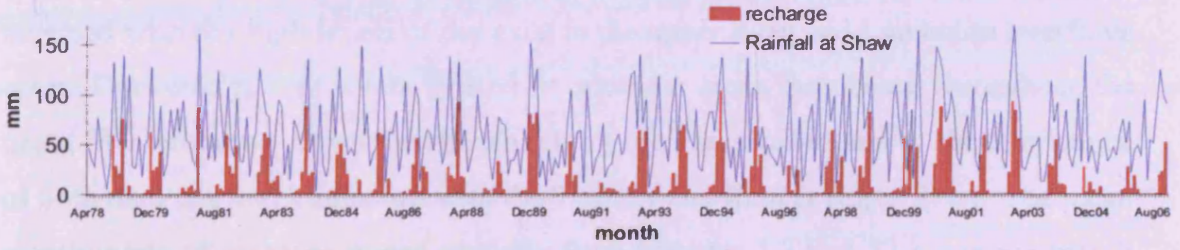

Figure 2.14 Monthly mean modelled recharge across catchment and rainfall between April 1978 and December 2006

Over the 28 year period, the mean monthly rainfall input was 61.7 mm for the entire catchment. Between 3 and 26 mm was lost on average as interception, however the majority of the catchment saw relatively low interception (around 3 mm), with the highest values over woodland, particularly coniferous, which maintains canopy cover during the winter (Figure 2.15A). Mean monthly runoff was between 37.4 mm and negligible (0.2 mm). The upper Pang and Lambourn catchments were characterised by relatively low runoff. The interfluve area between the upper Winterbourne and Pang valleys exhibited particularly high runoff. Built-up areas, characterised by impermeable surfaces also showed relatively high rates of runoff (Figure 2.15B).

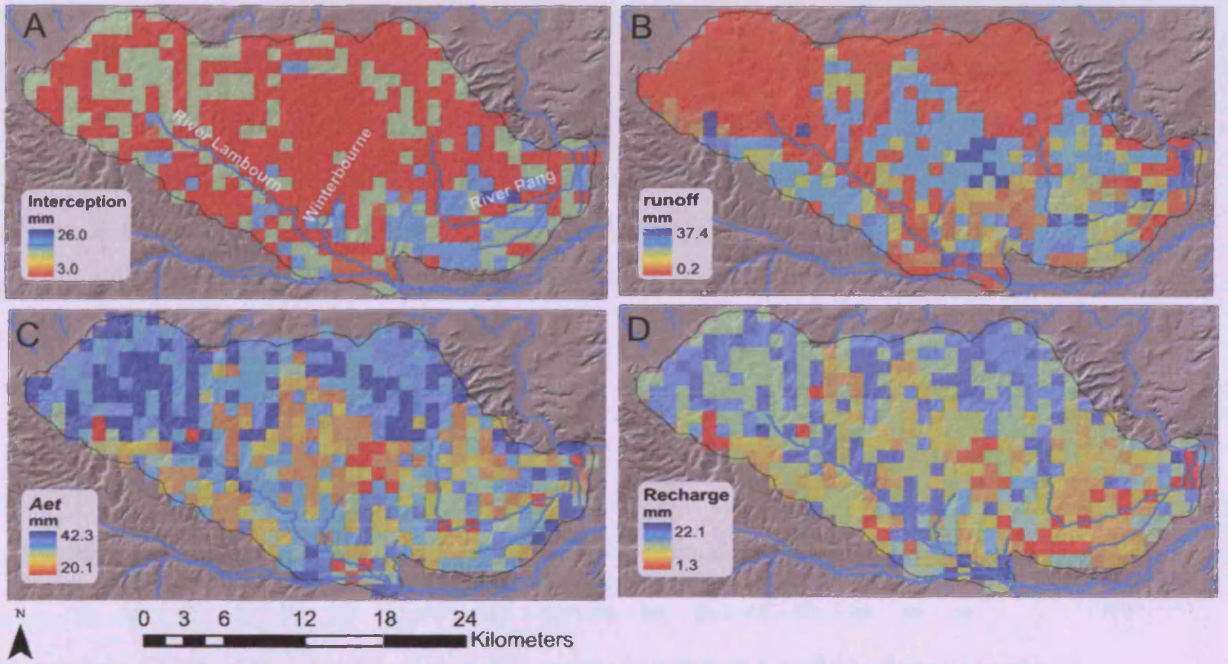

Figure 2.15 Distributed mean monthly interception (A), runoff (B), actual evapotranspiration (C) and recharge (D) from between April 1978 and December 2006.

The rates of *Aet* were more spatially variable than interception and runoff, ranging from between 20.1 and 42.3 mm per month (Figure 2.15C) and represent the largest proportion of the water balance (Figure 2.17D). Here, the runoff trend was reversed whereby high levels of *Aet* exist in the upper Pang and Lambourn interfluve areas. Conversely, low levels existed in sporadic areas distributed throughout the upper Winterbourne, upper Lambourn, along the Pang valley and at the confluence of both the Pang and Lambourn with the Thames and Kennet respectively. The mean monthly rate of recharge varied spatially from between 1.3 and 22.1 mm per month (15.6 and 265.2 mm/yr). The recharge values include both flux from the soil store and the bypass flow component (Figure 2.15D). Interestingly, areas of low *Aet* seem

to correspond to zones of low recharge. In addition, the areas to the south of the Pang valley also experienced very little recharge. The dominant recharge areas were the upper Lambourn and Pang interfluves and along the Lambourn and upper Pang valley. Over the 28 year period, net ΔSMD was negligible, indicating that the flux into the soil store equalled the flux out. High mean *SMDs* were an indication of a large C and D characteristic of wooded areas (see Appendix 1.16 for details). Here bypass flow was the primary recharge mechanism.

2.4.5 Temporal sensitivity analysis

A temporal sensitivity analysis was carried out to assess the impact of using daily, weekly or monthly calculations on mean monthly recharge across the catchment between April 1999 and March 2005 (Figure 2.16). Mean monthly recharge was 15.5, 15.7 and 19.2 mm for monthly, weekly and daily time steps respectively. During the winter months mean recharge was 29, 29.2 and 31.6 mm per month reducing to 1.9, 3.2 and 6.8 mm during the summer for monthly, weekly and daily time steps respectively.

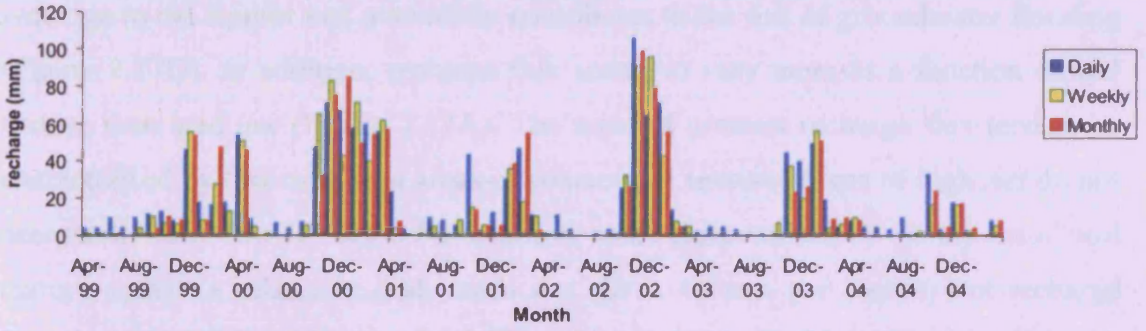

Figure 2.16 Comparison between using daily, weekly or monthly weather values on mean monthly recharge across the Pang/Lambourn from April 1999 until March 2005.

During this period, mean recharge was 3.7 mm less when calculated on a monthly basis compared to summed daily values, reducing to 0.2 mm for weekly accounting. This represents a 19% underestimation for monthly calculations in comparison to daily procedures. This variation was less during the winter months where mean modelled values are 2.6 mm less when calculated on a monthly basis in comparison to daily calculations, equivalent to an 8% reduction. This was reduced to 0.7% during the winter. The greatest difference lies in the summer months where there was a 72% reduction in recharge between daily and monthly accounting. This however only represents 4.9 mm of flux. Indeed, the majority of recharge took place

in the winter months, so the relative impact of this error on modelled groundwater levels and therefore flood risk assessment may be relatively small.

2.5 Discussion

The output from the recharge model has been successfully tested against local soil moisture field observations. In addition, the time step of the model was altered systematically to see if monthly recharge calculations were appropriate and provided an acceptable level of accuracy. The results provide an interesting opportunity to interpret the soil water balance of the Pang/Lambourn and provide the basis for groundwater flood risk assessment under scenarios of land use and climate change.

2.5.1 Soil moisture balance and the recharge regime in the Pang/Lambourn

GIS-DIRT output suggests that *Aet* and interception combined make up the majority of the water balance budget for the Pang/Lambourn and represent the proportion of rainfall returned back to the atmosphere. About one fifth of the rainfall ends up as recharge to the aquifer and potentially contributes to the risk of groundwater flooding (Figure 2.17D). In addition, recharge flux seems to vary more as a function of soil texture than land use (Figure 2.17A). The areas of greatest recharge flux tend to be characterised by low runoff on areas of coarser soil texture. Areas of high *Aet* do not necessarily have low recharge. For example areas characterised by 'sandy loam' soil texture exhibit a relatively high mean *Aet* (circa 40 mm per month) but recharge remains high (20 mm) because of the low runoff. Generally high clay content in the soil tends to lead to less recharge, as these less permeable soils encourage a greater proportion of rainfall to runoff.

Land use does not produce the systematic changes seen with soil texture (Figure 2.17C). Coniferous woodland does however seem to limit the volume of recharge substantially. This is predominantly due to perennially high interception rates accompanied by large values for the C and D. The result is a limited proportion of rainfall reaching the ground surface even during the winter months, and large *SMD*s developing that are reduced usually at a rate not limited by C. Conversely, recharge in suburban/rural developments tends to be above average. This is due to a large proportion of these areas not being vegetated, which limits interception and provides smaller values for C and D. This compensates for the relatively high

proportion of runoff over impermeable surfaces associated with such areas. Slope angle has a limited influence on the amount of recharge (Figure 2.17B), although there is a slight tendency for a counter intuitive increase in recharge on steeper terrain, where run off is reduced. The sample size here is relatively small (16 km^2) however.

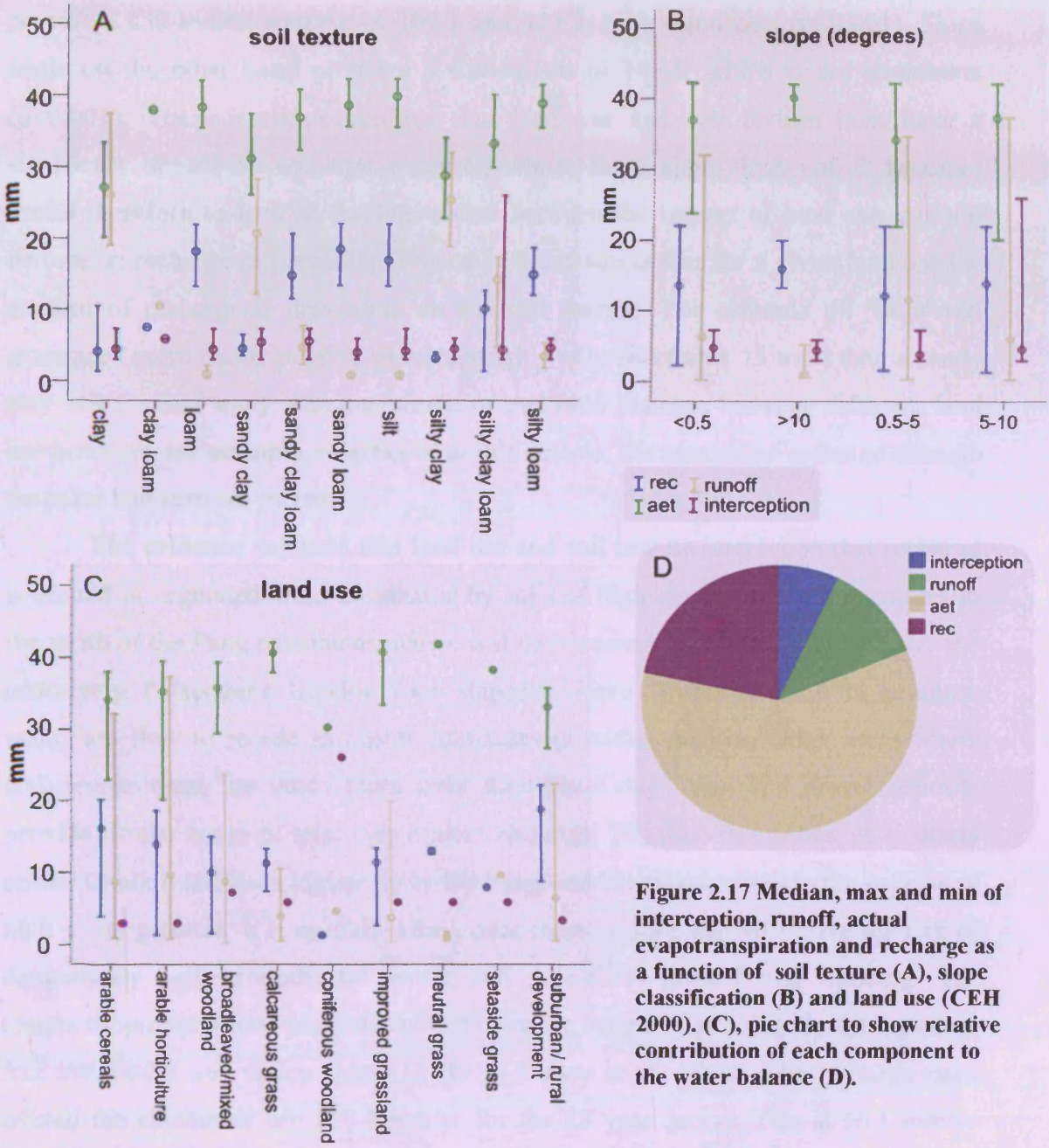

Figure 2.17 Median, max and min of interception, runoff, actual evapotranspiration and recharge as a function of soil texture (A), slope classification (B) and land use (CEH 2000). (C), pie chart to show relative contribution of each component to the water balance (D).

The relative impact of different catchment characteristics on recharge were confirmed using the Kruskal-Wallis test (Kruskal and Wallis, 1952). It was used to assess the difference between recharge associated with different soil texture, slope and land use. The Kruskal-Wallis test is a non-parametric analog of one-way analysis

of variance (ANOVA). In this case normality of the samples can not be assumed, especially given the small sample size. The result is chi-square value and associated significance value. By using this significance value we can accept of reject the null hypothesis. In this case, the null hypothesis is that soil texture, land use type and slope do not have an impact on mean recharge values. Land use and soil texture provide a Chi-square statistic of 109.8 and 413.3, both significant ($p<0.001$). Slope angle on the other hand provides a Chi-square of 14.65, which is not significant ($p<0.001$). These statistics confirm that land use and soil texture both have a significant impact on recharge volumes, whilst slope angle does not. It becomes useful therefore to look at the interaction between the impact of land use and soil texture on recharge in particular (Figure 2.18). It seems that for a given land use the amount of recharge is dependent on the soil texture. For example on 'improved grassland' more recharge takes place through a silty soil (circa 15 mm) than a sandy clay soil (circa 5 mm). The magnitude of this ratio changes between different land use however, for example, in areas of arable cereals, the amount of recharge through the same soil textures increases.

The evidence suggests that land use and soil texture interact so that recharge is limited in vegetated areas dominated by soils of high clay content. This applies to the south of the Pang catchment, where soil development has been influenced by the underlying Palaeogene London Clay deposits. Here, *SMD*s develop in summer, which are slow to recede as runoff dominates in winter months. Other areas where soil development has taken place over superficial clay, sand and gravel deposits provide similar zones of relatively limited recharge. The drift free zones, particularly on the Chalk interfluves higher up in the Pang and Lambourn provide the regions of high recharge rates. It is rainfall falling over these regions that will drive the risk of dangerously high groundwater levels, and potentially groundwater flooding. The results support previous suggestions that recharge occurs predominantly through drift free interfluves and valley sides (Griffiths, Binley et al., 2006). The recharge rates overall the catchment are 160.8 mm/yr for the 28 year period. This is 56.1 mm/yr greater than the estimate provided by Finch (2001) for the Pang catchment between 1972 and 1997 using land use data from 1990. The two figures are comparable given that recharge tends to be greater in the Lambourn.

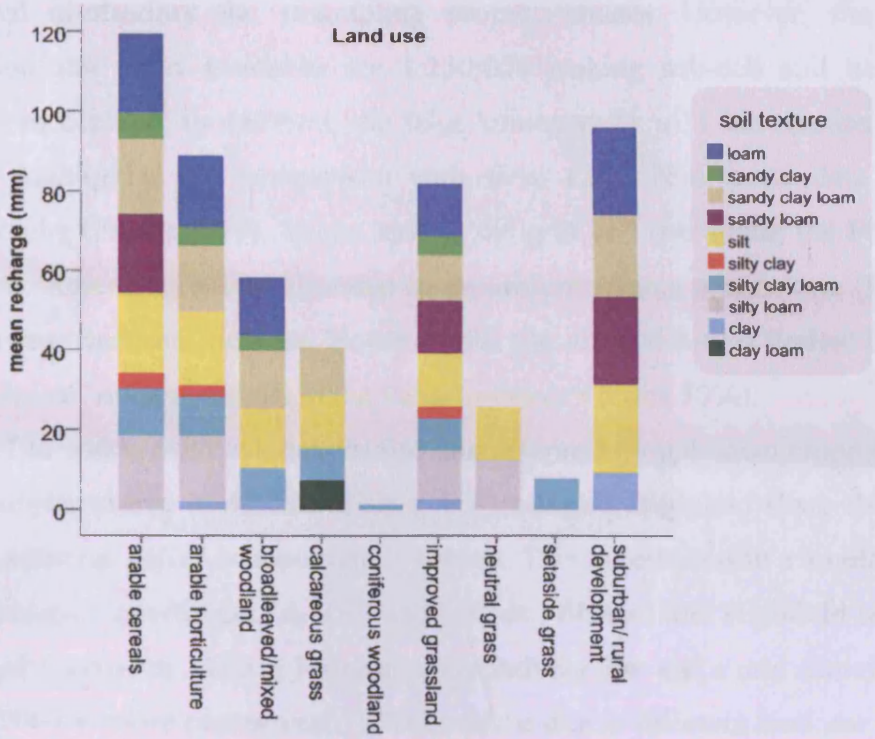

Figure 2.18 Stacked histogram showing mean recharge rate (mm) as a function of land use and soil texture.

2.5.2 Performance of GIS-DIRT

The observation that slope angle does not influence recharge significantly in the Pang/Lambourn is counter intuitive and in conflict with previous recharge studies (Finch, 2001; Lerner, 1990) and runoff parameterisation (Batelaan and De Smedt, 2007) i.e. coefficients on steeper slopes partition a greater proportion of precipitation to runoff. There are three likely explanations for this discrepancy; firstly, the terrain in the Pang/Lambourn is relatively homogenous and therefore there are limited differences in topography influenced runoff catchment-wide. In this case, land use and soil type play a more dominant role. Secondly, the influence of topography is not sufficiently represented in the parameters i.e. there should be a greater difference in the runoff partition between slope angles. Thirdly, it could be due to the resampling of the DTM to a 1 km gird and reclassification into only four slope categorises. These procedures may have introduced homogeneity to local topography, perhaps masking the impact of local steep areas on runoff in particular (see Appendix 1.8).

The same introduction of homogeneity also applies for soil and land use data. For example, two soil associations are lost in the resampling process, Block and Harwell (see Appendix 1.4 for details). Although they only make up a small proportion of total soil cover in the catchment, it illustrates the loss of precision and

increased uncertainty the resampling process creates. However, the maximum resolution soil maps available are 1:250,000 making sub-cell soil heterogeneity difficult to achieve. In addition, the false homogeneity of 1 km dominant land use data is highlighted by comparison with 1990 CEH 25m raster data and aerial photography (Figure 2.19). In the model, the grid cell containing the Frilsham soil moisture monitoring site is assumed to be uniform arable horticulture (Figure 2.9), which is an oversimplification. However, the use of 1990 data is limited by the large proportion of 'nodata' values in the Pang/Lambourn (circa 30%).

The coarse land use data is also characterised by unknown cropping regimes. For example, arable horticultural sites, Frilsham and Highfield share the same soil texture although differ in topographic setting. This is reflected in a similar model fit and correlation coefficient i.e. 0.72 and 0.79 at Frilsham and Highfield respectively. Observed maximum *SMD* at Frilsham are relatively low and a mid summer decrease during 2004 is more pronounced. This could be due to different land use locally and crop harvest schedules between the two sites. This highlights the potential difficulty of lumping horticultural land use into a single category. The summer dip at Frilsham is not simulated well in the model and could be due to the local harvest regime. The lack of fit however could be in part attributable to making comparisons between 1 km grid cells and point observations of *SMD*.

land use	*%*
grass heath	0.2
mown/ grazed turf	7.5
meadow/ verge/ semi-natural	26.8
rough/ marsh grass	0.3
bracken	0.1
deciduous woodland	10.2
coniferous woodland	1.5
tilled land	43.0
suburban/ rural development	9.1
continuous urban	0.4
inland bare ground	1.0

Figure 2.19 Areal photograph and land use from 25 m 1990 land use data for the grid cell representing Frilsham (There is a slightly different classification for land use in 1990 in comparison to 2000).

The difference between observed and modelled *SMD* could also be the result of adopting a single layered soil moisture store. The minimum observed *SMD* according to the neutron probe data is 2.2 mm indicating all sites are never actually

at *FC* when recordings were taken. It is likely that at least some horizons included in the calculation of the *SMD* up to the *ZFP* were not at *FC* simultaneously. It is therefore possible that the field *SMD* observations are not comparable directly to modelled *SMD*. Multi-layered soil models could model a profiled *SMD* more effectively (Dripps and Bradbury, 2007; Lerner, 1990; Rushton et al., 2006). In addition it might be useful to incorporate soil texture into the parameterisation of *C* and *D* (or equivalent parameters). At present soil texture does not directly influence *Aet* in GIS-DIRT. In other soil moisture models, soil texture plays a role in mediating *Aet* (Finch, 2001; Rushton, 2003). This could be another reason for the disparity between observed and modelled soil moisture.

The differences between observed and modeled *SMD* could also be due to the use of monthly time steps.The coarse temporal resolution leads to an underestimation of recharge in comparison to daily input. It could be that a bypass flow limit of 5 mm for daily calculations leads to a greater amount of bypass flow recharge, particularly during the summer when *SMD*s are usually developed and the soil is not at *FC*. Indeed, although the temporal sensitivity analysis suggests that making lumped monthly calculations underestimates recharge, these tend to be small except during the summer months. Groundwater flooding risk is a function of long term fluctuations in regional groundwater system as well as short term local changes that can be more rapid. The focus of GIS-DIRT is to provide a method which combines optimal temporal and spatial resolution for the task. This sensitivity analysis is therefore repeated when interfacing with a saturated flow model. If the impact on modelled groundwater heads is negligible, then the use of monthly models is plausible (see Chapter 5). Indeed, because the time scale of climate change scenarios are currently 30-100 years duration, coarse scale monthly models are the pragmatic alternative to daily or sub daily modelling techniques. If necessary the recharge values could be scaled up by the factor of underestimation. For example, summer recharge could be scaled by 72% and winter by 8%. Short term localised flood events would require very high resolution modelling techniques, in which the level of uncertainty would rise greatly, especially under scenarios of climate and land use change. The focus here is on longer term trends, so monthly calculations become more feasible. Daily or sub-daily calculations at a fine spatial resolution would be beneficial for example on a local study of the impact of a commercial abstraction on

a sensitive wetland zone. When assessing the impact of climate and land use change on the risk of groundwater flooding, the priorities change.

A further possible contribution to the difference between observed and modelled *SMD* is that rainfall is assumed to be equally distributed over the catchment. This is because climate change weather time series provided by stochastic downscaling is limited to lumped values at the catchment scale (see Chapter 5 for details). Because interfacing GIS-DIRT with such models is one of the purposes of the study, lumped rainfall values are initially used to provide consistency throughout the study. Indeed, the impact of using distributed rainfall as an alternative is assessed in section 2.4.2. Although distributed rainfall did not affect *SMD* development significantly, it could be that recharge volumes when the soil was at *FC* or bypass flow could be impacted upon.

Although the mechanisms of recharge are complex and varied, coarse scale estimations of potential recharge are useful and indeed provide the basis of more complex models. One of the main purposes of the recharge model is to compare the impact of change in the system, so to a certain extent, highly detailed recharge calculations are not so important (Bradford et al., 2002). If the model remains consistent through each scenario of change to be examined, what is important is the relative differences in the recharge regime, rather than the absolute value. Pragmatism and parsimony become increasingly important considerations when dealing with such a complex system.

2.5.3 Further work

- Similarly to the temporal sensitivity analysis, a future study might consider the impact of utilising a higher spatial resolution on recharge estimation.
- In order to improve model fit, the soil column should be split up into multiple horizons to represent a likely change in *FC* with depth. In addition, *SMD* estimation from field observations will have to take into consideration these multiple soil horizons.
- Higher resolution and deeper *SMD* monitoring is required to ensure periods of *FC* are recorded.
- Later versions of the model would include a facility to route the runoff over the DTM to account for overland flow and ultimately runoff recharge.

2.6 Conclusions

This chapter examines the fundamental structure of GIS-DIRT, which provides monthly calculations of distributed catchment-wide potential recharge. The implementation of the procedure directly in GIS facilitates interactive land use and climate change scenarios development, which becomes important later for future groundwater flood risk assessment. The Pang/Lambourn catchment in West Berkshire has been used as a case study in order to test the model against field measurements of soil moisture flux.

The modelled recharge rates across the catchment are 160.8 mm/yr between 1978 and 2006. Results have highlighted the importance of soil texture on the potential for recharge. The drift free zones, particularly on the Chalk interfluves higher up in the Pang and Lambourn provide more permeable soils and therefore dominate as regions of high recharge. Certain land use practices also have an important impact on the likelihood of recharge taking place too. Coniferous woodland in particular acts as a perennial barrier to rainfall reaching the surface and subsurface. Information such as this could be extremely useful in providing ways of managing the risk of groundwater flooding, perhaps by strategically managing the land in areas where the impact would be greatest. By combining the recharge model with a groundwater flow model, it would be possible to target recharge zones that provide the majority input to groundwater flooding affecting specific communities in the catchment.

Whilst distributed recharge calculations at 1 km scale is computationally efficient, introducing spatial homogeneity could be a problem. Limitations stem from modelling a continuous, locally specific process using coarse spatial and temporal resolution. A significant issue with calibrating and validating the recharge model has been the disparity between grid size (1 km) and point soil moisture measurements, which themselves are fairly sparse throughout the catchment. The discrepancies between modelled and observed *SMD* are therefore likely to be a function of the spatially coarse soil and land use data and paucity of local cropping data and comparing point with coarse grid. The model is useful however for modelling the relative impact of climate and land use change on the system.

Chapter 3 Cross-correlation analysis to assess recharge pathways in the vadose zone

3.1 Introduction

The combination of low hydraulic gradients and topography can lead to a deep unsaturated zone in Chalk catchments. For example the maximum vadose zone thickness in the Pang/Lambourn is around 143 m. Potential recharge from the soil zone (see Chapter 2) inevitably becomes attenuated as it passes through this zone. This chapter details a statistical technique to determine the time taken for rainfall to propagate from the surface to the groundwater table. This information is used to infer properties of the unsaturated (vadose) zone, providing an extension of the near surface GIS-DIRT model of potential recharge. The time taken for rainfall to perturb borehole hydrographs at seven sites in the Pang/Lambourn is used as a proxy for likely recharge pathways, for example via the pore matrix or fractures of the Chalk. The rate of the water table response to rainfall is particularly important for groundwater flood risk modelling as it will determine the likelihood, magnitude and duration of a flood (Pinault et al., 2005). In addition, the response timing can be considered when interfacing estimates of potential recharge with a saturated groundwater flow model. For example, it is useful to determine the appropriate model time step flux should be passed from the near surface soil store to the permanent groundwater table.

3.1.1 Recharge pathways though the vadose zone in Chalk

The porosity of Chalk is a function both of the intergranular pore matrix and fractures (Allen et al., 2007). The relevant contribution of fracture and matric flow to recharge through the vadose zone has been analysed using geochemical tracer, physical and statistical techniques. Chalk has a matric porosity of 25-40% but with a low matric permeability (Price, 1976). The saturated hydraulic conductivity of the Chalk intergranular matrix is typically only 3-5 mm/day, making matric pore flow very slow indeed. The fractures are heterogeneous in length and aperture, and contribute only 0.1 to 1% if the total porosity. However, it has been suggested that these fractures contribute significantly to aquifer permeability with flow rates of 0.1-100 m/day (Price, 1982).

The evidence for and frequency of rapid recharge through fractures varies between studies, likely as a function of site and investigative technique (Lee et al., 2006). Smith et al. (1970) for example used measurements of tritium concentration along the vertical profile in the Upper Chalk to determine the rate at which rainfall naturally infiltrates through the vadose zone. Tritium is a hydrogen isotope that peaked during widespread nuclear testing in the late 1950s. It was found that the rate of tritium percolation could largely be accounted for by movement through the Chalk matrix (i.e. relatively slowly). However, there was a concentration below the depth that this could be possible. The explanation given was that approximately 15% of the flux 'bypasses' the matrix and is conducted along fractures and fissures. Gardner et al. (1990) on the other hand used the isotope deuterium (a naturally occurring hydrogen isotope that is found in higher concentrations in rainfall in comparison to groundwater) to determine that matric flow was the only mechanism given an observed infiltration rate of 0.8 m/yr. Foster (1975) however pointed out that interpretation of isotopic and geochemical tracers is complicated by the potential for molecular diffusion between matric pore water and water in fractures.

Field measurements of matric potential and water content (physical methods) suggest that vertical hydraulic conductivity increases significantly (to over 100 mm/day) when pore pressures rise above -5 kPa. Negative pore pressure are equivalent to suction (Chae et al., 2010). This rapid response suggests that at higher pore pressures, fracture flow is initiated. Indeed, at a site on the Middle Chalk in Cambridgeshire these conditions occurred for 50% of the time during winter months (Jones and Cooper, 1998). Conversely at a site on the Upper Chalk in Hampshire, the pore pressure rose above -5 kPa on only one occasion during the winter suggesting that fracture flow here is relatively rare (Wellings, 1984). However, weekly measurements in this study could easily have missed short periods of fracture flow. Indeed responses to rainfall within 3 hours observed at 1 m depth at two sites on the Upper Chalk in Hampshire were not detected in weekly measurements (Hassan and Gregory, 2002). A study on the Upper Chalk in Hampshire suggested only matric flow took place on an interfluve site characterised by a vadose zone thickness of around 18 m. Hourly matric potentials were however only recorded up to a depth of 3 m, thereby not accounting for processes below this horizon (Haria et al., 2003).

Previous water content and matric potential data from unconfined sites within the Pang/Lambourn catchment suggest that matric potentials do not reach levels high

enough to initiate fracture flow because the soil zone and superficial deposits mediate flow into the vadose zone (Ireson et al., 2006). Further analysis of the same datasets however revealed that fast recharge pathways are activated but are sensitive to rainfall intensity. In this case, high rainfall intensity leads to an increase in matric potentials and the activation of rapid fracture flow (Ireson et al., 2009). Indeed fracture flow has been suggested only to occur when rainfall intensity is greater than the hydraulic conductivity of the matrix (Price, 2000). Similarly rapid recharge pathways were implicated during a flood event in the Somme Basin, France. Here, the switch from matric to fracture flow was due to accumulated wetness over several years in addition to short term high volumes of rainfall (Pinault et al., 2005).

Previous investigations of flow processes in the unsaturated zone have often focused on cross-correlation analysis of rainfall and groundwater level response time series (Calver, 1997; Flerchinger et al., 1992; Headworth, 1972; Lee and Lee, 2000; Mondal, 2004; Moon et al., 2004; Oakes, 1981). Figure 3.1 illustrates an example of a cross-correlation analysis between a single synthetic rainfall event and groundwater level response. In this example, a rainfall event of 10 mm/day is followed by a rise in groundwater levels between 8 and 13 days later. This is reflected in a significant cross-correlation at lag 11, which corresponds to the period of most rapid change. Response times can then be used to infer the process by which water percolates through the unsaturated zone (Chae et al., 2010) and have been found to be equitable to the results from tracer tests (Lee and Lee, 2000). The method has also been used to test for a third recharge mechanism, matric pulse percolation (Figure 3.2A). A matric pulse can produce a relatively rapid piston-displacement type response similar in velocity to fracture flow and is also dependent on antecedent moisture levels (Lee et al., 2006). The time (t) for a significant response over a distance (Z) in a one dimensional diffusive system (i.e. matric pulse) is given by (Barker, 1993; Price, 2000)

$$t = \frac{Z^2 C}{2Ku} \tag{3.1}$$

where C is specific moisture capacity. For typical suctions in the Chalk (10-150 kPa), values of C lie in the range of 0.0001-0.0007 m^{-1}. Ku is unsaturated hydraulic conductivity, which given the response timing, thickness and antecedent moisture content of the vadose zone can be used to infer the recharge mechanism.

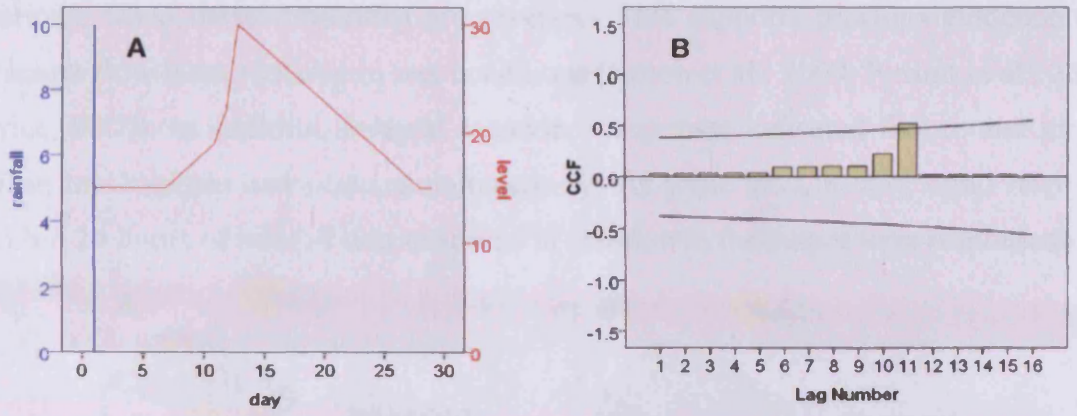

Figure 3.1 Cross-correlation between a synthetic daily rainfall series representing a single event and borehole response. Graph (A) shows a rainfall event and corresponding borehole response. Graph (B) shows the plot of cross correlations according to lag number (day).

Lee et al. (2006) used this cross-correlation technique and Equation 3.1 as a basis to analyse water table response to daily rainfall at sites on the Upper, Middle and Lower Chalk of southern England. At one particular site, a response time within one day through a vadose zone of 64 m suggested a mechanism based only on matric pore flow was out of the question. Using the matric pulse Equation 3.1 and typical values of C, Ku is required to be between 0.2 and 1.4 m/day, which is much greater than the saturated hydraulic conductivity of the Chalk matrix (3-5 mm/day). It is not feasible therefore that the flow was via a matric pulse either and so must be attributed to fracture flow. The time for the water table to respond was found to vary from less than 1 day to more than 4 weeks. It was concluded that recharge could have occurred via rapid fracture flow but mostly through a slower matric pulse (Lee et al., 2006).

In the same study, evidence was also found that the thickness of the vadose zone plays a role in determining whether rapid fissure flow or a slower matric response occurs (Lee et al., 2006). During dryer, summer/autumn conditions borehole responses were more typical of a slower matric pulse. During this time, the vadose zone is likely to be thicker increasing travel times. Specific moisture capacity (C) increases and unsaturated hydraulic conductivity (Ku) decreases with a decrease in water content, which may also explain the increase in travel times. Conversely, C decreases and Ku increases with water content and potential. This increase in water potential is likely to occur during wet periods, which is also when the vadose zone is likely to be thinner. The slower responses occurred during or at the end of dry periods, when both groundwater storage in the vadose zone and its matric hydraulic conductivity are relatively low. The rapid responses occurred during or after wet

periods, when these conditions are reversed. This supports previous evidence that fracture flow is more likely in wet conditions (Ireson et al., 2009; Pinault et al., 2005; Price, 2000). In addition, delayed secondary responses indicated fissure and matric pulse mechanisms can occur simultaneously. At some sites, a very rapid response within 24 hours of rainfall was observed in addition to the longer term responses.

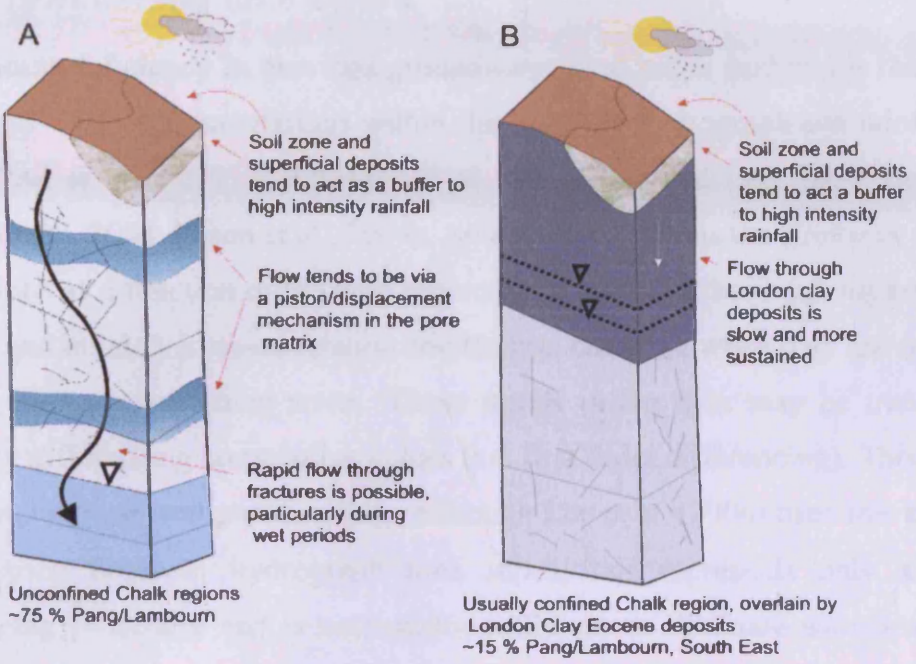

Figure 3.2 Schematic of vertical flow mechanisms through a typical Chalk vadose zone in (A) unconfined regions and (B) confined areas.

In summary, evidence suggests that in the Chalk, matric flow is the normal mode of recharge, which can lead to a reasonably rapid response as a result of a piston displacement process. However, the spatial and temporal variations in response time can only be partially accounted for using a diffusive model for propagation through the unsaturated matrix, suggesting that some fracture flow was occurring. Fracture flow will occur locally when the recharge rate approaches or exceeds the hydraulic conductivity of the matrix. In some previous cases however it is likely that fracture flow has wrongly been attributed to rapid piston matric flow. This dual porosity recharge mechanism in Chalk areas such as the Pang/Lambourn is summarised in Figure 3.2A.

The London Clay Formation is a non-aquifer and forms a confining layer over the Chalk (Brenchley and Rawson, 2006). As such, it is often assumed that little or even no recharge occurs through this layer, for example in the south east of the Pang catchment. Indeed, it has been suggested that the only method of recharge through this layer would be artificially through wells (Downing et al., 1972).

However, a report commissioned by the Environment Agency (EA, 1997) assessing the water quality in the London Basin suggested that a small amount of infiltration can take place via leakage through the London Clay cover. The likely mechanism of flow through the confining layer is therefore included in Figure 3.2B.

3.1.2 Prewhitening time series

A significant deficiency in previous groundwater time series analyses is the lack of attention given to autocorrelations within the borehole hydrograph and rainfall time series (Chae et al., 2010; Flerchinger et al., 1992; Lee and Lee, 2000; Lee et al., 2006; Mondal, 2004; Moon et al., 2004). An autocorrelation is the similarity between observations as a function of the time separation between. It has been suggested that spurious and inflated cross-correlation coefficients can arise when they are computed between autocorrelated time series. These trends in the data may be transformed usually by differencing consecutive values (i.e. first order differencing). This process of de-trending is termed prewhitening. Although Lee et al. (2006) used this approach for preparing borehole hydrograph time series, this represents only a simple prewhitening procedure and is not usually sufficient to eliminate autocorrelations. One method to avoid this problem is to prewhiten the data by fitting Autoregressive Integrated Moving Average ARIMA models to the data (Box and Jenkins, 1976). The residuals of the fitted ARIMA model are considered to be independent and normally distributed with mean zero and constant variance. By cross-correlating the residuals of the ARIMA models, the effect of autocorrelation is minimised (Chatfield, 2003; Lehman and Rode, 2000; Yamaguchi, 1986).

3.2 *Aims and objectives*

The aim of this chapter is to use time series analysis to determine the timing of water table response to rainfall events at a variety of sites in the Pang/Lambourn in order to gain an insight into vadose zone processes and the implications for groundwater flooding risk. This will be done by addressing a number of key objectives:

- Assess the impact of ARIMA prewhitening on cross-correlation analysis between rainfall and borehole hydrograph time series.
- Use cross-correlation analysis to determine the timing of water table response to rainfall events at a variety of sites in the Pang/Lambourn.

- Use time lags to gain an insight into the recharge flow paths of the Pang/Lambourn i.e. fracture flow, matric pulse or matric flow.
- Understand the role and potential impact of vadose zone processes in groundwater flood risk modelling.

3.3 Methods

The methodology makes use of long term daily (and in some cases hourly) borehole and rainfall data in the Pang/Lambourn and comprises three major steps. Initially ARIMA models were fitted to borehole hydrograph and corresponding rainfall time series at 7 sites. Secondly, a cross-correlation was performed between the prewhitened time series (i.e. residuals). Thirdly the likely recharge pathway was determined as a function of *C*, *Ku*, depth of vadose zone and lag time. There is an emphasis on the analysis of winter and spring time series, as this is when most recharge is likely to occur and groundwater flooding is a problem.

3.3.1 Prewhitening time series by fitting ARIMA models

An ARIMA time series model is potentially made up of 3 sub components; an autoregressive (AR), differencing/integrating (I) and moving average (MA) part, the order of which are represented by *p*, *d* and *q* respectively (see below). Hence the common notation ARIMA(*p,d,q*). In the past, the fitting of ARIMA models was time consuming and often reliant on expert judgment and trial and error (Lehman and Rode, 2000). Now, whilst it is important to consider the time series characteristics manually, software programs are available that will determine the best fit model automatically. In this case SPSS™ was used to fit models to the rainfall and borehole hydrograph time series prior to cross-correlation. The Box-Ljung statistic provided a measure of the overall significance of the residual autocorrelations i.e. measure of ARIMA model fit. A Box-Ljung statistic, Q>0.05 indicated the residuals were suitable for cross-correlation (Ljung and Box, 1978).

The univariate autoregressive (AR) model which forms part of the ARIMA assumes that an observation *X* at time *t* is predictable (to within a residual) from a weighted sum of the *p* previous observations i.e. the series is predicted from its immediate past

$$X_t = c + \sum_{i=1}^{p} \rho_i X_{t-i} + \varepsilon_t \qquad (3.2)$$

where $\rho_1, \ldots\ldots, \rho_p$ are parameters of the model, p is the order of model, c is a constant and ε_t is white noise i.e. a random number (Box and Jenkins, 1976). For example therefore, a third order autoregressive model would be represented by

$$X_t = c + \rho_1 X_{(t-1)} + \rho_2 X_{(t-2)} + \rho_3 X_{(t-3)} + \varepsilon_t \quad \textbf{(3.3)}$$

where ρ_1, ρ_2, ρ_3 are the autoregressive model parameters. Here, each observation is made up of a random error component and linear combination of three prior observations. The integration process involves removing the trend and drift from the data (i.e. makes non-stationary data, stationary). In the case of first order differencing, the first value is taken from the second, the third from the second etc. This would be repeated in second order differencing and over a specified lag (e.g. 365) for seasonal trends. A useful heuristic is to make the time series resemble white noise and reduce persistence in the autocorrelation plot (see Figure 3.5).

If the AR component represents the lingering effects of previous observations, the MA represents the lingering effects of q previous errors

$$X_t = \mu + \varepsilon_t + \sum_{i=1}^{q} \theta_i \varepsilon_{t-i} \quad \textbf{(3.4)}$$

where $\theta_1, \ldots\ldots \theta_q$ are parameters of the model, μ is constant and ε_t, $\varepsilon_{t-1}, \ldots$are error terms (Box and Jenkins, 1976). For example therefore, a third order moving average model is represented by

$$X_t = \mu + \varepsilon_t + \theta_1 \varepsilon_{(t-1)} + \theta_2 \varepsilon_{(t-2)} + \theta_3 \varepsilon_{(t-3)} \quad \textbf{(3.5)}$$

where θ_1, θ_2, θ_3 are the moving average model parameters. Here, each observation is made up of a random error component and a linear combination of three prior random shocks. An ARIMA (p,d,q) equation is obtained by combining the autoregressive, integrating and moving average terms. In this case the lag function L and d represents the nature of the differencing procedure in order to obtain a stationary series. The Box-Jenkins method does not require all the component models to be used at once, and parsimony is encouraged to limit the degrees of freedom.

$$X_t(1-L)^d = c + \varepsilon_t + \sum_{i=1}^{p} \rho_i X_{t-i} + \sum_{i=1}^{q} \theta_i \varepsilon_{t-i} \quad \textbf{(3.6)}$$

where L is the lag operator and d is the order of differencing (Box and Jenkins, 1976). SPSS™ ultimately provided a time series of ARIMA residuals upon which further analysis was performed.

3.3.2 Cross-correlation and recharge pathway analysis

The cross-correlation ρ_y between rainfall at time t (X_t) and borehole response at time t (Y_t) was determined for time lags, k, on a daily and where available, hourly basis

$$\rho_y(k) = \frac{\sum[(X_t - \mu_x)(Y_{t+k} - \mu_y)]}{\sigma_x \sigma_y} \quad (3.7)$$

where k is the 0,1,2.....n time lag between the two series (days or hours), μx and σx are mean and standard deviation of rainfall respectively and μy and σy are the mean and standard deviation of groundwater level. The process was carried out for selected time series following simple first order differencing of the borehole hydrographs. Secondly, the process was repeated for all the ARIMA residuals. This way, the impact of ARIMA prewhitening on the cross-correlation function (CCF) plot could be established. Significant correlations exceeded the 95% upper confidence level and negative lags were ignored as they do not provide any additional information: they simply represent those times when the two series are out of phase rather than in phase (Lee et al., 2006). Significant lags were substituted into Equation 3.1 along with the mean depth to groundwater during the time period. By adopting a likely range of C values of between 0.0001 and 0.0007 m^{-1}, a range of Ku values was established. These Ku values were then used to infer the vadose zone pathways operating in that area and time period. A borehole response that required Ku to greater than 10 mm/day was attributed to fracture flow. The borehole response time were also plotted against vadose zone thickness in order to discern any spatial or temporal pattern.

3.3.3 Field sites

Cross-correlation sites were chosen based on the availability of daily or hourly borehole records. An attempt was also made to draw from a range of vadose zone thicknesses and geological settings. Figure 3.3 illustrates the location of the selected boreholes and the nearest corresponding rain gauge with a complete (or nearly complete) record. Some sites were paired with more than one rain gauge, particularly at Saltbox and Hodcott, where hourly rainfall was only available from West Ilsley, but Peasemore offered a longer daily time series. Inter-annual and sub-annual (3 or 6 months usually) time series were investigated in order to assess the impact of

different groundwater conditions (i.e. vadose zone thicknesses) on significant lag times.

Northfield is located on the Upper Chalk approximately 1.5 km north east of the perennial source of the river Lambourn. The site is used for arable cereal farming and is overlain by river terrace deposits and a silty soil. The groundwater table here is generally 4 m below the ground although during wet periods it almost reaches the surface. Nearby rain gauges at East Shefford and Lambourn were used for the cross-correlation. Longacre is a grassy site on the Middle Chalk influve area north of the Lambourn valley, overlain by circa 3 m of superficial deposits and a silty soil. The vadose zone is about 13 m on average, although large scale fluctuations during wet periods elevate the groundwater table towards the ground surface. Similarly to Northfield, both Lambourn and East Shefford rain gauges were used for cross-correlation here. This was to make use of the different time periods covered by the gauges and assess the impact of using data from different locations.

Hodcott and Saltbox both lie on the interfluves north of the Pang valley. Borehole logs suggest both sites lie on the Middle Chalk although the position of Hodcott on a geological map suggests that it lies on the Upper Chalk. Both sites are characterised by superficial head deposits and silty soil but different land uses. Hodcott has a thicker vadose zone (16 m) compared to Saltbox (9 m). Despite a larger range of fluctuation (14 m) at Hodoctt, the groundwater does not come as close to the surface as at Saltbox (10-11 m fluctuation). Both sites were cross correlated with West Ilsley on an hourly and daily basis and Peasemore on a daily basis. Chapelwood is characterised by arable cereals, river terrace deposits and silty clay loam soil. It lies 2 km north of the Winterbourne valley at a site on the Upper Chalk. The vadose zone thickness and fluctuation zone is comparable to the site at Northfield. The rain gauge at Peasemore provided the longest time period for cross-correlation at almost four years.

Beenham and Newbury are both located on Palaeogene London Clay deposits, however differ considerably. Beenham lies relatively high in the South of the Pang catchment, adjacent to a tributary stream and is characterised by superficial gravel deposits, silty clay loam soil and arable land use. Newbury on the other hand lies adjacent to the Lambourn river close to the confluence with the river Kennet. It is overlain with alluvial deposits, loam soil and suburban development. Most striking is the difference in the depth to groundwater or piezometric surface, which is 50 m at

Beenham and negligible at Newbury. Indeed, at Newbury the well appears to be artesian, although there is a degree of uncertainty inherent in taking the top of the borehole from a 10m DTM. At both sites, the seasonal fluctuations are very small in comparison to the Chalk sites (1.5-3 m) and Bucklebury provided the rainfall data for cross-correlation analysis.

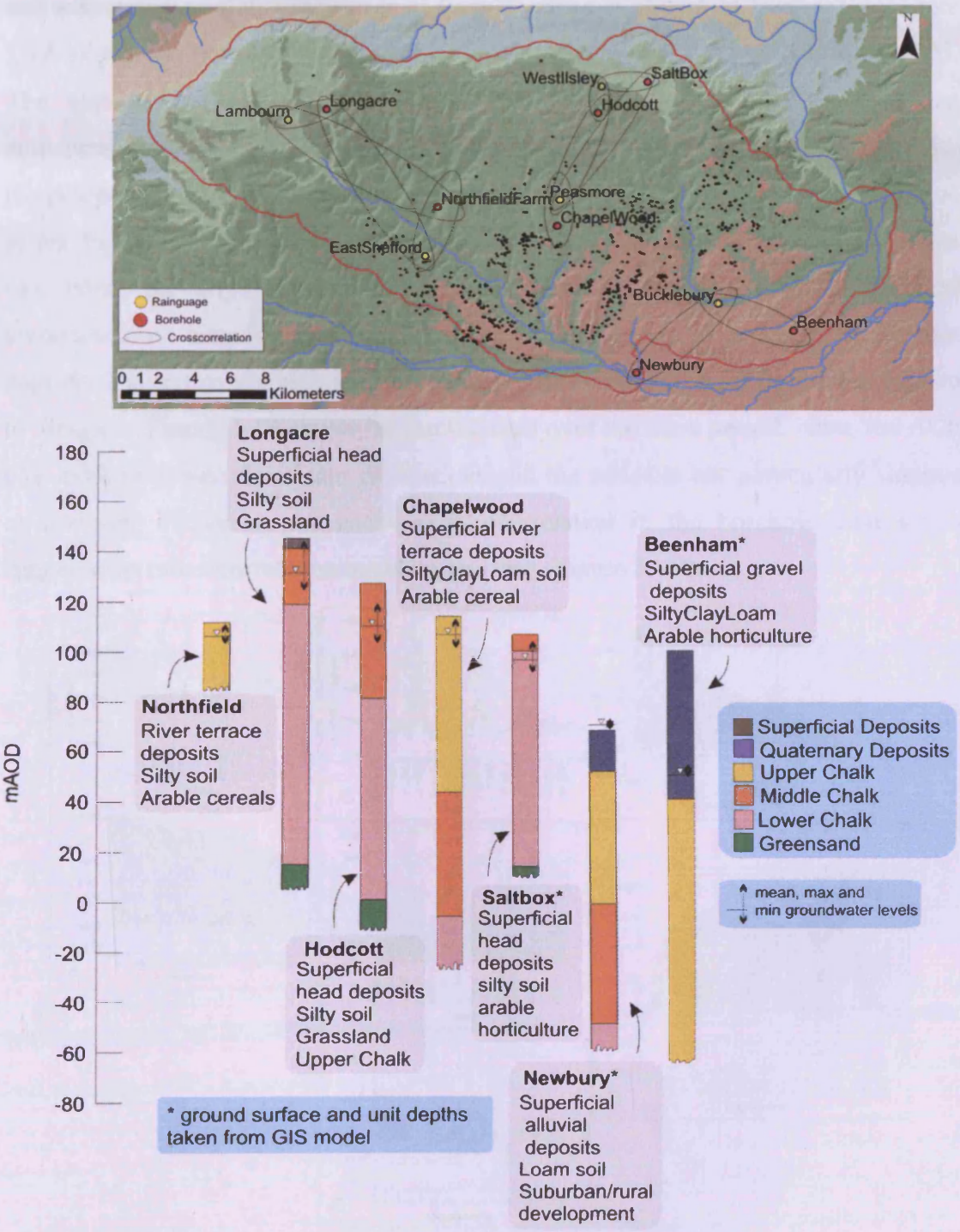

Figure 3.3 Location, logs, soil type, land use and groundwater table conditions (mean, max & min) associated with the boreholes used for cross-correlation analysis, along with the corresponding rain gauge locations.

3.4 Results

3.4.1 ARIMA prewhitening in comparison to first order differencing

The cross-correlation procedure between a daily borehole time series at Longacre and associated rainfall time series at East Shefford is shown in Figure 3.4. Figure 3.4A shows the borehole hydrograph from between spring 2002 until autumn 2005. The associated autocorrelation function (ACF) plot suggests there are strong autocorrelations up to lag 50 (at least). This means that each value is correlated with the proceeding 50 values, which is not surprising given the sinuous nature of the time series. Figure 3.4C shows the same time series after first order differencing. The data has been partially detrended, which is evident in the relatively reduced autocorrelation magnitudes and sinuosity of the time series. However, the ACF plot suggests a significantly high level of autocorrelation remains, with significant lags up to 50 again. Figure 3.4B shows the rainfall data over the same period. Here, the ACF plot exhibits fewer significant correlations and the series is not particularly sinuous or seasonal. However, the enduring autocorrelation in the borehole time series suggests the cross-correlation could be spurious (Figure 3.4D).

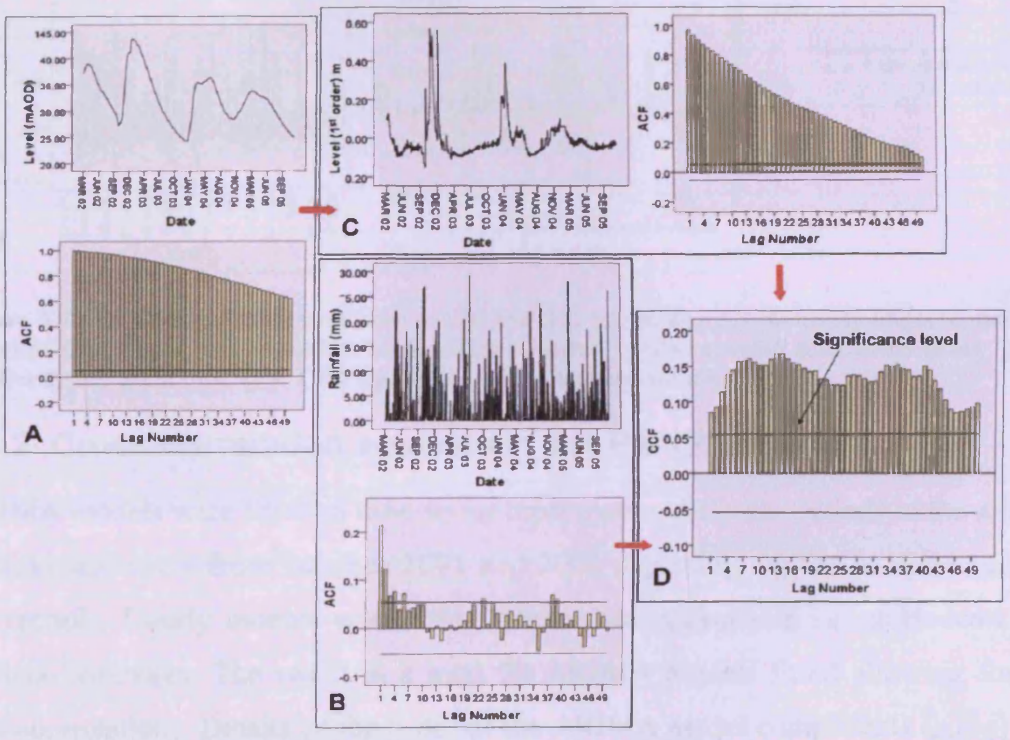

Figure 3.4 (A): Borehole hydrograph at Longacre and associated autocorrelation function (ACF) plot. (B): Rainfall at East Shefford timeseries and associated ACF plot. (C): Borehole timeseries following first order differencing and ACF plot. (D): Cross-correlation function (CCF) plot between B & C.

The impact of using ARIMA prewhitening on the ACF and CCF plots can be seen in Figure 3.5. Figure 3.5A and B show the residuals of a fitted ARIMA model and associated ACF plot for Longacre and East Shefford respectively. In both cases the residuals resemble white noise. In addition, the ACF suggests a marked reduction in the number of significant autocorrelations in comparison to simple first order differencing or no differencing (Figure 3.4A and C). The ARIMA residuals yield a Box-Ljung statistic of 0.90 and 0.73 for the borehole and rainfall time series, indicating the model fits well and there is no significant autocorrelation amongst the residuals It is apparent that the cross-correlation plot here provides a clearer indication of when significant lags exist in the data i.e. at lag 1,3,4,6, 26 and 40 (Figure 3.5C).

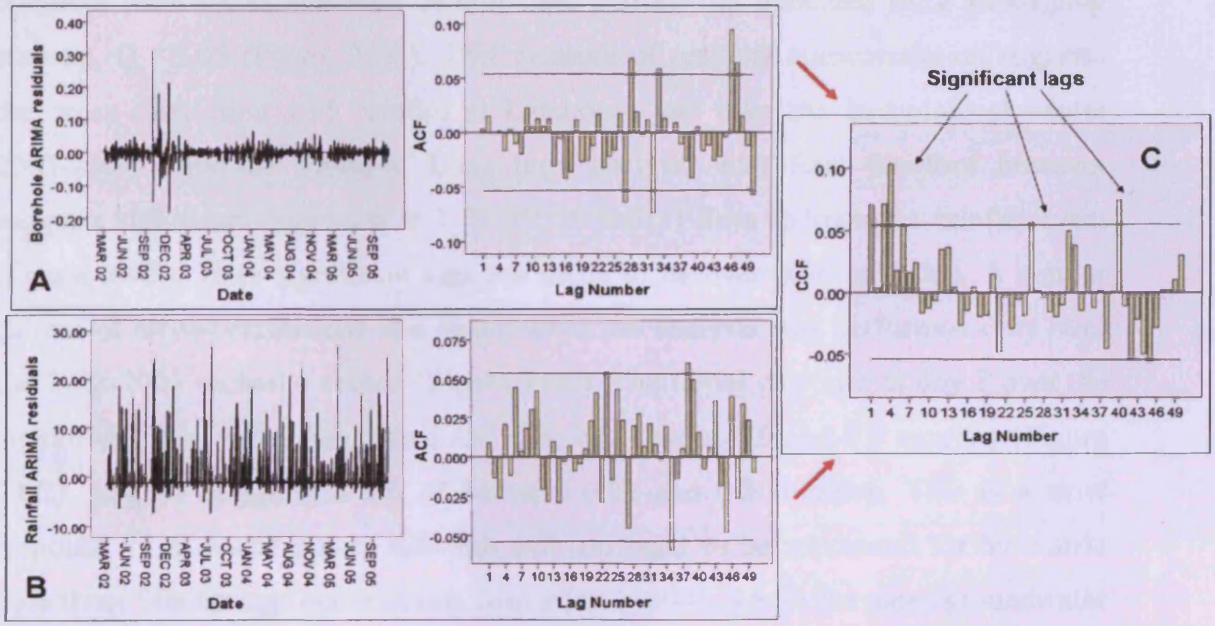

Figure 3.5 (A): Residuals from ARIMA model fitted to borehole hydrograph (Longacre) and associated ACF plot. (B): residuals from ARIMA model fitted to rainfall time series (East Shefford) and ACF plot. (C): CCF plot after ARIMA prewhitening.

3.4.2 Cross-correlation analysis in the Pang/Lambourn

ARIMA models were fitted to time series representing different periods of the annual hydrological cycle from between 2001 and 2006 depending on the completeness of the records. Hourly models were fitted where data is available i.e. at Hodcott and Saltbox boreholes. The result is a total 78 ARIMA models fitted allowing for 39 cross-correlations. Details of the order of the ARIMA model components (p,d,q) can be found in Appendix 2.1. Below is a summary of significant cross-correlation lags at each borehole over different time periods. These lag times were used to infer

recharge timing and pathways. For example, a relatively rapid initial response could indicate fracture flow, whereas a longer response could indicate a matric pulse mechanism. By substituting lag time and mean vadose zone depth into Equation 3.1 and assuming a range of C values of between 0.0001 and 0.0007 m^{-1}, the Ku range of the first and last significant lag provides an indication of matric pulse (m) or fracture flow response (f).

The borehole hydrograph for Northfield and the associated daily rainfall at East Shefford from August 2002 until December 2005 is shown in Figure 3.6A. There was a peak in groundwater levels in early 2003 corresponding to catchment-wide flooding. The consecutive seasonal peaks in 2004 and 2005 were considerably reduced. The cross-correlation analysis was limited by fitting ARIMA models to the borehole time series spanning certain time periods, as indicated by a Box-Ljung statistic, Q <0.05 (Figure 3.6C). This measure of residual autocorrelation suggests the cross-correlation with rainfall at Lambourn and over the hydrological winter 2003-2004 could be spurious. Long term analysis with East Shefford however suggests significant lags exist at 1, 9, 25, 29 and 31 days following a rainfall event (Figure 3.6B). Here significant lags are taken to be over 0.06 ($p<0.05$). A similar pattern of cross-correlations was found when the analysis was performed only over the 2002-2003 recharge season (Figure 3.6C). The initial response at day 1 over the interannual time series suggests a Ku value of between 0.9 and 6.3 mm/day (Figure 3.6C). Lag 31 suggests a Ku of between 0.03 and 0.2 mm/day. This is a slow response for a matric pulse, although still too rapid to be accounted for by matric pore flow. Similar lags occur during winter 2002–2003, where the mean groundwater table was generally closer to the surface. The lag at day one suggests a Ku of between 0.29 and 2.01 mm/day. The longest lag, 35, suggests a Ku of between 0.01 and 0.06 mm/day. All the responses are therefore characteristic of a matric pulse (m) of varying conductivity on a multi-annual scale as well as during the winter of 2002-2003.

Time series and CCF plots for Longacre and East Shefford can be seen in Figure 3.4 (without ARIMA prewhitening) and Figure 3.5 (with ARIMA prewhitening). ARIMA models were successfully fitted to the hydrograph for the time periods over which both Lambourn (1 km away) and East Shefford (10 km away) rain gauges operated. This allowed for a comparison between two different

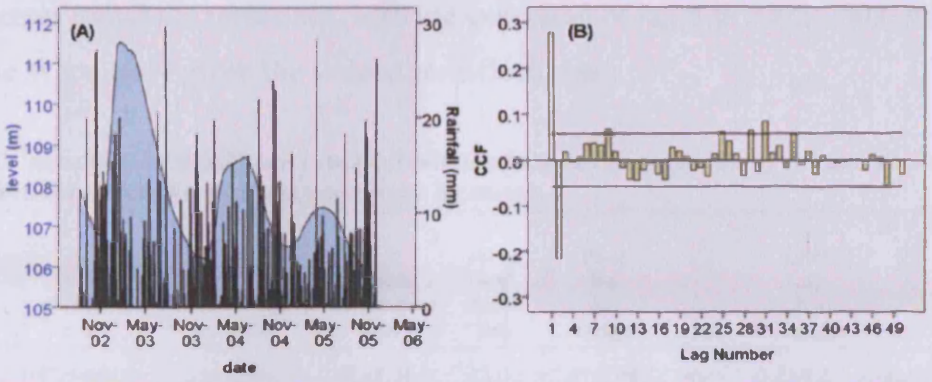

(C)

Time Series dates	Rain gauge location	Cross correlation lags	Mean GW depth (m)	First lag *Ku* range	m/f	Last Lag *Ku* Range	m/f
02/03-06/05	Lambourn	1*	4.10	0.85-5.89	m-m	0.85-5.89	m-m
08/02-12/05	EastShefford	1,9,25 29,31	4.23	0.9-6.27	m-m	0.03-0.21	m-m
10/02-03/03	EastShefford	1,7,25,29 31,36	2.40	0.29-2.01	m-m	0.01-0.06	m-m
10/03-03/04	Lambourn	1*	5.08	1.29-9.02	m-m	1.29-9.02	m-m
10/03-03/04	EastShefford	1*	5.08	1.29-9.02	m-m	1.29-9.02	m-m

* Box Ljung (BL) test indicates ARIMA residuals are significantly autocorrelated

Figure 3.6 Northfield farm borehole hydrograph and rainfall at East Shefford (A) and corresponding CCF plot (B). Summary of significant cross-correlation lags likely *Ku* and recharge mechanism for all time series and rain gauge locations (C).

rainfall time series albeit over slightly different periods. Long term cross-correlation analysis with Longacre and the rain gauge at Lambourn suggests significant lag times of 6, 14 and 33 days. A similar distribution of lags is seen when the cross-correlation is with East Shefford, although a quicker response is indicated, with a lag at day 1. This could be a result of the longer East Shefford time series including the winter of 2002-2003, where the mean vadose zone was shallower and the increase in borehole levels was greatest. This is supported by the lag at day 1 when the winter of 2002-2003 is isolated in the analysis. It is not seen during the winter of 2003-2004 using either Lambourn or East Shefford rain data (Table 3.1).

The initial response at day 1 during the interannual time series suggests a *Ku* value of between 8.15 and 57.04 mm/day, the upper bounds of which indicates a rapid fracture flow response. The last lag at 40 gives a *Ku* of between 0.21 and 1.43 mm/day, which is more associated with a matric pulse (m) suggesting that fracture flow and matric pulse flow can both occur. The winter of 2002-2003 has a shallower mean groundwater table in comparison with 2003-2004. This corresponds to a first lag at 1 in comparison to 6, suggesting a shallower water table allowed a faster response. The upper estimates of *Ku* values in both instances suggests fracture flow

can account for all the responses, with the exception of lag 4 in 2002-2003, where the response is too slow given the vadose zone thickness.

Table 3.1 Summary of significant cross-correlation lags at Longacre, likely *Ku* and recharge mechanism for all time series and rain gauge locations.

Time Series dates	Rain gauge location	Cross correlation lags	Mean GW depth (m)	First lag *Ku* range	m/f	Last Lag *Ku* Range	m/f
02/03-06/05	Lambourn	**6,14,33**	13.00	1.41-9.86	m-m	0.26-1.8	m-m
03/02-12/05	EastShefford	**1,3,4,6 26,40**	12.76	8.15-57.04	m-f	0.21-1.43	m-m
10/02-03/03	EastShefford	**1,4**	8.03	3.23-22.59	m-f	0.81-5.65	m-m
10/03-03/04	Lambourn	**6**	17.02	2.42-16.9	m-f	2.42-16.9	m-f
10/03-03/04	EastShefford	**6,8**	17.02	2.42-16.9	m-f	1.81-12.67	m-f

The borehole hydrograph at Chapelwood and corresponding rainfall time series at nearby (1.5 km away) Peasemore displays a peak in groundwater levels in spring 2003 (Figure 3.7A). The cross-correlation analysis is limited by the unsuccessful fitting of ARIMA models to the borehole time series over the 2003-2004 recharge season and autumn 2002 (as suggested by a Box Ljung of Q=0.01 in both cases). Multi-annual cross-correlation analysis suggests significant lag times at days 3, 4, 6 and 11 (Figure 3.7B). Given a mean groundwater depth during this period of 6.79m, the initial lag equates to a likely *Ku* of between 0.77 and 5.38 mm/day. The upper and lower values both suggest that this response is likely to be a matric pulse mechanism. The last significant lag at day 11 indicates a *Ku* of between 0.21 and 1.47 mm/day which again lies within the likely range of a matric pulse mechanism (Figure 3.7C). If infiltration took place at the rate associated with saturated conductivity (i.e. 3-5 mm/day), given a vadose zone thickness of 6.79 m, the response would take approximately 3.7 years. The rate of infiltration is therefore too rapid to be accounted for by pore matric flow.

A significant lag at day 1 during the recharge season 2002-2003 indicates a *Ku* range of between 1.03 and 7.17 mm/day given (Figure 3.7C). Despite this relatively rapid response, the shallow vadose zone (4.5 m) means a matric pulse mechanism is likely. Conversely, a lag at day 1 during the 2004-2005 recharge season could be attributed to fracture flow (*Ku* range between 4.4 -30.78 mm/day). This is due to the relatively thick vadose zone during this period (9.38 m), where a second matric response is also found at day 5. A slower response is detected during

the period from January to March 2003. Here, despite a shallow water table (1.69 m), the only significant lag exists at day 6. This suggests a range of *Ku* between 0.03-0.17 mm/day, well below the bounds typical of fracture flow.

Figure 3.8 shows the Hodcott borehole hydrograph, rainfall at Peasemore and associated cross-correlation function plot. A slightly shorter time series is covered by the West Illsey rainfall time series, which is geographically closer to the borehole site (see Figure 3.3). The hourly cross-correlation analysis with West Ilsley was limited by unsuccessful fitting of ARIMA models to rainfall and borehole time series (i.e. Box-Ljung Q<0.05). The lag times must therefore be treated with a degree of caution. However, it should be noted that a significant lag occurs at 1 hour, indicating the possibility of sub-daily responses to rainfall events. Generally, the hourly analyses show a more diffuse lag pattern than daily analyses (see Appendix 2.2).

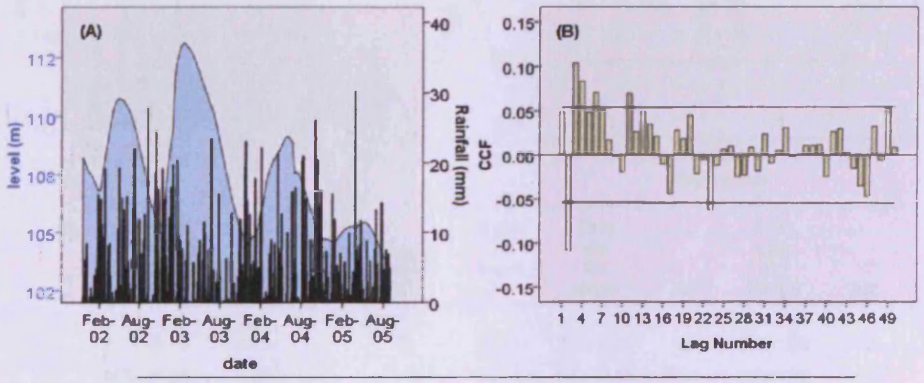

(C)

Time Series dates	Cross correlation lags	Mean GW depth (m)	First lag *Ku* range	m/f	Last Lag *Ku* Range	m/f
11/01-08/05	**3,4,6,11**	6.79	0.77-5.38	m-m	0.21-1.47	m-m
10/02-03/03	**1**	4.53	1.03-7.17	m-m	1.03-7.17	m-m
10/03-03/04	**1,8***	8.52	3.63-25.4	m-f	0.46-3.18	m-m
10/04-03/05	**1,5**	9.38	4.4-30.78	m-f	0.88-6.16	m-m
10/02-12/02	**6***	7.56	0.58-4.01	m-m	0.58-4.01	m-m
01/03-03/03	**6**	1.69	0.03-0.17	m-m	0.03-0.17	m-m

* Box Ljung (BL) test indicates ARIMA residuals are significantly autocorrelated

Figure 3.7 Chapelwood borehole hydrograph and rainfall at Peasemore (A) and corresponding CCF plot (B). Summary of significant cross-correlation lags, likely *Ku* and recharge mechanism for all time series and rain gauge locations (C).

Although the multi-annual Peasemore and WestIlsley time series cover slightly different periods, they both indicate an initially rapid response, followed by a longer secondary response. Peasemore gives significant lags at 1,2,3,41,49 in comparison to 2 and 30 at West Ilsley. In both cases the *Ku* estimations suggest an initial fracture flow response followed by a slower matric pulse response 30-49 days

later. For example the lag at 1 day indicates a *Ku* of between 13.4 and 93.8 mm/day (both within the bounds of fracture flow). The lag at 30 gives a *Ku* of between 0.44 and 3.1 mm/day (Figure 3.8C). The 2002-2003 recharge season follows a similar pattern of fast initial response and slower second response. When this is broken down further into 3 month periods, it suggests the rapid response occurs in the October to December 2002 (lag 7, *Ku* 2.02-14.16 mm/day) and a slower response in the following 3 months (lag 41, *Ku* 0.08–0.53 mm/day), despite a shallower vadose zone. The recharge season between October 2003 and 2004 is characterised by a relatively deep vadose zone (19.32 m) and rapid response. During this time, the upper *Ku* bounds of the lag at day 2 and 3 both suggest fracture flow.

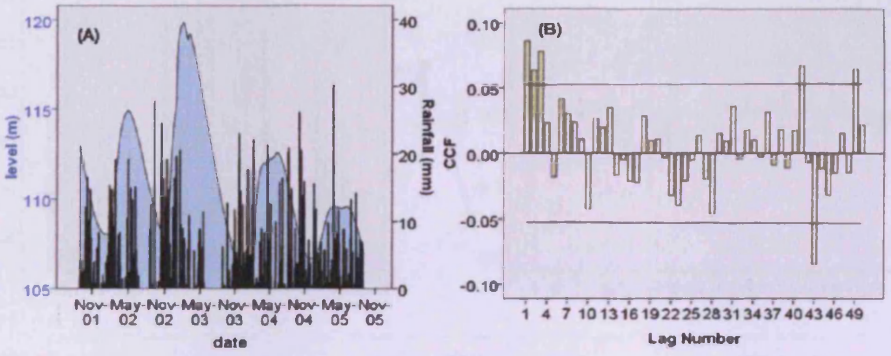

(C)

Time Series dates	Rain gauge location	Cross correlation lags	Mean GW depth (m)	First lag *Ku* range	m/f	Last Lag *Ku* Range	m/f
08/01-08/05	Peasemore	1,2,3,41 49	16.37	13.4-93.8	f-f	0.28-1.92	m-m
10/02-03/03	Peasemore	1,3,41	12.42	7.72-54.01	m-f	0.19-1.32	m-m
10/03-03/04	Peasemore	2,3	19.32	9.34-65.32	m-f	6.23-43.55	m-f
10/02-12/02	Peasemore	7	16.83	2.03-14.17	m-f	2.03-14.17	m-f
01/03-03/03	Peasemore	41	7.87	0.08-0.53	m-m	0.08-0.53	m-m
11/02-07/05	Westllsley	2,30	16.29	6.64-46.47	m-f	0.45-3.1	m-m

Figure 3.8 Hodcott borehole hydrograph and rainfall at Peasemore (A) and corresponding CCF plot (B). Summary of significant cross-correlation lags likely *Ku* and recharge mechanism for all time series and rain gauge locations (C).

The long term cross-correlation analysis between Saltbox and Peasemore is limited by the unsuccessful fitting of an ARIMA model. Figure 3.9A shows the borehole hydrograph at Saltbox and the associated rainfall time series at nearby Westllsley. This multi-annual series with Westllsley suggests lags at 1, 2 and 3 (Figure 3.9B). This results in an initial value for *Ku* of between 4.25 and 29.77 mm/day at lag 1 reducing to between 1.42 and 9.92 mm/day by lag 3. The upper bounds indicate a fracture flow mechanism as well as a matric pulse operating together at this location. Incidentally, the compromised analysis with Peasemore

suggests the same significant lag times (Figure 3.9C). A dual mechanism is also suggested by looking at the recharge seasons over 2002-2003 and 2003-2004 specifically. In this case, the depth of the vadose zone does seem to extend the maximum lag time. At a mean vadose depth of 11.38 m the max lag is 29 and at 6.12 m is 3. No significant lag is found at all between January and March 2003. Similarly to Hodcott, hourly analyses are hampered by significant Box-Ljung statistics. However, it is again worth noting the sub daily responses found at the multi-annual scale and winter scale. The lags are also more diffuse than daily cross-correlations between and range from less than a day up to day 39 (see Appendix 2.2 for details).

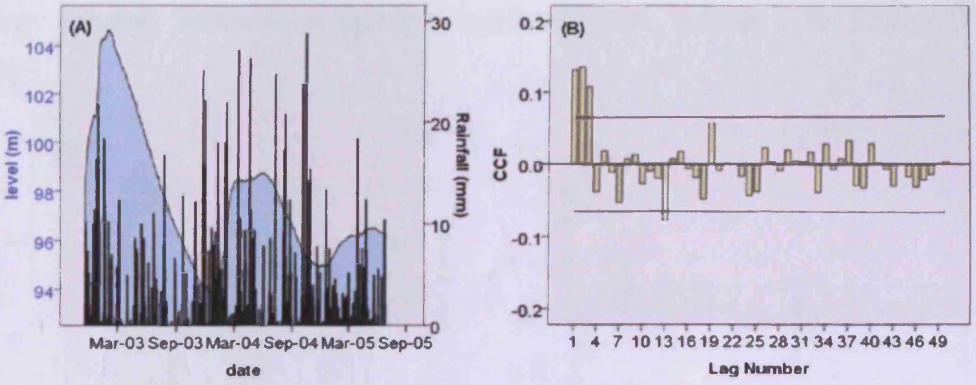

(C)

Time Series dates	Rain gauge location	Cross correlation lags	Mean GW depth (m)	First lag *Ku* range	m/f	Last Lag *Ku* Range	m/f
03/02-06/05	Peasemore	1,2,3*	9.22	4.26-29.78	m-f	1.42-9.93	m-m
10/02-03/03	Peasemore	1,3	6.12	1.88-13.11	m-f	0.63-4.37	m-m
10/03-03/04	Peasemore	2,3,10,29	11.38	3.24-22.67	m-f	0.23-1.57	m-m
10/02-12/02	Peasemore	3	9.01	1.36-9.47	m-m	1.36-9.47	m-m
01/03-03/03	Peasemore	none	3.17	-	-	-	-
11/02-06/05	Westllsely	1,2,3	9.30	4.33-30.31	m-f	1.45-10.11	m-f

* Box Ljung (BL) test indicates ARIMA residuals are significantly autocorrelated

Figure 3.9 Saltbox borehole hydrograph and rainfall at WestIlsley (A) and corresponding CCF plot (B). Summary of significant cross-correlation lags likely *Ku* and recharge mechanism for all time series and rain gauge locations.

Beenham borehole hydrograph is characterised by a flashy, spiky response and limited fluctuation (maximum range of 2.8 m). The cross-correlation with the nearby rainfall time series at Bucklebury is shown in Figure 3.10A. Between 1999 and 2004 significant lags exist at 1, 8, 9, 15, 16, 35 and 38 days (Figure 3.10B). Equation 3.1 and a typical range of C from 0.0001 to 0.0007 probably do not apply to the London Clay and so estimations of *Ku* can not be made. This same pattern is typically repeated for individual recharge seasons in 2000-2001, 2001-2002 and 2002-2003, where an initially rapid response is followed some weeks later by a secondary response (Figure 3.10E). Interestingly, the time series at Beenham is the

only one that includes the widespread flood event of 2000-2001. During the period October 2000 to March 2001, the initial response during this time is actually slower than during the same period in subsequent years. The borehole hydrograph at Newbury exhibits a similar flashy response and small range of fluctuation to Beenham (Figure 3.10C). Here however the cross-correlation with Bucklebury rainfall time series (Figure 3.10D) is limited by the unsuccessful fitting of ARIMA models as indicated by a Box-Ljung Q>0.05 (Figure 3.10F). Again, Equation 3.1 and a typical range of C from 0.0001 to 0.0007 probably do not apply to the London clay and so estimations of Ku can not be made. The cross-correlation of individual recharge seasons however suggests a rapid response, within 1 to 3 days (Figure 3.10F).

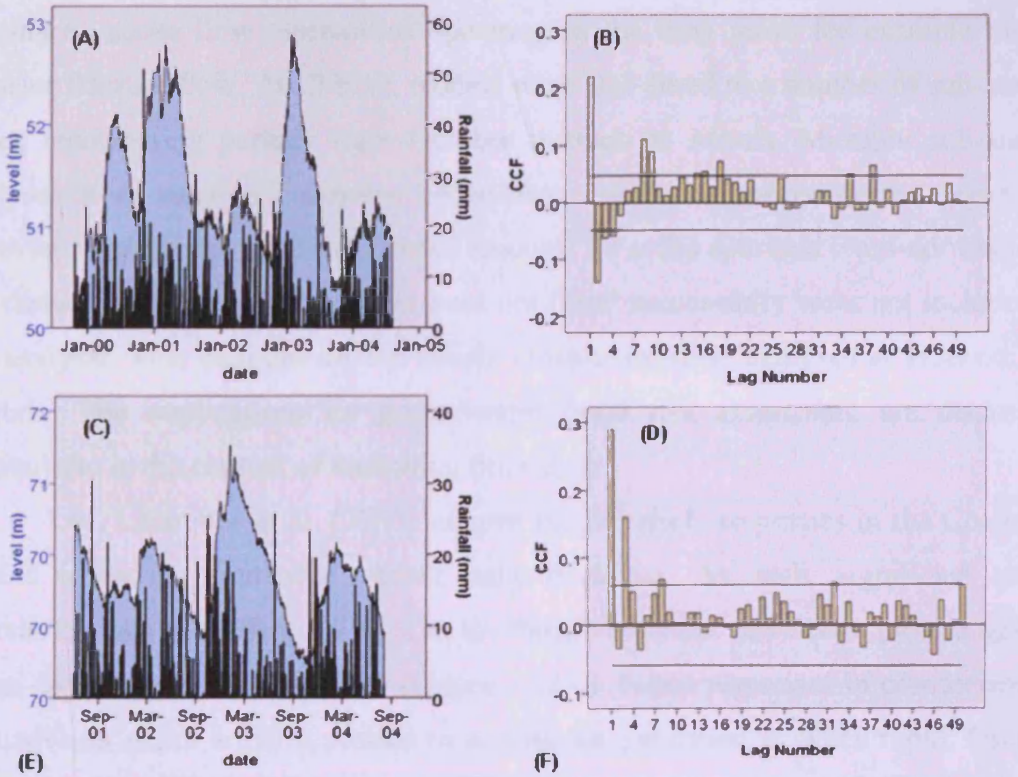

(E)

Time series dates	Cross correlation lags
10/99-08/04	1,8,9,15,16,18,35,38
10/00-03/01	6,12
10/01-03/02	1,14,22
10/02-03/03	1,8,9,12,19,20,30
10/00-12/00	6,12
01/01-03/01	13

(F)

Time series dates	Cross correlation lags
06/01-08/04	1,3,8,33*
10/01-03/02	1
10/02-03/03	1,3
10/02-12/02	1
01/03-03/03	3

*Box Ljung (BL) test indicates ARIMA residuals are significantly autocorrelated

Figure 3.10 Beenham (A) and Newbury (C) borehole hydrographs and rainfall at Bucklebury. Corresponding CCF plots for Beenham (B) and Newbury (D). Summary of significant cross-correlation lags, likely *Ku* and recharge mechanism for all time series at Beenham (E) and Newbury (F).

3.5 Discussion

With the exception of Saltbox, ARIMA models were successfully fitted to all long term hydrograph and rainfall time series. Pre-whitening by this method allowed the effective cross-correlation of relatively long, interannual time series not previously possible using simple first order differencing (Chae et al., 2010; Lee et al., 2006; Lehman and Rode, 2000; Mondal, 2004). A case study comparison of the impact of ARIMA prewhitening on the cross-correlation at Longacre showed that autocorrelations were reduced effectively. In addition, the cross-correlation plot using ARIMA prewhitening provides a clearer indication of when significant lags exist in the data (Figure 3.4 and Figure 3.5).

The cross-correlation of inter-annual series provided an indication of the dominant vadose flow mechanism operating in the long term, for example matric pulse or fracture flow. At all sites, models were also fitted to a number of sub-annual series representing periods from October through to March. Multiple sub-annual analyses were used to determine under what conditions the processes occur e.g. depth to groundwater table and rainfall amount. To avoid spurious cross-correlations, the cases in which ARIMA models were not fitted successfully were not included in the analysis. This includes all the hourly cross-correlation analyses at Hodcott and Saltbox. The implications for groundwater flood risk assessment are discussed, particularly in the context of modelling time steps.

Lee, Lawrence et al. (2006) suggest that borehole responses in the Chalk are related to locally controlled vadose zone thickness. As such, significant cross-correlation lags identified at 7 sites in the Pang/Lambourn have been plotted against mean depth to groundwater table (Figure 3.11A). Initial responses in comparison to groundwater depth are also plotted to provide an indication of when rapid, fracture flow type responses may have occurred (Figure 3.11B). Such responses may have consequences for groundwater flood risk assessment. For example, although the hazard is regarded as slow onset (Cobby et al., 2009) , an event could potentially be triggered relatively rapidly following rainfall.

At Northfield Farm on the Upper Chalk (Figure 3.3), the response to rainfall is rapid but includes a secondary response up to 31-35 days later. This pattern is dominant over the period August 2002 to December 2005 and is verified during a sub-period from October 2002 to March 2003. Both periods cover periods of high

and low rainfall and oscillations in groundwater conditions. It is difficult to say therefore when the fast and slow responses took place during these times. Indeed, the rapid response may have occurred when the groundwater table was near the surface in spring 2003. It is clear however that the river terrace deposits and vegetation cover of arable cereals did little to mediate a rapid response. Despite the rapid response, by substituting the lag time into Equation 3.1, the resulting *Ku* range indicates a matric pulse response. This suggests that the mean travel distance of 2.4 – 4.2 m within a day could be via a matric pulse. However, there may be a sub-daily response not picked up by the cross-correlations. Indeed (suspect) evidence of hourly lag analysis at Hodcott and Saltbox means this could occur at even deeper levels. The thickness of the river terrace deposits is unknown at Northfield. It could be that the rapid responses occurred as the groundwater table lies in this horizon when conditions are almost riparian.

The response over a multi-annual time series at Longacre (Figure 3.3) again indicates a rapid response (day 1-6), followed by a second slower response, 26-40 days later (Figure 3.11, A and B). Given a relatively deep vadose zone, the initial response at day 1 is likely to be a result of fracture flow (assuming a C of 0.0001). The longer lags are more likely to be a matric pulse mechanism (Figure 3.11, D). This provides support for evidence of a dual porosity in the Chalk vadose zone (Ireson et al., 2009; Price, 2000). The responses seem to vary as a function of mean depth of vadose zone. For example, the initial response in particular is at day 1 during October 2002 to March 2003 when the mean depth to groundwater table is 8 m in comparison to day 6 when the mean is 17 m (October 2003 to March 2004). However, in both cases, assuming a C value of 0.0001, both these initial responses could be attributed to rapid fracture flow. Here, the depth to the groundwater table seems to impact the timing of the initial response rather than the mechanism. Interestingly, the longer lags (>8 days) are absent in the 6 monthly time series. This could be because they cover a relatively wet period (October to March). Indeed the mean daily rainfall rate at East Shefford between March 2002 and December 2005 is 1.8 mm/day. Between October and March this is raised to 3.3 and 2.1 mm/day in 2002-2003 and 2003-2004 respectively. During dry periods, moisture content can be low in the vadose zone and so the matric pulse mechanism is slower. This combined with a longer travel distance means longer lags seem to be constrained to dryer periods, which was originally suggested by Lee, Lawrence et al. (2006). This

confirms previous observations that moisture levels of the unsaturated zone are an important influence on flow processes in Chalk (Price, 2000).

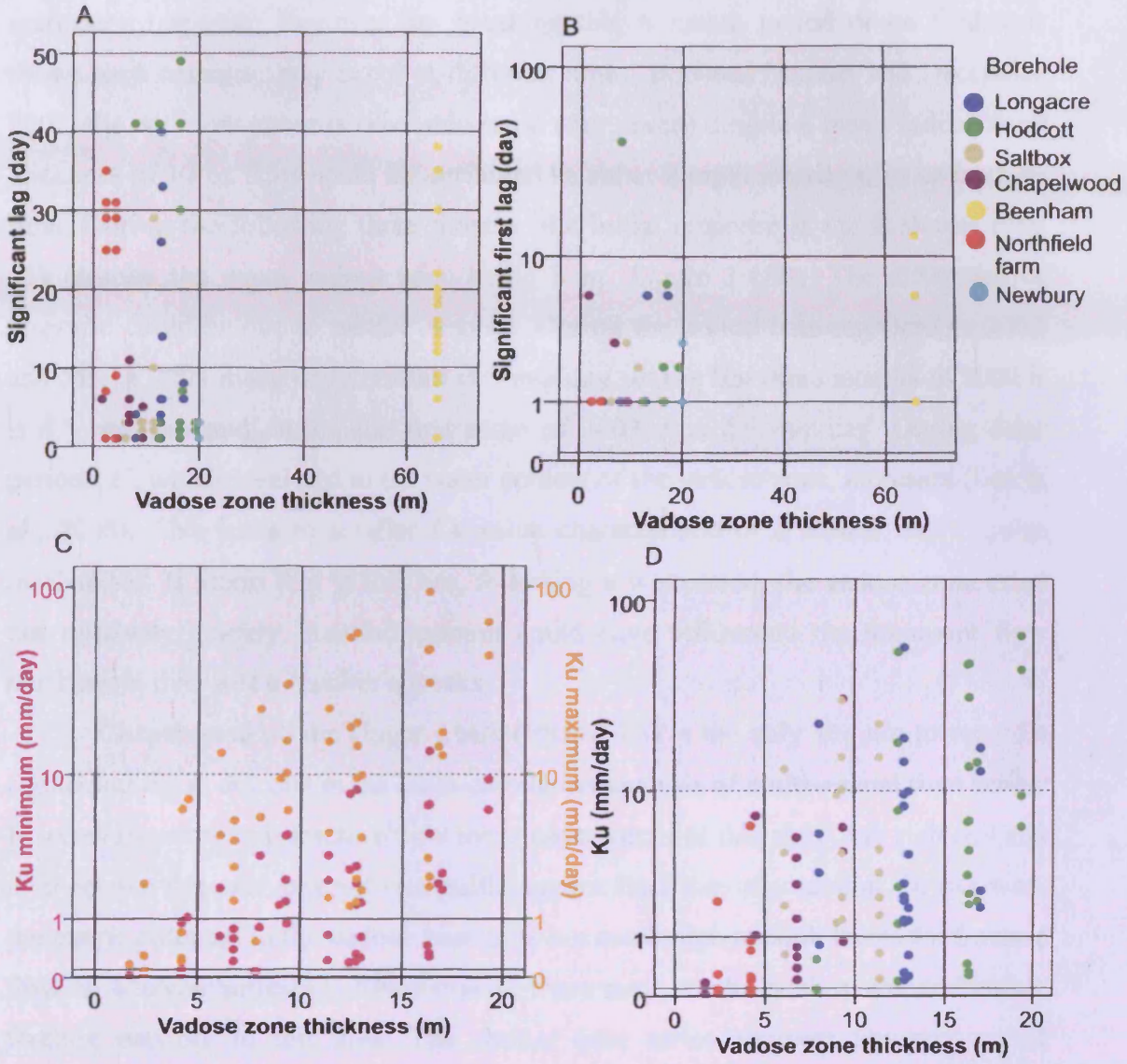

Figure 3.11 All (A) and first (B) significant lags as a function of mean vadose zone thickness and borehole including multi-annual and sub-annual series. Maximum and minimum estimated *Ku* depending on value of C, as a function of vadose zone depth (C) All estimated *Ku* values as a function of vadose zone depth at each site (D).

At Hodcott on the Upper Chalk (Figure 3.3) there is strong evidence of a fracture flow signal (Figure 3.11D). The cross-correlation with Peasemore between 2001 and 2005 suggests a significant lag at day 1 which, given a mean vadose zone thickness of 16.4 m, equates to a *Ku* values of between 13 and 94 mm/day. In this case even the lower bounds are within the accepted range of fracture flow. Even if this very rapid response only occurred at peak groundwater levels (i.e. within 7 m of the surface during February 2003), it still represents a fracture flow type response. There is also a clear secondary signal, associated with a matric response which can

be seen in Figure 3.11A. In addition, the cross-correlation analysis between October 2002 and March 2003 exhibits the familiar rapid initial response and slower secondary response. However, by breaking this 6 month period down further it shows each response may occur at different times. Between October and December 2002, the initial response is relatively rapid (day seven) despite a mean vadose zone thickness of 17 m. This could be attributed to either a rapid matric pulse or fracture flow. During the following three months, the initial response is much slower (day 41), despite the mean vadose zone being 8 m (Figure 3.11B). The difference in response could be due to rainfall amount. During the period between October 2002 and March 2003 mean daily rainfall is 3 mm/day. In the last three months of 2002 it is 4.5 mm/day and during the first three of 2003 it is 2.5 mm/day. During drier periods, C, which is related to the water content of the vadose zone, increases (Lee et al., 2006). This leads to smaller Ku value characteristic of a slower matric pulse mechanism. It seems that at this site, following a wet period, the vadose zone dried out relatively quickly. Rainfall amount could have influenced the dominant flow mechanism over just a number a weeks.

Chapelwood on the Upper Chalk (Figure 3.3) is the only site not to record a significant lag at day one in the cross-correlation analysis of multi-annual time series. It seems therefore that fracture flow tends not to occur at this site. Clay rich soil and river terrace deposits may act as a buffer against high intensity rainfall. In this way, the matric potential in the vadose zone does not reach high enough levels for fracture flow to become activated. Alternatively, there may not be such a comprehensive fracture network in this area. The shorter time series analyses however reveal contrasting evidence. During the period October 2002 to March 2003, there is a significant initial lag at day 1 (see Figure 3.11B). The shallow water table during this period (4.5 m depth) results in an estimated Ku range outside the bounds of fracture flow, although a sub-daily response could have been missed. The same season in 2004 to 2005 exhibits the same rapid initial response, despite a deeper vadose zone (9.4 m). Such a response suggests that fracture flow could actually be possible here, despite a modest mean rainfall rate of 1.8 mm/day during this time. This is in contrast to 3 mm/day on average during the period from 2002 to 2003. Further analysis at Chapelwood is hindered by the fitting of ARIMA models to some time series. The borehole response does however seem to be independent of vadose zone depth and mean rainfall rate.

The multi-annual cross-correlation analysis between Saltbox on the Middle Chalk and rainfall at West Ilsley (Figure 3.3) is the only site on the unconfined Chalk where the first and last response could be attributed to a fracture flow mechanism. However, sub-annual analysis does pick up evidence of a matric pulse response too. This could be because over the period from March 2002 to June 2006 the dominant mechanism is rapid fracture flow. During shorter sub-periods, e.g. from October 2002 to December 2002, a matric pulse mechanism is dominant or occurring simultaneously (October 2003 to March 2004). The response here does not appear to be due to vadose zone depth (Figure 3.11), neither mean daily rainfall rate or antecedent conditions. For example, the response between October and December 2002 is characteristic of a matric pulse despite a relatively high mean rainfall rate of 4.5 mm/day. The three months following exhibit no significant lags at all despite a mean depth to groundwater of just 3 m. The nuanced response to rainfall at Saltbox is clearly complex. Although evidence for fracture flow and transmission via a matric pulse is found, the conditions under which they occur is not clear here.

Cross-correlation analysis for two sites monitoring the confined Chalk aquifer at Beenham and Newbury (Figure 3.3) suggest direct recharge might be taking place here. However, Equation 3.1 and a typical range of C from 0.0001 to 0.0007 probably do not apply to the London Clay and so estimations of Ku can not be made. For this reason both sites are not included in Figure 3.11C and D. However, of particular interest is the evidence that rapid recharge appears to occur through the Palaeogene deposits. Usually recharge through Clay rich deposits to Chalk is regarded as negligible or at the least, slow and continuous (Jackson and Rushton, 1987). Here, a response within a day is seen at Beenham over a depth of approximately 66 m and over a shorter distance at Newbury. This rapid response is reflected in the 'spiky' appearance of the associated borehole hydrographs (Figure 3.10A and C). It is difficult to explain a response that resembles rapid fracture flow in an area where fractures are unlikely to be widespread and continuous. The result might be an artefact of the low fluctuation at these sites i.e. 2.8 and 1.5 m maximum at Beenham and Newbury respectively. Influence from upstream flow could be giving a false impression of a rapid response to individual rainfall events. However, the sites lie several kilometres away from the unconfined Chalk system. Assuming a typical maximum saturated conductivity (K, $[LT^{-1}]$) of the Chalk in this region of 180 m/day (Grapes et al., 2006) this explanation is unlikely. Beenham in particular

exhibits the largest spread of significant responses of all sites (Figure 3.11A). This could be indicative of a smeared recharge signal. Percolation could therefore constant throughout the year. However this does not explain only a rapid response at Newbury. The London Clay may be providing only a semi-confining layer for the Chalk aquifer. Percolation may be occurring rapidly via a modified piston displacement or fracture flow-like mechanism. At the same time, recharge may be occurring throughout the year, acting like a leaky reservoir.

3.5.1 Unsaturated flow and implications for groundwater flood risk

The response to rainfall events at all sites has been too rapid to be accounted for by intergranular matrix flow alone (typically only 3-5 mm/day). However the longest significant lag accounted for was 50 days, making it difficult to discern a matric pore flow signal. Over 50 days matric pore flow would travel only 250 mm. The majority of responses on the unconfined Chalk result in an estimated *Ku* within the range of <10 mm/day. Indeed when assuming a high value of *C*, only one *Ku* estimate is above the threshold (Figure 3.11C). This suggests that most recharge in the Pang/Lambourn occurs through a matric pulse, which agrees with findings of Lee et al. (2006) in similar geological setting. This suggests that a groundwater response over a significant distance can occur within one day via a matric pulse mechanism. Evidence for fracture flow was also found however, supporting the idea of a dual system of flow mechanisms in the Chalk (Ireson et al., 2009; Jones and Cooper, 1998; Smith et al., 1970).

In some cases, depth of the vadose zone seems to impact the timing of the first significant lag, e.g. at Hodcott and Longacre, although overall there is no significant trend (Figure 3.11B). Spearman's rank correlations of all, first and last lags against depth to groundwater (at all sites) results in correlation coefficients of 0.12, 0.07 and 0.04 respectively ($p>0.05$). It should be noted however that the average maximum lag is 26.5 for interannual analyses compared to 11.6 during the winter/spring months. This could reflect the longer lags being a function of responses during lower groundwater table conditions. Any influence of vadose zone thickness may be locally controlled or an artefact of wetter conditions i.e. rainfall intensity and antecedent conditions. It has been suggested for example that matric pulse speed and fracture flow initiation is locally controlled by rainfall rate and antecedent moisture

within the vadose zone (Ireson et al., 2009; Price, 2000). Lee et al. (2006) suggest that rainfall intensity (>5 mm/day) is a major factor in determining whether fracture flow takes place. Intra-site climatic variation is difficult to assess in this case given a relatively small sample size. However, some sites exhibit higher *Ku* values during wetter periods in comparison to dryer e.g. Longacre and Hodcott. Other sites however do not and in the case of Chapelwood exhibits a higher *Ku* during dryer periods. The critical level at which matric might switch to fracture flow cannot therefore be determined.

At all the sites on the unconfined Chalk there is evidence for a delayed secondary response. It is possible that the two distinct responses indicate separate fracture and matric pulse responses. In some cases, it has been possible to identify and provide explanations for periods when each is the dominant process. This was the case for example at Hodcott over the 2002-2003 period, where a wet period produced a rapid response followed by a dry period and slower response. This observation also highlights the possibility of variable matric pulse rates at the same site determined by prevailing climatic conditions.

The implications of the cross-correlation analysis in terms of groundwater flooding risk assessment and modelling are important. Firstly, the large range of *Ku* values illustrates that groundwater responses can be rapid even in the absence of fracture flow following high intensity rainfall and/or moist antecedent conditions. This suggests that although the conditions for groundwater flooding may take several recharge seasons to build up (Cobby et al., 2009), the triggering of an event may be rapid. In addition, the excess storage in the vadose zone may be converted to saturated horizontal flow as the water table rises rapidly. This was the suggested mechanism for the large magnitude flood event in the Chalk of northern France in 2000-2001 (Pinault et al., 2005).

Secondly, the groundwater table response to rainfall may be distributed over 40+ days in response to gradual vadose zone drying. An initially rapid response via matric pulse or fracture flow may subsequently slow if no further rainfall occurs. This smearing of a rainfall event should be taken into account when considering a model of flux between the soil zone and saturated flow. For this reason, a monthly recharge estimation procedure would account for initial and subsequent responses to rainfall. Applying daily recharge to a groundwater model would increase uncertainty as to when the flux would actually reach the water table. The monthly accounting

procedure described in Chapter 2 (GIS-DIRT) amalgamates daily rainfall into monthly values, which deals with the issue of when to apply recharge flux in the period following rainfall. Any issues with delayed recharge are therefore largely irrelevant.

Thirdly, both rapid and 'smeared' recharge appears to occur through the London Clay. The responses at Beenham and Newbury may at first resemble the unconfined response. Although the limited borehole fluctuations suggest any significant lags do not equate to the same amount of flux as the other sites, it is feasible that the lags are an artefact of a leaky pseudo-confining layer such as that originally proposed in Figure 3.2B. As such, GIS–DIRT does not discount recharge in any area of the catchment after the soil store.

3.5.2 Limitations

A significant cross-correlation at lag X between rainfall and borehole time series merely establishes a statistical relationship between the two. It does not directly reveal anything about the mechanism or reason for the response time. A borehole response may be due to other factors as well as vertical recharge for example lateral subsurface flow is difficult to discount. However, the water flux at each site would still have had to infiltrate the vadose zone and travel relatively quickly through the saturated zone. In this case the response is still the same, although the mechanism is slightly different to the proposed vertical fracture, matric pulse combination. Saturated conductivity values are also usually very low, limiting short to medium term responses particularly on interfluves. Evidence suggests that barometric pressure can influence groundwater levels in unconfined aquifers (Healy and Cook, 2002). In this case however hydrograph fluctuations are too significant or occur in confined sites. In addition, rainfall in the UK is usually associated with low pressure, so rises would be seen during the event rather than afterwards. Similarly trapped air is unlikely in a highly fissured system overlain by thin soils.

The impacts of pumping for public water supply or otherwise are difficult to assess as data is often classified and difficult to obtain. Such abstractions often operate at a similar rate on a daily basis, so any impact would be relative (Lee et al., 2006). Systematic weekly impacts would probably be observed in the borehole hydrographs or lag times and they are not. Irregular drawdowns or rebound should also be masked by using long term interannual time series.

A focus of this investigation has been interannual time series, during which time the vadose zone thickness could fluctuate markedly. The estimation of *Ku* from significant lag times and mean depth to groundwater can therefore be problematic. Shorter series are restricted to the winter or spring months. Limited inferences can therefore be made about flux mechanisms outside the winter months, when the vadose zone is likely to be thickest. At sites where the mean groundwater table is within circa 5 m of the surface, the maximum *Ku* estimation will always be within the bounds of a matric piston displacement mechanism. Improving sub-daily lag analysis to individual rainfall events would help this problem.

Finally, localised responses could be influenced by nuanced differences in site properties. These could include fracture development, Quaternary weathering, local weather conditions and ultimately complex combinations of all influencing factors. Such complexity hinders the development of a distributed catchment-wide vadose zone model for example, based on groundwater depth, soil properties, superficial geology, bedrock geology and antecedent moisture conditions.

3.6 Conclusions

This chapter has highlighted the efficacy of using ARIMA prewhitening as a tool for ensuring the robust cross-correlation analysis of borehole hydrographs with rainfall time series. 7 sites were analysed in the Pang/Lambourn for various time periods between 2000 and 2006. Statistically significant lags are interpreted as the time taken for the water table to respond to a rainfall event at a daily or sub-daily time scale. This has been found to vary from less than a day up to 7 weeks, though most fell within 40 days.

A rapid response (1–3 days) can occur at a site irrespective of vadose zone thickness or geological setting. At unconfined sites, these rapid responses can be attributed to either a matric pulse mechanism or in some cases, fracture flow. By assuming a likely range of antecedent moisture, represented by C, the *Ku* of the Chalk matrix can be estimated. Using a conservative value of C, most initial responses and all final lags can be attributed to this matric pulse mechanism. Even during relatively wet periods, the matric pulse seems to be the dominant mechanism by which recharge occurs. The prevalence of rapid responses ensures there is little association between depth of vadose zone and lag time. Because *Ku* of the Chalk matrix is dependent on the C, the rate of flux is liable to change. This is reflected in

secondary peaks up to several weeks after the initial response. These responses could be delayed responses to the same rainfall event. As the vadose zone is drained and the matric potential is reduced, C is increased and Ku is subsequently reduced. For example, an initial response could be via fracture flow. As the vadose zone dries out, this response could revert to a matric pulse. This is characteristic of the dual porosity of the Chalk. The large range of Ku values illustrates the importance not only of the material properties but also antecedent moisture conditions.

The implications for modelling groundwater flood risk are that groundwater table responses can be rapid even in the absence of fracture flow. In addition, the response can also be smeared over 40+ days. This smearing of a rainfall event should be taken into account when considering a model of flux between the soil zone and saturated flow. Although monthly recharge accounting allows for this delayed flux, the potentially rapid onset of a flood is not. In addition, recharge appears to occur through the London Clay in the south of the Pang catchment and so flux to the Chalk in these areas should not be discounted.

Chapter 4 Regional groundwater flow in the Pang/Lambourn: MODFLOW modelling

4.1 Introduction

This chapter looks at the saturated hydrogeology of the Pang/Lambourn catchment as a foundation for advanced mathematical modelling using two distinct methodologies. Firstly, a depth integrated, single layered MODFLOW model domain is parameterised using the inverse modelling technique PEST (Doherty, 2003). Secondly, a multi layered model is developed using the Graphical User Interface (GUI) Visual MODFLOW (VMF) (WH, 2000). In both instances, distributed recharge from GIS-DIRT provides a reliable input source. By coupling GIS-DIRT and groundwater flow models, a comprehensive representation of climate, surface and sub-surface hydrology is achieved. This can later be used to assess the risk of groundwater flooding in changing climate and land use conditions. Comparing the two techniques also provides an opportunity to identify the strengths and weaknesses of both approaches for groundwater flooding risk assessment.

4.1.1 Chalk hydrogeology, aquifer properties and Darcy's law

The Chalk is often regarded as having 'dual porosity'(Allen et al., 2007), whereby the primary mechanism for groundwater flow in the Chalk is via fractures up to about 2 mm diameter (Morel, 1980). Storage of water is however within both fractures and the pore matrix. This interaction of properties can leave Chalk catchments vulnerable to the dichotomy of being at risk from both prolonged and rapid contamination from pollutants (Jackson et al., 2007). Pollutants may reside in the pore matrix for a long period before being released for rapid flow through the fracture system. The same processes may contribute to the nature of groundwater flooding risk (DEFRA, 2006a; DEFRA, 2006b; Green et al., 2006; Pinault et al., 2005), which is discussed in further detail in Chapter 6.

Evidence has also been found for karstic-type rapid flow in the Chalk of southern England (Macdonald et al., 1998). Indeed extremely rapid (6000 m/day) groundwater flow through a discrete fracture system was observed using tracer tests at 'Blue Pool', near the perennial source of the river Pang (Figure 4.1) (Banks et al., 1995). However, a greater proportion of flow occurs through a network of smaller fractures (Rushton, 2003) and flow is laminar even in the vicinity of pumped

boreholes (Morel, 1980). This means Darcy's law (Equation 4.1) and numerical groundwater modelling is applicable in Chalk aquifers, where turbulent flow is minimal.

Hydraulic conductivity (K, [LT^{-1}]) describes the ease with which water moves through the rock and depends on pore size, arrangement and fractures as well as the dynamic characteristics of the fluid (water) such as viscosity and is defined by Darcy's Law (Darcy, 1856),

$$Q = -KA\left(\frac{\partial h}{\partial l}\right) \tag{4.1}$$

where Q is the volume of water per unit of time [L^3T^{-1}], A is the cross sectional area [L^2], at a right angle to the flow direction, through which the flow occurs. ***dh/dl*** is the hydraulic gradient [-]. A related property, transmissivity (T, [L^2T^{-1}]) is the capacity of an aquifer to transmit water and is equal to K multiplied by the saturated thickness of the aquifer [L]. Specific Storage (Ss, [L^{-1}]) of a saturated aquifer is defined as the volume of water that a unit volume of aquifer releases from storage under a unit decline in hydraulic head. The storage coefficient (S, [-]) is the volume of water released in a confined aquifer per unit surface area per unit decrease in hydraulic head. It is equal to the Ss multiplied by the aquifer thickness. Water derived from S is relative to; the expansion of water as the aquifer is depressurised (pumped) and, compression of the aquifer.

Aquifer properties data for the Chalk are available from 2000 pumping tests at approximately 1300 locations through England (Allen et al., 2007). Data from Yorkshire and Lincolnshire in north east England exhibit the highest T values (median 1800 m^2/d). This may be due to the relative hardness of the Chalk, allowing for fractures of greater aperture. Data from the Thames Basin on the other hand suggests a lower median value of 580 m^2/d (Allen et al., 2007). In contrast, different regions of the Chalk exhibit a similar range of S, from between 10^{-4} and 0.01, although these values are usually different to those used in modelling exercises (Allen et al., 2007). Several studies have highlighted the vertical and areal heterogeneity in Chalk aquifer properties (Grapes et al., 2006; Owen and Robinson, 1978; Rushton et al., 1989). For example field values of T in the Thames basin have been estimated to be between 1 and 8000 m^2/d (Morel, 1980). Such a large range in T is likely to be due to preferential flow paths which have important implications for localised groundwater flood risk.

4.1.2 Geology and Hydrogeology of the Pang/Lambourn region

The Chalk in England is made up of the North and South Province (Allen et al., 2007). The Pang/Lambourn catchment lies on the Southern Province. Indeed, the bedrock of the catchment is primarily made up of Upper, Middle and Lower Chalk formations (Figure 4.1). The formation members of the Southern Province and their spatial distribution in the Pang/Lambourn are detailed in Appendix 3.1. Members of the Palaeogene deposits predominant in the south east of the domain and underlying Greensand, outcropping in the north, are also detailed. Detailed hydrogeological studies were undertaken in the Pang/Lambourn during the 1960s and 1970s for the West Berkshire Groundwater Scheme (Owen, 1981). The scheme aimed to maintain flow in the Thames and Kennet for water supply to London during periods of drought by abstracting from the Chalk aquifer. Although the project has had mixed success, the rich data and borehole infrastructure legacy endures. Since much of the hydrogeological data collected is tied to the formations rather than the members, the focus is on these.

Cross sections of the Upper, Middle and Lower Chalk (Figure 4.1), are based on a three dimensional geological model developed by the British Geological Survey (BGS) and are validated by borehole logs (see Figure 3.3). The Upper Chalk is composed of soft white chalk with numerous flints. Middle Chalk in contrast is generally flintless. The Lower Chalk is also virtually devoid of flints but contains a high proportion of terrigious material. The lower 30 m of the Lower Chalk comprises Chalk Marl which has low permeability. Indeed, there is generally a gradient from high hydraulic conductivity to low from Upper to Lower Chalk (Allen et al., 2007). The total thickness of the Chalk is an average about 200 m and the geological structure is relatively simple, dipping south-east at about 1° toward the centre of the London Syncline. The major flow of groundwater in the aquifer is generally restricted to the uppermost 10 m below the water table. In the south east, the Chalk passes under softer impermeable Palaeogene strata which results in confined groundwater conditions (Figure 4.1).

Finch et al. (2004) highlighted the importance of topographical and geological structures in the focusing of localised groundwater movement to the surface. Significant hardbands exist at the interface between Chalk formations and are associated with spring development and preferential flow paths (Allen et al., 2007), most notably at the foot of the scarp slope bounding the catchment in the

north and north west (Figure 4.1). Here, the Lower Chalk is at outcrop where the contrast in hydraulic properties at the base of the scarp slope and groundwater table intersection has resulted in a line of perennial springs which drain eventually into the Thames, the Bristol Avon and the Hampshire Avon.

Springs and stream accretion occur catchment wide determined in part by lithology (Allen et al., 2007). For example, the Totternhoe Stone, which is an alternative name for the Zig Zag member of the Lower Chalk represents a relatively impermeable bed that impedes downward flow of the groundwater, encouraging it instead to escape to the surface (Allen et al., 2007). The base of the Middle Chalk is identified by the nodular Melbourne Rock (up to 5 m thick). This is underlain by a few metres of marly beds and is considered a preferential flow horizon and provides numerous springs. The Chalk Rock (alternative nomenclature for Lewes Nodular Chalk, up to 8 m thick) at the base of the Upper Chalk provides another important preferential flow horizon in the area. The Stockbridge rock (up to 5 m thick), lies towards the top of the Seaford Chalk member of the Upper Chalk. The thin porcelainous limestone horizon also has an important influence on groundwater flow and stream base flow in this an surrounding areas (Brenchley and Rawson, 2006). Springs also occur at other levels in the Upper and Middle Chalk, but they are usually small and tend to dry up during the summer and autumn. The interface between the Chalk and Palaeogene Clay deposits, particularly in the South of the catchment also seems to provide a hot-spot for springs due to hydraulic conductivity contrasts (Figure 4.1).

The topography of the drainage network also influences groundwater drainage. The orientation of the Pang perpendicular to the regional flow direction acts as a drain in wet seasons. In contrast flow in the Lambourn river is parallel to regional groundwater gradients. In contrast, flow in the upper Pang is predominantly perpendicular. More specifically the location of hardbands and intersecting dry valleys seems to focus this discharge, creating springs and potential flooding 'hot spots' (see Chapter 6) as well as irregular stream gaining profiles. The perennial source of the Pang (Figure 4.1) is the 'blue pool' spring complex near Bucklebury. Here, rapid discharge is focused all year round via karstic-like features. In contrast, the Lambourn flow follows the regional groundwater gradient. This leads to a more uniform flow accretion profile. Any variation that does occur is ascribed again to

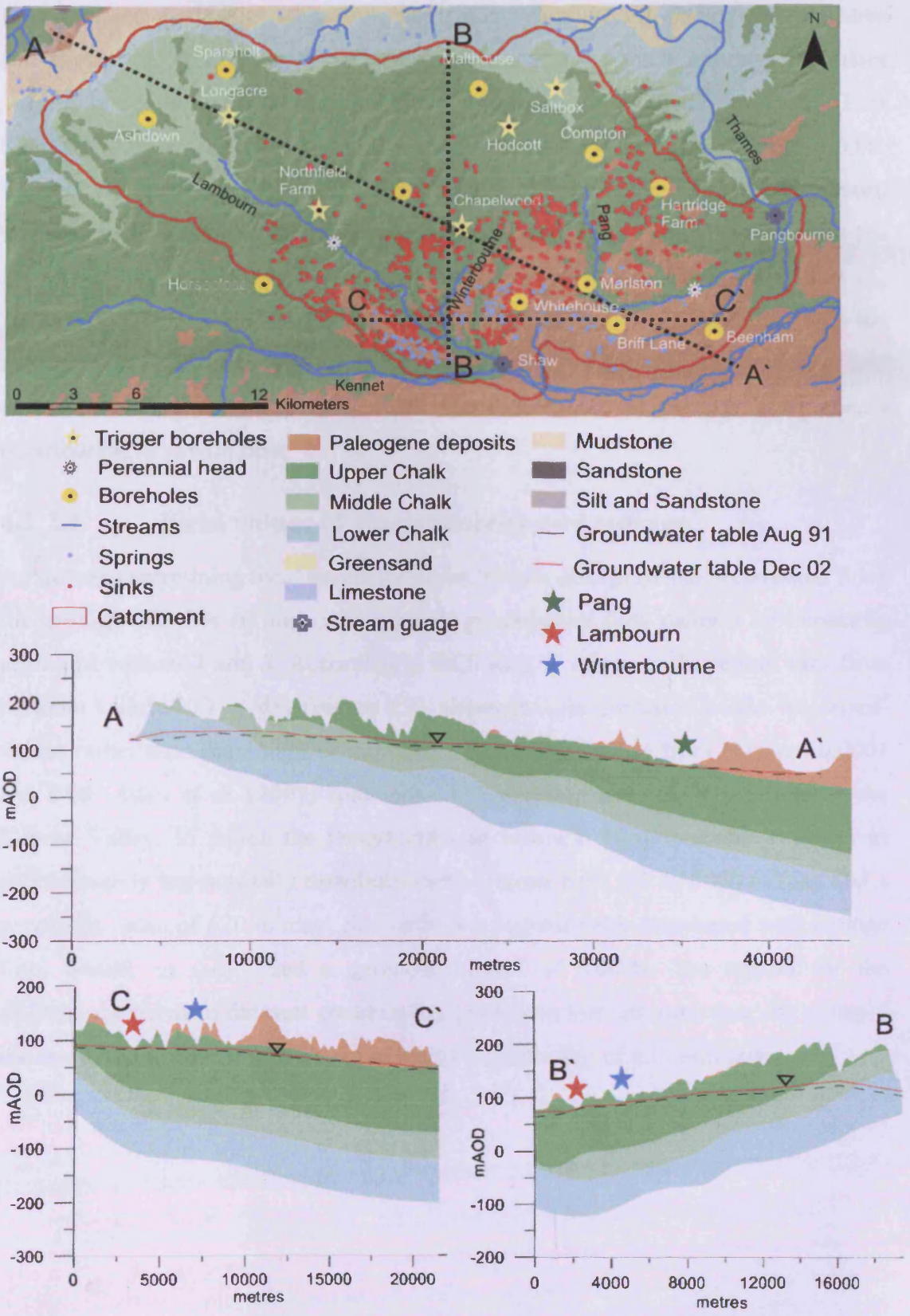

Figure 4.1 Geological map of the Pang/Lambourn Upper, Middle and Lower Chalk and Palaeogene formations; selection of representative boreholes and locations of EA trigger boreholes, streams and perennial stream heads and location of cross sections Below are the cross sections incorporating an interpolated groundwater surface from December 2002 and August 1991.

locally-scaled geological structures; variations in underlying geological structures and topography (Griffiths et al., 2006). The source of the Lambourn fluctuates seasonally between spring sources at Lambourn village in wet periods and near East Shefford (Figure 4.1). The Pang at Pangbourne has a Base Flow Index (BFI) of 0.86, whereas the Lambourn is 0.84 at Shaw (Figure 4.1). Further up in the Lambourn valley the BFI rises to 0.98 but remains around 0.87 in the Pang. This indicates the Lambourn has an almost exclusively groundwater fed flow regime (Griffiths et al., 2007). All BFI values show the streams are in close hydrological contact with the aquifer. This is the case even the Pang, which comprises a significant portion of less permeable Palaeogene deposits, where runoff is likely to provide a significant contribution to stream flow.

4.1.2.1 Field values of transmissivity and storage

As well as determining local spring locations, stream discharge and preferential flow, the geology also has an impact on regional groundwater flow patterns by impacting areal and vertical T and S. According to BGS data, T values in the region vary from between 1 and 3200 m^2/day (Figure 4.2), although these are based on the 'preferred' values rather than maximum or minimum. Values of S range from between 0.0001 and 0.08. Allen et al. (2007) summarise 117 pumping tests at 74 locations in the Kennet Valley, to which the Pang/Lambourn belongs. They describe T values as approximately log-normally distributed with a range from 0.5 to 8000 m^2/day and a geometric mean of 620 m^2/day. Similarly, S is log-normally distributed with a range from 0.0001 to 0.071 and a geometric mean of 0.0006. The reason for the discrepancy between datasets could be from pumping test interpretation, for example the estimated aquifer thickness or the use of the reporting of different tests.

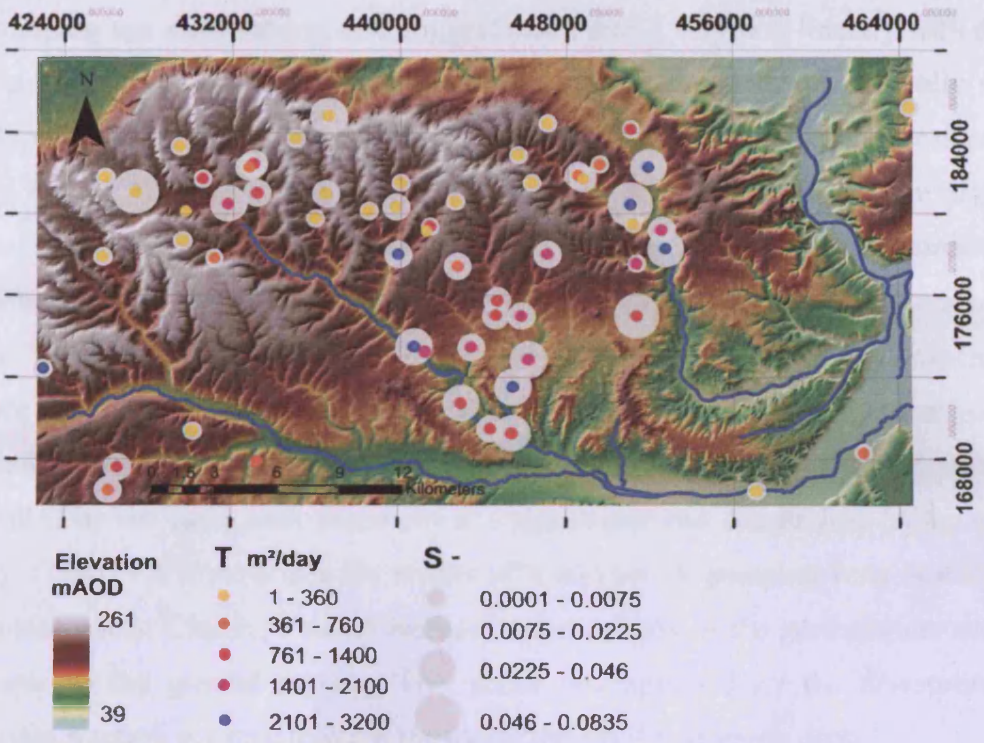

Figure 4.2 Location and value of 'preferred' point transmissivity and storage estimations based on pumping tests and provided by the BGS (Allen et al., 2007).

Previous numerical modelling of the region has highlighted the established trend that T is much greater in the main valleys (2000 m^2/day) than within the interfluves (50 m^2/day). Similarly, S are estimated to range from 0.015-0.03 to <0.005, within the valleys and interfluves respectively (Griffiths et al., 2006; Rushton et al., 1989). Others suggest higher values of 600 – 10800 m^2/day and 0.35 and 2 for T and S respectively (Grapes et al., 2006). An observed reduction in T away from the valleys can be due to a reduction in permeability due to a smaller frequency of fractures or a thinning of a high permeability layer. This could be because groundwater flux is generally greater in the valleys allowing a greater dissolution of fractures. Conversely on the interfluves, groundwater is more likely to become saturated with calcium carbonate as it passes through the thicker vadose zone, therefore reducing its fracture enlarging efficacy (Allen et al., 2007; Rushton et al., 1989). A similar variation for S was also suggested, which could be accounted for in similar fashion. What is generally agreed upon is that areal variation in T across the region is accounted for by three parameters (Allen et al., 2007);

1. Depth to minimum rest water level (i.e. thickness of vadose zone).
2. Saturated thickness of the aquifer.
3. Distance away from winter flowing streams.

Pumping test observations also suggest that T and S vary non-linearly with depth (Owen and Robinson, 1978; Rushton et al., 1989). Permeability is generally more developed towards the top of the Chalk. T within the Upper Chalk is greater than that within the Middle and Lower Chalk (680 m^2/day in comparison to 570 m^2/day). S values are also higher in the Upper Chalk due to a greater density of fractures. This could be due to a higher degree of weathering in the relatively shallow zones of the Chalk. Indeed, it is usually Upper Chalk in which the groundwater table fluctuates (Figure 4.1). It is this fluctuation which accelerates dissolution and enlargement of fractures. This apparent correlation between S and T would be expected if both were controlled by the same rock property i.e. fracture size and distribution (Allen et al., 2007). Figure 4.3 summarises the results of a number of pumping tests at different rest water levels. Clearly, T and S increase exponentially as the groundwater surface is nearer to the ground surface. This could be explained by the dewatering of important fracture systems towards the top of the aquifer as levels drop.

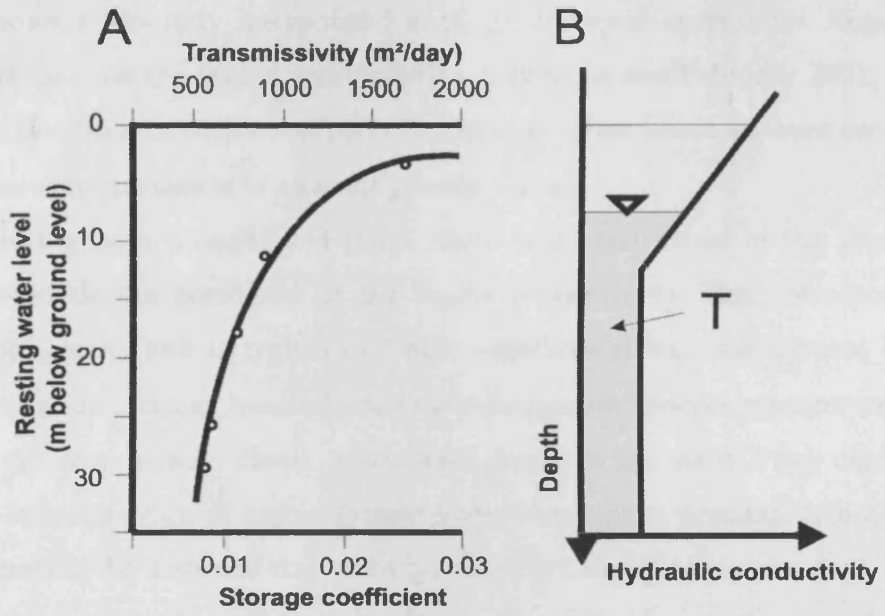

Figure 4.3 (A) Non-linear decrease in T and S estimated from pumping test at progressively deeper rest water level (Owen and Robinson, 1978). (B) Vertical distribution of transmissivity used in a groundwater flow model of the Kennet valley (Rushton et al., 1989).

If a groundwater model is to be used to simulate and predict flows at high groundwater levels, it will be important to take into consideration the changes in T and S with depth. Rushton et al.(1989) used a 'cocktail glass' vertical distribution of T to represent this vertical anisotropy. In their model, T is represented as being fairly constant throughout most of the thickness of the aquifer. However, in the top few metres, within the zone of water table fluctuation, T increases non-linearly. This is

the case both in the valleys and on the interfluves (Figure 4.3B). This phenomenon may be particularly important to model for groundwater flooding risk analysis. As groundwater levels rise, flow may be accelerated leading to a reduction in residence time between recharge and discharge.

4.1.2.2 Groundwater levels

The groundwater table cross sections included in Figure 4.1 are taken from mean monthly observation borehole values interpolated using the kriging method (Hughson et al., 1996; Kitanidis, 1999). Groundwater levels include the description of the piezometric surface in confined areas. Kriging interpolation is appropriate when there is a spatially correlated distance or directional bias in the data. In this case, groundwater levels are broadly expected to reflect the general trend in topography (see Appendix 3.2 for details of the kriging method used). The observation borehole locations used in the interpolation are shown in Figure 4.4, which shows a similarly interpolated areal groundwater surface for August 1992, during which time the region was suffering a drought and February 2001, during a period of flooding. In both cases perennial stream valley locations were used to 'fix' the groundwater surface at or near the ground surface.

During both drought and flood, there is a clear dome in the groundwater surface towards the northwest of the region (Figure 4.4). This corresponds with higher topography and is typical of Chalk interfluve areas, characterised by lower conductivity and storage. Similarly there is evidence of a steeper gradient in contours towards the east in both cases. A localised dome in the south Pang catchment is likely to reflect a ridge of higher ground under Palaeogene deposits. Interestingly, it would normally be assumed that recharge levels are negligible in this area, therefore limiting the propagation of a raised dome. A sustained annual smeared recharge signal through the less permeable confining layer could be feeding the elevated groundwater surface (see Chapter 3). During the period of higher regional groundwater levels, the dome of groundwater at the interfluves in the north west develops in height as well as migrating eastwards. This coincides with a tightening of the groundwater contours, particularly in the upper Pang and all along the Lambourn. It is possible that the dome is feeding this increased regional gradient and associated increase in discharge during the flooding episode in 2001.

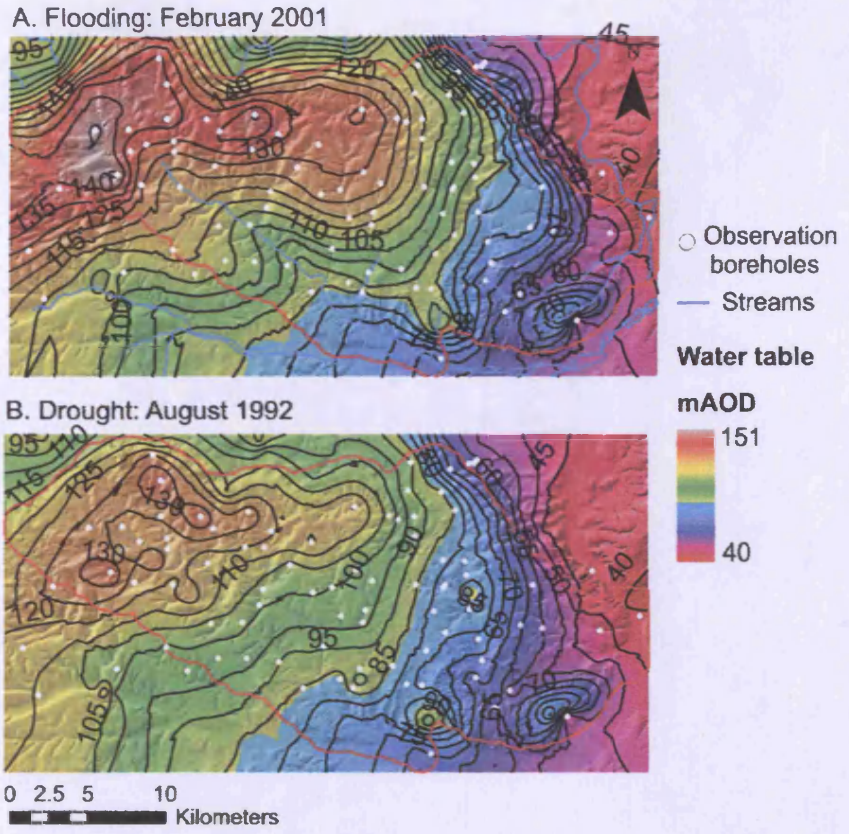

Figure 4.4 Monthly mean groundwater levels for (A) February 2001 and (B) August 1992, interpolated using the ordinary kriging method between observation boreholes within and beyond the boundary of the Pang/Lambourn surface water catchment.

Observation boreholes have been highlighted which provide a comprehensive sample of different hydrogeological settings (Figure 4.1). A comparison between hydrographs for the representative boreholes can be found in Appendix 3.3. Ashdown Park (164 mAOD) and Sparsholt Down (176 mAOD) boreholes are representative of Chalk interfluves characterised by the dome-like groundwater surface (Figure 4.4). Both hydrographs exhibit large seasonal fluctuations (20-30 m), primarily due to recharge fluxes from the surface. Neither borehole is overlain by superficial deposits which could act as a barrier to infiltration (Figure 1.2B). Oak Ash (173 mAOD), Horseclose (139 mAOD) and Hartridge (128 mAOD) boreholes are still relatively high up on the interfluves but are overlain with or in close proximity to Clay-with-flints superficial deposits. Localised runoff recharge processes are more likely to be occurring in this area. Individual responses here are likely to be a localised interaction of recharge and local flow processes. Seasonal fluctuations remain high at these sites; between 8 to 20 m per annum. Compton (99 mAOD) and Malthouse (129 mAOD) represent boreholes along the ephemeral Pang valley. Maximum fluctuations here too remain fairly high, between 15–20 m.

Marlston (75 mAOD) lies within 200 m of the lower Pang, approximately 5 km upstream of the perennial head and is overlain with river terrace deposits. Here the hydrograph is associated with low fluctuations (circa 2 m) close to the ground surface. This is to be expected in the vicinity of a Chalk stream in close hydrological contact with the aquifer. Whitehouse (104 mAOD) and Beenham (101 mAOD) are both overlain by Palaeogene deposits. Whitehouse is in a region not likely to be confined perennially, allowing for fluctuations up to 8 m annually. This could be the result of locally focussed recharge fluxes. Beenham on the other hand exhibits annually stable levels approximately 40 m beneath the ground surface indicating fluctuations are inhibited to an extent by the confining Palaeogene deposits. This could be due to a smearing of the recharge signal through the less permeable confining deposits, discussed in Chapter 3.

Due to the large number of observation boreholes in the catchment, these representative boreholes can provide a useful sub-sample to assess the success of the modelling, particularly during transient simulations. The locations of EA trigger boreholes are also highlighted in Figure 4.1. These are important for groundwater flood risk assessment and warning systems (see Chapter 6) and so simulation here was also a particular focus in the model development.

4.1.3 MODFLOW, Visual MODFLOW and PEST

MODFLOW is a three-dimensional finite-difference groundwater flow model (Harbaugh et al., 2000; McDonald and Harbaugh, 1988). The model domain (aquifer) is broken down into grid squares and the governing equation is solved using iterative methods at the centre point of each grid square. The governing partial differential equation used in MODFLOW is

$$\frac{\partial}{\partial x}\left(Kx\frac{\partial h}{\partial x}\right)+\frac{\partial}{\partial y}\left(Ky\frac{\partial h}{\partial y}\right)+\frac{\partial}{\partial z}\left(Kz\frac{\partial h}{\partial z}\right)=Ss\frac{\partial h}{\partial t}+W \qquad (4.2)$$

where t is time [T], h is groundwater head [L], K is the hydraulic conductivity [LT^{-1}], Kx,, $K y$ and Kz are hydraulic conductivities along the x, y and z axis respectively. Ss is the specific storage of the porous material [L^{-1}]. W is a volumetric flux per unit volume representing sources and/or sinks [L^3T^{-1}]. $W<0$ represents flow out of the system and $W>0$ for flow into the system. W can be broken down further to represent constituent sources and sinks for example,

$$W = R + Qr + Qs + Qg \qquad (4.3)$$

where *Qr*, *Qs* and *Qg* represent discharge from rivers and springs and groundwater respectively and *R* is recharge [L^3T^{-1}]. In this case recharge flux is constrained by implementing GIS-DIRT. When Equation 4.2 is combined with boundary and initial conditions, it describes fully saturated, transient three-dimensional groundwater flow in a heterogeneous and anisotropic medium. MODFLOW solves the finite difference form of the partial differential in a discretised aquifer domain, represented using rows, columns and layers. It is a modular code and numerous packages have been developed to simulate different boundary conditions, e.g. springs, rivers, observation wells and abstractions.

When modelling an aquifer, certain assumptions are often made. For example, a single layered (two dimensional) confined aquifer can be represented by,

$$\frac{\partial}{\partial x}\left(Tx\frac{\partial h}{\partial x}\right)+\frac{\partial}{\partial y}\left(Ty\frac{\partial h}{\partial y}\right)=S\frac{\partial h}{\partial t}+W+L \qquad (4.4)$$

where *Tx* and *Ty* are components of transmissivity [L^2T^{-1}]. *S* is the storage coefficient [-] and *W* is flow into and out of the system [L^3T^{-1}]. In this case vertical flux between multiple layers could be via a leakage (*L*, [T^{-1}]) term determined by vertical hydraulic conductivity and layer thickness (also referred to as *VCONT*, [T^{-1}]). When modelling regional Chalk aquifer systems, it is common for the conditions to be assumed to be confined. This means that *T* does not vary during a transient simulation, which maintains numerical stability and allows long transient simulations, including extreme climatic conditions.

Parameter estimation (PEST) techniques have been widely used in groundwater model calibration studies (Bravo and Jiang, 2002; Hill, 2007) to inversely provide a distribution of aquifer properties given known inputs and outputs from the system, for example recharge and groundwater levels. PEST inversely parameterises the discretised aquifer domain such that the groundwater levels (i.e. model result) at cells representing the location of observation boreholes are optimised (Alcolea et al., 2006; Doherty, 2003). Values of *T* (or *K*) and *S* (or *Ss*) are systematically perturbed, the model ran, and model error iteratively minimised. Often the parameters are constrained by estimates of the maximum and minimum values, although there is limited control on the resulting areal (or vertical) distribution.

A second popular method of parameterisation is where prior data and knowledge are used in conjunction with 'trial and error' calibration to minimise the error and develop realistic water fluxes and balance (Rushton, 2003). Usually, the

process of assigning conductivity and storage values throughout the domain is done using a GUI such as VMF. VMF provides a straight forward and user-friendly data pre- and post-processing environment. The user can import distributed parameter values from GIS, such as recharge values (e.g. from GIS-DIRT). Alternatively, values can be input manually to model. Boundary locations and conditions, including rivers, drains can also be assigned in the same way. By interactively viewing and modifying the model domain, intuitive modifications can be made to develop the conceptual model. Integrated post-processing visualisation allows for relatively rapid calibration procedures. For example, results at individual observation boreholes, or groups, can be extracted and residuals calculated interactively (WH, 2000).

4.1.4 Groundwater modelling in the Pang/Lambourn

Despite the esoteric nature of Chalk hydrogeology, several groundwater models of the Pang/Lambourn region have been documented from the earliest in 1976 (Connorton and Reed, 1978; Morel, 1980; Oakes and Pontin, 1976; Robinson, 1976). Rushton, Connorton et al. (1989) for example developed a vertically non-linear mathematical model on a 1 km grid for the entire Kennet valley, which included the Pang and Lambourn sub-catchments. The model was used for predictive purposes, with a particular emphasis on the use of groundwater for river augmentation. Here, the main issue to be addressed was the yield of pumping wells during periods of low groundwater levels and low stream flows. An important consideration was that rapid lateral transfer of recharge through the aquifer to streams reduces the quantity of water that is stored and available during the summer months. This same rapid response could have important consequences for groundwater flooding risk and is linked to the high values of T in the Upper Chalk (Figure 4.3). Using the model, it was suggested that river augmentation under the Thames Groundwater Scheme could operate successfully during a dry year but full recovery could take three years.

Although modelling vertical anisotropy has been identified as important in the Chalk (Rushton et al., 1989), some models still employ a single integrated layer (Grapes et al., 2006). Later models were characterised by an increased grid resolution (Clausen et al., 1994) and a greater focus on resource management and ecology protection (Grapes et al., 2006). In addition, other models were also developed across other Chalk aquifers in the UK (Cross et al., 1995) and France (Korkmaz et al., 2009). More recently, the research emphasis seems to have shifted to modelling

unsaturated flow in the Chalk (Ireson et al., 2009). There have been no published accounts of numerical modelling for the purpose of assessing the impact of climate and land use change on groundwater flooding risk.

4.2 Aims and objectives

The aim of this chapter is ultimately to develop a saturated groundwater model for the Pang/Lambourn, with an emphasis on simulating extreme (high) groundwater flow conditions using recharge input from GIS-DIRT. This model will later be used for groundwater flood risk assessment. The objectives are to:

- Inversely parameterise a single layered, depth integrated MODFLOW model domain to recreate borehole hydrographs across the domain over periods of groundwater flooding and drought.
- Make use of the field aquifer property data and visual MODFLOW to simulate the physical properties of the Pang/Lambourn aquifer over several layers and recreate borehole hydrographs and river base flows.
- Determine the implications both approaches have for our conceptual understanding of regional and local groundwater flow in the Pang/Lambourn.
- Assess which method is best for modelling multiple climate and land use scenarios and flood mitigation strategies in the Pang/Lambourn and elsewhere.

4.3 Methods

Two contrasting modelling methodologies have been developed. One was a single layered domain inversely parameterised using PEST in which the boundary of the model coincides with the surface water catchment. A second model incorporates the different hydrological properties of the layered Chalk formations in an extended domain where rivers and spring lines act as the boundaries to the model. The following section details the development of each model.

4.3.1 Single layer groundwater model (PEST)

The Chalk aquifer of the Pang/Lambourn catchment was implemented as a single integrated layer using MODFLOW 2000 (Harbaugh et al., 2000). The top and bottom of the aquifer were determined from the three dimensional geological model provided by BGS representing the top of the upper and bottom of the lower chalk

respectively (Figure 4.1). To avoid model instability at the interface between a high and relatively low conductivity layer, the Palaeogene London Clay deposits in the south of the catchment are not modelled (Figure 4.1). Instead, the entire system is assumed to be confined (layer type 0 is MODFLOW). In doing so, S and T values remain constant throughout the simulation which prevents the numerical instability inherent in modelling unconfined systems, where values of T are dependent on K and the (unknown) saturated thickness of the aquifer at that particular stress period. It was also assumed that the London Clay would have little impact on catchment scale groundwater flood risk assessment. For instance, none of the EA trigger boreholes are in this region (Figure 4.1).

The groundwater divide and model boundary were considered to coincide with a 1 km buffer of the surface water catchment (Figure 4.1) and so the boundary of the active model domain was assigned as a no flow boundary. The model covered a total area of 554 km^2, split up into 100 x 100m cells, giving a total of 55400 active cells (430 columns and 220 rows). In order to aid the integration of GIS-DIRT, the active domain boundary coincides exactly with that of the recharge model (see Chapter 2 for details). Downscaling of the 1 km recharge output was achieved by implementing a resampling step into the original GIS-DIRT code breaking down the grid cells to 100 m. The raster cells were then converted to comma separated files (.csv) and compiled into a large transient recharge file (.rch) using a VBA macro implemented in Microsoft Excel™. The recharge time series constrains the MODFLOW model runs to between April 1978 and December 2006, a total of 345 stress periods. The initial heads for the model corresponded to an interpolated groundwater surface for April 1978. The locations of the river cells (i.e. Lambourn, Pang and Winterbourne) were digitised from OS Meridian vector data (see Figure 4.1). The river stage for each cell was taken to be the top of the Chalk and the bottom 0.2 m below. The river bed conductance (Kv) was assigned a value of 300 m^2/day across the model, comparable to Grapes et al. (2006). Accurate and widespread pumping data was difficult to obtain due to data privacy restrictions and therefore the model is assumed to be a naturalised system.

Spatially continuous T and S values are defined inversely based on groundwater level observations and recharge flux from GIS-DIRT. The process of inverse parameterisation was performed with pilot points at locations including observation boreholes (Doherty, 2003). In this method, T and S were optimised at an

array of points and values are interpolated across the model domain before each model run. Initially maximum and minimum values are assigned at each pilot point according to field data and previous modelling studies. For example, T constraints were between <1 and 10000 m^2/day (later exceeded by factorisation of entire array) and S between 0.1 and $1e^{-6}$. After the model is run, automated incremental adjustments are made to the values at the pilot points and re-interpolated. This iterative procedure is carried out for T and S distributions in turn until an optimal spatial distribution is reached by minimising the error between observed and modelled groundwater heads. The Preconditioned Conjugate-Gradient (PCG) solver package was used for each model iteration (Hill, 1990).

Finally, a sensitivity analysis was carried out using the calibrated model, where a single borehole was used (Briff Lane, Figure 4.1) to assess the impact of systematically perturbing T, S and recharge flux into the model. The Root Mean Square (RMS) error was used as the primary quantitative indicator of how well the model performed. The RMS provides a measure of how much a dependent series varies from its model-predicted level, expressed in the same units as the dependent series (Kelly, 2003). The smaller the RMS, the more accurate the simulation is. The equation for RMS can be found in Appendix 3.4.

4.3.2 Multi-layer Visual MODFLOW model

The Chalk aquifer of the Pang/Lambourn was also developed into a multi-layered model using VMF (Harbaugh et al., 2000; McDonald and Harbaugh, 1988). Early versions of the model consisted of layers based on the zone of maximum groundwater fluctuation and individual geological members of the Chalk. Due to the constraints of VMF however, the model was ultimately limited to the three Chalk formations allowing for the observed tendency of an increase in T from Lower to Upper Chalk. Similarly to the single layered model, the confining Palaeogene Clay layer dominating the lower Pang catchment is not simulated. Model cell size remains 100 m over 748 km^2 i.e. 420 columns and 220 rows. Although this is 10 fewer columns than the single layered model described above, a greater proportion of the domain is active (Figure 4.5). GIS-DIRT was used to provide recharge data over the extended domain (see Appendix 3.5). Annual average recharge between January 1990 and December 2005 was used in the calibration of the steady state model (between 14 and 297 mm/yr). Monthly recharge over the same time period was used

in the transient model. The modelled time period was shorter than the single layered model to allow for longer model run times, however it still included extreme drought and flood events.

The VMF model areal domain was extended beyond the single layered model to make use of the natural groundwater catchment divide of the River Kennet in the south, River Thames in the north east and spring line at the base of the scarp slope in the north and north west (Figure 4.5). Boundary conditions were chosen to reflect this; the river Thames and Kennet were assigned as Constant Head Boundaries (CHB) equivalent to the ground surface. Although these river levels are likely to fluctuate, particularly during a flood event, for monthly time steps this is a pragmatic assumption. In addition this assumes the groundwater surface is in direct contact with these river valleys all year round. In the north, the spring complexes along the scarp are assumed to be approximately equivalent to the bottom of the lower Chalk. This is based on the assumption that the springs generally flow from the base of the Lower Chalk at the interface with the underlying Greensand formation (Figure 4.5). The eastern boundary is treated as a General Head Boundary (GHB) in order to avoid unnecessarily extending the model domain to all natural boundaries i.e. the confluence of the River Kennet with the River Thames to the east. Groundwater heads equivalent to the ground surface were assigned, with a distance of 1000 m and average hydraulic conductivity (K) of 1 m/day, comparable to nearby calibrated values of Chalk K (Figure 4.9). A no flow boundary was assigned around the remaining cells of the domain boundary. The CHB and GHB boundary conditions are equivalent in each of the three model layers (Figure 4.5).

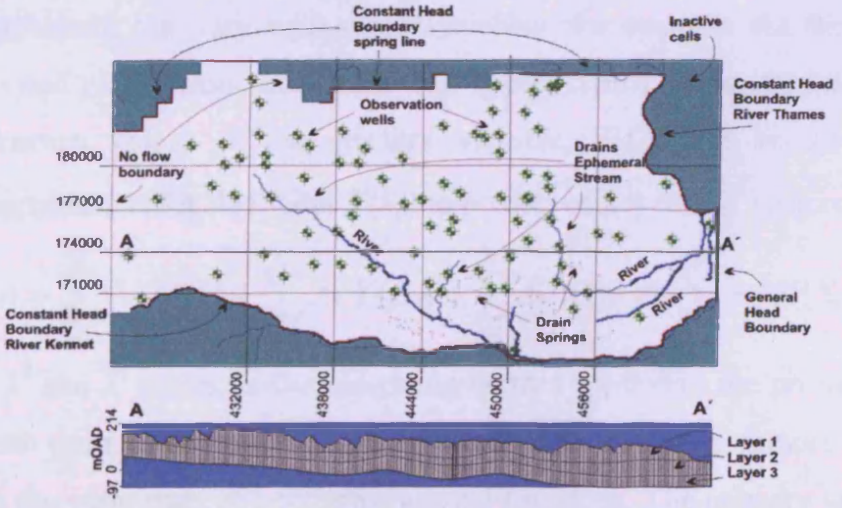

Figure 4.5 Active model domain and areal distribution of major boundaries conditions in the VMF model (layer 1). A-A' cross section across layers 1-3 representing the Upper, Middle and Lower Chalk formations.

Rivers are assigned using the river package, which simulates the influence of a surface water body on the groundwater flow. In lieu of field data, the river stage was assumed to be at the ground surface and the channel 0.9 m deep, 5 m wide and with a riverbed thickness of 0.1 m. The *K* value of the riverbed material is assumed to be 1 m/day, comparable to the conductivity of the GHB in the east. The default conductance formula in VMF (WH, 2000) converts *K* to a conductance range of between 300 and 6000 m^2/day, the lower bounds of which is comparable to the value adopted by Grapes et al. (2006). Similarly to Grapes et al. (2006) ephemeral streams and springs outside the northern scarp area are assigned as drains. In contrast to the river package, groundwater is only ever discharged at a drain cell, while no contribution is made from surface water. Drain, i.e. spring or stream, elevation was assumed to coincide with the ground surface and vertical *K* was kept equivalent to perennial river reaches (1 m/day). *K* values for rivers and drains were later factorised during the calibrating process to improve the simulation of base flow in the Pang and Lambourn.

Field values of *T* and *S* (Figure 4.2) were converted to *K* and *Ss* assuming an aquifer thickness between the groundwater table in February 2001 and the bottom of the Chalk. *K* and *Ss* were then interpolated using cokriging which is similar in principle to kriging, except that it uses information on several variables to produce a continuous interpolated prediction surface. Cross-correlations between the primary variables and all other variables are used to make better predictions. It is useful when interpolating between sparse data points where other correlated variables are sampled more frequently. This makes it ideal for *K* and *Ss* which are measured sporadically over the catchment, but vary with other variables, for example the distance away from valleys and vadose zone thickness. Cokriging extends the concept of kriging by using the known values of the primary variable, $Z(S_i)$, and known values of correlated variables, $Y(S_v)$, $X(S_t)$ and $K(S_d)$ to predict values of $\hat{Z}$ at position S_o;

$$\hat{Z}(S_o) = \sum_{i=1}^{N} \lambda_i{}^1 Z(S_i) + \sum_{v=1}^{N} \lambda_v{}^2 Y(S_v) + \sum_{t=1}^{N} \lambda_t{}^3 X(S_t) + \sum_{d=1}^{N} \lambda_d{}^4 K(S_d) \qquad \textbf{(4.5)}$$

where λ^1 λ^2 λ^3 and λ^4 represent the weighting factors applied to the primary, second, third and forth (correlated) variables respectively. The weighting factors in this case are based on the variogram and cross-variogram functions. The primary variable here is either *K* or *Ss*. The other correlated variables are, depth of the vadose zone, aquifer thickness and distance from valleys (Hughson et al., 1996; Kitanidis, 1999). The

cokriging procedure was carried out in ArcGIS where the vadose zone depth was assumed to be the groundwater table in August 1992 to the top of the Chalk. See Appendix 3.6 for datasets used and the resulting distribution of *K* and *Ss*. The average standard error of prediction is 6.4 m/day and 0.00001 m^{-1} for *K* and *Ss* respectively. This is comparable to the error associated with ordinary kriging using just point values of *K* and *Ss*. However, the benefit of a weighting model in data sparse regions gives added benefit. Zones were delineated in VMF using groundwater contours and assigned to the distributed values of *K* to allow local calibration control (Appendix 3.7). Trial and error calibration of *K* was performed on the steady state model by multiplying zones by 'factors'. 45 zones were assigned to each of the three layers in the model. An effort was made to maintain a graduation of factor values from Lower to Upper Chalk in order to reflect the observation of higher *K* towards the surface. In such a way a pseudo-cocktail glass vertical distribution of *K* was modelled. The entire *Ss* array was also factorised to recreate a similar vertical distribution. The Waterloo Hydrogeologic Solver for Visual MODFLOW was used for each model run (Harbaugh et al., 2000).

The RMS error was used as the primary quantitative indicator of how well the model performed. In addition, a water budget for the entire domain was carried out to assess the major influences on groundwater flow in the Pang/Lambourn. Base flow analysis was also carried out for both the Pang at Pangbourne and Lambourn at Shaw to allow riverbed *K* values to be constrained (see Figure 4.1 for gauge locations). The base flow component was separated form daily observed flows using the WHAT method (Lim et al., 2005) and averaged out to monthly values. This was then compared to net river leakage out including drainage from ephemeral portion of the streams i.e. drains.

4.4 Results

The single and multi-layered models were calibrated and compared against observation boreholes across the Pang/Lambourn and each other. The major focus of the modelling exercise was to assist in groundwater flood risk analysis making adequate long-term simulation of EA trigger boreholes (peaks) important. The models were also tested in detail across a select number of boreholes that represent a sample of hydrogeological settings.

4.4.1 Single layer model calibration and output

The process of inverse parameterisation using PEST resulted in an areal distribution of T and S as shown in Figure 4.6A and B. The values of T converged upon ranged from between 3 m^2/day to 30000 m^2/day. It is difficult to discern any significant spatial pattern in the areal distribution although zones of high T appear to occur in the headwaters of the Lambourn and Pang, perpendicular to the Lambourn and in the lower reaches of the Pang. These features do not seem to correspond to topography or geology, including aquifer thickness. The value of S varies between 0.069 and $1e^{-6}$ and was generally greater in the south of the catchment. An exception was a localised zone of higher values in the north west of the Lambourn valley. Aside from this zone, high storage seems to be associated with the regions overlain by Palaeogene deposits, where the Chalk is often confined and the stream flow is perennial.

The comparison between observed and modelled groundwater levels from 1978 to 2006 provided almost 20,000 data points (n=19481) and resulted in an optimum RMS error of 7.01 m (Figure 4.6C). The graph suggests there was an overall tendency for the model to simulate groundwater levels below observed. This is particularly the case at sites at and above 120 mAOD, where fluctuations and margin for error are usually greatest. Indeed, between 100 and 120 mAOD there is a spread downwards below observed, indicating the model is overestimating groundwater levels considerably. There is another significant anomaly between about 10 and 80 mAOD, where modelled values are overestimated. A closer analysis of mean, maximum and minimum borehole levels suggested that the model tended to overestimate the maximum value of a hydrograph time series (Figure 4.6D).

Testing the model at the EA trigger boreholes yielded an RMS of 6.93 (n=1327) and a reasonably linear relationship (Figure 4.6E), albeit with a tendency for the model to underestimate groundwater levels. The good model fit is supported by a visual interrogation of the time series hydrographs in which the seasonal fluctuations are reconstructed well (Figure 4.7). In some instances however, peaks in groundwater levels occur up to 2 months before field observations. For example, at Chapelwood the observed peak of 113 m in March/April 1995 was matched by a modelled peak in February of the same year. A particularly extreme example occurs at Saltbox during December 1986 when a minimum in observed groundwater levels appears to coincide with a modelled maximum. At other sites however, the peaks coincide more consistently, particularly during wet periods e.g. in February 2001 and

2003. In addition, the peaks are not as sustained as they are in reality; observed groundwater levels tend to recede between May and June, whereas modelled values have already usually dipped sharply by April. Often when observed groundwater levels peak later than April, the model peaks and recedes too soon. The timing of troughs are more consistently modelled although the magnitude of the recession is usually over estimated. Indeed there does seem to be an issue reconstructing the low groundwater levels of drought periods in the early 1990s and mid 2000s. Here,

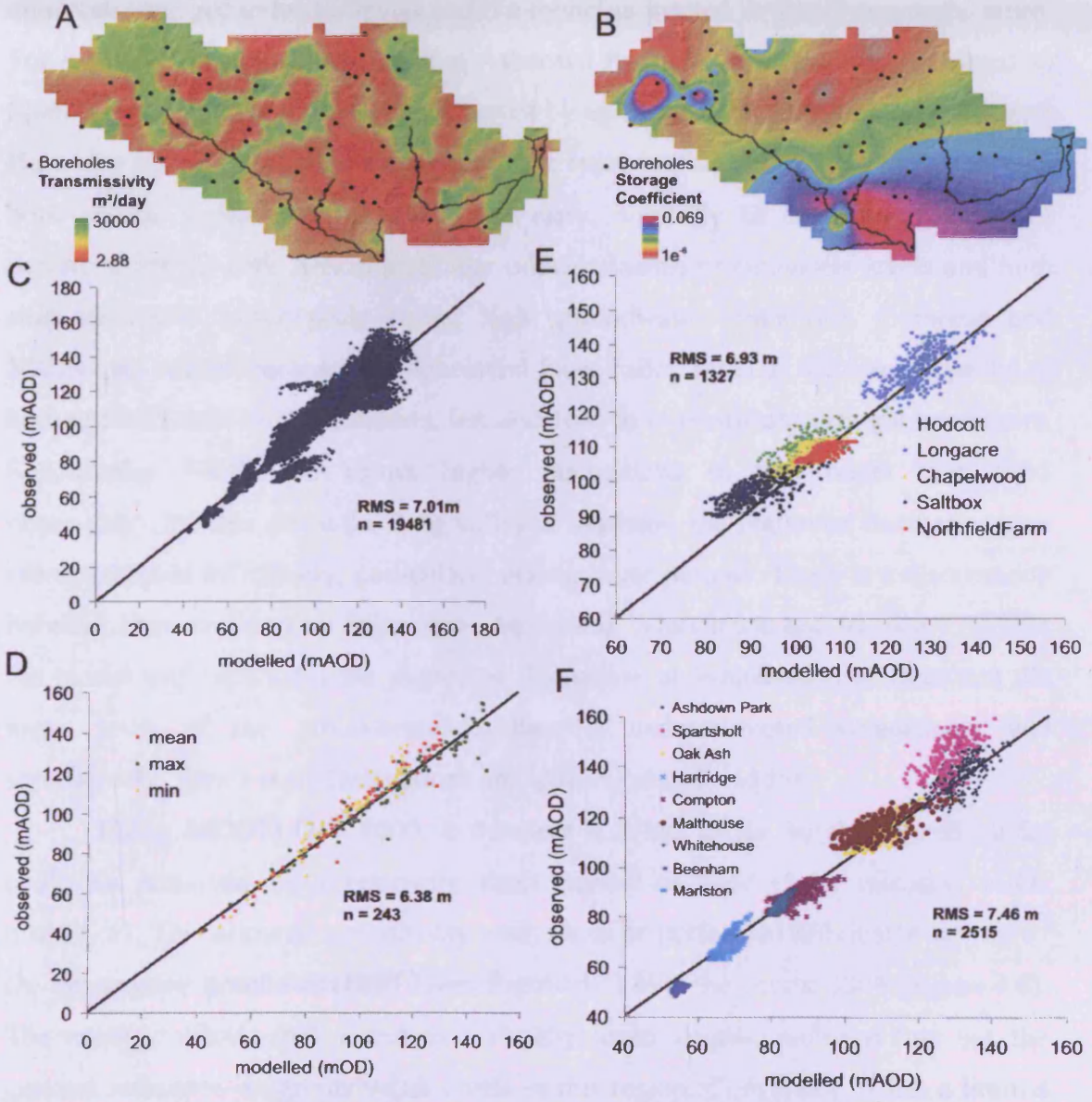

Figure 4.6 *T* (A) and *S* (B) distribution of the single layered MODFLOW model inversely parameterised using PEST (Location of river cells and observation boreholes also shown). (C) Modelled groundwater levels plotted against observations for all observation boreholes over the duration of the transient model. (D) Mean, min and max modelled groundwater level at each borehole, (E) EA trigger boreholes and (F) a catchment wide representative selection in comparison to observations

modelled data falls well below observed records. In contrast, the major flood events of 2000-2001 and 2002-2003 seem well modelled in most cases. The peak in groundwater levels is clearly discernable with absolute values close to reality, if not slightly elevated.

Interrogating a select number of boreholes that represent a cross section of hydrogeological settings provided a RMS of 7.46 (n=2515), comparable with the trigger boreholes (Figure 4.6F). Once again there is a tendency for the model to underestimate groundwater levels and the model is limited in simulating some areas. For example the large fluctuations at Ashdown Park are recreated well compared to Sparsholt Down, which are underestimated by up to 25 m (Figure 4.7). Oak Ash and Hartridge provide more consistently accurate reproductions of hydrographs, although both exhibit a tendency to recede too early, similarly to the trigger boreholes described above. Oak Ash in particular underestimates groundwater levels and both sites exhibit a lower peak during high groundwater conditions. Compton and Malthouse, which represent the ephemeral Pang valley seem to recreate the peaks of high groundwater level conditions, but also tend to overestimate drought conditions. Specifically, Malthouse shows higher fluctuations in the model than field observation. Further down the Pang valley at Marlston, the shallower fluctuations are recreated more effectively, particularly during dryer periods. There is a discrepancy between sites confined by Palaeogene deposits at Whitehouse and Beenham. Whilst the model underestimates the degree of fluctuation at Whitehouse, at Beenham the mean level of the groundwater surface is underestimated consistently and significantly. Small-scale fluctuations are however accounted for.

Using MODFLOW 2000, a transient solution to the single layered model could be achieved in a relatively short period of time (5-10 minutes, 1GHz processor). This allowed a sensitivity analysis to be performed efficiently for one of the observation boreholes (Briff Lane, Figure 4.1) over the course 2004 (Figure 4.8). The results indicate that T and to a slightly lesser degree, recharge flux has the greatest influence on groundwater levels in this region. Conversely, S has a limited impact. In addition, by factorising recharge up to three times, the seasonality also becomes more pronounced.

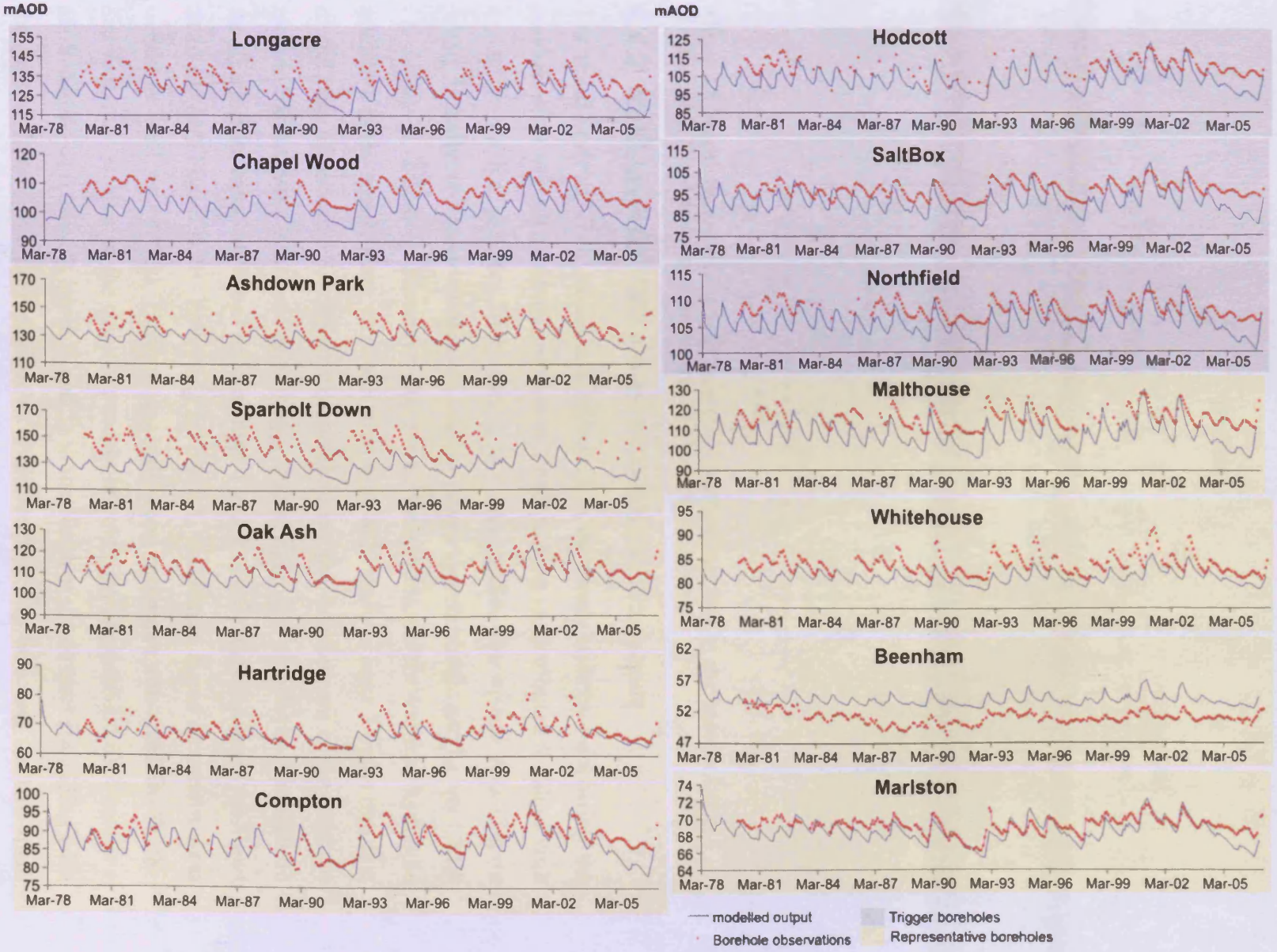

Figure 4.7 Modelled output and borehole observations for EA trigger and representative boreholes between March 1978 and December 2006.

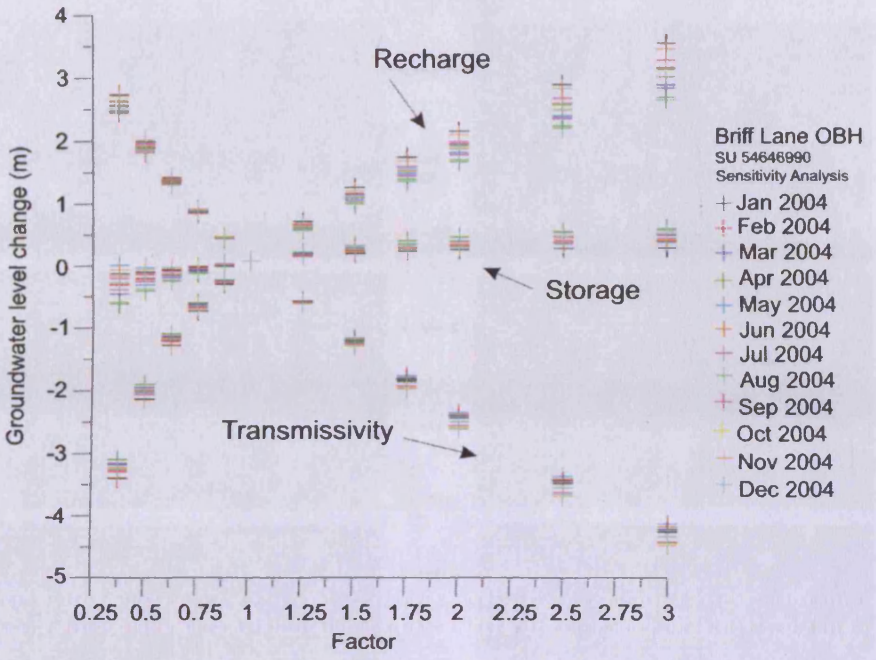

Figure 4.8 Sensitivity analysis at Briff Lane (SU546699) during 2004 by the factorisation of distributed *T*, *S* and recharge from between 0.25 and 3.

4.4.2 Multi-layered VMF Model calibration and output

The multi-layered VMF model was calibrated in the steady state by minimising the residual error at each borehole and overall RMS, leading to distributed *K* values with a positive vertical gradient from layer 2 to 1 and smaller one from 3 to 2 (Figure 4.9A). Initially, the observation wells monitored the Upper, Middle and Lower Chalk i.e. layers 1, 2 and 3. However, there was little evidence for vertical hydraulic gradients in the steady state, so observation were only made in layer 3 in the transient model (see Appendix 3.8). *Ss* was calibrated during the development of the transient model. Values were factorised assuming a single 'zone' for each layer. Similarly to the *K*, a higher value of *Ss* was used in layer 1 and 2 to reflect the tendency for *K* and *Ss* to co-vary Figure 4.9B. Following calibration, distributed *K* and *Ss* exhibit areal trends as well as vertical. Because a single zone technique was used in *Ss*, the distribution is similar to the original product of cokriging (Appendix 3.6). There is a marked zone of relatively lower *K* and *Ss* in the North of the domain coinciding with the groundwater dome characteristic of the interfluve area bisecting the two main river catchments. A notable low also occurs in the south east of the Pang catchment, which coincides with another local dome of groundwater. Notable zones of higher *K* and *Ss* exist in the upper Lambourn and Pang valleys. In comparison, the remaining regions of the catchment are relatively average and more homogenous.

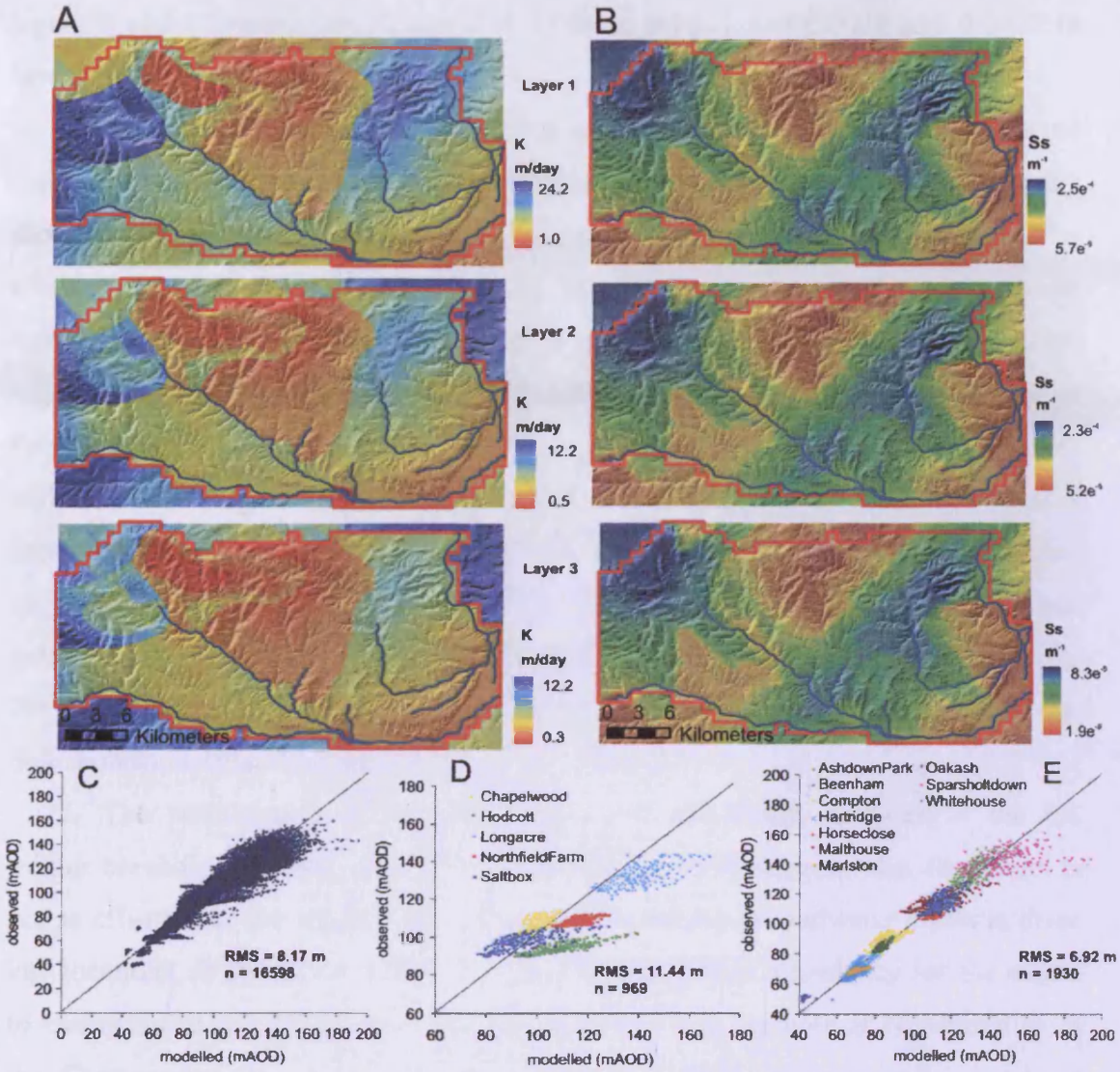

Figure 4.9 (A) Distributed *K* values and (B) *Ss* values for layer 1-3 in Visual MODFLOW. (C) Modelled groundwater levels vs observations at all observation boreholes for the durations of the transient model. Modelled groundwater levels vs observed at (D): trigger boreholes and (E): a catchment wide representative selection.

In order to allow comparisons with the single layered model, distributed values of *T* and *S* are shown in Appendix 3.9. These values were calculated by multiplying the values of *K* and *Ss* by the layer thickness, producing a difference in aerial distribution. In areas where the layer is thin e.g. in layer 1 (Upper Chalk) at Middle Chalk outcrop, values of *T* are much lower than in other regions where the same layer is thicker. For this reason, *T* ranges considerably higher than *K* across the region and the 'cocktail glass' vertical distribution of aquifer properties (Figure 4.3) is only obvious for *K*. However, some vertical and areal *T* trends are clear; including higher *T* and *S* in the valleys in layer 1 and a general decrease in *T* and *S* with depth. Mean *T* in layer 1 is 321.2 m^2/day in comparison to 155.6 m^2/day and 227 m^2/day in

layers 2 and 3 respectively. Mean S is 0.006 in layer 1 and 0.0048 and 0.0029 in layers 2 and 3.

The enlargement of the model domain in comparison to the single layered approach led both to an increased number of observation boreholes and necessary shortening of the modelled time period to accommodate an extended run time. The aim was therefore for the transient model to reproduce mean monthly groundwater levels from January 1990 to December 2005 at 86 boreholes (192 stress periods) (see Figure 4.5 for locations). In addition, an attempt to simulate base flow for the rivers Pang and Lambourn was also made. Comparing all modelled groundwater levels with observed (Figure 4.9C) gave a RMS of 8.17 m suggesting that overall error is greater than the single layered model. This is despite a smaller sample of data points to compare (n=16598). There was a tendency for the model to overestimate groundwater levels as suggested by the drift below the linear 1:1 line (Figure 4.9C). This discrepancy is greatest at sites with relatively high groundwater levels e.g. Sparsholtdown (Figure 4.9E).

The performance of the model was also specifically assessed at the EA trigger borehole locations. An RMS of 11.44 m (n=969) suggests that the model is not as effective as the single layer model at reproducing groundwater levels at these key locations. With the exception of Chapelwood, there is a tendency for the model to overestimate groundwater levels (Figure 4.9D). For example at Northfield farm the discrepancy is up to 18 m during the spring of 2001 i.e. circa model day 4139 (Figure 4.10). More generally, the relatively large RMS statistic is reflected in hydrographs that do not compare very well. The seasonality is reproduced with peaks in groundwater levels coinciding, however the magnitude of the oscillations is not always comparable. At Saltbox and Hodcott for example, oscillations are considerably more pronounced than observations suggests. A positive aspect of the model is that flood peaks are clearly discernable as time series maximums.

Similarly to the single layered model, the VMF version was tested at a representative cross section of sites (Figure 4.9E). There is one more borehole than the single layered model; Horseclose is not within the more restricted domain. At these sites, the VMF model outperformed the other approach, providing an RMS of 6.92 m (n=1930). The RMS of the representative boreholes is almost half that of the trigger boreholes. This is reflected in reasonable fitting hydrographs across the catchment (Figure 4.10). The Drift free interfluves represented by Ashdown and

Sparsholt are much improved from the single layered model. Fluctuations are synchronous and absolute values accurate, even during periods of drought. The boreholes representing drift covered interfluves exhibit a similarly good fit. Groundwater levels at Horseclose however are generally overestimated by a consistent 2-5 m. Compton and Malthouse in the ephemeral Pang valley present a mixed result. At both sites, levels are simulated adequately, although at Compton some peaks are underestimated, whilst others (e.g. during the flood of 2000-2001) are overestimated. This occurs to a lesser extent at Malthouse too. Further down the Pang valley, the more shallow oscillations at Marlston are modelled accurately during dryer seasons. During periods of higher groundwater levels the modelled fluctuations are however too pronounced in comparison to observations. In areas overlain by Palaeogene deposits there is a difference in model fit depending on whether the Chalk is confined all year or only during high water levels. Whitehouse for example exhibits larger fluctuations which are reconstructed favourably by the model. At Beenham, whilst the model simulates the subtle fluctuations, the groundwater levels here are much too (circa 15 m) low. In all cases, the flood peaks of 2000-2001 are clearly discernable as time series maxima.

The proportion of water flux accounted for by constituent processes in the transient model was calculated for the entire time period, a relatively wet period (October 2000-September 2001) and dry period (August 1991-July1992). During the entire model duration, the largest proportion of groundwater into the system is provided by recharge and the largest flux out is via CHBs (Figure 4.11A). The flux out to constant CHBs is flow into the rivers Kennet and Thames and spring line to the north and north west. Net river leakage out is minimal in comparison, which represents flow out into the rivers Pang and Lambourn. Throughout the entire simulation, water entering storage is in equilibrium with water coming out of storage. During particularly wet (Figure 4.11B) and dry (Figure 4.11C) periods, this equilibrium is upset. For example, during a wet period, recharge flux is the dominant process making up most of the 998,146 m^3/day mean input into the system. During this time, a greater proportion of water leaves storage than enters. During the dry period, this is reversed and a greater proportion of water enters storage. Recharge makes up far less of the overall input flux of 288,393 m^3/day, which is maintained to an extent by CHBs. At all times, the proportion of flux to the rivers and drains is small and fairly constant.

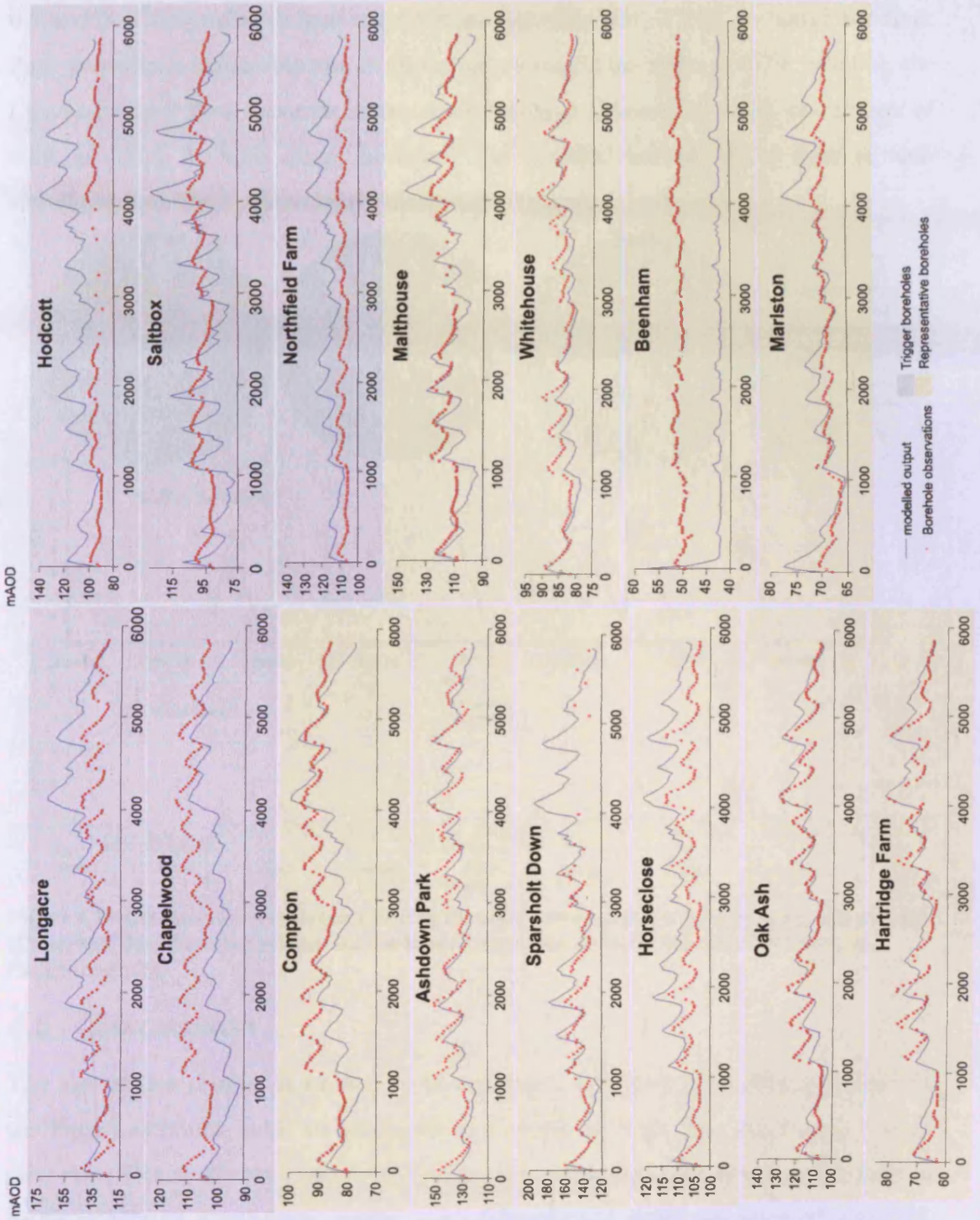

Figure 4.10 Modelled output and borehole observations for EA trigger and representative boreholes across the catchment. Time in (model) day from January 1990 to December 2005.

Modelled base flow in the Pang and Lambourn at Pangbourne and Shaw gauging stations respectively was calibrated by reducing the vertical conductivity (K) of the riverbed and drain parameters by 1000 to 0.001 m/day. Prior to this adjustment, the proportion of water lost from the system through base flow was too high. This adjustment resulted in riverbed conductance being corrected to between

0.3 and 6 m^2/day using default conductance formula (WH, 2000). Although the river Pang provides a reasonable match (Spearman's rank correlation of 0.79, $p<0.01$), the Lambourn base flow becomes increasingly too high (Spearman's rank correlation of 0.64, $p<0.01$). In both cases, however, the seasonal nature of the flow is well simulated, and flood peaks clearly discernable (Figure 4.11D and E).

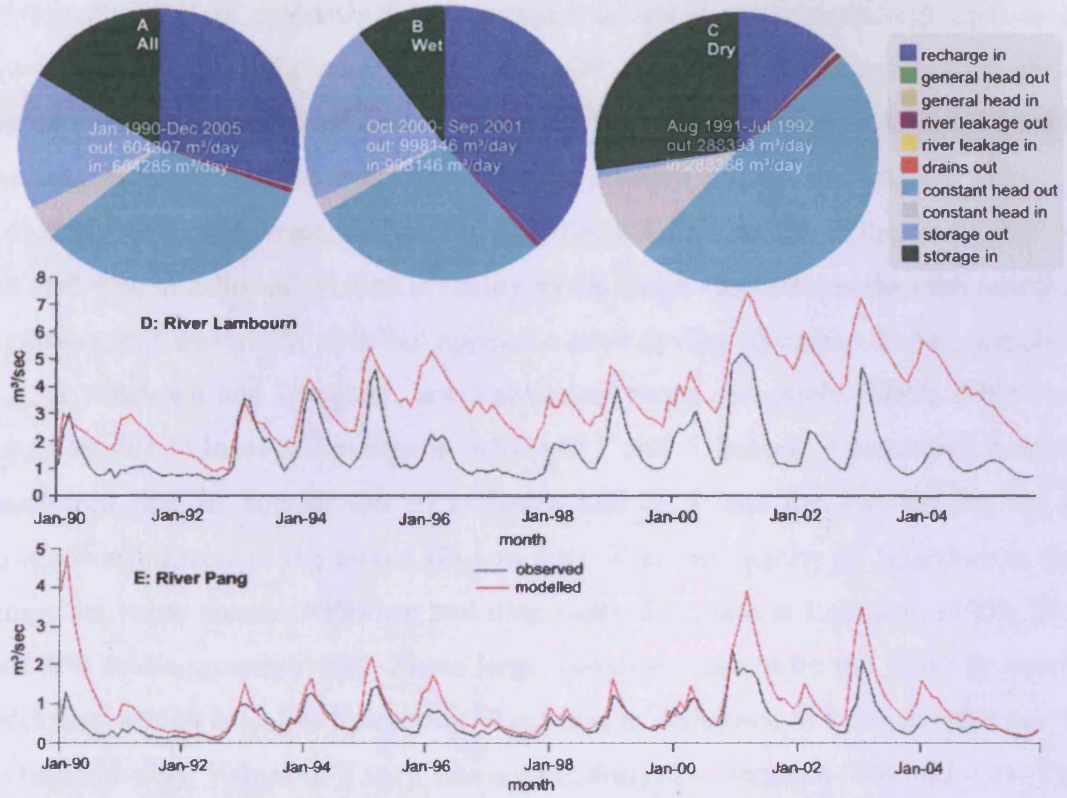

Figure 4.11 Catchment water balance during the entire simulation period (A), a wet (B) and dry (C) period. Base flow comparison for the River Lambourn at Shaw (D) and River Pang at Pangbourne (E).

4.5 Discussion

The aim of this chapter is ultimately to develop a saturated groundwater model for the Pang/Lambourn, with an emphasis on simulating high flow conditions. To do this, the efficacy of two distinct modelling methodologies was compared. Firstly, a depth integrated single layer model was parameterised using the inverse modelling technique, PEST. Secondly, a three-dimensional multi-layered approach was adopted using VMF. The two methodologies make use of field data available in the Pang/Lambourn to differing degrees and are assessed by looking at simulated groundwater levels in different areas of the domain and overall. The focus has been to provide an adequate simulation of groundwater flow at the regional scale as well as developing a useful tool that can aid groundwater flood risk management. The success and perhaps more importantly the limitations of each method provide an

insight into the groundwater processes as well as providing tools for climate change impact studies and flood risk assessment (see Chapters 5 and 6).

4.5.1 Single layered model

The single layered (two dimensional) model, parameterised using PEST performs reasonably well in reconstructing boreholes across the catchment, reflected in an overall RMS error of circa 7 m (Figure 4.7C and D). Trigger and representative boreholes yielded a RMS of 6.93 m and 7.46 m respectively (Figure 4.7E and F). The success is not replicated everywhere in the domain and is not divided along the originally proposed conceptual zonations (Figure 4.1). The site at Sparsholt, high up on drift free interfluves exhibits in reality much larger fluctuations than the modelled hydrograph. Conversely, sites that appear to have similar characteristics to Sparsholt, e.g. at Ashdown and Longacre, are represented more accurately. These differences could be due to local differences in values of T and S. Indeed, a sensitivity analysis suggested that in comparison to recharge and S, T has the greatest impact on groundwater levels in the model (Figure 4.8). T in the vicinity of Sparsholt is four times the value around Ashdown and nine times the value at Longacre (9000, 2400 and 850 m^2/day respectively). These large variations cannot be put down to aquifer thickness, which is less at Sparsholt (59 m) than at Ashdown or Longacre (89 and 99 m respectively). Values of S vary less significantly, i.e. between 0.04 and 0.01. This elevated value of T is likely to have the effect of dampening groundwater fluctuations by increasing the ease with which inflows (e.g. recharge) can flow away from the area.

Elsewhere in the catchment, the distributed values of T and S (Figure 4.6) converged upon by PEST bare little resemblance to the conceptual understanding in which variation is a function of distance from valleys, vadose depth and aquifer thickness. The maximum value of T (30000 m^2/day) exceeds the maximum value obtained by pumping tests in the Kennet valley (8000 m^2/day) by almost four times and maximum modelled values (2000 m^2/day) by fifteen times (Rushton et al., 1989). Values of S on the other hand are comparable with pumping test values (0.0001–0.07) in the Kennet valley (Allen et al., 2007).

Using pilot points in conjunction with PEST provides an optimisation of T and S given the borehole observations. Certain areas could be forced into these exceptionally high values of T as they interact to provide greater accuracy at other,

observed points in the domain. This process is likely to produce anomalous values both of T and S and also groundwater levels. It is likely that the distribution of T and S converged upon is one of a large number that could provide an equivalent level of fit. It so happens that the one converged upon contains these anomalous points. The pilot point methodology seems to sacrifice the fit of some boreholes for others and in doing so limits the successful fit of all the boreholes.

Another interesting modelled hydrograph was at Beenham in the south east of the Pang catchment (Figure 4.1), where mean groundwater levels consistently exceed observations. This is despite local T values of circa 9000 m^2/day (aquifer thickness 307 m). It could be that fluctuations are exaggerated by not including the confining low conductivity Palaeogene deposits, which would reinforce the importance of this layer in regulating groundwater behaviour in this region. However, EA trigger boreholes are not situated in this areas and the questionable importance of this region to groundwater flooding processes makes this observation less important.

There are also variations in model fit with time whereby extremely dry seasons tend to be simulated less well. There is also a tendency for the receding limb of the modelled hydrograph to occur too early annually. Both could be because the single layer approach restricts the opportunity to represent the vertical heterogeneity of the aquifer system. Just as a 'cocktail glass' vertical distribution of T and S mediates extreme high and low groundwater levels (Rushton et al., 1989), so it could delay the decline in seasonal levels. Further evidence for this is found in the consistently large troughs during the summer months at the trigger borehole sites. The flood peaks are modelled more closely but by lowering the mean levels. Still in some cases, flood peaks exceed observations e.g. at Northfield and Saltbox.

Uncertain GIS-DIRT based recharge values may have propagated into the model and provides a possible explanation for inconsistent performance. At monthly time steps, GIS-DIRT may underestimate recharge; particularly during the summer months (see Chapter 2). The focus of recharge during the hydrological winter (April –October) could be a factor in the early reduction of groundwater levels. In addition, there may be sub-monthly borehole responses to rainfall not well modelled (see Chapter 3). This could explain the model-wide underestimation of groundwater levels and mismatch in groundwater level maxima. There is also a degree of spatial uncertainty in GIS-DIRT which could lead to inaccurate local recharge fluxes and therefore modelled borehole responses in some areas. Indeed, the sensitivity analysis

carried out at Briff Lane (Figure 4.8) suggests increasing recharge elevates groundwater levels and extremes in seasonality i.e. the difference between the annual maximum and minimum. However, according to local long term GIS-DIRT values, Sparsholt receives more recharge (21 mm/month) than Ashdown (17.5 mm/month). In addition, evidence from the other VMF model suggests the same recharge values can be compensated for by different model structure and parameters. The difference in modelled hydrographs between the two models is marked, despite the same recharge input, for example, groundwater levels recede too early ay Oak Ash in the single layer model, but are more effectively modelled using VMF.

Given the scale and complexity of the groundwater system in the Pang/Lambourn, it is not surprising a single layered model with simple no-flow boundary conditions restricted PEST from converging on a solution that more closely resembles the conceptual understanding of the system as well as replicating levels at all the observation borehole sites. Previous modelling attempts certainly highlighted that the cocktail glass vertical distribution significantly improved the performance of previous models in representing levels and stream flow (Rushton et al., 1989). It also provides a possible explanation for the unusual areal distribution of T and S converged upon by PEST and subsequent factorisation. Indeed, evidence for Karstic behaviour of the Chalk at Blue Pool (Banks et al., 1995) suggests a highly non-linear system. The T and S distribution may reflect the esoteric preferential flow paths that pervade the Chalk.

4.5.2 Three-dimensional VMF model

The detailed three-dimensional method adopted in the VMF model addresses some of the deficiencies of the single layered approach. By interpolating T and S values from BGS pumping tests the extreme values generated by PEST are replaced by less extreme values from field investigations. Cokriging ensures values of T (or K) and S (or Ss) are constrained by the conceptual understanding of the system in areas where data is sparse. In addition the simulating of groundwater flow where hydraulic conductivities vary non-linearly with depth was addressed by introducing multiple layers into the model. The enlarged domain allowed for a more reasonable assumption that the rivers Kennet and Thames and spring line provide the natural groundwater divide boundary in the region (Rushton et al., 1989).

By combining the distribution of K and Ss (Figure 4.9) with more realistic boundary conditions, the steady state model was well calibrated (RMS=6.3 m) by manually factorising zones. Notable adjustments were made to increase K in the Upper Lambourn valley and reduce it in the interfluves area between the two river catchments during the calibration procedure. The decrease reflects the lower T values away from the valleys on the interfluves. However, the requirement to increase values in the Upper Lambourn may be due to local preferential flows paths or the assumption of no pumping wells. There were particular difficulties in calibrating levels at Letcombe (6 km east of Longacre) and Newbury (lower Lambourn valley), where modelled levels were lower than observed and at Northfarm and Hodcott (upper Lambourn and Pang valleys respectively, see Figure 4.1), where modelled levels were significantly higher. By constraining the calibration zones to 45 per layer, it was difficult to calibrate these localised areas without disrupting other nearby sites.

Mean values of T and S were adjusted to decrease from layer 1 to 3 representing the transition from Upper to Lower Chalk formations (see Appendix 3.9 for T and S distributions). It became evident that the vertical movement of water from layers 2 and 3 to layer 1 is negligible; suggesting the dominant direction of regional flow is horizontal. Summing T and S over the three layers shows the range of T varies from between 11 and 2128 m^2/day and S between 0.0002 and 0.03. This is similar to the range used in previous models (Rushton et al., 1989). There is a distinct zone of low T and S in the interfluves between the Pang and Lambourn, which is characterised by a groundwater dome. Generally, the Pang and Lambourn valleys exhibit elevated values, although there is localised variation due to aquifer (i.e. layer) thickness.

Performance of the transient model is better in some areas than others, generating an overall RMS error greater than the previous modelling approach (8.17 m). Simulation at the trigger and representative boreholes (Figure 4.1) gave a RMS error of 11.44 m and 6.92 m respectively, the latter an improvement on the previous model. The fluctuations on the drift free Middle Chalk interfluves at Ashdown and Sparsholt are modelled reasonably well. At Longacre however the model overestimates levels during the 2000-2001 flood by approximately 25 m. The recharge is equivalent at the sites, with values of between 211 and 249 mm per annum on average. The sum of T across the three layers at Longacre is 89.7 m^2/day

in comparison to 497 m^2/day at Ashdown and 42.9 m^2/day at Sparsholt. The thickness of the Chalk is 113m, 89 and 65 m respectively. It is likely that the relatively high value of T at Ashdown compensates for the thin (1 m) Upper Chalk layer of higher K that would be able to mediate extremely high levels during flood events. Data for Sparsholt during the 2000-2001 flood event is missing, but we could assume that it would behave in a similar way to Longacre.

Other modelled EA trigger borehole sites on the Middle Chalk exhibit a similar inability to mediate large fluctuations. For example Saltbox has a summed T value of 167 m^2/day, with a negligible input from the high K layer 1. The result is a realistic mean modelled groundwater level but with excessive oscillations. Northfield farm and Chapelwood, on the Upper Chalk have a greater input from layer 1, which moderates the fluctuations. In these cases however, the mean groundwater levels are either too high or low. The issues with simulations at the trigger boreholes suggest localised issues with the vertical and areal distribution of T. However, the modelled representative borehole hydrographs indicate that some aspects of the model are successful. The suggestion that layer 1 thickness is responsible for successful modelling is supported by Oak Ash and Hartridge. Here, there is a substantial Upper Chalk contribution to T of 257 m^2/day and 583 m^2/day respectively. The modelled hydrographs exhibit fluctuations very similar to field observations, with none of the extreme peaks seen at Longacre for example. It seems that a thin layer 1 reduces the 'pseudo-cocktail glass' vertical T effect, even on the interfluves. The site at Marlston also exhibits extreme peaks symptomatic of low T in layer 1, where levels are up to about 6 m too high during high groundwater periods. This is despite being relatively low in the Pang valley, where T is expected to be generally high. Layer 1 T value is 813 m^2/day of a 1240 m^2/day total for all 3 layers. This is offset however by a layer thickness of 106 m of a 233 m thick aquifer. It seems that high K values in layer 1 can be offset when the thickness of the layer is either too large or small.

In addition to calibrating groundwater levels, VMF was also used to determine a catchment-wide water balance for the entire model duration and wet and dry periods (Figure 4.11A, B and C). An interesting observation was that a significant proportion (over a half) of the water flux was determined by CHBs during dry periods. Although this is reduced in wet periods and overall, it may be considered an over-reliance on fixed heads to solve for distributed values. However, the position and value of the constant heads are conceptually sound, given they

represent the actual location of the River Kennet, Thames and spring line. A further consideration is the relatively insignificant role of river outflow (and inflow) on the system. Despite this it is useful to calibrate these values, given the potential role in groundwater flood events. As such, riverbed K and drains simulating the ephemeral Pang, Lambourn and Winterbourne were reduced to obtain a reasonable match (Figure 4.11D and E). The overestimation of the river Lambourn base flow is likely to be symptomatic of a wider overestimation of groundwater levels. The relatively large flux from the CHBs may be a contributing factor.

4.5.3 Limitations and insights from the MODFLOW models

Both the successes and limitations of the models have provided an insight into the groundwater system in the Pang Lambourn. As is usual with most modelling endeavours, future refinement is likely to be needed. The single layered approach using PEST is constrained by the simple domain structure, and boundary conditions, forcing T and S to values not seen in pumping test analysis. The vertical heterogeneity suggested by pumping tests and borehole logs can not be represented in the model. The translation of the conceptual model to VMF has also been limited, despite cokriging T and S over multiple layers. There are a number of plausible reasons for this, including:

- The original BGS values of T and S are based on unknown aquifer thickness. These were converted to K and Ss for input into VMF using an arbitrary aquifer thickness value (i.e. the difference between the high groundwater levels in February 2001 and the base of the Chalk). Given the confined system assumption, K is converted back to T in VMF by multiplying by layer thickness, which is greater than assumed aquifer thickness. This could therefore lead to an underestimation of T generally.
- The original BGS values of T and S seem conservative in comparison to some of the values of T and S given for the region elsewhere, e.g. T up to 8000 m^2/day (Allen et al., 2007). Unreliable T and S values could contribute to a potential lack of significant cross correlation between Ss, K and aquifer thickness, vadose depth and distance from valleys. Cokriging does not work effectively with a lack of cross correlation, as seen in the equivalent error when compared with ordinary kriging.

- The minimum 1 m thick layers can lead to low T values when importing the distributed K values. It seems factorising layer 1 to increase T was insufficient to recreate the pseudo-cocktail glass effect in all areas. Equally the impact of high T values is reduced in thicker layers. The trial and error factorisation of zones and layers does not seem to have compensated for these shortcomings in all areas of the domain.

More generally, both models suffer from a lack of abstraction data. By assuming a naturalised system, it could be that modelled boreholes would be affected and areal and vertical T and S distributions would have to compensate. The impact of pumping however is generally localised in the Chalk, which is exemplified by the limited impact such pumping had on the flooding in 2000-2001 (DEFRA, 2006a). Despite the apparent lack of impact however, any change in the use of the Chalk aquifer as a resource should be accounted for in future models.

Whilst boundary conditions in the VMF model are more realistic than the single layered model, the values of the CHB and GHB conditions remain static through the transient simulation. It is likely that conditions at these boundaries change with time. For example, stream levels fluctuate, particularly during a flood and also may dry out. Indeed the concept that the River Kennet and Thames are in close contact with the aquifer remains uncertain. It would also be useful to gather more field data on the rivers in the catchment. At present the Pang, Lambourn and tributaries are represented by a constant channel width and river bed conductance. Although these values are consistent with previous modelling attempts (Grapes et al., 2006), it is unlikely that they remain consistent along the profiles in reality. Indeed the base flow analysis could be improved with added information.

In summary, any further work could benefit from cherry picking aspects of both modelling approaches. The enlarged VMF domain could be constrained by more transient boundary conditions. The vertical distribution of K should be irrespective of Upper, Middle or Lower Chalk, perhaps in accordance with the zone of fluctuation, where dissolution would be more aggressive. Pumping test data could be used to constrain T and S values during PEST calibration, which could also include boundary conditions and base flow. Finally, a stochastic methodology could be adopted to account for model uncertainty e.g. stochastic finite element methods (Renard, 2007). This method would also allow for a continuous domain, without the

constraints of a layered system. The Palaeogene deposits could also be integrated without the associated model instability.

4.5.4 MODFLOW models for groundwater flood risk assessment

It has been shown that the single layered model adequately reconstructs a wide range of observed hydrographs. Importantly, the flood peaks seen at the EA trigger borehole during 2000-2001 were modelled effectively. On the other hand, the VMF model simulates a broad cross-section of the domain using a more physically based parameterisation process. Here however, the trigger boreholes are not modelled as well. The 100 m resolution of the models means however they are not well suited for predicating local-scale discharge patterns during flood events. River flows, springs and diffuse locations that would discharge during regionally high groundwater levels are still poorly understood. It is feasible that only a small number of spring locations are mapped and river accretion profiles are not known except in localised cases, especially under high groundwater conditions (Bradford, 2002a; Griffiths et al., 2006). There is evidence for example that discharges to the rivers and localised alluvial aquifers are partly dependent upon lateral water movement in the unsaturated zone (Grapes et al., 2006). This lateral movement is likely to be due to preferential flow paths along planar fractures and hard bands (marls and flints). The simple observation of these alluvial aquifers is enough to suppose that a groundwater flow model representing only the saturated Chalk is likely may be too simplistic to be used directly as flood risk model. In addition, the flow of water over the surface after emerging is not modelled.

The magnitude, location and timing of flood discharges are however related to the large scale seasonal variation in groundwater levels (Pinault et al., 2005). By being pragmatic the models could therefore be used as a flood risk management tool, whereby the level of risk is assigned based on the frequency of regionally high groundwater levels. For example we can make an assessment of the risk that the EA trigger boreholes will reach the flood peaks or trigger levels. By doing so a quantitative measure of risk could be established. Secondary data sources on flood extents, discharge locations and damage could be ascribed to water levels at these (or other) boreholes. By applying weather time series associated with scenarios of climate and land use change into the model, we can make an assessment of the risk that the EA trigger boreholes will reach the flood peaks in the future. If risk is likely

to generally increase, there may be a need to invest in more refined nested models, particularly in areas most vulnerable. Grapes et al. (2006) describe how catchment-scale groundwater models can be used to investigate specific floodplain wetland systems by nesting models. A similar approach is probably suitable for groundwater flooding, where a general model, like those presented here would assess regional fluxes. More refined models (with adequate boundary conditions) would make better use of more refined data collected at sites deemed at risk of groundwater flooding.

The PEST method of inversely parameterising the groundwater model has been successful in recreating a wide selection of borehole hydrographs over a long period of time. Because the recharge values are well constrained and there is a large number of monitoring boreholes, it makes sense to utilise inverse parameter estimation techniques for groundwater flood risk assessment elsewhere. Indeed it appears more successful at modelling the trigger boreholes. This way, maximum use can be made of the recharge model to converge on a suitable distribution of T and S. Continuous, accurate surface data to constrain recharge e.g. land use and soil type, are easier and cheaper to obtain than aquifer properties.

4.6 Conclusions

Modelling a large scale heterogeneous, esoteric system such as the regional Chalk aquifer of the Pang/Lambourn valley is problematic. Here, a single layered, depth integrated MODFLOW model was inversely parameterised based on a large number of transient groundwater level observations. This was juxtaposed against a three-dimensional, multi-layered approach using Visual MODFLOW. By interpreting the successes and failures of both methods a number of insights have been made into hydrogeological processes. For instance, the result of the inverse parameterisation process provided a highly heterogeneous distribution of aquifer properties (T and S). This is likely to be the result of non-linearity and preferential flow paths in the system. The Visual MODFLOW model was parameterised by cokriging field values of aquifer properties with distance from valleys, aquifer thickness and vadose zone thickness data. Despite introducing variation into the vertical distribution of hydraulic conductivity, the model did not simulate groundwater levels as well as the single layered model due in part to localised layer thickness.

The primary aim of the modelling procedure has been to develop a groundwater flood risk assessment tool. The single layered model was more effective

at modelling groundwater fluctuations at EA trigger boreholes, used to assess short to medium term groundwater flooding risk. Although the model is too coarse (100 m) to be used to identify localised discharge zones accurately, the frequency of peaks at these locations would provide a useful indication of flood risk. In combination with GIS-DIRT recharge model the method is also easily transferable to other catchments. In addition, by applying climate change scenarios to this model it would be possible to gauge whether investing in model refinement is worthwhile in the future. Only through more refined nested modelling and local data collection regarding preferential flow paths, could the modelling advance by any significant extent. Secondary data on past flood events could help identify where this refinement should be prioritised. Utilising stochastic modelling e.g. using a mixed finite element approach could also help address the uncertainty. Model refinement could include the conceptual advances made in the multi-layered Visual MODFLOW model, including an extended model domain.

Chapter 5 Integrated modelling for climate and land use change impact assessment

5.1 Introduction

The aim of this chapter is to quantify how changes in land use and climate may affect the groundwater system in the Pang/Lambourn. Ultimately this information can be used to better manage water resources and groundwater flood risk in this region and similar settings throughout the UK. The methodology involves combining the recharge and groundwater flow models developed in earlier chapters. Scenarios of climate change can then be applied to this integrated model by downscaling output from a GCM. Similarly land use modification scenarios can be developed and applied to the recharge model. The resulting ensemble of outputs from the model can then be used to quantitatively assess the range of likely impacts.

5.1.1 Climate change impacts on hydrology and hydrogeology

There is overwhelming evidence to suggest that human activities are significantly influencing global climate systems, with rapid increases in global temperature associated with anthropogenic inputs of CO_2 since the second half of the 18th century (Mann et al., 2008). These influences are expected to continue and bring about future dramatic changes in temperature, precipitation and other climatic variables (IPCC, 2007). Recent worldwide climate predictions based on large numbers of GCM scenarios together with observations suggest that during the next 100 years it is 'very likely' that heat waves and heavy precipitation events will become more frequent (IPCC, 2000; IPCC, 2007). Such changes may have significant consequences for global hydrological balances.

The UK Climate Impacts Programme (UKCIP) has produced three series of climate projections for Great Britain in 1998 (Hulme and Jenkins, 1998), 2002 (Hulme et al. 2002) and 2009 (Jenkins et al., 2009). By the end of this century in Britain, average annual temperatures may rise by between 1°C and 5°C with greater warming in the summer and autumn months (Hulme et al., 2002). Precipitation may also increase by up to 30% in winter and reduce by up to 50% during summer. The intensity of winter precipitation events are also predicted to increase (Hulme et al., 2002). More recently, the UKCIP09 predictions have assigned probabilities to

regional changes, where the greatest changes are expected in the South East (Jenkins et al., 2009). These predicted changes are supported by ongoing observations of exiting trends. For example, between 1770-1800 and 1970-2000 annual precipitation in England and Wales increased by only 24 mm yet winters became 55 mm wetter and summers 45 mm drier (Jackson et al., 2006). Similarly, there has been a UK-wide increase in the frequency and magnitude of high river flows during the last 30–50 years. Modelling studies also suggest there is likely to be a further increase in the magnitude and frequency of fluvial flooding in the future (Prudhomme et al., 2003).

Fundamental climatic shifts are likely to have an impact on groundwater resources in Britain (Herrera-Pantoja and Hiscock, 2008; Holman, 2006; Jackson et al., 2006; Wilby et al., 2006; Younger et al., 2002; Yusoff et al., 2002) and elsewhere in the world (Brouyere et al., 2004; Loaiciga, 2003; Scibek and Allen, 2005; Scibek and Allen, 2006; Scibek et al., 2007; Woldeamlak et al., 2004). In previous hydrogeological impact studies on the Chalk, Younger et al. (2002) adopt the approach of applying downscaled GCM output to a groundwater flow model of the Yorkshire Chalk aquifer. Year-round increases in groundwater discharge were predicted to be likely in the first half of the 21st century (9% increase in total annual average flow). Other studies have predicted no real change from present seasonal groundwater levels or base flow rates e.g. in a Chalk valley in Belgium (Brouyere et al., 2004). Others predict a reduction in recharge rates (17-35%) leading to a substantial decrease (14%) in autumn base flows in a Chalk valley in East Anglia (Yusoff et al., 2002). Herrera-Pantoja and Hiscock (2008) suggest this reduction in recharge is likely to extend to sites all over Britain. If recharge rates and groundwater levels vary significantly in the Chalk aquifers during the coming century, the risk to resources, quality and flooding is likely to also change. Other studies highlight the large degree of uncertainty inherent in making such predictions, for example Wilby et al. (2006) demonstrate a large range of outcomes for their water quality modelling of the Kennet valley depending on the GCM used. Despite evidence that climate change will impact groundwater resources, no study has looked at the future risk of groundwater flooding in a Chalk catchment.

5.1.2 Land use change impacts on hydrology and hydrogeology

Socio-economic drivers can impact upon the local hydrological system through land use change pressures brought about by population growth and economic

development (Krysanova et al., 2006; Webber et al., 2001). It would be unreasonable to expect the landscape to remain constant over the next 100 years while the climate changes markedly (Holman, 2006). Indeed, it has been recognised that assessing socio-economic driven land use modification in conjunction with climate change is important: "Whilst the use of climate scenarios as inputs into vulnerability, impact or adaptation assessments is well established, there is far less experience of using socio-economic scenarios. However, studies to assess climate change impacts suffer from serious weakness if by default they merely assume that the projected future climates will take place in a world with a society and economy similar to today" (UKCIP, 2001). As such land use change is an important consideration in managing water resources and more specifically groundwater flooding risk.

Upland catchment management studies initially highlighted the key role of land use in the hydrological cycle (Law, 1956). Seminal work carried out at the source of the Rivers Wye and Severn at Plynlimon, Mid Wales found for example that 15-20% of rainfall is lost to transpiration from grassland in comparison to 30-40% over full forest cover (Hudson et al., 1997). Hydrological processes such as evapotranspiration from the land surface are driven by meteorological controls but mediated by characteristics of the land use (e.g. crop type) and soils. For example, climate change may lead to greater evaporative demand during warmer summers. However, actual evapotranspiration may be reduced because of increasingly frequent periods of soil moisture deficit determined by the rooting depth of the overlying crops (Arnell, 1996). Similarly Reynard et al. (2001) provide river modelling evidence to suggest that increasing forest cover by 50% in the Thames and Severn catchments could counter-act the impact of climate change on fluvial flood risk over the next 50 years. As expected, a large increase in the urban cover of the catchments also has a significant effect, increasing both the frequency and magnitude of floods beyond the changes attributed to climate alone.

Land cover is a key variable in determining groundwater recharge and so changes to land use may increase or reduce flux into the groundwater system (Finch, 2001). The physical processes involved in these changes are hinted at by Finch (2000), who noted that the area of deciduous woodland in Britain is increasing as a result of government policy. Observed soil moisture deficits are much larger under woodland in comparison to grassland (up to 1 and 3 m respectively). In addition, over a simulated 25 year period, mean annual runoff and soil drainage for the

woodland was less then half those for grass. This may have consequences for increasing the risk of depletion in groundwater resources. Moiwo Juana (2006) assessed the impact of land use change on distributed groundwater recharge and discharge over a large area (circa 47,000 km^2) in western Jilin, China. Here an emphasis was put on calculating the recharge that would be lost as natural woodland areas are replaced with more impervious urban areas. Mean recharge values of 159.8 mm/yr (37% annual rainfall) were reduced to between 26 and 79 mm/yr over developed land. By assuming hypothetical natural conditions of woodland over the entire catchment, average recharge rises to 263 mm/yr, suggesting woodland promotes recharge in comparison to developed land. More recently, a study of the impact afforresation may have on the water resources of a sandstone aquifer in Nottinghamshire, UK found that although recharge was reduced by almost 50%, groundwater levels were not significantly affected (Zhang and Hiscock, 2010).

Investigations that have explicitly examined the impact of land use change on Chalk aquifers have tended to focus on groundwater vulnerability to pollution (Whitehead et al., 2002). Indeed, a study of groundwater recharge rates across the Chalk dominated East Anglia region suggested that climate change may be more important for water resources (and groundwater flooding risk) than socio-economic drivers at the regional scale (Holman, 2006). However it has be shown that local socio-economic impacts can be highly significant, especially where they result in major land use changes (Moiwo Juana, 2006).

In the Berkshire Downs (site of the Pang/Lambourn), it has even been suggested that direct anthropogenic influences could mask the impact of climate variability and change on groundwater fed stream discharge. These influences could include groundwater abstractions, flood relief measures, changes in river management and agricultural practice (Bradford, 2002a). More specifically, Finch (2001), used a distributed recharge model to find that land use changes in the Pang catchment from 1990 to 1997 had little effect on the volume of recharge, only on the distribution. Here the dominant observed land use change was an increase in the area of tilled land at the expense of grass. It was observed that the increase in recharge due to the replacement of grass by cereal crops was balanced by the reduction in recharge caused by the small increase in coniferous forest. The mean annual recharge to the catchment in 1990 was therefore 104.7 mm compared to 106.2 mm in 1997 (assuming equal climatic conditions). Whilst the overall impact on groundwater

recharge in the Pang was neutral, particular locations within the catchment varied significantly. Either way, the influence of the atmosphere upon the groundwater system is mediated by groundwater recharge. GIS-DIRT (see Chapter 2) partitions recharge as a function of land use cover, soil properties and slope making it ideal for predicting the effects of land use change as well as climate change.

Changes to soil properties are also an important consideration. Soils in the future may not have the same infiltration properties as current datasets suggest. Crop changes can introduce localised changes to carbon cycling, for example a reduction in soil organic carbon, which can affect surface sealing. Changes in tillage practices can also have an impact on the run off potential of soils (Holman, 2006). Indeed, Chapter 2 suggested that the spatial distribution of recharge in the Pang/Lambourn catchment is dominated by soil texture rather than land use (although woodlands and urban settlement locations did have a significant impact on recharge flux). Usually it is land use and not soil properties that socio-economic systems influence directly, although the choice of land use can be influenced by and could potentially alter the soil and its properties (Rounsevell et al., 1999). The impact of soil changes over time is however outside the scope of this study.

5.1.3 Climate change impact modelling

The UKCIP02 (Hulme et al. 2002) scenarios are the focus of this research as the more recent UKCIP09 (Jenkins et al., 2009) models were not available in time to incorporate into study. The UKCIP02 scenarios are the result of running Global or Regional Climate Models (RCM) based on a selection of greenhouse gas emission scenarios and climate sensitivities developed by the Intergovernmental Panel on Climate Change (IPCC, 2000). Estimated atmospheric greenhouse gas concentrations range from 540 ppm CO_2 or equivalent in the low scenario to 920 ppm in the high scenario, compared with a pre-industrial value of 280 ppm. These represent four plausible 'futures' ranging from rapid economic growth with intensive use of fossil fuels ('High Emissions') to increased economic, social and environmental sustainability with cleaner energy technologies ('Low Emissions'). For each of the four UKCIP02 scenarios, changes are described for three future thirty-year time-slices: 2011 to 2040 (the '2020s'), 2041 to 2070 (the '2050s') and 2071 to 2100 (the '2080s'). All changes in climate are given relative to the baseline period of 1961 to 1990.

Impact assessments of climate change on local hydro(geo)ology require time series of weather variables for specific catchments. Such series are not directly available from RCMs in UKCIP02. Indeed, the finest resolution RCM, HadRM3H (Hulme et al., 2002) has 50 km grid cells and so does not effectively simulate the distributed patterns of climate e.g. rainfall, at the local scale. A solution has been to develop synthetic time series of weather variables by simply perturbing past time series (Bloomfield et al., 2003; Jyrkama and Sykes, 2007; Woldeamlak et al., 2004). Here, past weather time series are factorised using predicted changes in the long-term mean for different weather variables and climate change scenarios. Effectively, the same historic climate is used as a model of future climate, with shifts being introduced only in the magnitude of each event in the series. Change factors are defined by comparing the climate model output for the control baseline (usually 1961-1990) with the output from future climate scenarios. The factors are calculated for the grid cell overlying the study area and applied to locally observed time series (Yusoff et al., 2002).

The downside of simple perturbation is that changes in the frequency and magnitude of extreme events cannot be modelled effectively. An alternative is therefore to apply a statistical downscaling model (Scibek and Allen, 2006; Wilby et al., 2006). Similarly to the perturbation technique, the approach relies on deriving factors of change for from a control baseline to future scenarios. However, instead of simply factorising past time series these factors are applied to observed weather statistics from which new, synthetic time series are generated. Kilsby, et al. (2007) describe a stochastic Weather Generator (WG) methodology for use in climate change impact studies. Here, the Environment Agency Rainfall and Weather Impacts Generator (EARWIG) produces an internally consistent series of meteorological variables based on the output from a range of GCMs and RCMs including the HadRM3H associated with UKCIP02. Initially, a stochastic model produces a time series of rainfall from which other variables are derived. These include temperature, humidity, wind, sunshine and potential evapotranspiration. By combining gridded observed rainfall statistics along with change factors from the UKCIP02, these time series can be provided at the catchment scale up to 5 km resolution (see Section 5.3.1 for details). The EARWIG method has subsequently been used in a wide range of climate impacts, from fluvial flood risk (Kay et al., 2008), to groundwater recharge (Holman et al., 2009) and even railway line buckling risk (Dobney et al., 2010).

5.1.4 Socio-economic and land use change modelling

Despite an emphasis on the importance of socio-economic influenced land use change in potentially mediating the impact of climate changes (UKCIP, 2001), most groundwater studies tend to assume a 'business as usual' approach, where such complexities are ignored (Jackson et al., 2006). A notable exception to this is the application of a regional, multi-sectoral and integrated assessment of the impacts of climate and socio-economic change in the UK, RegIS, to groundwater recharge (Holman, 2006; Holman et al., 2005a; Holman et al., 2005b). RegIS is a research methodology for stakeholder-led, regional impact assessment that evaluated climate change impacts as well as adaptation options, comprising interactions between coastal, agricultural, water and biodiversity sectors. Underlying the framework are drivers and associated Socio-Economic Scenarios (SES); world markets, global sustainability, national enterprise and local stewardship. It is argued that such scenarios help to quantify the effect governance and societal values may have on land use and resource management in the future (Shackley and Deanwood, 2003). A summary of the core characteristics of the four SESs can be found in Appendix 4.1.

In the RegIS approach, stakeholder meetings and complex sector modelling was used to develop distributed datasets of potential changes for the difference scenarios (Holman, 2006). For example urban growth is related to population pressures determined by the SES. The agricultural land use distribution is then based on profitability arising from costs, prices and subsidies according to the socio-economic scenario adopted and predicted yields for each crop-soil type combination. For example a 5 km grid of changes in urban area was developed for the 2050 time slice under the national enterprise scenario. Similar datasets are produced for agricultural land use, where simulated crop and irrigation prices dictate areas given over to potato crops and sugar beet are likely to increase dramatically under the national enterprise scenario. Other impacts simulated include saline intrusion into coastal aquifers and areas lost to high flood risk. The combined effect of climate and land use change on the groundwater system were then be assessed at the regional scale

The RegIS process however comes with a long list of caveats (Holman, 2006). For example, scenarios of urban development are unconstrained by water availability. Similarly water availability did not constrain crop types. Feedbacks such

as the impact of land use change on market supply and demand is also lacking. Other sources of uncertainty include not knowing whether biomass crop production would increase infiltration through improved soil organic matter and structure, or decrease through significantly higher soil water use (Holman, 2006; Holman et al., 2005a; Holman et al., 2005b). Downscaling the SES to the regional scale and assessing the impact on key activities e.g. agriculture, housing, transport remains a complex challenge. In addition, while the uncertainty in climate scenario development is high, socio-economic feedback in terms of land use development is even more so.

Alternatives to the RegIS approach include investigating past change on the system (Finch, 2001), arbitrary changes based on general trends (Moiwo Juana, 2006) or interactive scenario development (Jessel and Jacobs, 2005). Local government planning strategies also provide robust tools to formulate likely scenarios in the short to medium term. For the Pang/Lambourn region, these could include; the Berkshire Structure Plan: 2001-2016 prepared by the Berkshire Unitary Authorities Joint Strategic Planning Unit (2005); The South East Plan developed by The South East England Regional Assembly (2006) and West Berkshire District Profile prepared by West Berkshire Council (2007).

5.2 Aims and objectives

The aims of the study are summarised in Figure 5.1 and are made up of three key objectives:

- Interface the GIS-DIRT model developed for the Pang/Lambourn (see Chapter 2) with an ensemble of climate change weather time series from EARWIG. Assess the impact of each scenario on recharge. This model is called EARWIG-DIRT.
- Modify the land use distribution of GIS-DIRT based on a socio-economic scenario developed from local planning documents. Assess the impact these changes will have on total and distributed recharge. The integrated model is termed Socio-Economic Change–Distributed Recharge Transient model (SEC-DIRT).
- Assess the impact of both climate and land use change recharge scenarios on long term future groundwater levels by interfacing them with a groundwater flow model developed in MODFLOW (see Chapter 4). This will be done by

comparing baseline and change scenario borehole hydrograph time series at a range of locations representing different hydrogeological settings.

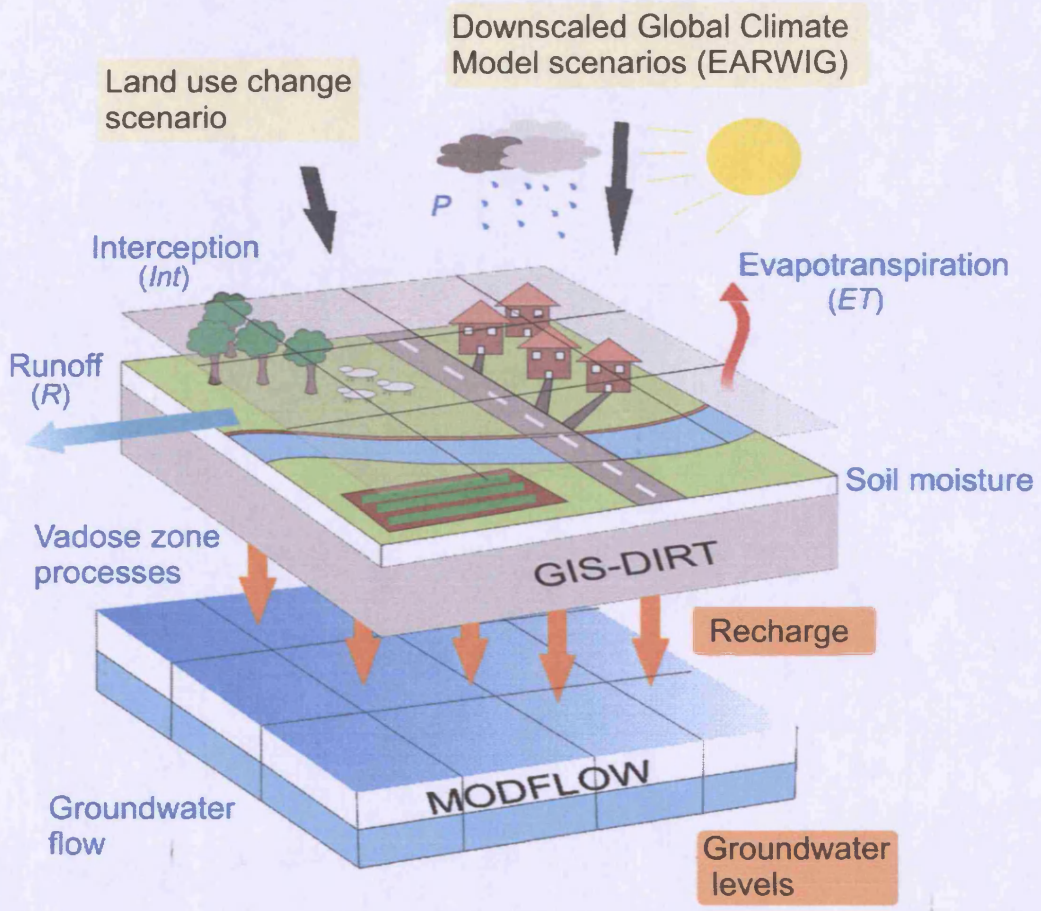

Figure 5.1 Schematic diagram detailing the integration of climate and land use scenarios with the coupled GIS-DIRT and MODFLOW model.

5.3 Methods

5.3.1 Climate change impacts: EARWIG-DIRT and MODFLOW

HadRM3H was the RCM used in conjunction with EARWIG to develop time series of rainfall and potential evapotranspiration for the Pang/Lambourn. The HadRM3H RCM, developed at the Hadley Centre of the UK Meteorological Office was derived from the HadCM3 GCM. Boundary conditions were derived from the global atmosphere model, HadAM3H, which is intermediate in scale between the coarser resolution HadCM3 and HadRM3H (Fowler et al., 2007). HadRM3H ensemble output was used to produce the UKCIP02 climate change scenarios for the UK. Out of the four UKCIP change scenarios, low and high were used and assumed to be the bounding limits of potential impacts. Both high and low emissions scenarios were

therefore implemented at the 2020, 2050 and 2080 time slices, as well as the baseline period (1961-1990). Being a stochastic process means many iterations of the WG are required to give a range of outcomes. For each scenario therefore, an ensemble of five time series was generated in order to address uncertainty issues.

The EARWIG method downscales GCM or RCM output to the catchment scale (<1000 km^2) across Britain (Kilsby et al., 2007). The process was used to provide time series for input into GIS-DIRT for the Pang/Lambourn and can be broken down into five stages:

1. 5 km gridded daily rainfall data is generated for the observed period 1961-1990 by combining multiple regression and inverse distance weighted interpolation taking into account geographic and topographic factors. The relationship between observed rainfall and other climatic variables is defined using regression analysis.
2. RCM rainfall data is used to derive factors of change from current climate state to define climate change scenarios. These are comparable to the factors used in simple time series perturbation studies.
3. A Stochastic Neyman-Scott Rectangular Pulses (NSRP) model of daily rainfall is fitted to the 'current climate' i.e. baseline 1961-1990 at each 5 km grid cell and then re-fitted for possible future scenarios using the change factors.
4. A WG model based on the regression relationships between daily climatic variables and daily rainfall is applied to the synthetic rainfall time series. For the future, all regression weights and explained variances are assumed not to change, although the mean and standard deviation temperature is changed according to the scenario.
5. Synthetic weather time series are generated on a 5 km grid throughout the UK. Other variables include daily mean temperature, daily temperature range, vapour pressure, sunshine duration and wind speed.

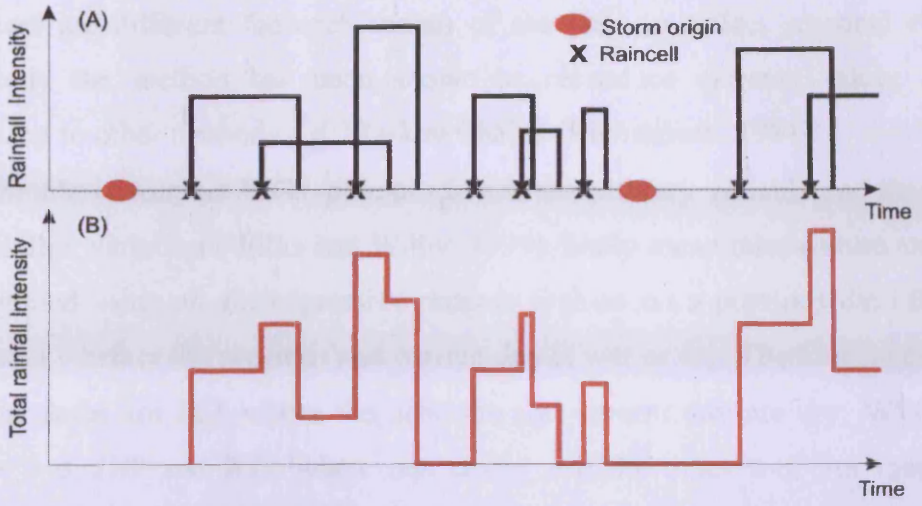

Figure 5.2 Schematic of the NSRP model. (A) Arrival of individual storm systems and associated rain events through time. (B) Total rainfall intensity as a sum of individual rainfall events.

The NSRP rainfall model forms the primary basis of the WG, from which other climate variables are derived. It is a clustered point processes model, broadly relating to underlying physical dynamics. Rainfall is associated with clusters of "rain cells" making up "storm events". The timing of cells is a function of a set of independent and identically distributed random variables representing the time intervals between the storm origin and birth of the individual cells. The parameters are as follows:

λ The average waiting time between subsequent storm origins [T]

β The average waiting time of the rain cells after the storm origin [T]

η The average cell duration [T]

ν The average number of cells per storm

ξ The average cell intensity [LT^{-1}]

The storm arrives with the arrival rate λ. Each storm generates a random number C, with mean value ν, of rain cells separated from the storm origin by time intervals that are exponentially distributed with parameter β. The duration of each rain cell is exponentially distributed with parameter η. The intensity of each rain cell is exponentially distributed with parameter ξ. Finally, the total rainfall intensity is equal to the sum of the intensities of all the active cells at the moment (Kilsby et al., 2007). The schematic, Figure 5.2 illustrates the structure of the model. Analytical expressions are used to fit sets of parameter values (λ, β, η, ν and ξ) corresponding to rainfall time series statistics; mean rainfall amount, proportion of dry days, the variance and skewness of daily rainfall and the lag-1 autocorrelation coefficient. This is done by minimising the weighted sum of squared differences. The model

parameters are different for each month of the year to reflect seasonal changes. Importantly the method has been shown to reproduce extreme values well in comparison to other methods e.g. Markov Chains (Richardson, 1981).

Similarly to most WGs, precipitation is the primary variable and determines other weather variables (Wilks and Wilby, 1999). Daily mean temperature and range are generated using an autoregressive process (values on a previous day) that also depends on whether the previous and current day is wet or dry. The four precipitation transition states are *DD*, where the previous and current day are dry; WW, where both are wet; *DW* and *WD*, where one is dry and the other wet. For mean daily temperature (*Ti*, [°C]) during a *DD* period,

$$T_i = a_1 T_{i-1} + b_1 + e \tag{5.1}$$

wet period (*WW*),

$$T_i = a_3 T_{i-1} + b_3 + e \tag{5.2}$$

dry, wet transition (*DW*),

$$T_i = a_5 T_{i-1} + a_6 P_i + b_5 + e \tag{5.3}$$

dry (*WD*) transition,

$$T_i = a_9 T_{i-1} + a_{10} P_i + b_7 + e \tag{5.4}$$

where, P_i is daily precipitation [L], weights (a_1 to $_{10}$, b_1 to $_7$) have been determined by regression analysis of the observed data and e is a random variable from a normal distribution. Equivalent equations apply to temperature range (*Ri*), albeit with relevant regression weighting. The other variables (X_i) are then determined by regression analysis. For example, vapour pressure, sunshine duration and wind speed corresponds to j (1 to 3)

$$X_{ij} = c_j + d_j P_i + e_i T_i + f_j R_i + g_j X_{i-1,j} + e \tag{5.5}$$

where c, d, e, f and g are regression parameters. These inter-variable relationships maintain both the consistency between and within each of the variables (Kilsby et al., 2007). For climate change scenarios it becomes necessary simply to perturb the mean and standard deviation of these variables where required by scaling the time series. Daily temperature range, vapour pressure and wind speed do not seem to alter under GCM and RCM projections of climate change. In addition, sunshine hours cannot increase, so it is only necessary to perturb the mean and standard deviation of the

mean temperature for each half month period (Kilsby et al., 2007). Precipitation of has previously been perturbed in the NSRP before the WG is initiated.

The EARWIG user interface allows interactive selection of multiple 5 km grid cells or groups of cells making up pre-defined river catchments (see Appendix 4.2 for an example). Catchment output is achieved by simple averaging across a number of 5 km squares. For this reason, a limit of 1000 km^2 is recommended for a single basin, well below the combined surface area of the Pang/Lambourn. The RCM or GCM, time slice and climate scenario was selected from a menu and a defined number (five in this case) of daily time series of 30 years duration was generated providing a spreadsheet-based ensemble. The variables of interest in this study were rainfall and potential evapotranspiration (*Pet*). *Pet* was calculated from the weather variables generated by the WG using the MORECS Penman-Monteith formula (Monteith, 1965). At this stage, the EARWIG WG baseline data (1961-1990) was validated against observed data.

EARWIG rainfall and *Pet* data was run through the recharge model GIS-DIRT for the baseline, high (h) and low (l) emissions scenarios at each of the time slices (2020, 2050, 2080), providing an ensemble of distributed monthly recharge time series. By interfacing the EARWIG stochastic WG with GIS-DIRT distributed recharge model, a new model structure EARWIG-DIRT is created. This structure allows any new rainfall and *Pet* time series combination to be input, allowing interactive scenario development as climate science advances. Under all scenarios, the land use is assumed to remain unchanged from the observed distribution given by the dominant land cover in 2000 (see Figure 1.2).

A transient, single layered MODFLOW model developed using PEST inverse parameterisation was used to assess the impact of the recharge scenarios on groundwater flow in the Pang/Lambourn (see Chapter 4 for details). This model was chosen because it simulated groundwater levels more accurately over a longer time period than the VMF model. In addition, the model run time was shorter, allowing a larger number of scenarios to be processed efficiently. The recharge data was converted from ArcGIS raster grids to recharge (.rch) files and input into the model. This provided an ensemble of groundwater head time series at each observation borehole. The distributed groundwater heads at the end of each simulation were used as the initial heads for the next. For example the final time step of a baseline scenario simulation was used as the initial heads for a 2020 time slice. Groundwater level

simulations at a representative number of sites were assessed closely in order to determine the impact of climate change at the local scale (see Figure 4.1 for borehole locations). An independent samples t test (Wheater and Cook, 2005) was used to determine whether groundwater time series were significantly different from the baseline for each climate change scenario.

In addition, a temporal sensitivity analysis was carried out to determine the impact of using daily or monthly recharge calculations on modelled groundwater levels. To do this, recharge calculated using daily weather data for two sample years (1999 and 2004) was aggregated to monthly values and input into the groundwater model. Any differences in levels can then be compared with the impacts of change on the system to make an assessment of the suitability of monthly recharge calculations. The differences in transient and mean modelled levels at EA trigger boreholes (for location see Figure 4.1), according to recharge time step is assessed. These are in turned compared with observed heads. Northfield, Longacre, Chapelwood, Hodcott and Saltbox boreholes are chosen for their relevance to groundwater flood risk (see Chapter 6).

5.3.2 Land use change impacts: SEC-DIRT and MODFLOW

Land use was modified according to trends highlighted in regional planning documents and RegIS study (Holman et al., 2005b). This method reflects a balance between arbitrary large scale modifications e.g. applying woodland everywhere (Moiwo Juana, 2006) and complex, stakeholder led downscaling of national socio-economic scenarios (Holman, 2006; Jessel and Jacobs, 2005). Here, the West Berkshire District Profile (West Berkshire Council, 2007) suggests a population growth of 7% by 2028 in the region. Due to increases in housing density of up to 40%, this is translated here into approximately a 5% increase in urban/suburban land cover in the catchment, the majority of which is around already established towns and villages (Figure 5.3A and B). The same report explains there are "a number of pressures on the local landscape through changes in farming practices and development", although these pressures are not themselves explicitly detailed. Other trends are picked up by The South East Plan developed by The South East England Regional Assembly (2006). Here, it is suggested that "tree cover is growing and wildlife is generally thriving". As such, coniferous and deciduous woodland has been increased by approximately 5% in the modified land use change scenario (Figure

5.3C). Nuanced changes in the agricultural land use of the region are not quantified in regional development reports and are therefore largely arbitrary.

The recharge model (SEC-DIRT) was parameterised using the modified land use distribution (see Figure 5.3B and C). For details on parameterisation of the transient recharge model refer to Chapter 2. Generally this represents an increase in urban and suburban areas and increase in coniferous and deciduous woodland alongside a decline in arable cereals and horticulture. The changes were spatial as well as in terms of overall coverage. For example, the percentage change is grassland (all varieties) is small, although the location of the grassland varies considerably. In order to allow a comparison between the relative impact of land use and climate to be explored, the ensemble of h2020 weather time series were used. Only the 2020 time slice is considered given the relatively short term land use predications made by the regional planning documents. The distributed recharge data from SEC-DIRT was interfaced with the MODFLOW model providing an ensemble of groundwater level time series at each observation borehole. A representative number of sites were assessed closely in order to determine the impact of land use change at the local scale (see Figure 4.1 for borehole locations). An independent samples t test (Wheater and Cook, 2005) was used to determine whether groundwater time series were significantly different from the baseline in the land use change scenario.

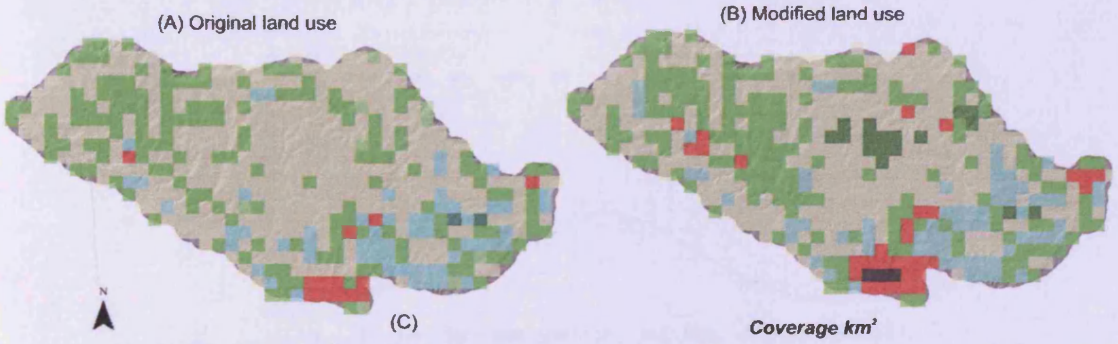

(C)

land use	Coverage km² old	new	change	% change
Improved grassland	156	159	3	0.54
Arable cereals	161	137	-24	-4.33
Suburban/ rural development	13	32	19	3.43
Calcareous grass	9	9	0	0.00
Arable horticulture	153	128	-25	-4.51
Broadleaved mixed woodland	57	67	10	1.81
Set-aside grass	1	1	0	0.00
Coniferous woodland	2	17	15	2.71
Neutral grass	2	1	-1	-0.18
Continuous urban	0	3	3	0.54

Figure 5.3 (A) Original 1 km, 2000 dominant land use raster (B) Future modified distribution representing the 2020s. (C) Summary table of percentage and surface area changes. The changes are based on trends identified in the West Berkshire District Profile (West Berkshire Council, 2007) and The South East Plan (The South East England Regional Assembly, 2006).

5.4 Results

5.4.1 EARWIG baseline climate validation

The ensemble output from EARWIG was summarised for the baseline and climate scenarios and compared against past observations in the Pang/Lambourn (Figure 5.4). The monthly mean of the baseline ensemble compare reasonably well against observed values over a similar time period (1961-1990 in comparison to 1978-2007). The mean difference in *Pet* is circa 7 mm/month and 1.5 mm/month in rainfall. The observed *Pet* statistics are interestingly similar to the h2020 scenario statistics (Figure 5.4C). Any mismatch between the baseline and observed however is dwarfed by the difference between the baseline (and observed) values and those of the climate change scenarios (with the exception of h2020). This is especially the case for h2080 which exhibits around a 37 mm/month increase in *Pet* and 4.5 mm/month decrease in rainfall compared with the baseline. In addition, the temporal distribution of rainfall under climate change scenarios alters in comparison to both the baseline and observed values. For example, the winter months tend to see an increase in mean rainfall, and the summer months a decrease.

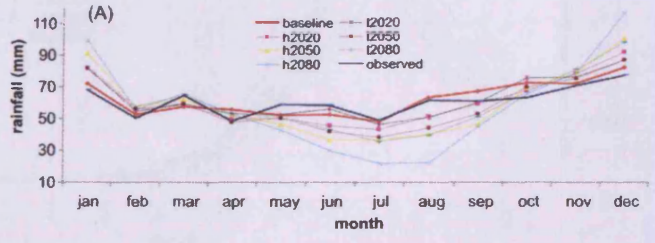

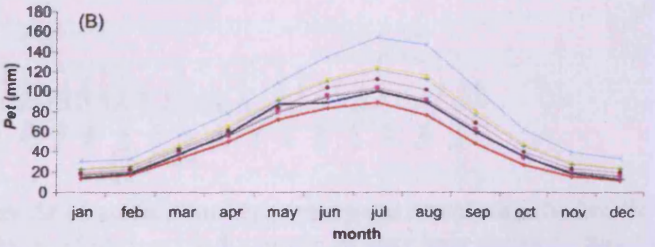

(C)

Potential Evapotranspiration (mm)

	Baseline	h2020	h2050	h2080	l2020	l2050	l2080	MORECS 1978–2007
mean	44.72	53.39	65.69	81.66	52.06	58.03	63.52	51.61
max	88.87	103.93	125.05	153.74	101.95	112.17	121.90	100.12
min	12.04	16.55	23.33	30.58	15.38	19.24	22.52	12.89
sd	29.08	33.08	38.47	46.37	32.59	35.45	37.75	33.13

Rainfall (mm)

	Baseline	h2020	h2050	h2080	l2020	l2050	l2080	Shaw 1962–1990
mean	62.37	61.04	59.67	57.99	62.70	58.75	60.39	60.91
max	82.58	92.30	100.59	117.03	87.26	87.24	98.49	77.45
min	47.80	43.30	36.29	21.84	46.22	38.30	35.43	48.38
sd	10.89	15.70	21.36	29.56	13.71	16.22	19.23	8.87

Figure 5.4 (A) EARWIG baseline mean monthly rainfall in comparison to climate scenarios and field observations at Shaw gauging station. (B) Mean monthly *Pet* comparisons. (C) Summary statistics.

5.4.2 Climate change impacts on recharge and groundwater levels

Monthly mean modelled recharge across the Pang/Lambourn (554 km^2) was calculated for each 30 year distributed time series provided by the EARWIG-DIRT. The result is an ensemble of high and low climate scenarios for the 2020, 2050 and 2080 time slices in comparison to the baseline (Figure 5.5A). Transient mean areal recharge for two example time series (one baseline, one h2080) can be seen in Figure 5.5B. Each data point is equivalent to a distributed recharge dataset and each time series is represented as one entry in the ensemble (Figure 5.5A). Figure 5.5 B shows that most recharge occurs between October and March, irrespective of change scenario. As such, it is useful to look more closely at changes specifically at these times. Figure 5.5C shows box plots of monthly recharge amounts only during hydrological winter (October to March). Box plots show the minimum, first quartile, median, third quartile and maximum (outliers are >1.5 interquartile range).

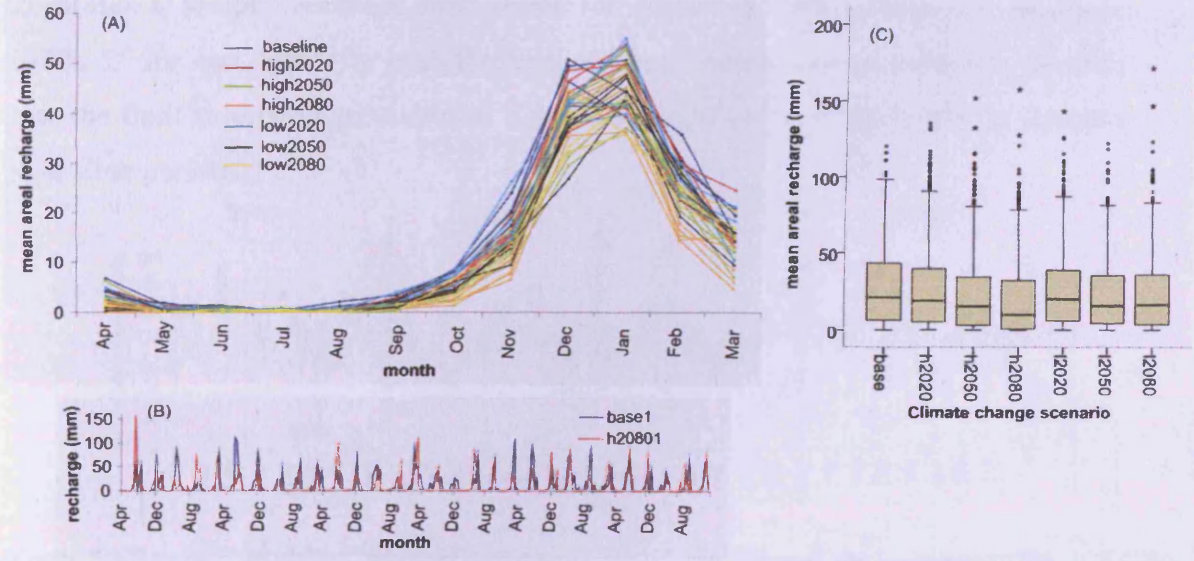

Figure 5.5 (A) Ensemble of mean monthly recharge across the catchment for the baseline, high and low climate change scenarios. (B) Example 30 year long recharge time series for one baseline and one high2080 scenario. (C) Box plot of median monthly recharge and extreme event outliers across the catchment during winter months for the baseline and each climate change scenario.

There is a trend to a decline in average recharge volumes relative to the baseline for all climate change scenarios, especially during the 2080 time slices. Taking a mean of 27.4 mm/month for the baseline, the 2020s show a reduction of between 5.5 and 5.6% for the high and low scenario respectively. The 2050s show a reduction of between 18 and 17.6%, whilst the 2080s exhibit a greater range of between 27 and 17.5% reduction. Interestingly, the number of extreme events

remains high and in some cases the magnitude of these events exceeds those in the baseline. The maximum monthly recharge amount during the baseline ensemble is 120.4 mm in comparison to between 135.4 and 143.1 mm during the 2020s (high and low respectively). This rises to between 151.7 and 122.3 mm during the 2050s and up to 157.4 and 171.2 mm during the 2080s. Throughout the simulations, land use is assumed to remain constant, including seasonal changes in vegetation cover. Relative distributed recharge patterns are not therefore significantly altered (see Appendix 4.3).

Interfacing the distributed recharge time series with the groundwater flow model will help determine if these extreme recharge events would merely replenish a depleted aquifer or lead to dangerously high regional groundwater levels. As such, the climate change recharge data was input into the MODFLOW model, providing an ensemble of groundwater level time series at each observation borehole, including representative boreholes discussed in Chapter 4 (see Figure 4.1). Figure 5.6 illustrates a sample borehole time series for Ashdown Park through the baseline, 2020s, 2050s and 2080s for both the high and low climate change scenarios. In each case the final simulated groundwater levels were used as the initial heads for the next time slice period.

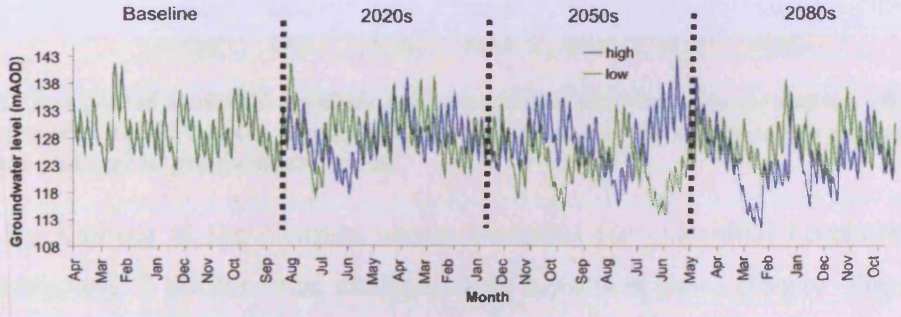

Figure 5.6 Example modelled borehole hydrograph time series through the baseline, 2020s, 2050s and 2080s at Ashdown Park using one sample high and low climate scenario.

Ensemble time series for all boreholes are summarised in Figure 5.7A and B. Each box plot represents 145800 monthly values (30 years × 5). The percent change ($\Delta\%$) from the baseline is calculated for each scenario and time slice for the mean, maximum and minimum,

$$\Delta\% = \frac{(\mu B - \mu C)}{\mu B} 100 \tag{5.6}$$

where μB is the baseline mean, maximum or minimum across the ensemble and μC the climate scenario and time slice mean maximum or minimum across the ensemble.

The 2020 time slice sees a mean decrease of between 0.6 and 0.5% across all boreholes for the high and low scenario respectively relative to the baseline. The 2050s shows a reduction of between 2.5 and 2.3%. For the 2080s, it falls further to between 3.8 and 2.2%. The maximum (peak) groundwater levels are reduced in a similar manner, up to 7.1% for the low scenario during the 2050s and 2080s. Minimum levels remain largely unchanged. These statistics are summarised for all scenarios in Figure 5.7C.

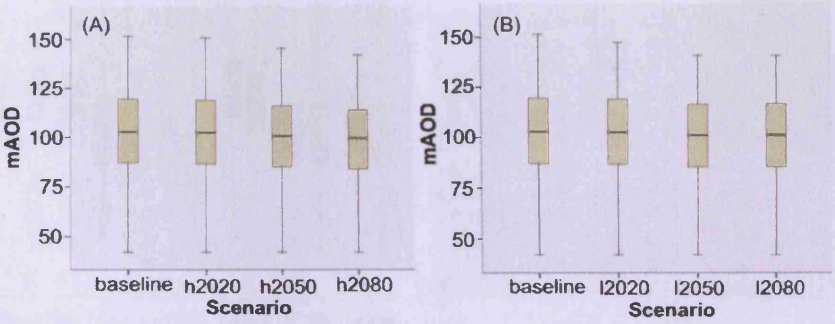

(C)

Scenario	Mean mAOD	% change	Max mAOD	% change	Min mAOD	% change
Baseline	100.7	NA	151.6	NA	42.2	NA
h2020	100.1	-0.60	150.8	-0.53	42.2	0.00
h2050	98.2	-2.48	145.3	-4.16	42.2	0.00
h2080	96.9	-3.77	141.9	-6.40	42.1	-0.24
l2020	100.2	-0.50	147.4	-2.77	42.2	0.00
l2050	98.4	-2.28	140.8	-7.12	42.2	0.00
l2080	98.5	-2.18	140.8	-7.12	42.2	0.00

Figure 5.7 Box plot of modelled borehole levels catchment wide for high (A) and low (B) climate change scenarios relative to the baseline. (C) Summary table of mean, maximum and minimum percentage changes in groundwater levels.

By looking at the changes across scenarios for individual boreholes of the Pang/Lambourn, it allows local changes to be examined more closely. Figure 5.8A shows box plot summaries for boreholes on the interfluves at Ashdown (164 mAOD) and Sparsholt (176 mAOD), for different climate scenarios. The graph suggests a dramatic decrease in average groundwater levels with time, as well as maximum and minimum values, relative to the baseline. In order to quantify the changes from one scenario to another, Figure 5.8B summarises the percentage change in groundwater levels at the two sites, including variation within individual scenario ensembles. A t test carried out in each case confirms a statistically significant deviation from the baseline ($p<0.5$). There is variation within climate scenarios, as well as between. For example, at Sparsholt, the high scenario during the 2020 time slice provides a mean reduction in groundwater level of 1.1 m. This is however bounded by a maximum

increase of 0.8 m and decrease of 2.2 m. Similarly, extreme low values for the h2080 scenario at Ashdown are bounded between a reduction of 6 and 1.4 m. Extreme high levels are bounded by a reduction of between 5.7 and 13.1 m during the same scenario.

(A)

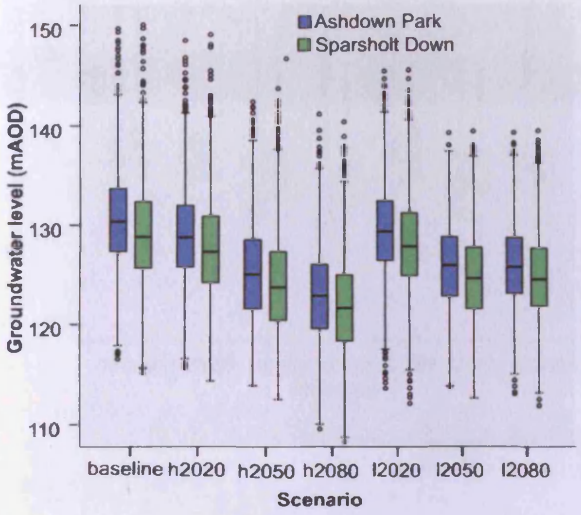

(B)

scenario	mean GW level % change min	mean	max	extreme GW level % change low min	low max	high max	high min	t test
h2020	-2.2	-1.1	0.8	-0.8	3.5	-0.8	-7.4	8.9**
h2050	-5.6	-4.0	-2.2	-2.3	-0.2	-4.9	-11.1	31.7**
h2080	-7.3	-5.9	-5.5	-6.0	-1.4	-5.7	-13.1	46.5**
l2020	-2.0	-0.8	-0.3	-2.5	3.1	-2.0	-7.6	6.7**
l2050	-5.5	-3.5	-2.5	-2.4	2.0	-6.9	-10.4	29.3**
l2080	-4.6	-3.4	-2.6	-3.0	2.8	-6.9	-9.2	29.4**
h2020	-2.2	-1.1	0.8	-0.7	3.1	-0.6	-7.5	8.1**
h2050	-5.4	-3.9	-2.1	-2.3	-0.2	-4.2	-11.3	28.8**
h2080	-7.0	-5.7	-4.5	-6.0	-1.3	-6.4	-12.3	42.9**
l2020	-2.0	-0.8	-0.1	-2.6	3.0	-3.0	-7.3	6.0**
l2050	-5.3	-3.4	-2.4	-2.2	1.9	-7.1	-9.7	26.6**
l2080	-4.4	-3.3	-2.5	-2.8	2.7	-7.1	-9.0	26.6**

Figure 5.8 (A) Box plot of modelled groundwater levels at Ashdown and Sparsholt across climate scenarios. (B) Summary statistics for climate change scenarios. ** t test significant, P<0.05.

Other representative boreholes are summarised in Figure 5.9. Significant t test results were found at all sites under all scenarios and time slices ($p<0.5$), suggesting all climate change scenarios had an impact on groundwater levels catchment wide (see Appendix 4.4). Details of intra-scenario variations of mean, maximum and minimum levels can also be found in Appendix 4.4. Oak Ash (173 mAOD), associated with influves overlain with superficial deposits and Malthouse (129 mAOD) along the ephemeral Pang, both exhibit a decline through time and across climate scenarios (Figure 5.9A). Nuanced differences however exist between the responses. Malthouse shows a greater overall decline, for example -4.8% mean for h2080 in comparison to -3.4% at Oak Ash. There is also a greater decline in minimum and maximum values, suggesting a greater reduction in groundwater level fluctuation at Malthouse (Figure 5.9A).

Whitehouse (104 mAOD) is overlain by Palaeogene deposits but usually remains unconfined and Compton lies along the ephemeral Pang (99 mAOD). Again, mean and extreme groundwater levels at these locales decreases dramatically across the scenarios (Figure 5.9B). The low emissions scenario, although providing a statistically significant shift, shows a less marked decrease generally. The reduction

in the mean and extreme values at Compton is greater than at Whitehouse, with Compton being more comparable to Malthouse (Figure 5.9A).

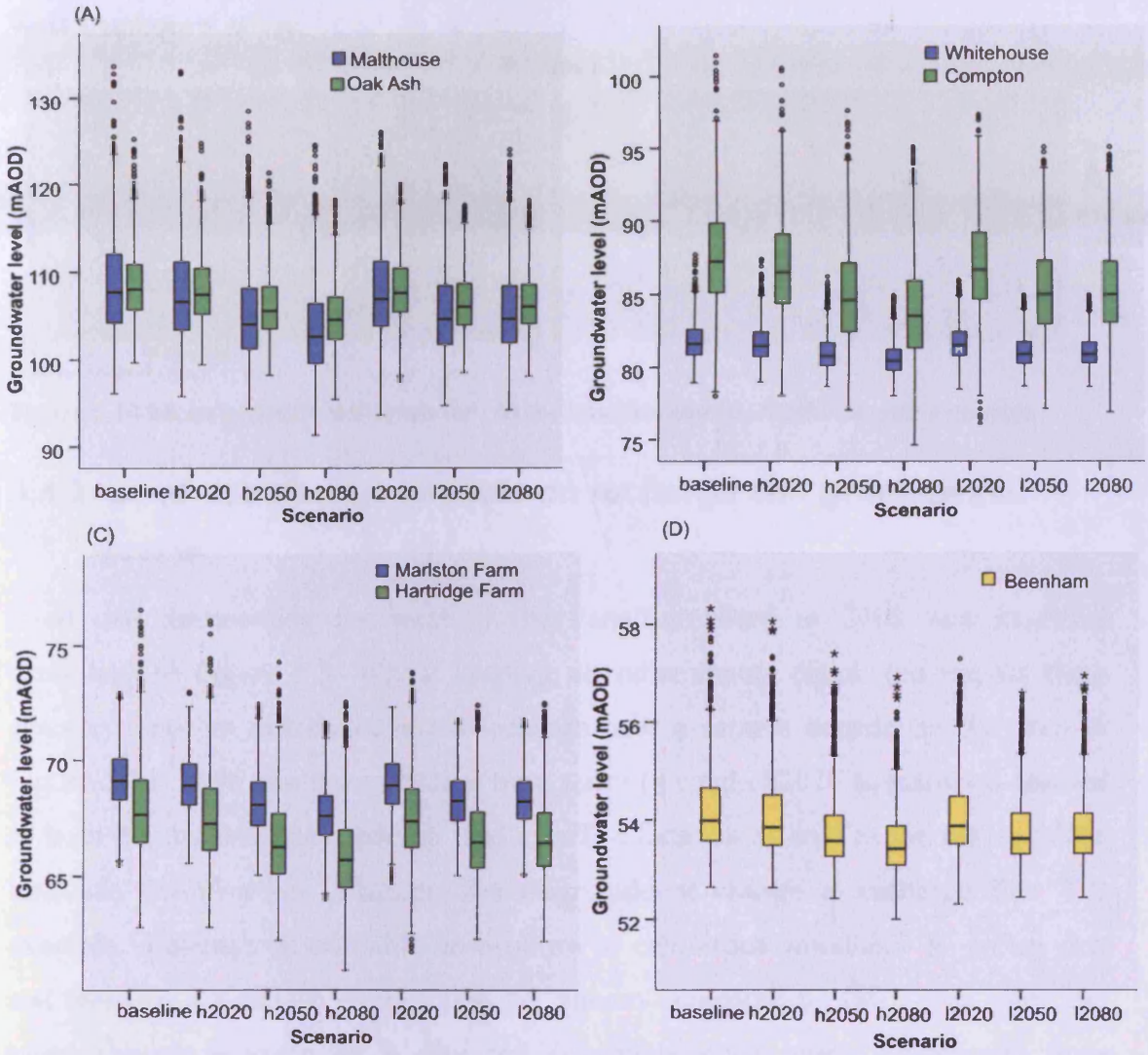

Figure 5.9 Box plots of modelled groundwater levels across climate scenarios at Malthouse and Oak Ash (A), Whitehouse and Compton (B), Marlston and Hartridge (C) and Beenham (D)

Marlston (75 mAOD) lies near the perennial source of the Pang, Hartridge further up the interfluves (128 mAOD) and Beenham is usually confined under the London Clay (101mAOD). All disparate sites exhibit the same fundamental shift to a lower mean, minimum and maximum groundwater level under the climate change scenarios (Figure 5.9C and D). Indeed, all three show indications of significant shifts in the groundwater regime. Hartridge, with the greatest range seems to exhibit the largest decrease in mean and extreme values across the scenarios. This continues a trend of sites of relatively large fluctuation suffering the largest decrease. Figure 5.10 illustrates mean groundwater levels for the entire model domain across the ensemble for the baseline and h2080 climate scenario. At this large scale, it is difficult to pick

up on the subtle changes in groundwater levels. However, it possible to see the reduction in groundwater levels generally and particularly the mound in the north west Lambourn valley.

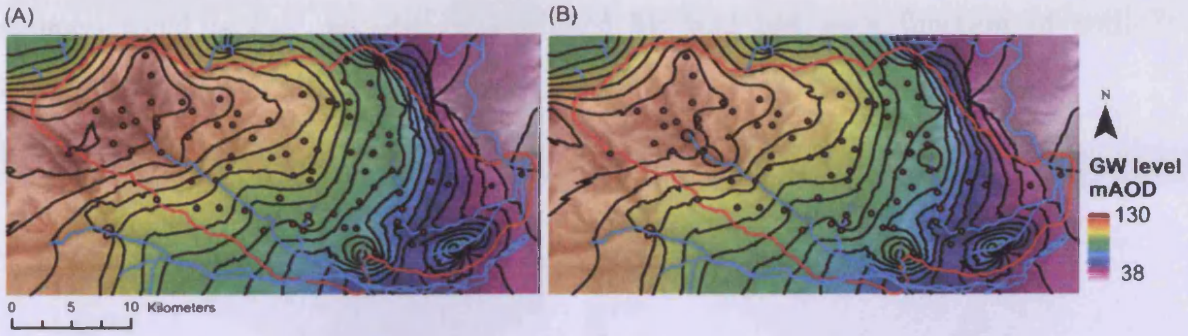

Figure 5.10 Mean groundwater levels for (A) the baseline and (B) h2080 climate scenarios.

5.4.3 Land use change impacts on recharge and groundwater levels

Land use representing the state of the Pang/Lambourn in 2000 was modified according to Figure 5.3. Whilst keeping all other inputs equal, the impact these changes have on distributed mean recharge over a sample decade can be seen in Figure 5.11. Here, the same weather time series (a single h2020 scenario) is applied to both the original and modified land use. The location as well as the nature of the land use modification influences the magnitude of change in recharge flux. For example, a change from arable horticulture to coniferous woodland on a clay rich soil leads to a decrease of 94.4 mm per annum compared to 180.5 mm when the same change is made on a silty soil (equitable slope angle). A change from calcareous grass to coniferous woodland on the same silty soil leads to relative decrease of 115 mm per annum. Similarly, changing from arable cereals to improved grassland leads to a decrease of 54.7 mm in clay rich soil but 90.2 mm over a more silty soil. Indeed, better draining soils seem to amplify the land use changes. Deciduous woodland improves the potential for recharge in comparison to permanent grassland by about 30 mm per annum. On the other hand, decreases of between 12.8-36 mm are seen where arable horticulture is replaced by deciduous woodland. This dichotomy reinforces the importance of perennial vegetation die off in the recharge process. Elsewhere, increases are seen where grassland is converted to arable land (40–90 mm per annum). Suburban development also leads to an increase in recharge, as interception is more limited. For example converting grassland to suburban rural development leads to an increase in recharge of 108.8 mm per annum on a silty soil.

The increase is more modest when developing arable land (typically 18–43 mm). However, as suburban development moves towards continuous urban development however, decreases in recharge in the region of 32 mm per annum are seen. The common trend is that recharge is mediated by land use as a function of soil properties, and to a much lesser extent topography i.e. slope angle.

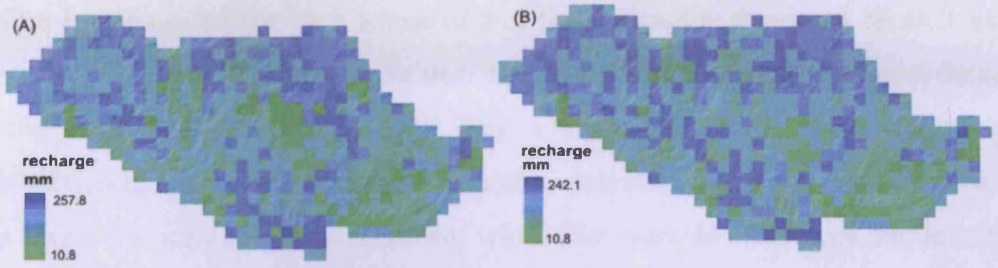

Figure 5.11 Annual mean distributed recharge (mm/yr) over a ten year period of a h2020 weather time series for the modified land use (A) and original land use (B).

As well as nuanced differences in the spatial distribution of recharge, land use change impacts on the overall volume of water entering the groundwater system (Figure 5.12A). There is trend to a decline in average recharge for the land use change scenario relative to the original h2020 values. Mean monthly recharge is 14.47 mm for the baseline in comparison to 13.39 mm for h2020, 12.44 mm in the land use change scenario and 10.17 mm for the h2080 scenario. During the winter months, the h2020s shows a reduction in recharge of 5.5% per annum in comparison to the baseline. The land use scenario (luh2020) demonstrates a reduction of 12.3%. The frequency and magnitude of the extreme recharge events however remain equitable to the h2020 scenario. The maximum recharge event in a single month across the ensemble is 135 mm and 132 mm for the h2020 and luh2020 scenarios respectively (Figure 5.12A).

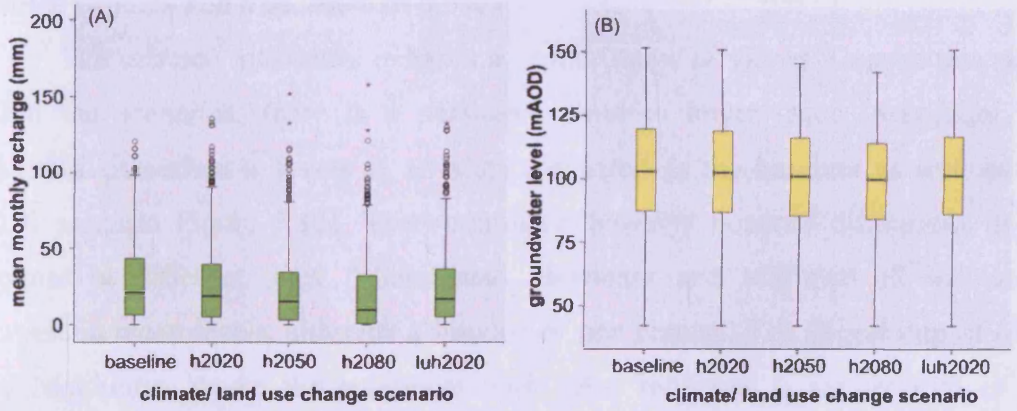

Figure 5.12 Box plots summarising (A) mean monthly recharge during hydrological winter and (B) mean modelled groundwater levels at all observation boreholes, for the baseline, high climate and land use change scenarios.

The land use change recharge data was input into MODFLOW providing an ensemble of groundwater head time series at each observation borehole, including the 5 EA trigger boreholes. Ensemble time series for all borehole sites are summarised in Figure 5.12B. Each box plot represents 145800 monthly groundwater level values (over 30 × 5 years). The percent change ($\Delta\%$, see Equation 5.6) from the baseline is calculated for each scenario and time slice for the mean as well as the extreme maximum and minimum values. The luh2020 scenario sees a mean decrease in recharge of 1.7% from the baseline. This is in comparison to a 0.6% reduction for the h2020 scenario. The maximum reduction was for the h2080 scenario, where mean levels dropped by 3.8% catchment wide. The extreme maximum and minimum values are reduced by 0.6 and 0.2% respectively in the luh2020. This is a slightly greater impact than in the h2020, where maximum levels drop by 0.5% and the minimum remains unchanged from the baseline.

Individual boreholes were examined more closely for the local impact of land use changes. Figure 5.13 shows box plot summaries for Ashdown, Sparsholt, Oak Ash, Malthouse, Whitehouse, Compton, Marlston, Hartridge and Beenham boreholes across the scenarios. Table 5.1 summarises the percentage changes in groundwater levels from the baseline, including variation within individual scenario ensembles. A t test is also carried out in each case confirming a statistically significant deviation from the baseline and the h2020 climate scenario ($p<0.05$). There is variation within the land use change scenario ensemble as well as between the baseline and other scenarios. This intra-scenario range is most pronounced at Ashdown, where the mean groundwater table falls by 2.5%, bounded by a reduction of 8% and increase of 0.6%. In addition, relative to the baseline, the minimum level ranges from an increase of 3.1% and a decrease of 6.5%.

The extreme maximum exhibits a similar range of values. Despite this range within the scenarios, there is a persistent trend to lower mean, maximum and minimum groundwater levels at all sites compared to the baseline as well as the h2020 scenario Figure 5.13). There are again however nuanced differences in the response at different sites. Whitehouse, Beenham and Marlston all indicate a decrease in mean levels, although a fraction of one percent. The largest impact of all is at Malthouse, where the maximum high value reduction is almost 13% of the baseline. Indeed it is the maximum groundwater levels that are affected more than the minimum all sites under the land use modification scenario. An interpolated

mean groundwater surface illustrates this general reduction in groundwater levels, which is however difficult to discern at the catchment scale (see Appendix 4.5).

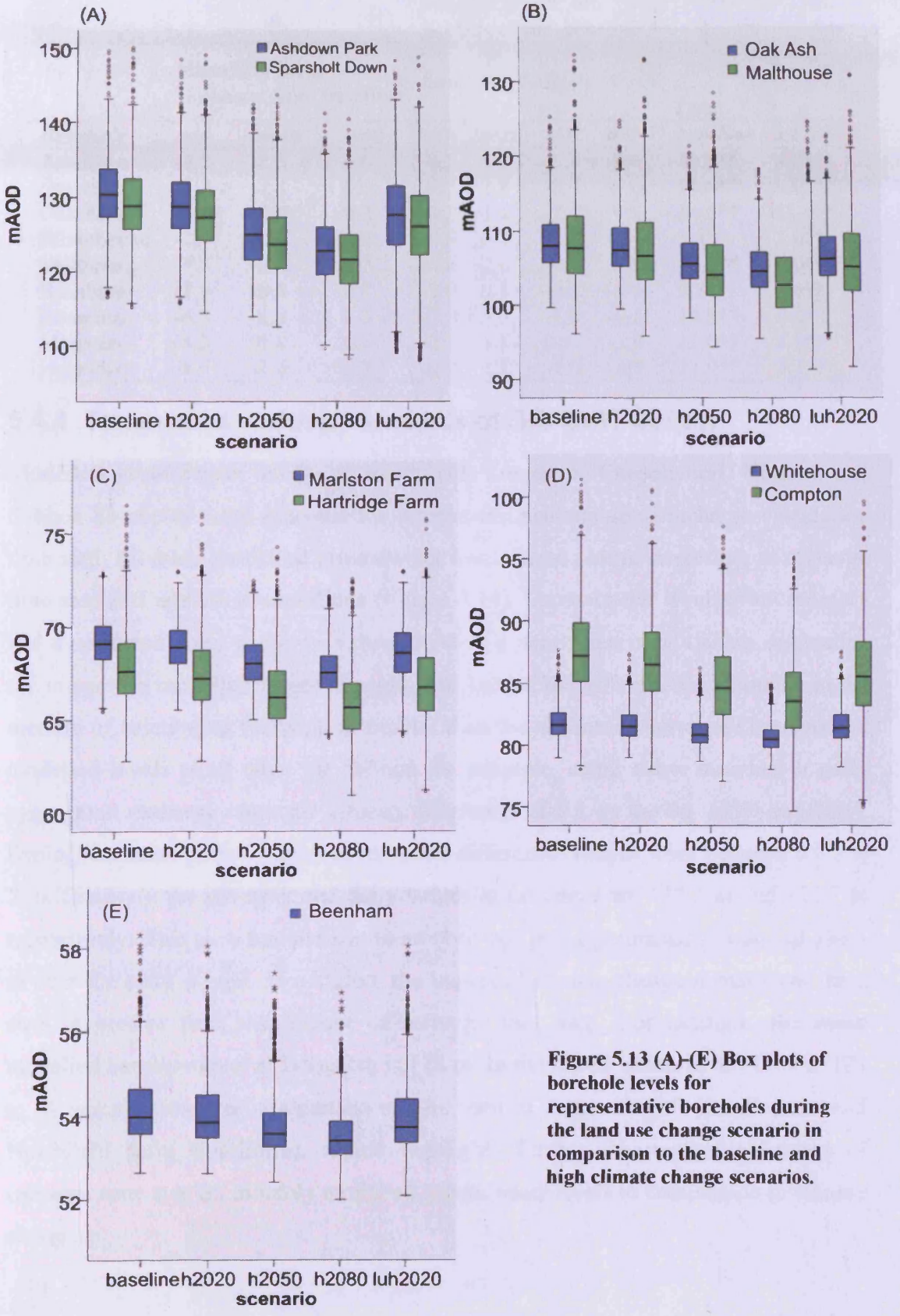

Figure 5.13 (A)-(E) Box plots of borehole levels for representative boreholes during the land use change scenario in comparison to the baseline and high climate change scenarios.

Table 5.1 Summary statistics for all representative boreholes for the land use change scenario relative to the baseline and h2020 scenario. ** t test significant, p<0.05

	Mean GW level % change from baseline			Extreme GW level % change from baseline					
				Low		*High*		*t test*	
Borehole	***min***	***mean***	***max***	***min***	***max***	***max***	***min***	***baseline***	***h2020***
Ashdown	-8.0	-2.5	0.6	-6.5	3.1	-0.9	-9.4	16.8**	9.2**
Sparsholt	-7.8	-2.4	0.6	-6.3	2.8	-0.9	-9.6	16.0**	9.0**
Oak Ash	-5.3	-1.8	0.2	-4.2	1.6	-2.0	-9.9	14.6**	11.1**
Whitehouse	-1.9	-0.3	0.6	-0.9	0.7	-0.2	-4.4	5.8**	3.0**
Malthouse	-7.1	-2.4	0.3	-4.6	2.0	-2.1	-12.9	13.1**	9.0**
Beenham	-1.6	-0.5	0.2	-1.0	0.5	-0.5	-4.6	9.3**	5.0**
Compton	-6.3	-2.0	0.3	-3.9	2.8	-1.8	-9.6	14.3**	9.0**
Marlston	-3.2	-0.8	0.4	-2.1	1.5	0.1	-3.4	12.0**	8.0**
Hartridge	-4.4	-1.4	0.3	-2.7	1.7	-1.0	-8.3	12.9**	8.1**

5.4.4 Temporal sensitivity analysis of GIS-DIRT output

Modelled groundwater levels at Northfield, Longacre, Chapelwood, Hodcott and Saltbox boreholes were assessed for differences attributable to recharge calculation time step. Monthly modelled groundwater levels were plotted according to recharge time step and against observations (Figure 5.14). Groundwater levels from monthly and aggregated daily recharge values provide a near linear relationship suggesting the impact on modelled levels is negligible. Indeed the difference attributable to the method of calculating recharge is smaller than the difference between observed and modelled levels at all sites. At Saltbox for example, using either monthly or daily aggregated recharge leads to a mean difference of 0.1 m during 1999 and 2004. During the same period model-observation differences ranges from between 6.9 and 7 m. Similarly the monthly and daily values at Longacre are 127.3 m and 126.7 m respectively. This is in comparison to an observed mean groundwater value of 133.1 m over the same period. In addition, the impact of climate change scenarios at these sites is greater than the impact of recharge time step. For example, the mean modelled baseline level at Longacre is 128 m. In the h2080 scenario this falls to 121 m. A sample transient comparison can be seen in Appendix 4.6 (for Hodcott and Northfield farm boreholes), which highlights further the negligible impact of recharge time step on monthly modelled groundwater levels in comparison to climate change.

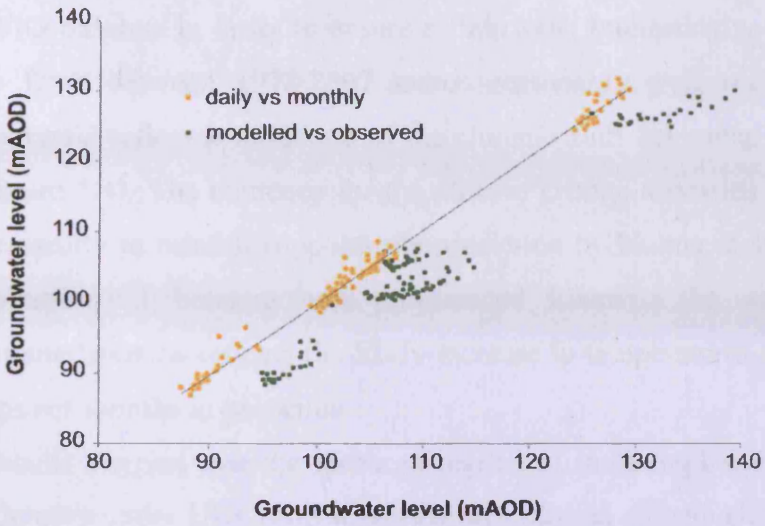

Mean groundwater level 1999 & 2004

	Northfield	Longacre	Chapelwood	Hodcott	SaltBox
Monthly	105.4	127.3	101.4	102.3	90.6
Daily	105.7	126.7	101.6	102.6	90.5
Observed	108.0	133.1	107.6	110.6	97.5
h2080	103.9	121.2	99.4	99.0	87.1

Figure 5.14 Modelled levels at EA trigger boreholes during 1999 and 2004 as a function of either daily or monthly recharge calculations, in comparison to observations and the h2080 climate scenario.

5.5 Discussion

The aim of this chapter has been to assess the impact of climate and land use change on the future recharge regime and groundwater levels in the Pang/Lambourn. To do this the integrated recharge and groundwater flow models developed in previous chapters were systematically perturbed according to likely future scenarios. Scenarios of climate change are applied to this integrated model by downscaling output from the RCM, HadRM3H. In addition, a modified land use scenario was developed in conjunction with regional planning documents to assess the relative impact on the hydrogeological system. The focus has been on developing a useful tool to quantify the potential changes in groundwater levels under scenarios developed by UKCIP02 (Hulme et al., 2002). Ultimately the changes to the groundwater regime discussed here will be used to assess the risk of groundwater flooding in the future (see Chapter 6).

Firstly, the stochastic WG, EARWIG was used to generate an ensemble of synthetic rainfall and potential evapotranspiration time series. The baseline (1961-1990) statistics match up well with the corresponding observed time series, considering the relatively low number of iterations of the WG. The relatively small discrepancy is not important as the climate change scenarios will be assessed relative

to the EARWIG baseline in order to ensure a 'fair test'. Interestingly, the observed *Pet* statistics from between 1978-2007 match reasonably well with the h2020 scenario. This could reflect a validation of the climatic shift beginning in the 2020s time slice (Figure 5.4). The tendency for the climate change scenarios to exhibit an increased seasonality in rainfall supports the prediction by Hulme et al. (2002) that winter precipitation will become more pronounced. Likewise the increase in *Pet* during the summer months reflects the likely increase in temperatures generally and during the summer months in particular.

The results suggest that the recharge regime of the Pang/Lambourn will be altered considerably under UKCIP02 scenarios of projected climate change. There is a declining trend in average (mean and median) recharge volumes relative to the baseline for all climate change scenarios, particularly during the 2080 time slices. Overall, there is a range of between 5.5% (h2020) and 27% (h2080) reduction in recharge rates relative to the baseline over the next century. This is in agreement with previous studies that also suggest a marked reduction in recharge in East Anglia and other sites in Britain (Herrera-Pantoja and Hiscock, 2008; Yusoff et al., 2002). This decrease is despite an increase in winter rainfall– a period when recharge is conceptually most likely to occur. The consequence of wetter winters could be countered by a concurrent increase in temperatures and *Pet* during the same period. Also drier, warmer summers could deepen soil moisture deficits and delay the recovery of the soil to field capacity.

Interestingly although the trend is to a decline in recharge flux, the number of extreme recharge events remains high and in some cases the magnitude of these events exceeds those simulated in the baseline. For example, a maximum monthly recharge value of 171.2 mm is seen during the l2080 scenario in comparison to 120.4 mm during the baseline. This observation could reflect the forecast increase in the intensity of winter precipitation events. These periods of exceptionally high rainfall may lead to peaks in recharge, even in the absence of a soil moisture deficit, via bypass flow. Indeed this increase in rainfall intensity is expected to be highest in the south east of Britain (Hulme et al., 2002), the region in which the Pang/Lambourn is located. This suggests that monthly recharge calculations can pick up nuanced changes in rainfall intensity as well as volume.

The spatial and temporal distribution of recharge remains largely unchanged under the variety of climate change scenarios. The winter and spring months,

between October and April remain the dominant months of recharge flux (Figure 5.5) and relative distributed values remain stable. This is likely to be because the land use, soil and slope parameters remain unchanged throughout. It seems therefore that surface hydrology dominates distributed recharge, whereas climate influences the magnitude of the flux. In this case, uniform weather conditions are assumed over the catchment. Although the relative spatial pattern of recharge remains similar throughout the climate scenarios, it is important to maintain the distributed nature of the data. This is because, when applying these values to a groundwater model, the location of these changes could be significant. A reduction in flux at one point could potentially have different consequences for water resource management and groundwater flood risk than a reduction of similar magnitude elsewhere.

The mean and maximum groundwater levels are reduced through the time slices and across the climate scenarios. This generally mirrors reductions seen in the recharge flux. These findings appear to contradict predictions of increased groundwater levels in the Yorkshire Chalk in the first half of the 21st century (Younger et al., 2002) but confirm other reports of decreased (14%) base flow in East Anglia over a similar period (Yusoff et al., 2002). The later figure is associated with a 17-35% drop in recharge rates, suggesting a discrepancy between flux into the system and out. A similar discrepancy is seen here, where the maximum reduction in average groundwater levels of 3.8% is considerably less than the 27% decrease in average recharge entering the system during the same period. Equally, the higher extreme recharge events are not translated into high groundwater levels. Whereas maximum recharge values increased, peak groundwater levels are reduced up to 7% from the baseline. A possible explanation of this could be that these extreme recharge events simply replenish a depleted aquifer rather than leading to high groundwater conditions. This observation has important consequences for groundwater flooding risk (see Chapter 6). The discrepancy between recharge and groundwater level decrease, as a percentage from the baseline is more difficult to explain. It is not possible to directly equate recharge input with a direct and equivalent rise in groundwater levels. The maintenance of levels could be due to the release of water into and out of storage. This process may dampen any extreme changes in the future risk of groundwater flooding.

All boreholes exhibit a general trend of decline in groundwater levels across time slices and scenarios. Indeed, a contour comparison between the baseline and

h2080 scenario indicates a subtle change to a gentler groundwater gradient, particularly in a north-easterly direction, west of the Upper Pang valley. However, it has been necessary to compare individual boreholes to assess nuanced local impacts. There is a trend of a reduction in climate change impact with site elevation (mAOD) and seasonal fluctuation range. This applies to mean, maximum and minimum values as well as the spread within the scenario ensemble. The percentage change in mean groundwater level is greatest on the drift free interfluve sites at Ashdown (164 mAOD) and Sparsholt (174 mAOD). Conversely, Beenham (101 mAOD) exhibits the smallest impact, with a maximum reduction of about 1 m in the mean during the h2080 scenario. This pattern is likely to be a reflection of dominant local hydrogeological processes. For example, sites monitoring the interfluves are more directly influenced by recharge flux. This is supported by the relatively large values of potential recharge in these areas (see Figure 5.1B) and relatively large seasonal fluctuations in the groundwater surface (20-30 m). The site at Beenham is usually confined under Palaeogene deposits reducing the amount of recharge and fluctuations. Climatic changes therefore have less of an influence here. Other sites lie along a continuum where the exposure to recharge mediates the relative impact of climate change on groundwater levels. Table 5.2 shows a ranking of impact of the h2080 scenario, which could equally apply to the other scenarios. An impact rank of one is an indication that the site shows the largest relative reduction in mean groundwater levels. The order of impact based on hydrogeological setting and elevation is clear.

Table 5.2 Climate impact ranking of a selection of boreholes, including fluctuation ranges, altitude and hydrogeological setting.

Borehole	*Hydrogeological setting*	*Observed Recharge (mm/yr)*	*Impact rank*	*Fluctuation Range m*	*Elevation mAOD*
Ashdown	Interfluve	212	1	20-30	164
Sparsholt	Interfluve	249	2	20-30	176
Malthouse	Upper pang valley	245	3	15–20	129
Compton	Upper pang valley	110	4	15–20	99
Oak Ash	Interfluve & deposits	145	5	8-20	173
Hartridge	Interfluve & deposits	136	6	8-20	128
Marlston	Lower Pang Valley	116	7	2	75
Whitehouse	Paleogene, not confined	121	8	8	104
Beenham	Paleogene, confined	116	9	<1	101

The exposure of the groundwater system to climate change impacts is likely to reflect local aquifer properties. Higher transmissivity (T) and storage (S) in valleys may produce a more dampened response to recharge. As flux is channelled away relatively quickly or released from storage, the relative impact of climate change is attenuated. Again, this is also a possible explanation for the discrepancy between the change in recharge flux and groundwater levels at the boreholes. Recharge in the surrounding areas will also impact the exposure of a site. For example, the Compton borehole site receives relatively little recharge but is relatively exposed to climate impacts. This could be because it lies in an island of reduced recharge surrounded by zones of 200 mm/yr or more.

By comparing the baseline with climate and land use scenarios, it is possible to explore the relative contribution of each in modifying the recharge regime. There is a decline in average recharge rates in the land use change scenario (luh2020) relative to both the baseline and equivalent climate change scenario (h2020). This is exemplified during the winter months, where the percentage decrease in the mean relative the baseline is over double in luh2020 compared to h2020 (12.3% and 5.5% respectively). The frequency and magnitude of extreme recharge events remains equitable. This suggests that land use can significantly impact upon the recharge regime just as changes to climate might. Where climate is a key driver of extreme events, land use can control mean local input levels. Although it is difficult to compare directly due to local differences, these findings support the previous studies that have highlighted the importance of land use in the recharge regime (Finch, 2001; Holman, 2006). Just as in Finch (2001), the land use changes produced nuanced differences in the spatial distribution of recharge. Evidence suggests that the location and nature of the land use modification influences the magnitude of change in recharge flux. In addition, whilst the changes are driven by land use, they are mediated by soil properties. This is expected in a system where land use does not produce the systematic variation in recharge associated with soil texture (see Figure 2.17). Soil texture is a determinant of recharge potential via a runoff parameter. The degree of actual recharge is a function of land use which largely dictates interception, and evapotranspiration via the root constant and wilting point.

The mean and maximum groundwater levels are reduced in the land use change scenario relative to the baseline and equivalent climate change scenario. This suggests that the land use modifications amplify the reduction in groundwater levels

catchment wide. The contour comparison between h2020 and luh2020 (Appendix 4.5) suggests that regional groundwater flow patterns remain similar despite the changes in distributed recharge. Regional flow is more likely dominated by aquifer parameters, T and S. This is supported by assessing the impact ranking of climate and land use change scenarios on select boreholes (Table 5.3). Here, a comparison is made between the relative impact of h2020 and the land use change scenario luh2020 on groundwater levels at select boreholes. The impact is simply a rank of percentage change from the baseline. The h2020 ranking is similar to h2080 and luh2020, suggesting local reductions in groundwater levels may be unaffected by land use modification. However by plotting the mean percentage changes in recharge and groundwater levels for a land use change scenario (Figure 5.15), it is possible to see that some boreholes are not affected equally. For example, Oak Ash lies in the vicinity of a relatively large afforested zone. The reduced recharge flux seems to have created a more pronounced decrease in groundwater levels here than in other areas. Similarly, Compton is sited near a zone of increased recharge, thereby attenuating the catchment-wide reduction in groundwater levels. Therefore although recharge changes may be dissipated catchment-wide, they still may affect groundwater levels at the local scale.

Table 5.3 Climate and land use change impact ranking of a selection of boreholes, including fluctuation ranges, altitude and hydrogeological setting.

Borehole	*Recharge (mm/yr)*	*Impact rank luh2020*	*Impact Rank h2020*	*Impact Rank h2080*	*Fluctuation Range m*	*Elevation mAOD*
Ashdown	212	1	1	1	20-30	164
Sparsholt	249	2	1	2	20-30	176
Malthouse	245	2	2	3	15–20	129
Compton	110	3	2	4	15–20	99
Oak Ash	145	4	4	5	8-20	173
Hartridge	136	5	3	6	8-20	128
Marlston	116	6	5	7	2	75
Whitehouse	121	8	6	8	8	104
Beenham	116	7	6	9	<1	101

Finally, a temporal sensitivity analysis was carried out using recharge values calculated on a daily or monthly basis. It was found that the magnitude of error using monthly input values was small in comparison to observation-model differences (a detailed discussion of model fit can be found in Chapter 4). This is despite the

groundwater model being shown to be sensitive to recharge flux (see Figure 4.8). The difference between monthly and daily recharge calculations is not significant enough to impact upon groundwater levels significantly. In addition, the impact of climate on the groundwater system outweighs the impact of using monthly or daily data. Taking Northfield borehole as an example, the mean groundwater level modelled using monthly data is 105.4 m in comparison to 105.7 m when using daily data. The observed mean level is 108 m. Over 30 years the baseline climate data gives a value of 106.2 m in comparison to 103.9 m for the h2080 scenario. Climate impacts modelling, relies on calculating relative impacts of different climate regimes, so by keeping the method constant it provides a fair test. These tests suggest that monthly (Vandewiele et al., 1992) or longer (Batelaan and De Smedt, 2007) time steps provide a meaningful alternative to daily accounting procedures.

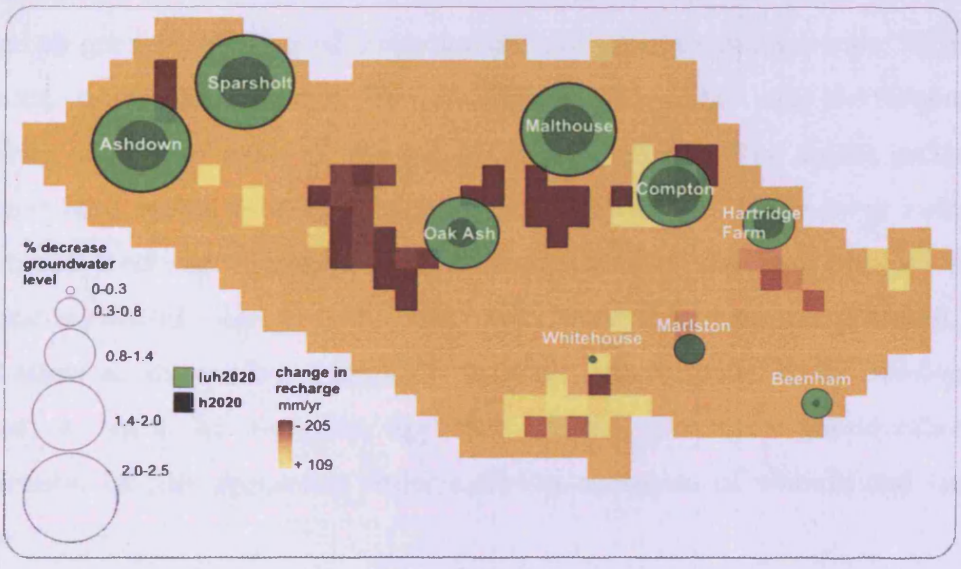

Figure 5.15 Comparison of percentage decrease in mean groundwater level between the h2020 and luh2020 scenarios. Grid indicating zones of reduced recharge for a sample 10 year period following land use modification.

5.5.1 Limitations and further work

The EARWIG WG method relies on 'learning' the detailed behaviour of weather from observations and using it in statistical relationships (Kilsby et al., 2007). Although these relationships can be interpreted with some physical sense (e.g. dry days in summer will on average be warmer than wet days), there is no explicit basis in physics or meteorology. There is no guarantee therefore that the generated series, particularly under a changed climate, will always reproduce the correct weather

behaviour. This is likely to be the case for some weather extremes (e.g. hot dry spells), particularly when future climates produce conditions outside of the range of those previously observed. Likewise, the sensitivity of using monthly lumped weather data as the basis for modelling changes in recharge has only been tested on past climate data. The predicted shifts in seasonal rainfall intensity (Hulme et al., 2002; Jackson et al., 2006) may not be well accounted for. The runoff and interception parameters could be inaccurate under such changes.

The UKCIP02 project has now been superseded by UKCIP09 (Jenkins et al., 2009). Future climate impact studies in the UK would use the scenarios available here instead. The focus would be more on running a greater number of iterations, creating a Monte Carlo stochastic methodology. This would include using output form a wider range of GCM/RCMs in a further attempt to account for uncertainty in climate change predictions. In the same way, more land use scenarios would be required to get a better idea of the potential influences catchment-wide. With more resources, downscaling from UKCIP SES would allow the development of ensembles similar to those developed for climate change. The model architecture presented here makes it easy to interactively develop and test a large number of raster based land use distributions. The development of feedback between climate and socio-economic change, in a similar vein to the RegIS project (Holman, 2006) would allow an even more integrated, dynamic system model to be developed. In addition, a focus of such an approach should take into consideration, the modification of soil properties under different scenarios of climate and land use change.

5.6 Conclusions

The future impact of climate and land use changes on the hydrogeological system of the Pang/Lambourn catchment, West Berkshire has been investigated. Potential changes in the groundwater regime can then be used to assess the risk of groundwater flooding in the future. Output from the regional climate model HADRM3H has been downscaled to the catchment scale using the EARWIG WG. UKCIP high and low climate scenarios were integrated into a distributed groundwater recharge model, implemented in ArcGIS™, EARWIG-DIRT. In addition, a land use change scenario was also developed from local planning documents and applied to the same recharge model (SEC-DIRT). The ensemble of

climate change scenarios suggests that the recharge regime will be altered considerably. There is a range of between 5.5 and 27% reduction in recharge rates relative the baseline over the next century. The recharge data was interfaced with a MODFLOW model, where mean groundwater levels at observation boreholes are reduced by up to 3.8% against the baseline. Sites in the catchment that exhibit the largest annual fluctuations are most sensitive to the reduction in recharge.

The land use change scenario was characterised largely by afforestation and urbanisation. This resulted in a reduced recharge rate of 6.8% on top of the climate change impacts during the winter months. In addition there were nuanced differences in the spatial distribution of recharge. Whilst these changes are driven by land use, they are mediated by soil properties. Groundwater levels dropped, suggesting land use modifications in this case amplify the reduction under climate change. This amplification is more pronounced at sites adjacent to zones of reduced recharge. For example, at sites receiving flow from regions exhibiting an increase in recharge, groundwater level reduction was less marked. Targeted land use modification has the potential therefore to be a powerful resource management and groundwater flood risk mitigation tool.

Chapter 6 Integrated modelling for groundwater flood risk assessment

6.1 Introduction

The aim of this chapter is to assess the current and future risk of groundwater flooding in the Pang/Lambourn. To do this, the integrated groundwater model is combined with detailed socio-economic data. Firstly, the past and current risk to property and livelihoods is assessed using GIS based hazard mapping. Secondly, the impact of climate and land use scenarios on the risk of flooding in the future is quantified using a borehole trigger frequency methodology. Thirdly, the cost benefit of mitigation by targeted land use modification is investigated by implementing advective transport of groundwater flow in MODFLOW and combining this with a GIS based recharge risk model.

6.1.1 Groundwater flooding hazard and risk assessment

It is estimated that of the 1.7 million properties are at risk of groundwater flooding in England and 382,407 of these are located on major Chalk aquifers (Jacobs, 2004). Between 2000 and 3000 of those were directly affected by groundwater flooding in 2000-2001, although this number is likely to be underestimated (Bradford, 2002a; Jacobs, 2004). Other notable groundwater flooding events have taken place in 1993-1994, 1994-1995 and 2002-2003. Table 6.1 summarises the types of flood events that can occur within a permeable Chalk catchment. Types 2 and 3 are the principal categories into which groundwater flooding events are categorised. Each one is characterised by a relative input from groundwater, but both are caused by greater than average recharge over several seasons, leading to a regionally high water table (Bradford, 2002b). Indeed a Chalk basin responds as a filter that is sensitive to rainfall fluctuations over a multiyear timescale (Pinault et al., 2005). Long term climatic changes are therefore likely to influence the risk of groundwater flooding.

The dual porosity of Chalk makes catchments such as the Pang/Lambourn particularly vulnerable to groundwater flooding. The relatively low storage capacity of the fissure system in the chalk unsaturated zone can result in large and sometimes rapid groundwater level rises in response to recharge (Jacobs, 2004). In addition, the low to moderate permeability does not allow elevated groundwater levels to be

dissipated readily (Jacobs, 2006). Finally, the exchange of groundwater from the matrix into the fissure system when levels start to recede slows the recovery and thus perpetuates any flooding event (Green et al., 2006). The schematic in Figure 6.1 summarises the processes and consequences of groundwater flooding in a typical Chalk catchment. In this case, the hazard is defined as occurring above the head of the stream. Previously, in an attempt to distinguish groundwater from other types of flooding DEFRA (2006a) exclude flooding events downstream of the perennial head. Others however, do not make sure a distinction (Jacobs, 2004). It is unclear whether the flood statistics for properties affected are only for regions above the perennial head of the streams.

Table 6.1 Classification of flood types in permeable catchments (adapted from Bradford, 2002b).

Type of flood event	*Characteristics*
1 Flash flood with limited groundwater component	Short duration, high peak flows usually associated with runoff from high intensity summer storms on scarp slopes or frozen ground. May contain considerable debris and sediment.
2a High groundwater discharge ('groundwater surge')	Moderate to large 'clearwater' flows in winter/spring following greater than average recharge during autumn/winter. High groundwater component.
2b Quick runoff peaks super- imposed on high groundwater discharge	As 2a but with short duration peaks associated with winter storms, direct runoff from less permeable parts of the catchment and saturated valley floor, and/or rapid snowmelt with frozen soils.
3 High water table winter/spring	Localised flooding from standing groundwater in headwater regions during winter/spring.

Fluvial and coastal flood risk assessment strategies are usually focused on design flood estimations in which for example a 1 in 100 year flood extent is based on the statistical evaluation of past events (Shaw, 1994; Smith, 2003; Smith and Ward, 1998). Statistical modelling of groundwater flooding is problematic however as each flood peak is rarely independent of another. In addition, events on which to base probabilities are rare and often produce one sustained 'peak' that can last several weeks or even months (Jacobs, 2006). Despite the drawbacks, statistical procedures developed originally for less permeable catchments have been adapted to estimate the frequency of annual maxima flood peaks in permeable catchments (Robson and Faulkner, 1999). Probabilities have also been assigned to the 'volume-duration' of flood events, which have been identified as more disruptive than the actual peak flow in groundwater flooding events (Bradford, 2002b). These statistical

models however assume a stationary climate which precludes them from being used in any medium to long term future predictions. More recently, a simple regression model has been developed to assess the annual groundwater flood risk in Brighton, UK (Adams et al., 2010). The model uses annual groundwater level minima and autumn and winter rainfall to determine to subsequent annual maxima and hence groundwater flood risk. However the analysis of risk is limited to the short term.

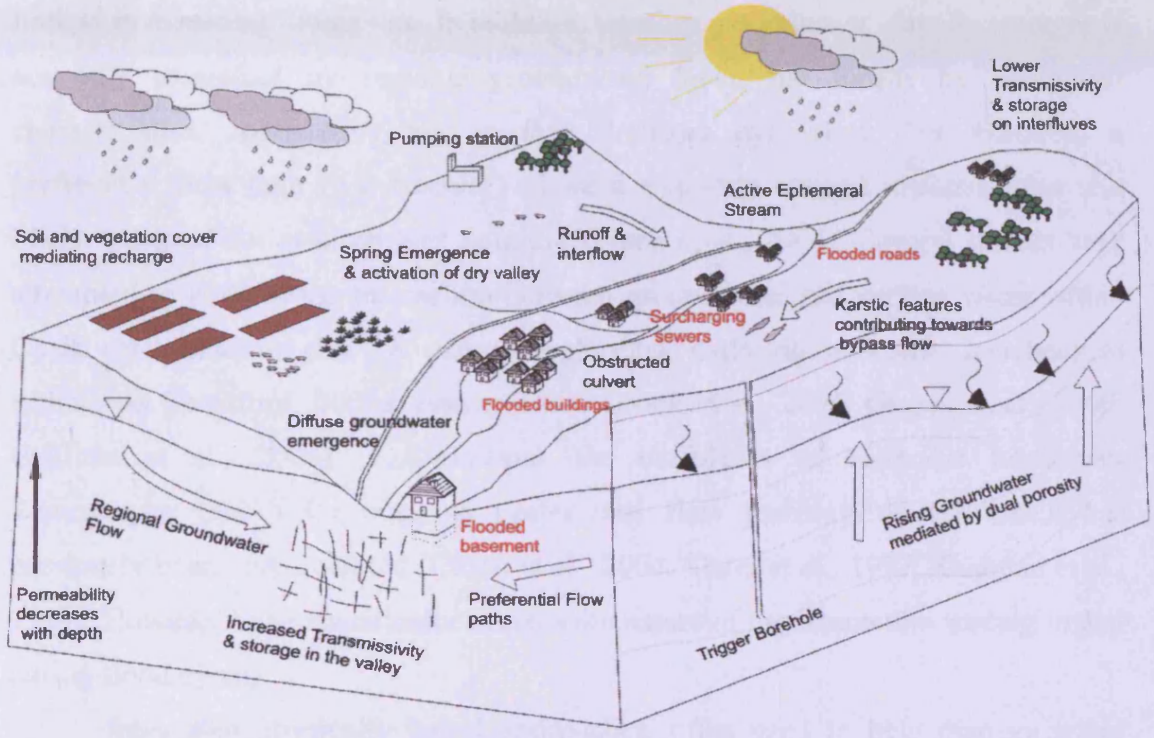

Figure 6.1 Processes and possible consequences of catchment-wide high groundwater conditions above the perennial head of the stream leading to flooding.

Previous reports on groundwater flooding risk make reference to the importance of considering climate change in future risk assessments (Jacobs, 2006). Likewise, reports detailing the potential impact of climate change on groundwater resources suggest flooding risk would be affected (Jackson et al., 2006). However, in addition to land use change, no attempt has been made so far to quantify the impacts explicitly (Cobby et al., 2009). Pinault et al. (2005) provide a possible method for incorporating climate change into a long term future assessment of groundwater flooding. They developed an inverse transfer model that simulated borehole and stream hydrographs in the Somme Valley, northern France given a time series of rainfall and evapotranspiration. By introducing an ensemble of perturbed time series representing climate change during the late 20th century it was found these changes had modified the risk of groundwater flooding in the region. However, the inverse

transfer model was site specific and did not give an indication of future risks. Indeed the study served to highlight further the need for future impact studies.

In order to assess the spatial distribution of the groundwater flooding risk, Groundwater Emergence Maps (GEMs) have been developed based on observations of groundwater levels and basic topographic data (Jacobs, 2004; Morris et al., 2007). However, they still suffer from being based on past conditions and so are therefore limited in assessing future risk. In addition, whether groundwater actually emerges is not only controlled by regional groundwater levels but locally by geological characteristics, topography and surface drainage hydraulics. For example, a preferential flow path (e.g. fracture) adjacent to poorly drained lowland areas is a likely 'hotspot' for groundwater flooding (Finch et al., 2004). Several studies have attempted to address the interaction between groundwater and surface water within Chalk catchments in the UK using geophysical, hydrological and/or geochemical techniques (Bradford, 2002a; Buttle, 1994; Crook et al., 2004; Grapes et al., 2005; Griffiths et al., 2006). For example, the usefulness of Electrical Resistivity Tomography (ERT) for mapping preferential flow pathways in the Chalk has previously been demonstrated (Crook et al., 2004; Slater et al., 1997; Zaidman et al., 1999). However none specifically address the nature of the interaction leading to and during flood events.

Integrated physically based approaches, often used to help manage water resources (Yusoff et al., 2002) provide an ideal method of investigating changes in future groundwater levels (see Chapter 5). They offer a robust representation of surface water/groundwater interaction across an entire catchment and are ideal for modelling the impact of both climate and land use change on the system (Finch, 2001). However, until this study, groundwater modelling exercises have focused on low flows (Cross et al., 1995). Even now, the resolution of the models presented in Chapters 4 and 5 could be too low resolution (100 m) to simulate localised groundwater discharge and flooding at the local scale.

A hybrid approach could be a way of combining the benefits of a statistical approach, physical modelling and hazard mapping. An example could be the integration of mathematical modelling, hazard mapping and flood risk proxies under climate change scenario ensembles e.g. the return period of a particular groundwater level. This would allow the current and future spatial dimension of the hazard to be

determined. The approach can be supplemented and validated by secondary sources, for example anecdotal evidence about past (and coming) flood events.

6.1.2 The socio-economic impact and mitigation of groundwater flooding

Equation 1.1 states that risk is a function of both hazard and vulnerability. As such it is important that socio-economic determinants of vulnerability are taken into consideration in a risk assessment of current and future groundwater flood risk. Indeed, given the prolonged inundation duration of groundwater floods, (up to several months) socio-economic stress has the potential to be more pronounced than with short term fluvial or coastal flooding (Green et al., 2006). Impacts associated with groundwater flooding may include (DEFRA, 2006a):

- Flooding of basements below ground level.
- Overflowing of sewers and drains.
- Sustained flooding of buried services or other assets below ground level.
- Inundation of farmland, roads, commercial, residential and amenity areas.
- Flooding of ground floors of buildings above ground level.

Not included in this list are the potential secondary hazards that would be associated with prolonged exposure to groundwater inundation. These might include health problems, particularly exposure to harmful micro-organisms and psychological distress. The level of risk perception associated with groundwater flooding is also low in comparison to fluvial and coastal flooding, decreasing the level of preparedness (Kreibich et al., 2009).

Researchers have highlighted the need to integrate relevant socio-economic data with models of physical processes for managing environmental systems (Wheater and Peach, 2004), mitigating environmental hazards in general (Chen and Blong, 2003; Haque et al., 2006) and flood hazards in particular (Brown and Damery, 2002). However, there is limited information on the economic and social costs of groundwater flooding. The Association of British Insurers for example keeps no record of the specific losses associated with flooding from groundwater (ABI, personal communication, 2009).

The integration of socio-economic data with hydro(geo)logical models was initiated by the RegIS project in part to assess the impact of climate and land use change on aquifer recharge (Holman, 2006). However, this was not extended to

consider the influence the aquifer system may have on the risk of flooding to communities and assets at or near the surface. Other studies have focused more on the socio-economic impact and not on the physical processes. This includes the groundwater flood hazard maps (mentioned above), which have been used to assess the number of properties at risk in the UK (Jacobs, 2004; Morris et al., 2007). In addition, there has been a survey study of the economic cost to the village of Hambledon in Hampshire following groundwater flooding in late 2000 (Green et al., 2006). It was concluded that the extended duration of groundwater flooding results in substantially higher flood losses than would be predicted using standard 'depth-damage' calibration curves. Here, damage data was collected by Hambledon Parish Council for approximately 100 households in the village. It was concluded that a flood duration of 1 week resulted in losses which are 240% of the building fabric damages usually expected during a flood of similar depth. This figure rises to 360% for a flood duration of 3 months.

Whilst the approach at Hambledon is site specific, an existing framework for integrating socio-economic data into risk assessments have been developed for fluvial flood risk in the UK (Tapsell et al., 2002) and Germany (Fekete, 2009) and for storm surge risk in the US (Rygel et al., 2006) and involves the development of social economic vulnerability indices. Tapsell, et al. (2002) for example, developed a Social Flood Vulnerability Index (SFVI) using focus groups and census data. They identified a number of key variables that determined the vulnerability of the population to the flood hazard beyond simply being within a hazardous zone i.e. a flood plain. These included the number of elderly people (75+), lone parents, people with pre-existing health problems and financial deprivation. In this case, deprivation was a function of unemployment, overcrowding, non-car ownership and non-home ownership. GIS was used to intersect conventional EA indicative floodplain extents with census output zones containing information about the highlighted variables.

Integrating detailed socio-economic data into a risk assessment can be used to inform the cost benefit of potential mitigation strategies. Such mitigation strategies can take 3 forms: proactive, reactive and warning. Current warning systems comprise of an informal network of EA trigger boreholes. When groundwater reaches a predefined level at these sites, it provides an indication that flooding may be imminent and warnings issued if necessary (Jacobs, 2006). This information can then be used to inform reactive procedures e.g. pumping. In fact, groundwater abstraction

infrastructure was used successfully in 2003 and 2007 to lower groundwater tables to alleviate problems at a number of locations in the Pang/Lambourn, for example Lambourn, Great Shefford, East Ilsley and Compton (Jacobs, 2008). However, mitigation by groundwater pumping is not usually tenable, given the problems of discharging water into already full watercourses (Cobby et al., 2009). Other reactive measures might include traffic diversion and calming to avoid increased damage from bow waves, temporary local flood proofing or even evacuation. Proactive mitigation options could be controlling development in inappropriate locations, installing permanent sumps, pumps and drainage systems and public education to encourage maintenance of drainage pathways. In reality the distinction between these is often blurred and can be used in combination. The final option is of course to 'do nothing'. This option may become increasingly viable should climate change impact assessment reveal a likely reduction in the frequency and severity of future groundwater flooding (Cobby et al., 2009).

6.1.3 Pang/Lambourn groundwater flooding case study

Groundwater flooding occurred throughout the Pang/Lambourn catchments during the wet winter and spring of 2000–2001. Local residents of Compton and East Ilsley, led by the Parish Council mapped and photographed the extent of the surface water in the upper reaches of the Pang (Figure 6.2). During this time, the Pang left the confines (Figure 6.2C) of its ephemeral, largely artificial (Figure 6.2B) channel and usually dry valleys became activated (Figure 6.2A). Hazards included surcharging sewage networks, damage to roads, inundation of properties and long term transport difficulties from blocked communication networks (Jacobs, 2006). The 'clear water' nature of the flood is particularly evident in Figure 6.2C. There was no systematic evaluation of the socio-economic cost of the flooding in this area or elsewhere in the catchment. However there are a number of database records kept by the EA and local emergency services which provide an indication of where significant problems occurred.

During this period, Finch et al. (2004) made use of aerial photography and temperature measurements to determine the locations of gaining reaches along the Pang valley during the flood. Figure 6.3 shows stream flow normalised from above Compton to approximately 2 km south of Hamstead Norreys estimated using temperature observations along the Pang in February 2001. Significant groundwater

gaining reaches are found all along the length, although primarily around Hamstead Norreys and south of Compton (locations can be seen in Figure 6.2). In this region of the upper Pang, the orientation of the valley north-south perpendicular to the prevailing groundwater flow direction east-west, resulted in the channel acting like a drain for unprecedented regional groundwater levels. It was suggested that hard bands and associated zones of increased permeability acted as conduits, focusing these outflows into certain localities (Finch et al., 2004). It was also suggested that a dry valley perpendicular to the stream may also have been a focus for this preferential flow (see Figure 6.2).

Figure 6.2 Map of flood extent made by local resident and photographs (A-C) of flooding in the Upper Pang valley, spring 2001.

Conversely to the Pang, the Lambourn valley runs parallel to the regional groundwater flow direction (Figure 4.4A), and so flow accretion was probably more linear (although no measurements were made by Finch et al., 2004). In both cases the flooding was largely a function of the large-scale head ward migration of both the Pang and Lambourn under regionally high groundwater conditions. Localised flooding resulted from drainage difficulties (see damaged culvert, Figure 6.2 B), and focused discharges at activated springs.

Sub-surface geophysical investigation using ERT has previously been used to investigate groundwater-surface water interaction along the Pang at Frilsham (circa

4.5 km downstream from Hampstead Norreys). A 3 m resistive layer (125-200 Ω/m) was found overlaying a less resistive zone (50-100 Ω/m). This was interpreted to coincide with the transition from a heterogeneous flint gravel layer to underlying homogenous, weakly weathered chalk. Within this Chalk layer, relatively small fluctuations in resistivity (~3%) are attributed to weathering and therefore permeability (Crook et al., 2004). Using ERT may allow a greater understanding of the interplay between the regional water table, topography and variations in the permeability of the aquifer in determining the locations of flooding hotspots. Such information could be used to locally refine hazard maps.

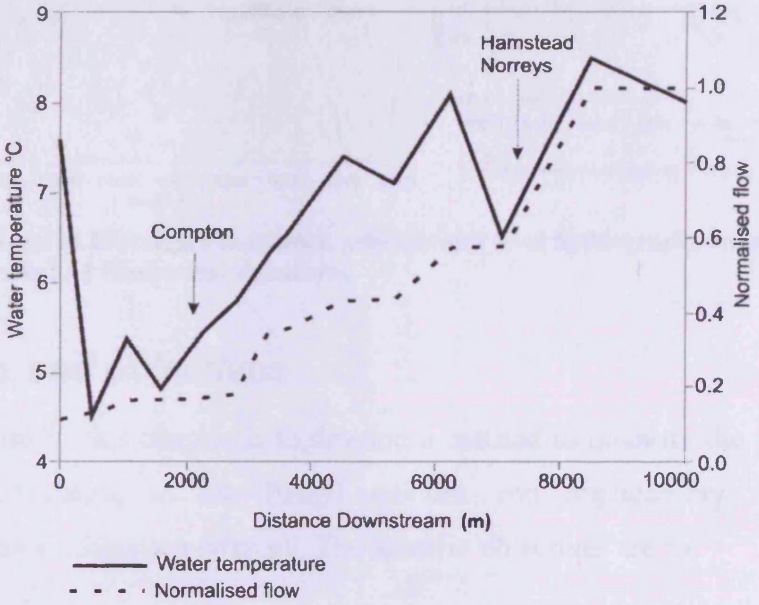

Figure 6.3 Profiles of water temperature and estimated normalised flow along the river Pang 18th February 2001 (Finch et al., 2004).

In response to the flooding in 2001, the EA now use key observation boreholes across the Pang/Lambourn to assess the short term risk of groundwater flooding. If trigger levels are exceeded at these points, levels across the catchments are monitored more closely and warnings issued if necessary. These trigger levels provide a useful focus in determining the frequency with which dangerously high groundwater levels may be reached under simulated conditions of climate and land use change (Figure 6.4). Apart from the UK wide hazard maps (Morris et al., 2007), there has been no formal analysis on the risk of groundwater flooding to the communities within the Pang or Lambourn catchments currently or into the future. This is despite the recent introduction of statue (Great Britain, *Flood and Water Management Act 2010*) which has given the EA and local authorities in the UK a statutory requirement to manage flooding from groundwater.

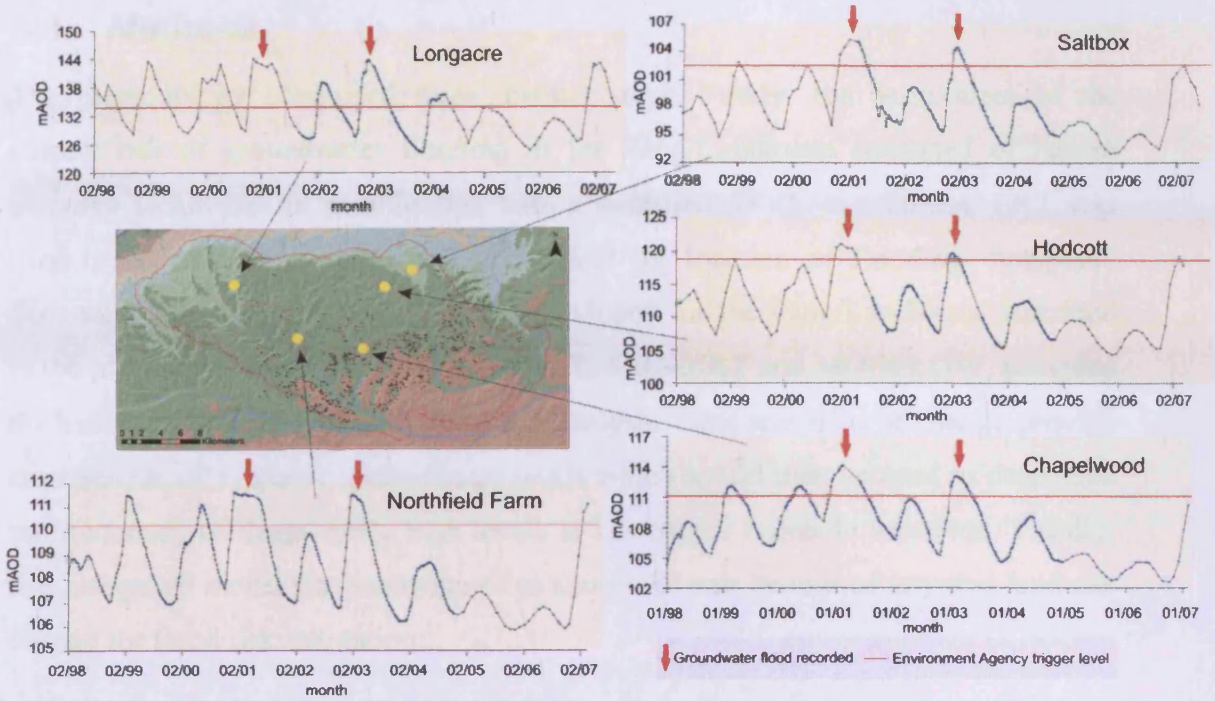

Figure 6.4 Location of EA trigger boreholes, groundwater level hydrographs from 1998 until 2007, trigger levels and flood event signatures.

6.2 *Aims and objectives*

The overall aim of this chapter is to develop a method to quantify the future risk of groundwater flooding in the Pang/Lambourn and applicability of land use modification as a mitigation strategy. The specific objectives are to:

- Assess the current risk of groundwater flooding in the Pang/Lambourn catchment using hazard mapping in combination with a socio-economic vulnerability index developed specifically for groundwater flooding.
- Determine how this risk may alter under scenarios of climate and land use change by applying scenarios to the integrated catchment model. Synthetic groundwater level time series at trigger borehole locations will provide a proxy indication of flood risk.
- Investigate targeted land use modification as a risk mitigation tool by identifying zones contributing recharge to flood discharges. The cost of making changes to the land use in order to limit recharge can then be weighed against the benefit of flood risk reduction.

6.3 Methods

The methodology comprised three distinct steps. Firstly, the assessment of the current risk of groundwater flooding in the Pang/Lambourn consisted of hazard mapping techniques in combination with a modified SFVI. In addition, ERT was used in an attempt to refine and understand the location of flooding 'hotspots'. Secondly, the physically based models developed for the Pang/Lambourn described in the previous chapters i.e. EARWIG-DIRT, SEC-DIRT and MODFLOW, provided the basis of future groundwater flood risk analysis. Here scenarios of change provide an ensemble of synthetic groundwater levels which would then be used to determine the frequency of dangerously high levels at EA trigger borehole locations. Thirdly, this integrated model was interrogated to assess the cost benefit of targeted land use change for flood risk mitigation.

6.3.1 Current groundwater flooding risk

Flood hazard maps were developed using groundwater level interpolation in conjunction with a DTM. In this case, the groundwater surface was taken to be February 2001 levels interpolated using the ordinary kriging method constrained by the DTM at known surface water locations (see Appendix 4.2 for details of interpolation method and Figure 4.4A for interpolated surface). A simple GIS based spatial analysis query was used to determine areas where groundwater is within 2 or 5 m of the ground surface during this period of known flooding. This was further contextualised and validated using mapped surface water extents from local residents and the EA during the 2000-2001 floods. The hazard was defined both for above the perennial head and the entire catchment.

An ERT survey was used in an attempt to refine the hazard mapping and assess the mechanism of focused gaining reaches suggested by Finch et al. (2004) during the flooding of 2000-2001 in the upper Pang valley (see Figure 6.3). The resistivity of a particular rock or soil sample depends on porosity and degree of water saturation (Loke, 2010) and so it was anticipated that preferential flow paths may be discernable. The field site chosen was circa 800 m north of Hampstead Norreys observation borehole and has been subject to flooding during periods of regional high groundwater levels (Figure 6.5A). It is situated on the Upper Chalk overlain with sand and gravel superficial deposits (Figure 6.5B), which is supported by

nearby borehole logs at Woodend and Hampstead Norreys. The same boreholes provided groundwater level information that can be used in the ERT interpretation. The local soil type is Coombe 1, which is described as a well drained, calcareous, fine silty soil (Figure 6.5C). Rainfall data at Yattendon (see Appendix 1.6 for location) was also used in the subsurface characterisation.

Three resistivity lines were taken parallel and sub-parallel to the identified gaining reach (Figure 6.5D). Lines 1 and 2 were 355 m in length and line 3 was 245 m in length each with 5 m electrode spacing, capable of providing data up to 50 m depth. The location of each electrode was ascertained using a Differential Global Positioning System. Once plotted in GIS, LIDAR data provided altitude information. An Iris Instruments Syscal switch 72 ERT was used to collect the data and the RED2DINV program used the smoothness-constrained least-squares method inversion technique (Sasaki, 1992) to produce a 2D vertical model of the subsurface from the apparent resistivity data. The resistivity [Ω/m] of the profile was used to determine the presence of preferential flow paths and other hydrogeological features that might be relevant to focused groundwater discharge during a flood.

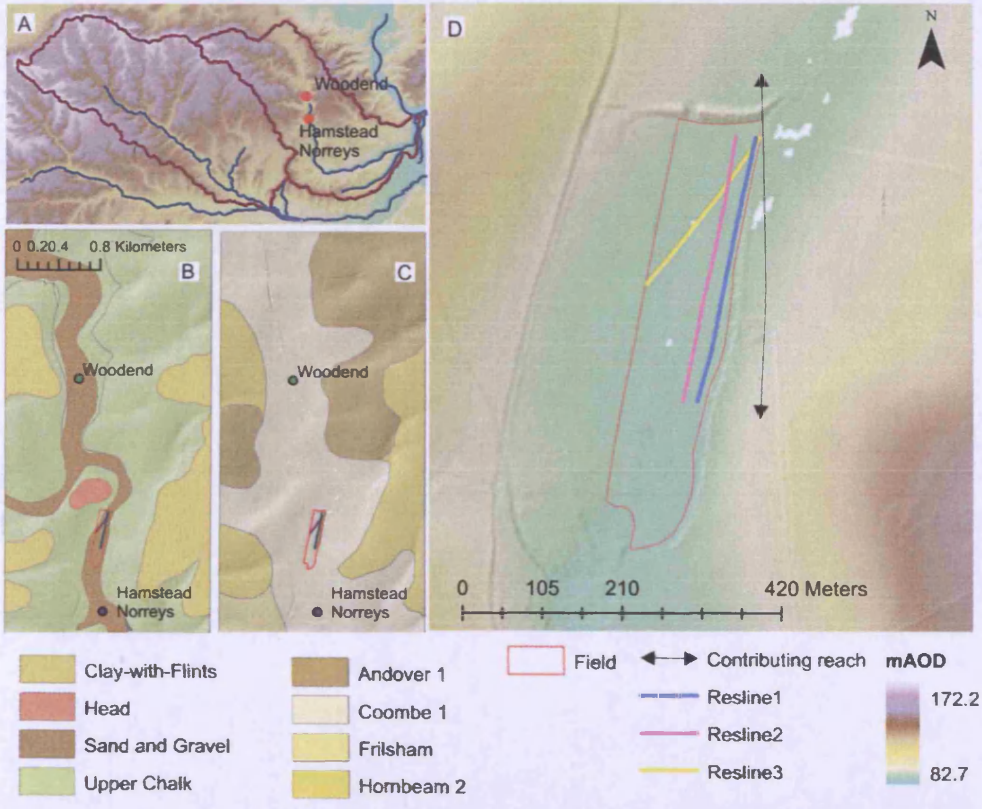

Figure 6.5 Location of ERT study site in the Upper Pang valley (A) and locally in relation to bedrock and superficial geology (B) and soil (C). Local topography and position of resistivity lines in relation to the gaining reach of the river Pang (D). LIDAR topographic data supplied by EA, 2009.

To determine flood risk, the vulnerability of local populations, infrastructure, interests and investments was assessed. In this case, Ordnance Survey (OS) Meridian (up to 50:000 scale) and Mastermap (up to 1:1250 scale) vector data was used to determine the urban areas and number of buildings that could potentially fall within the delineated hazard zones. This was done by overlaying the OS data with the hazard maps in GIS. The resulting risk areas were calculated above the perennial head of the Pang and Lambourn as well as the entire catchment.

In order to refine the risk analysis, a modified SFVI (Tapsell et al., 2002) was developed and integrated into the analysis. Here, census data at the highest available spatial resolution, Output Area (OA) provides the basis for identifying those areas that are more exposed to the negative consequences of groundwater flooding. It is a Composite Additive Index (CAI) based on a financial-deprivation indicator, three social characteristics and a built environment factor. Census data is provided by the Office of National Statistics (ONS) via the MIMAS (University of Manchester) CASWEB online portal (ONS, 2001a). All the original CASWEB data codes for the datasets can be found in Appendix 5.1. OA delineation is provided by the ONS via UKBORDERS (ONS, 2001b). The Townsend Index (Townsend et al., 1988) was used to identify financially deprived areas and is made up of four percentage indicators; unemployment, U_n [%], overcrowding, O_v [%], non-car ownership, N_c [%] and non-home ownership, N_h [%] for each census OA in the Pang/Lambourn,

$$U_n = \frac{U_r}{E_a} 100 \tag{6.1}$$

where U_r is the number of unemployed residents aged 16-74 and E_a is the number of economically active people aged 16-74.

$$O_v = \frac{O_b}{H} 100 \tag{6.2}$$

where O_b is the number of households with over 1 people per room and H is the number of households in the OA.

$$N_c = \frac{C_h}{H} 100 \tag{6.3}$$

where C_h is the number of cars or vans per household.

$$N_h = \frac{H_r}{H} 100 \tag{6.4}$$

where H_r is the number of households in rented accommodation. Based on previous focus group research, Tapsell et al. (2002) suggest three more social indicators of flood risk vulnerability. These include the proportion of long term sick, S_i [%], single parent households, S_p [%] and elderly residents, E_r [%],

$$S_i = \frac{H_s}{H} 100 \tag{6.5}$$

where H_s is the number of households suffering from a limiting long-term illness.

$$S_p = \frac{H_{sp}}{H} 100 \tag{6.6}$$

where H_{sp} is the number of single parent households with dependent children.

$$E_r = \frac{E_y}{R_s} 100 \tag{6.7}$$

where E_y is the number of residents aged 75 and over and R_s is the all residents living in the OA. There is an added risk associated with flooding of basements during groundwater flooding (Green et al., 2006), and so an additional basements, B_h [%] factor was also integrated,

$$B_h = \frac{B}{H} 100 \tag{6.8}$$

where B is the number of households in which the lowest level is below ground. The raw percentages (U_n, O_v, N_c, N_h, S_i, S_p, E_r, B_h) for all OAs were transformed to minimise the skew and kurtosis of the data (see Appendix 5.2 for the transformation method used for each indicator). These values were summed to provide a CAI after being standardised as z scores (z),

$$z = \frac{(x - \mu)}{\sigma} \tag{6.9}$$

where x is the score to be standardised, μ is the mean of the population and σ is the standard deviation. In order to prevent any undue bias towards financial deprivation, the four Townsend indicators (U_n, O_v, N_c, N_h) were summed and multiplied by 0.25 before being added to the other variables. The Social Groundwater Flood Vulnerability Index (SGFVI) was calculated only for OAs with at least a portion within the Pang or Lambourn catchment. It is therefore only an indication of relative risk within this region. The resulting values were then categorised into five bands using natural breaks (Jenks, 1967), representing different degrees of vulnerability: very high, high, average, low and very low. Jenk's data classification method ensures

maximum variance between categories and minimum variance within categories, i.e. classes are based on natural groupings inherent in the data.

In addition to the OS data and SGFVI, an attempt was made to survey the local population in the villages of East Ilsley and Compton to assess the cost and impact of groundwater flooding at the household level. An article detailing the study and its purpose was published in a local magazine and distributed throughout the villages (Appendix 5.3). Residents were encouraged to respond to a detailed online survey (Appendix 5.4). Unfortunately, the survey proved unsuccessful, with only one respondent taking part.

Finally, the hazard and vulnerability analyses were combined to provide a comprehensive assessment of the past and current risk of groundwater flooding in the Pang/Lambourn. For example, the number of buildings within the hazardous zones and also within a highly vulnerable area could be identified using GIS spatial analysis. Risk mapping was also contextualised and validated with point flood incidence data from the EA and local fire and rescue services.

6.3.2 Future groundwater flood risk under climate and land use change

Synthetic groundwater level ensembles based on climate and land use change scenarios (Chapter 5) were used to determine the flood risk relative to the baseline (1961-1990). Output from the depth integrated, single layered MODFLOW model (interfaced with EARWIG-DIRT and SEC-DIRT) was used to assess the relative frequency of trigger levels and flood peaks (February 2001) at EA trigger borehole locations (Figure 6.4). The frequency of level breaches was assessed for the baseline, climate and land use change scenarios across all the time slices. Because these hazard proxies are used instead of specific modelled discharges to springs and streams, risk could be assigned to the entire region in a generalised way and may therefore include high base flow fluvial flooding downstream. The percentage deviation from the baseline in the frequency of a trigger or flood level being breached, $f\Delta$ is given by,

$$f\Delta = \frac{(f\alpha - f\beta)}{f\alpha} 100 \qquad (6.10)$$

where $f\alpha$ is the frequency of breaches (or flood peaks) in the baseline and $f\beta$ in the climate or land use change scenario across the ensemble. The percentage increase or

decrease in the hazard occurrence can then be combined with the vulnerability data described above to provide future risk assessments.

6.3.3 Mitigation of flood risk by targeted land use modification

The upper Pang valley was used to develop a land use modification impact analysis. The multi-layer VMF model developed in Chapter 4 was used for recharge zone delineation by reverse particle tracking. This is because particle tracking is not available in the DOS based version of MODFLOW used to develop the single layered model. The surface flood extent mapped by a local resident (Figure 6.2) provided the 'discharge zone' along which particles were placed. The model was run in steady state and based on calculated flow paths, the particles were tracked back towards their point of origin at the surface into the groundwater system (Robinson and Reay, 2002). Appendix 5.5 illustrates an example of the results of particle tracking in VMF. In a second simulation, a refined number of particles were located along reaches of the identified by temperature analysis (see Figure 6.3) as significantly gaining during the flood of 2000-2001 (Finch et al., 2004). In both cases, the particle tracking results were subsequently imported into GIS and the recharge zones delineated as polygon shapefiles.

Table 6.2 Ranking of slope classification, soil texture, land use and discharge stream reach according to relative recharge sensitivity.

Recharge sensitivity rank	*Slope (%)*	*Soil texture*	*Land use (1990) 25 m*	*Recharge zone*
1	0.5-5	Silty/clay/loam	Coniferous	Not gaining
2	5-10	Silt	Broadleaved	Gaining
3	<0.5		Grass	
4	>10		Arable horticulture	
5			Suburban/rural dev	

The recharge zones are then combined with GIS-DIRT recharge data. Firstly, areas of higher mean recharge are identified as having the greatest potential for reducing the input into the system. To do this, each land use (25 m 1990 CEH data) was ranked according to 'recharge potential' based on the in depth analysis of GIS-DIRT results (see Figure 2.17). Differing scales and nomenclature from 2000 1 km data required a subtle re-assignment of some land use categories, e.g. bracken is treated as grass (see Appendix 5.6 for equivalent 2000 and 1990 categories). Using the same principle, slope angle classification and soil texture were also ranked. The recharge zones were also ranked depending whether they discharged to the gaining

reaches or not (see Table 6.2). The respective raster datasets were then summed, providing a CAI of recharge potential. A high score would suggest that land use change at that point might have a relatively large impact on reducing groundwater flood risk.

6.4 Results

6.4.1 Current groundwater flooding risk

A GEM based on where the groundwater surface lies within 2 or 5 m of the DTM during periods of known flooding (i.e. February 2001) can be seen in Figure 6.6A. Surface water flood extents, mapped by a local resident above Hamstead Norreys, and catchment wide by the EA are shown in Figure 6.6B. Spatial analysis in GIS suggests that 34.4 km^2 of the Pang and Lambourn is within 5 m and 21.8 km^2 within 2 m of the groundwater table during this time. These values are shared equally between the two basins i.e. 11.2 and 10.6 km^2 for the Pang and Lambourn respectively within 2 m. 6.9 and 3.9 km^2 of the ephemeral portions of the Pang and Lambourn respectively are within 2 m, indicating a high level of risk from groundwater. Likewise, 11.2 and 6.6 km^2 of these areas are within 5 m.

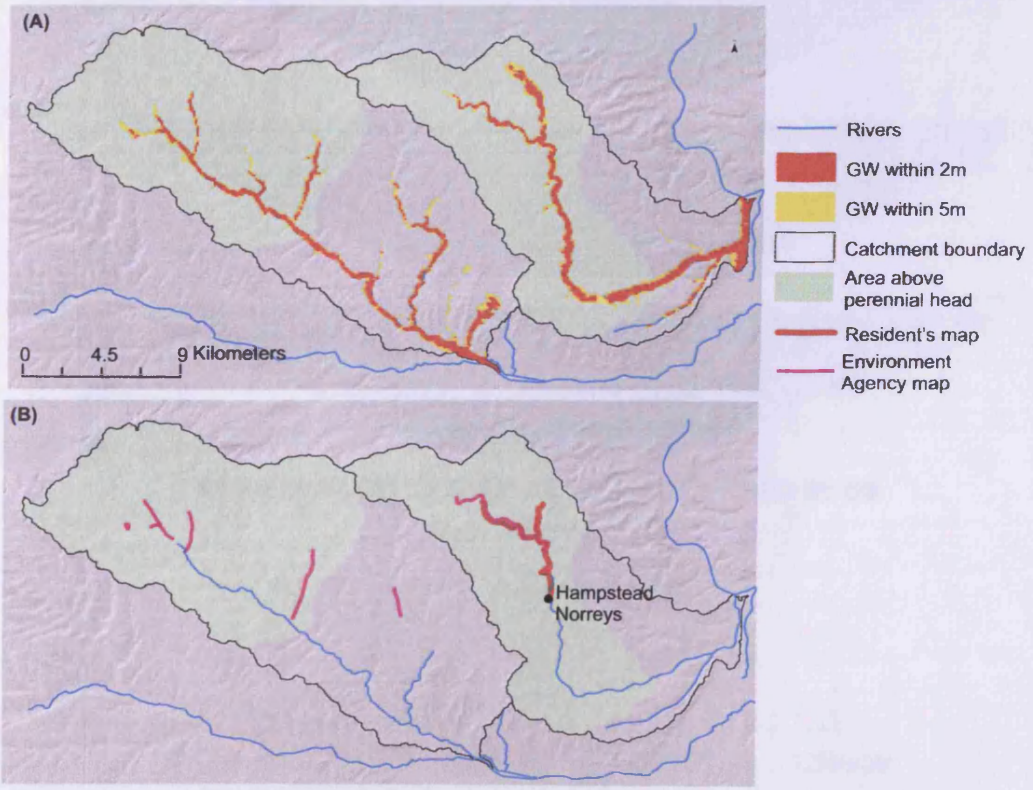

Figure 6.6 GEM where the groundwater surface is within 5 or 2m of the surface during February 2001 (A) and mapped areas of flooding during the same period (B).

A summary of the ERT survey carried out on the 3rd September 2008 is shown in Figure 6.7 (profiles 1-3). The distance along each line is from the north east corner of the study field (see Figure 6.5). Vertically, the data for each profile can be divided into 3 distinct layers. Layer (a) is characterised by heterogeneity and relatively high resistivities, typically between 300-900 Ω/m. In some areas this reduces to as low as 25 Ω/m, for example within the first 40 m along the profiles. This is particularly the case in profile 3, where layer (a) exhibits considerably lower resistivity than the other two profiles. However, there was a rain shower at approximately 3pm (0.4 mm at Yattendon gauge), potentially affecting only profile 3. At approximately 5 m depth, there is a transition to layer (b), a largely homogenous layer of lower resistivity, typically between 25 and 100 Ω/m. At around 70 mAOD there is another transition to layer (c), where resistivity is slightly higher again, between 150-300 Ω/m. Finally, there is evidence for a possible fourth layer at around 40 m depth, where resistivity appears to decrease again.

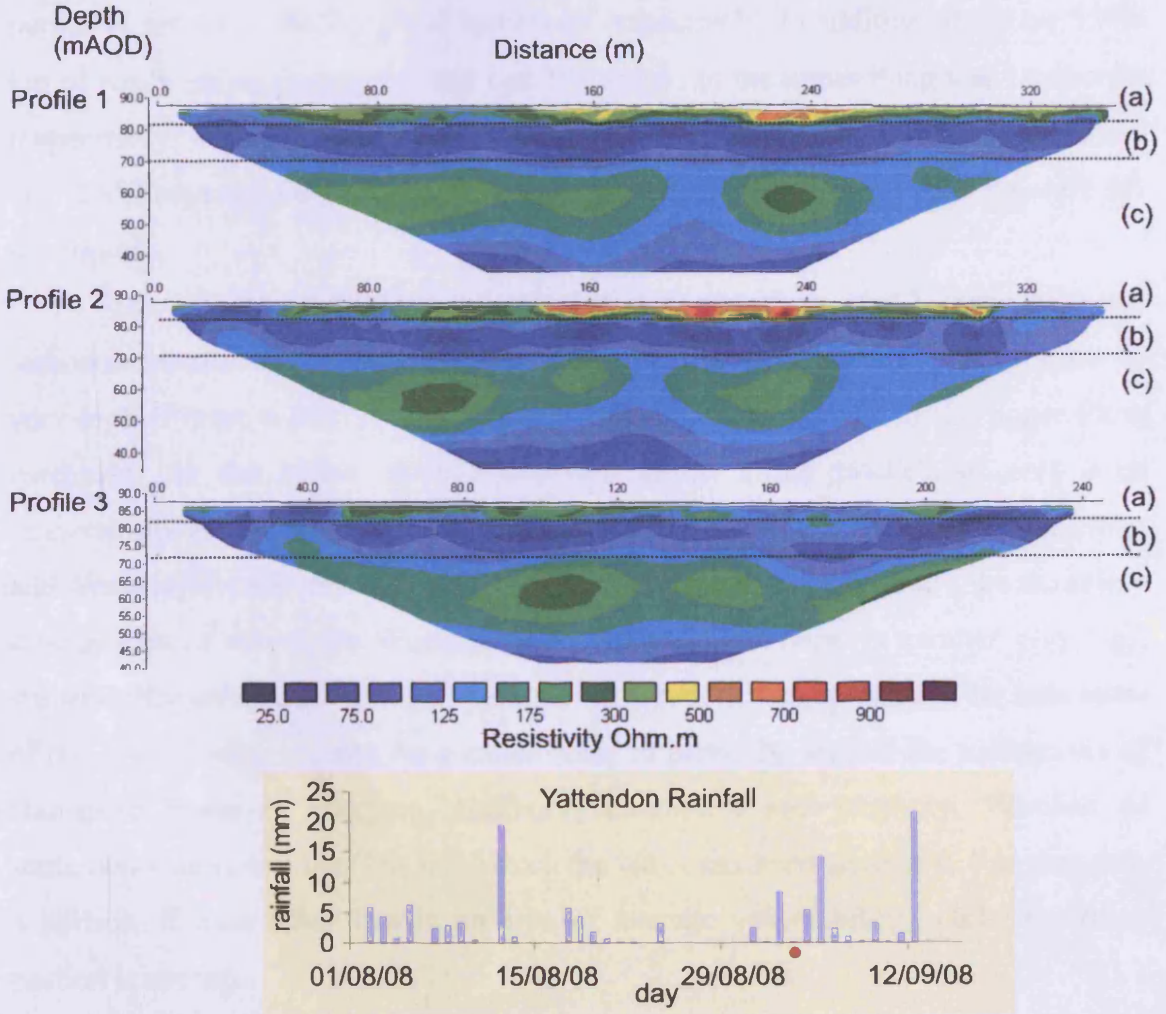

Figure 6.7 ERT profile lines (1-3) at a field site north of Hampstead Norreys in the upper Pang valley and daily rainfall at Yattendon before, during and after the survey period.

Observations at Woodend (03/09/08) and Hampstead Norreys (19/09/08) suggest the groundwater level is between 5.5 m and 2.3 m respectively below the ground surface in this area. This coincides with the transition from layer (a) to (b), and could account for the marked difference in resistivity. In addition, borehole logs at Woodend and Hampstead suggest that superficial gravel deposits are 3.5 m and 3 m thick respectively. They consist of very clayey gravel grading into pebbly clay head and finally into Chalk and could account for the heterogeneity and contribute to the low resistivity in layer (a). Following rainfall, very high resistivities may have reduced in line 3, though the heterogeneity characteristic of the gravel remained. However, there was considerable rainfall recorded at Yattendon (14 mm) during the previous 24 hours, suggesting a transient impact and rapid drainage.

Based on OS Meridian data, there are 27.1 km^2 of 'urban areas' within the Pang/Lambourn catchment boundary, representing concentrated areas potentially vulnerable to groundwater flooding (Figure 6.8A). 6.9 km^2 and 4 km^2 lie above the perennial source of the Pang and Lambourn respectively. In addition, there are 559.6 km of roads across the region. 144 and 104 km lie in the upper Pang and Lambourn respectively. Within the Pang catchment the OS Mastermap database suggests there are 19537 separate buildings- 12613 lie above the perennial head (see Figure 6.8B for zoom).

The SGFVI has a minimum value of -6.8, maximum of 9.2, mean of 0 and standard deviation of 2.6 and is classified into relative vulnerability from very low to very high (Figure 6.8C). A zone of very high vulnerability lies in the upper Pang catchment, in the region surrounding East Ilsley. Other pockets of very high vulnerability exist towards to confluence of the Lambourn and Pang with the Kennet and Thames respectively (at Newbury and Pangbourne in particular). Immediately downstream of where the Winterbourne joins the Lambourn, is another very high vulnerability area. Areas of high vulnerability are more widespread and include areas of the upper Lambourn and Pang catchments, in particular around the settlements of Hamstead Norreys, Compton, Eastbury, Lambourn and Eastbury. Portions of settlements lie across the OAs into which the index has been generated. For example, a portion of East Ilsley lies in an area of average vulnerability, whilst the other portion is average.

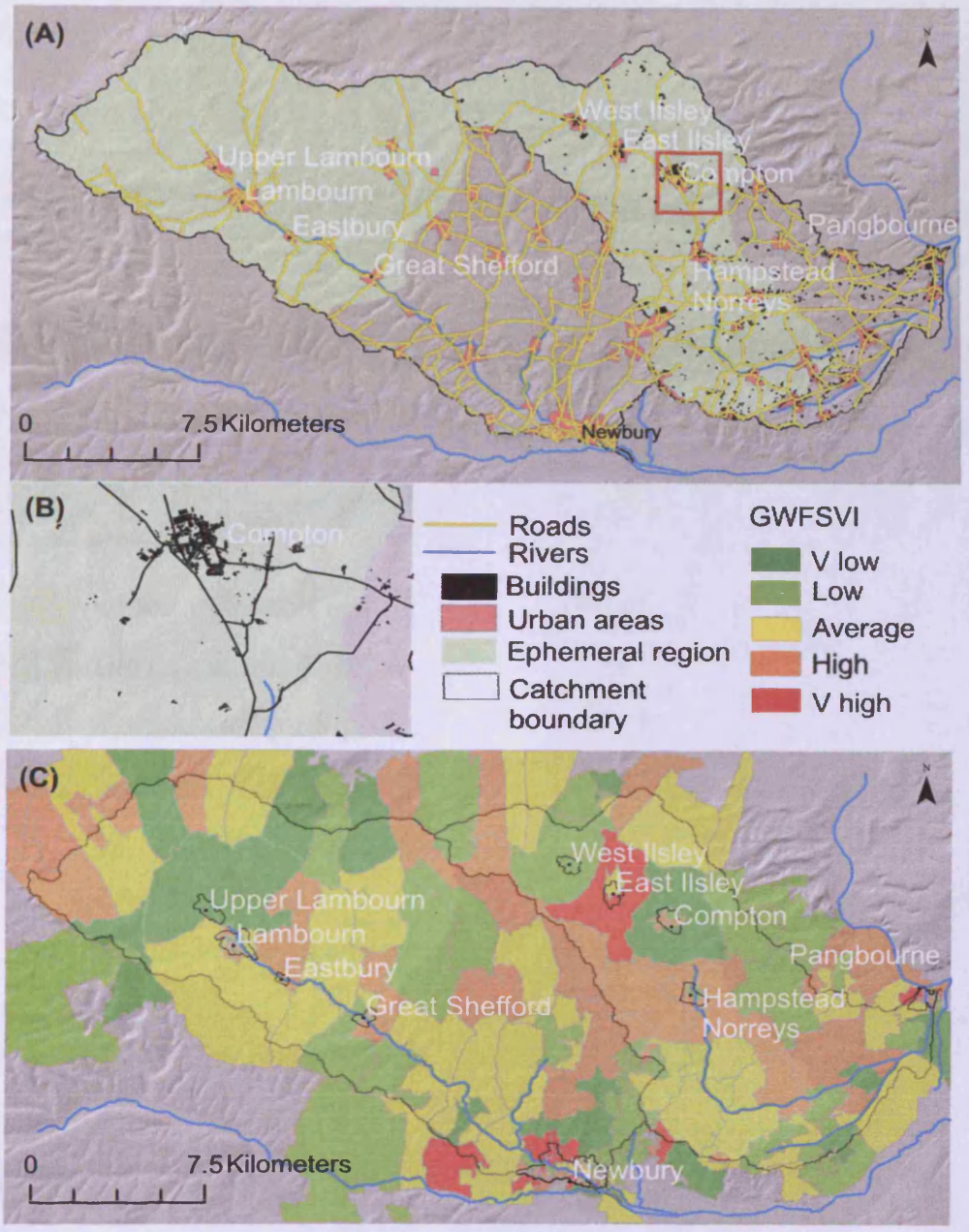

Figure 6.8 (A) Building locations taken from OS Mastermap and road and urban areas taken from OS Meridian dataset. (B) Close-up of OS Mastermap building locations at Compton. (C) Pang/Lambourn SGFVI.

The final step is to combine the hazard (Figure 6.6) and vulnerability mapping (Figure 6.8) to provide an analysis of risk (Figure 6.9). The risk areas shaded yellow in Figure 6.9A are where hazardous zones (i.e. groundwater within 2 m during February 2001) intersect with urban areas. The risk areas shaded red are where these urban areas in turn lie within zones of high or very high vulnerability. The inset (Figure 6.9B) illustrates the same principle being applied to a sub-region of OS Mastermap data, allowing risk to be delineated at the building scale.

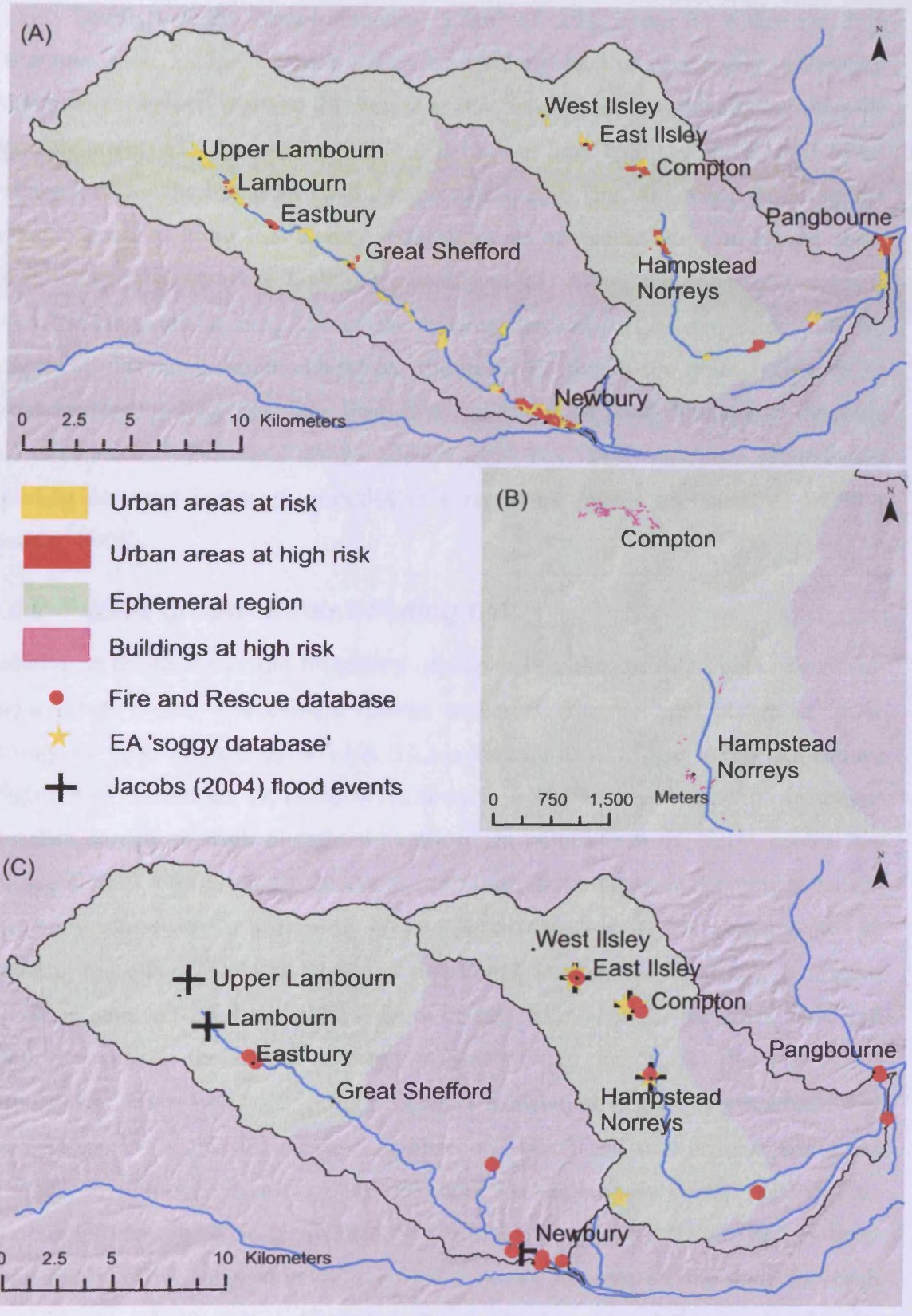

Figure 6.9 (A) Risk map combining hazard assessment and vulnerability analysis of urban areas. (B) Individual buildings in the upper Pang at high risk from groundwater flooding. (C) Validation of risk with point incidence of flooding from fire and rescue, EA database and Jacobs (2004).

Throughout the Pang/Lambourn, 5 km^2 of urban areas lie within the 2 m hazardous zone. 1.7 km^2 of these areas are considered high or very highly vulnerable. Along the ephemeral reaches, 2.2 km^2 is at risk, which is shared equally between the two catchments (1.1 km^2 each). 0.8 km^2 is high or very highly vulnerable (0.2 km^2 and 0.6 km^2 for the Lambourn and Pang respectively). The Mastermap data suggests within the entire Pang catchment, 3603 buildings lie within the 2 m hazard zone, 1422 within high or very high vulnerability areas. Along the ephemeral reaches, 2406 buildings are at risk, 755 of these being deemed particularly vulnerable. By way of a risk assessment validation, Figure 6.9C shows the point incidence of groundwater flooding incidence from between 2000 and 2004. The spatial database is a combination of fire and rescue call-out data[†], EA 'soggy database' groundwater flooding data and incidents recorded in a report by Jacobs on behalf of DEFRA (Jacobs, 2004).

6.4.2 Future groundwater flooding risk

Relative to the baseline, the frequency of trigger breaches or flood peaks decreases under the high and low climate change scenarios, progressively becoming fewer through the time slices (Figure 6.10). This is the case at all trigger borehole locations (Figure 6.4). Based on Equation 6.10, there is a 62.7% mean reduction in trigger breaches across all high climate time slices, in comparison to 72.1% across low (Figure 6.10A). For the 2020, 2050 and 2080 time slices the mean decrease in breach frequency across both scenarios is 29.9%, 80.6% and 91.7% respectively. In addition, there is a 75.3% reduction in flood peak frequencies for all high scenarios in comparison to 92% for all low (Figure 6.10B). Similarly, for the 2020, 2050 and 2080 time slices the mean decrease in peaks were 59.4%, 93.7% and 97.9% respectively. Each borehole location exhibits a different degree of sensitivity. For example, during the l2020 scenario, Saltbox and Northfield farm exhibit reductions in trigger level breach frequency of 6.3% and 8.9% respectively (Figure 6.10A). This is in comparison to 32%, 68.8% and 58.8% at Longacre, Chapelwood and Hodcott respectively. This same relative sensitivity is not necessarily repeated for each scenario e.g. h2020, where Chapelwood exhibits less of a reduction (18.8%) in comparison to Northfield (22.2%).

[†] All flood incidents between December and May 2000 to 2004 are assumed to be groundwater origin

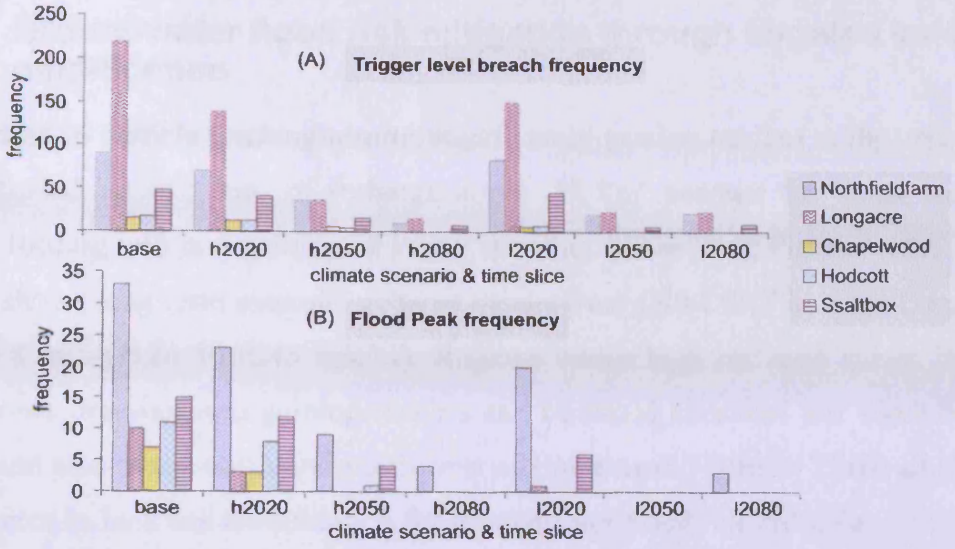

Figure 6.10 Frequency of trigger level breach (A) and flood peaks (B) across climate change scenario ensembles.

Relative to the baseline and h2020 climate change scenario, the frequency of trigger breaches and flood peaks reduces at all locations under the land use change scenario (Figure 6.11). There is a 49.3% decrease in mean trigger breach frequency under the land use change scenario. This is in contrast to a 24.8% decrease under the equivalent high climate change scenario and time slice (Figure 6.11A). These reductions are more marked for flood peak frequencies, where the land use change scenario exhibits a reduction of 67.7% from the baseline (Figure 6.11B). There are again differences in the sensitivity of the boreholes to land use change. For example, Longacre exhibits a reduction of 37% in trigger breach frequency during h2020, in comparison to 18.8% at Chapelwood. Following land use change, Longacre reduces by 46.6% but Chapelwood by even more (50%).

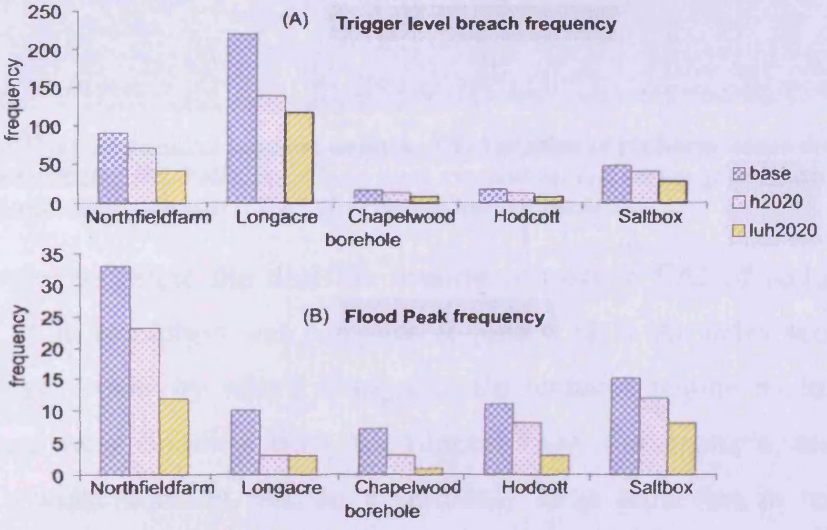

Figure 6.11 Frequency of trigger level breach (A) and flood peak breach (B) across land use and climate change scenario ensembles.

6.4.3 Groundwater flood risk mitigation through targeted land use modification

According to particle tracking results, significantly gaining reaches in the upper Pang are supplied by 16.3 km^2 of recharge zones. 15 km^2 account for 'other recharge' zones, feeding into less gaining or losing stretches of the Pang Figure 6.12A. Figure 6.12B shows long term average recharge values from GIS-DIRT in a local rank from 1 (109.8 mm/yr) to 30 (245 mm/yr). Regions where high recharge values intersect with zones draining into gaining reaches can be found clustered just south of West Ilsley and also to the north and north west of Hampstead Norreys. These areas could be targeted in land use modification for groundwater flood risk reduction.

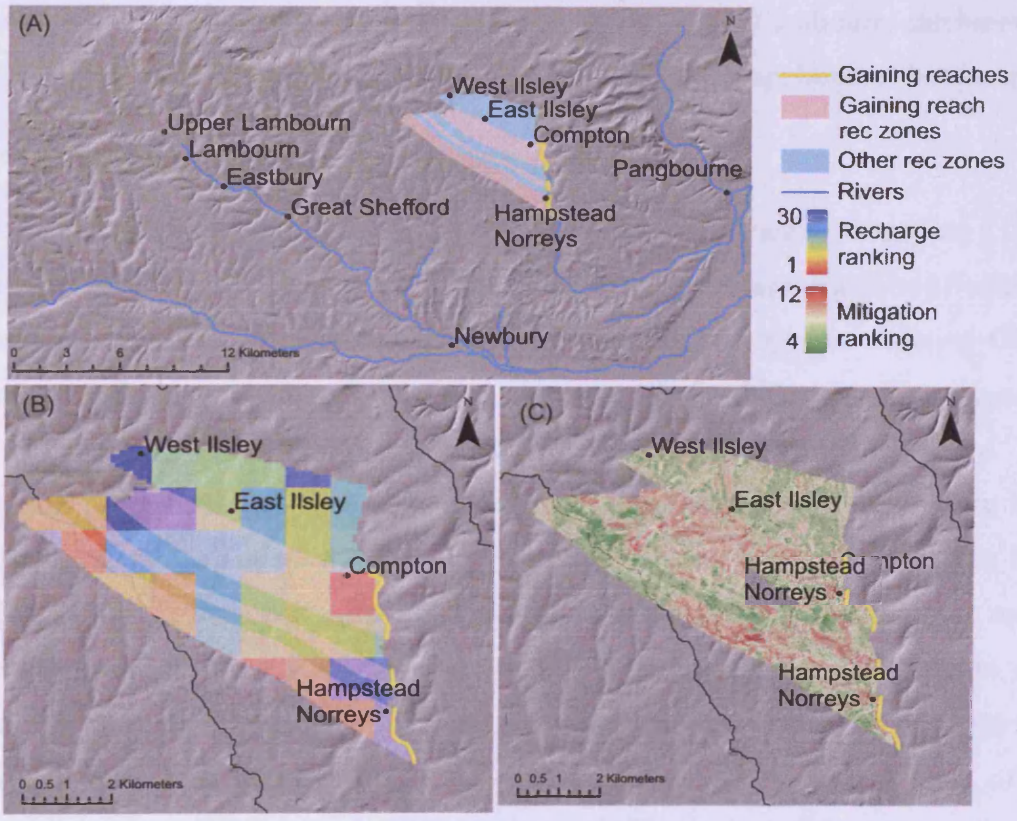

Figure 6.12 Mitigation decision support analysis. (A) Location of recharge zones delineated using particle tracking. (B) Ranking of long term mean observed recharge rates overlain with gaining reach recharge zones. (C) CAI of recharge impact potential.

In order to refine the decision making process, a CAI of recharge impact potential at 25 m resolution was compiled (Figure 6.12C). An index score of 10-12 represents high sensitivity where changes to the recharge regime could impact the risk of groundwater flooding along the (upper) Pang. For example, conversion to coniferous woodland could lead to a relatively large reduction in recharge and potentially groundwater flood risk. In total there is 8.5 km^2 where flood risk could be

highly sensitive to land use change. Spatially, there is a tendency for highly sensitive areas to concentrate along the recharge zones that drain to the Pang during floods. According to either the 1990 or 2000 land use data (Figure 5.3), the majority lies on arable/horticultural land, with a mean slope of 10%. Andover 1 soils also dominate these areas, which are characterised by a well drained, silty texture.

6.5 Discussion

The aim of this chapter was to combine GEMs, climate and groundwater modelling and socio-economic datasets in order to assess the risk of groundwater flooding at present and in the future. In addition, a decision support tool for mitigation by targeted land use modification was developed. The Pang/Lambourn catchment is used as a case study although the methodologies are equally applicable elsewhere.

6.5.1 Current groundwater flooding risk

Spatial quantification of the current groundwater flooding hazard is based on a GEM and suggests between 22 km^2 and 34 km^2 of the Pang/Lambourn could be affected by groundwater flooding. Previous studies have made an attempt at validating GEMs against specific groundwater flood events (Jacobs, 2004). A flood event however is only likely to be recorded where populations, buildings etc. are concentrated. This validation procedure therefore is reserved until after aspects of vulnerability have been integrated. However, where groundwater emergence during a flood has been mapped locally, it does coincide with the where the water table is within 2 m on the GEM (Figure 6.2). There has been some debate in the literature with regards to what constitutes a groundwater flood (DEFRA, 2006a; Jacobs, 2004). In this instance, hazard analysis was conducted both above and below the perennial head of the stream. By using GEMs as a proxy for hazard, the need to differentiate between flood types is diminished (Table 6.1).

An ERT survey was conducted parallel to the main valley in order to characterise preferential flow paths and potentially refine the GEM. The results of the ERT at the site north of Hampsetad Norreys suggest an upper layer (a) of relatively high resistivity (300-900 Ω/m) circa 4-5 m thick (Figure 6.7). This is likely to be due to the water table, which is between 5.5 and 2.3 m below ground level and the transition from heterogeneous superficial gravel deposits to Chalk bedrock. A similar transitional change was also found at Frilsham (further down the Pang valley)

which was due to the water table (Crook et al., 2004). The difference in absolute resistivity values between the site at Hampstead Norryes and Frilsham could be due to site specific superficial geology or antecedent conditions. Indeed, the importance of antecedent conditions was highlighted by a period of rainfall during the survey, when the resistivity of layer (a) appeared to drop along profile 3 (Figure 6.7). The water appears to have infiltrated rapidly into well-drained calcareous fine silty soil. Alternatively, it could simply reflect local groundwater levels in what is likely to be a seasonally riparian area, or the heterogeneity of superficial deposits. Indeed there were localised zones of very low resistivity in layer (a) along lines 1 and 2. This result however opens the possibility of conducting ERT in 4D, allowing the real time imaging of recharge through the vadose zone.

Compared to the upper zone, Layer (b) is more homogenous and has a resistivity of typically between 25-100 Ω/m. This coincides with the transition to saturated bedrock at the boreholes and matches well with a zone of 'homogenous weakly weathered Chalk' identified by Crook, Griffiths et al. (2004) at Frilsham (50-100 Ω/m). The ERT at Frilsham however did not detect a third horizon, layer (c) at a depth of 15 m characterised by slightly higher resistivity, circa 150-300 Ω/m. It could be that layer (b) represents a zone of increased fractures and associated permeability. Borehole fluctuations at Woodend and Hampstead Norreys extend only over the first 5-6 m below the ground surface, suggesting that water table fluctuation is not responsible for any increased dissolution of the fracture system. Although a zone of relatively high permeability may exist between 5 and 15 m, it does not provide a mechanism for regional scale drainage. Suggestions that dry valleys perpendicular to the main valley could act as draining conduits or hardbands provide preferential flow paths (Finch et al., 2004) is still valid. The survey did however reinforce that regional scale processes could be mediated by the local impact of a seasonal riparian gravel aquifer. Indeed elsewhere in the Lambourn catchment, it has been suggested that dry valleys perpendicular to the main river act as 'drains' focusing groundwater flow. However, the discharge to the river is ultimately mediated by local gravel aquifers (Griffiths et al., 2006). There is still scope to refine regional GEMs by sub-surface characterisation and identification of flood discharge 'hotspots'.

The vulnerability analysis accounts for all assets potentially at risk within the Pang/Lambourn, both within the ephemeral and perennial sub-catchments. This

allows a hierarchical assessment from estimates of urban areas in km^2 through to accounts for specific buildings. Previous risk maps however, did not take into consideration the relative vulnerability of the populations living within the urban areas or buildings (Morris et al., 2007). Fluvial or coastal flooding research has a rich history of in-depth vulnerability analysis, so the methodology was adopted from this body of research (Tapsell et al., 2002). The result was the SGFVI, which had the added dimension that those properties with basements would be more vulnerable to flooding form groundwater (DEFRA, 2006a; Green et al., 2006).

The hazard and vulnerability analyses were overlain to produce risk maps. Similarly to previous studies (Cobby et al., 2009; Jacobs, 2004), regions where groundwater levels are within 2 m of the surface were defined as hazardous. Throughout the Pang/Lambourn, 5 km^2 defined as urban are within these zones and are therefore considered 'at risk'. The 2 km^2 at risk in the Pang catchment is accounted for by 3603 at risk buildings. In both cases, statistics are given for regions above and below the perennial head to cater for differing groundwater flood definitions. It is difficult however to compare results with previous studies given there are no statistics available at the catchment scale using previous GEMs (Jacobs, 2004). Validation was carried out by using point incidence data. Although, as was suggested earlier, whether groundwater actually emerges is not only controlled by regional groundwater levels but locally by geological characteristics and topography controlling subsequent overland flow (Finch et al., 2004). In addition to this, there is the possibility that all individual flood incidents were not recorded. There is however a reasonable match between recorded events from 2000-2004 and at risk areas. Notable exceptions include Great Shefford in the upper Lambourn, where a portion of the settlement is deemed at high risk, but no incidents were recorded (Figure 6.9).

A novel development beyond previous risk mapping was the integration of a SGFVI. Using this indexing method, the 3603 buildings at risk in the Pang can be further classified into 1422 highly vulnerable and 2181 less vulnerable. Similarly, catchment wide, the 5 km^2 at risk urban areas, can be classified into 1.7 km^2 high risk and 3.3 km^2 less vulnerable. Such an index is difficult to validate using flood event locations alone, as they provide no indication of the relative financial and social impact. A survey of the impacts soon after an event would help validate the SGFVI. It is possible that the survey attempted as part of this study (Appendix 5.4) was too long after the major flooding of 2000-2001, resulting in poor participation numbers

as groundwater flooding had fallen away as a priority for residents. Just as groundwater inundation mapping during and soon after a flood event is important to improve physical modelling and hazard maps, so is detailed surveying of households. Only this way, can the risk maps incorporating the SGFVI be validated and improved. The inventory carried out at Hambledon (Green et al., 2006) could provide the basis for socio-economic impact assessment across the Pang/Lambourn and other Chalk catchments. Although this is beyond the scope of the current study, explicit examination of acute social, health or psychological stress of flooding could also be examined in the context of prolonged groundwater inundation.

6.5.2 Future groundwater flood risk

Previous attempts at groundwater flooding risk assessment do not consider the impact of a future non-stationary climate or land use change (Cobby et al., 2009). In this study, mathematical modelling of the climate and groundwater system has been combined with proxy flood indicators. The frequencies of trigger level and flood peak breaches at key boreholes are assessed for the baseline ensemble and each climate and land use change scenario. This gives an indication of the risk of groundwater flooding in the future relative to a baseline. Although not the same as frequency magnitude calculations associated with fluvial flood risk (Shaw, 1994), it provides a robust measure of relative risk based on the physical processes of rainfall infiltration and groundwater flow. The scenario ensemble technique also allows for the quantification of uncertainty in the flood risk predictions.

The recharge regime of the Pang/Lambourn will be altered considerably under scenarios of projected climate change (Figure 5.5). There is a trend to a decline in average recharge volumes relative to the baseline for all climate change scenarios, especially during the 2080 time slice. Interestingly, the number of extreme recharge events remains high and in some cases the magnitude of these events exceeds those seen in the baseline. By focusing on the relative frequency with which key boreholes breach trigger levels or reach flood peaks, it has been demonstrated that changes to the recharge regime will have an impact on the likelihood of dangerously high groundwater conditions that may result in flooding. Groundwater flooding risk will diminish considerably over the next 100 year period. This reduction appears to be irrespective of a high or low climate scenario and is progressive through the time slices (Figure 6.10). The 2080 time slice, representing 2070 to 2100, exhibits

between a 97–98% decrease in flood peak frequency depending on climate scenario. Using this proxy, this represents an almost complete eradication of groundwater flood risk. Indeed, the greatest reduction in risk is found under the 'optimistic' UKCIP low emissions, low climate sensitivity scenario. This suggests that changes to the hydrological cycle under moderate climate change might impact the risk of groundwater flooding more than if a dramatic change took place. It could be that the increase in short term, high intensity rainfall associated with climatic change (Hulme et al., 2002; IPCC, 2007) will compensate the reduction in overall recharge if emissions and sensitivity are both high. It could be argued however that the focus given over to the management of groundwater flood risk will become less warranted over time. In this case, finite resources would be better allocated to surface water flooding associated with short-term heavy rainfall and drought alleviation.

There is a suggestion that the reduction in groundwater flood risk may not be equivalent across the Pang/Lambourn. Reduced sensitivity to climate change at Chapelwood, Saltbox and Northfield boreholes could be due to localised modelled preferential pathways in the Chalk aquifer or recharge 'hotspots' (see Figure 6.10). Indeed, the land use change scenario (Figure 5.3) produced nuanced differences in the spatial distribution of recharge. Overall there is a trend to a decline in average recharge volumes and amplitude of extreme events in comparison to the baseline and control h2020 scenario (Figure 5.12). Relative to the baseline value of trigger level breaches, there is a 49% decrease in frequency under the land use change scenario. This is in contrast to a 25% decrease under the control h2020 scenario. This suggests that although climate forcing is likely to be the primary factors in mediating the risk of groundwater flooding this coming century, land use may also play a part. Spatial variations in recharge could have implications for the spatial variation in groundwater flooding risk. This has been highlighted by the differences in the sensitivity of some boreholes to land use change (Figure 5.15). However, the differences in flood proxy frequency reduction between boreholes cannot simply be put down to land use change. This is because changes happen in the 'rank of sensitivity' between climate scenarios as well as between climate and land use scenario. The trigger boreholes are however not necessarily tied to groundwater flood risk at a particular location, rather they are indicative of generalised risk. The differences between boreholes could therefore be viewed as another level of uncertainty in risk quantification.

The flood proxy frequency analysis can be combined with risk mapping discussed previously in order to develop pseudo-probability risk maps. For example, the 3603 buildings currently deemed at risk in the Pang catchment (see Figure 6.9), would see a decrease in that risk of between 25% and 94% over the next century (h2020 and h2080 respectively), assuming unchanged land use. Uncertainty of such statistics is quantifiable and exists between scenarios, within scenario ensembles and between proxy measures (i.e. using borehole trigger or flood frequencies). As an example, the groundwater flooding risk associated with the coming 20 years (i.e. the 2020s) can be broken down as follows: depending on the climate sensitivity and global greenhouse gas emissions, the reduction in borehole trigger breach frequency will be between 25% (high) and 35% (low). The 35% consists of a range between 16.7% and 37% reduction across boreholes in the domain. The 25% consists of a range between 17% and 37%. The risk reduction is therefore between 16.7% and 37% catchment wide over the next couple of decades. This range does not include intra-scenario differences or the use of flood peaks instead of trigger breach frequency. Validation of such predictions will continue throughout the coming century.

6.5.3 Mitigation options

The mitigation option of doing nothing to prevent groundwater flooding (Cobby et al., 2009), appears to be an increasingly realistic option given the evidence of a decreasing risk. Continuing uncertainty however, means it is prudent to assess possible mitigation strategies. The risk analysis framework also allows the testing of proactive mitigation measures, in this case targeted land use modification. A local index of recharge potential was developed for the upper Pang in order to identify where efforts to modify recharge could be focused (Figure 6.12). A conditional statement then represents the mitigation decision making process. Here, α represents the total baseline (i.e. current) cost of flooding [£/m^2] or intangible costs e.g. anxiety, so that

$$\textit{if} \qquad (\alpha \times A)\lambda > \beta \tag{6.11}$$

then the mitigation procedure is cost effective

where A is a factor that reduces or increases the costs depending on frequency changes under climate or land use change. The cost is further mediated by λ, which is a measure of vulnerability as a function of the SGFVI. This can then be weighed

against the cost of mitigation β, which in this case is the cost of land use modification [£/m^2]. This change could for example be from tilled land to coniferous woodland. If the left hand side of Equation 6.2 is greater than the left, the mitigation procedure is cost effective. The modelling procedure outlined could provide values for A and λ but would require two additional datasets:

1. Cost of converting land (β). The majority of the highly sensitive areas lie on arable or horticultural land. The cost of converting to coniferous woodland or implementing a sustainable drainage system [£/m^2] would need to be calculated. This is made more complex by issues of land ownership and is beyond the scope of this study.
2. The cost of a flood (α) to property and livelihoods in pounds as well as secondary ill effects to health [£/m^2].

The gathering of such data is complex and would require survey and stakeholder engagement processes. The on-line survey attempted during this study and modified depth, duration, damage curves (Green et al., 2006) could provide the basis for a possible methodology. The risk model framework could be used to run multiple scenarios of mitigation options in order to determine the optimum solution. Although the framework cannot offer solutions, the purpose of this study is to illustrate how the methodology might work. It offers an interactive framework in order to encourage greater stakeholder engagement in the decision making process. Indeed, a similar algorithm could be implemented for other mitigation procedures e.g. installing additional pumping wells or improving surface drainage.

6.6 Further work

The SGFVI was calculated only for census OAs with at least a portion within the Pang or Lambourn catchment. It is therefore only an indication of relative vulnerability within this region. The census in 2011 will provide an ideal opportunity to develop the SGFVI for the entire UK. By combining a UK-wide SGFVI and GEM, it would be possible to highlight the areas of the country that are most vulnerable to groundwater flooding. This would ensure that finite resources could be allocated in areas where they are most needed. Similarly these is a need to use the model framework to assess the impact of climate change on groundwater flooding risk elsewhere in the UK in order to confirm that the reduction in risk in not specific to the Pang/Lambourn.

In this study, the future predictions of flood risk are limited to extreme high and low climate sensitivity and CO_2 emissions scenarios. In addition, the HadRM3H was the only climate model used to generate these scenarios. The integration of the latest UKCIP09 climate change scenarios, including a greater number of climate models and scenarios would help refine impact predictions. Also, further land use change scenarios would be required to get a better idea of the potential influences. Indeed, the model architecture makes it very easy to interactively develop and test a large number of raster based land use distributions.

The region may see a shift in risk from groundwater flooding to fluvial and pluvial flooding. Droughts are also likely to become more of a problem as the risk of groundwater flooding diminishes. As such, it becomes more vital to steer the research and modelling focus towards these risks. Higher spatial and temporal resolution modelling is required to better account for high rate, short term rainfall on pluvial and fluvial flooding risk perhaps with less of an emphasis on a groundwater contribution.

6.7 Conclusions

Climate change and groundwater modelling has been integrated with socio-economic data to provide a robust analysis of current and future risk of groundwater flooding in the Pang/Lambourn catchment. Hazard maps were integrated with a novel SGFVI to identify at risk urban areas and specific buildings. In this case, 5 km^2 of 'urban area' lies within a groundwater flood hazard zone, 1.7 km^2 of which is at relatively high risk. In the Pang catchment for example this represents 3603 buildings in the hazard zone, 1422 at high risk. These risk areas have been validated using point flood incidence databases.

Using EA trigger borehole levels as a proxy for flood risk, climate change scenarios suggest that the risk of groundwater flooding in the catchment will decrease considerably (25-98%) over the next century. Further significant modification of the risk could occur through changes in land use. Uncertainty exists however and a methodology for the cost-benefit of mitigation through focused land use modification is considered. The flexible model framework will encourage local level climate adaptation behaviour and integrated stakeholder engagement. Emphasis should however be moved away from groundwater flooding risk towards short duration, high intensity surface water flooding and drought mitigation.

Chapter 7 Conclusions and further work

7.1 Conclusions

The principal aim of this thesis has been to test the hypothesis that ..."global changes in climate and socio-economic systems are likely to have an impact on groundwater recharge and flooding risk within Chalk catchments of the UK..." This was broken down further into a series of research questions linked to the Driver Pressure State Impact Response (DPSIR) framework. In order to address these in Chapters 5 and 6, an integrated atmosphere, hydrosphere, biosphere and geosphere model was developed for the Pang/Lambourn catchment in Chapters 2-4. Initially therefore, conclusions are made about this integrated model and the dominant processes at this site:

1. A distributed, transient recharge model was developed using GIS (GIS-DIRT) for the Pang/Lambourn catchment and tested against field observations of soil moisture. By applying observed weather data, between 1978 and 2006, the mean recharge rate was found to be 160 mm/yr. This means that about one fifth of rainfall potentially ended up as recharge to the aquifer and contributed to the risk of groundwater flooding.
2. Land use and soil texture interact to influence the distribution and magnitude of recharge in the Pang/Lambourn suggesting an opportunity to manage recharge and therefore groundwater flood risk through land use modification.
3. A temporal sensitivity analysis of monthly calculations suggested that winter recharge is underestimated by up to 8% in comparison to a daily calculation. However, this does not have a significant impact on modelled groundwater levels.
4. ARIMA prewhitening of rainfall and borehole hydrographs has allowed the robust cross-correlation analysis between the two time series. This analysis suggested that groundwater flow from the soil, through the vadose zone to the permanent groundwater surface is either via a matric piston displacement mechanism or via fractures. Groundwater level responses can be rapid or 'smeared' over a number of weeks. A monthly groundwater model time step, will adequately account for both rapid and longer term recharge.

5. Rapid (sub-daily) responses to rainfall are possible through a relatively deep vadose zone. Therefore local groundwater flood risk may have a slow onset but rapid 'activation period'. Evidence for rapid infiltration of rainfall was also found during a geophysical investigation of a possible preferential flow path in the Pang valley.
6. Borehole responses suggest that recharge occurs through the London Clay in the south of the Pang/Lambourn and so is accounted for in GIS-DIRT.
7. Inverse parameterisation of a single layer MODFLOW model constrained by output from GIS-DIRT results in a highly heterogeneous distribution of aquifer properties (transmissivity and storage). This is likely to reflect the non-linearity and preferential flow paths characteristic of the Chalk.
8. A second MODFLOW model introduced vertical heterogeneity and the domain was also extended up to the extent of the groundwater catchment. Despite this, the single layer model simulated the EA trigger boreholes more effectively. It was therefore deemed more suitable for use as a flood risk assessment.

The integrated atmosphere, surface water, vadose zone, groundwater model architecture developed here for the Pang/Lambourn would be applicable to any other Chalk catchment in the UK and beyond. Indeed, the emphasis throughout the construction of the model has been on the use of a generic GIS data structure for simulations where possible. Once the model was set up for a catchment, the original DPSIR related research questions developed from the hypothesis could then be tested. In this case, the results for the Pang/Lambourn could provide an indication of the changes expected at other Chalk catchments, particularly nearby in the south of England.

How will climate and socio-economic changes (drivers) translate into regional pressures, for example rainfall amounts, temperature ranges and land use modification?

- Output from the regional climate model HADRM3H was downscaled to the Pang/Lambourn catchment scale using the EARWIG weather generator. The most extreme prediction based on an ensemble of UKCIP climate change scenarios (h2080 scenario) suggested a 37 mm/month increase in mean

potential evapotranspiration and a 4.5 mm/month decrease in mean rainfall relative to the climate baseline of 1961-1990.

- A future land use modification scenario was based on trends identified in regional planning documents covering the next 20 year period. The changes were characterised largely by predictions of increased afforestation (5% increase in woodland cover) and urbanisation (4% increase in urban/suburban cover).

What will the impact be on the state of the groundwater system i.e. recharge rate and groundwater levels?

- The EARWIG-DIRT coupled model suggests that over the coming century under climate change, recharge in the Pang/Lambourn will be reduced by between 5.5 and 27% relative to the baseline.
- An increase in afforestation and urbanisation will lead to a decrease of 5.5% in overall recharge. In addition, distributed recharge patterns will be affected, the magnitude of which are mediated by soil type.
- Changes to the recharge regime under climate change will reduce mean groundwater levels by up to 3.8% against the baseline. The largest reductions will be seen at interfluve sites which currently exhibit the largest fluctuations.
- Changes to the spatial distribution of recharge as a result of land use changes will impact groundwater levels locally.

How will this impact on the risk of groundwater flooding to those living in the region?

- Groundwater flood hazard maps of the Pang/Lambourn suggest that about 22 km^2 of the Pang/Lambourn may be exposed during high groundwater levels. 5 km^2 of urban development areas lie within these hazardous zones and are therefore deemed at risk. In the Pang catchment this is accounted for by 3603 buildings.
- A Groundwater Flooding Social Vulnerability Index was based on the socio-economic composition of regional settlements. Combined with the hazard maps, it was suggested that 1.7 km^2 of urban areas could be considered highly or very highly at risk from groundwater flooding. In the Pang catchment, of the 3603 buildings in the hazard zone 1422 are deemed at high risk.

- Both high and low climate change scenarios predict a considerable decrease (25-98%) in the frequency of groundwater flood events over the coming century. This decrease is progressive through the time an irrespective of CO_2 emissions and climate sensitivity.
- Land use modification led to a further 24.5% reduction in the risk of groundwater flooding on top of climate change impacts during the 2020 time slice.
- Uncertainty of risk reduction statistics is quantifiable and exists between scenarios and between proxy measures. For example, the groundwater flooding risk associated with the 2020s can be broken down as follows: depending on the climate sensitivity and global greenhouse gas emissions scenario, the reduction in borehole trigger breach frequency will be between 25% and 35%. This 35% consists of a range between 16.7% and 37% reduction across boreholes in the domain. The 25% consists of a range between 17% and 37%. The risk reduction is therefore between 16.7% and 37% catchment wide over the next couple of decades.

Will there be an appropriate response to the change in risk and what should it be?

- An index of recharge potential was developed for a sub-region of the upper Pang known to be susceptible to groundwater flooding. Regions where high recharge values intersect with zones draining into gaining reaches are regarded at high sensitivity areas. Land use modification of these areas could help mitigate against flood risk.
- The cost benefit of land use modification is mediated by the reduced future risk of groundwater flooding. It is likely that the cost to communities of flooding will reduce and so investing in mitigation becomes less economical.

7.2 Wider implications and further work

This study has successfully developed a method for down-scaling future predications of climate and land use change to assess the impact on regional groundwater flooding risk. This type of interdisciplinary work is vital to provide robust predictions of the potential risks associated with a changing climate and socio-economic future in the UK and beyond. It provides an opportunity to effectively communicate the effects

climate change will have on individual groups of people. Indeed, by customising and individualising the impacts of an abstract threat of global change, the impetus to adapt may become stronger. In addition, the cost and benefit of adopting adaptation or mitigation strategies can be assessed objectively. I strongly suggest that such an integrated approach be adopted as the standard in any future climate impact studies on groundwater resources. By combining data and processes from other sectors as well, it provides a powerful spatial planning tool in order that multiple 'win-win' benefits might be realised.

Studies such as this one also highlight the need to focus on potential positive aspects of change and the need for pragmatic adaptation. In some cases for example climate change may bring about beneficial effects, for example here in the reducing the risk of groundwater flooding. However, only by validating the model against the incidence of groundwater flooding over the coming decades will this conclusion be confirmed. At the same time, ongoing improvements could be made to the model that could refine such predictions, for example using more up to date climate modelling and scenarios (e.g. UKCIP09).

In light of the likelihood that groundwater flooding risk may be reducing in Chalk catchments of the UK, the option of 'doing nothing about it' is attractive. At the same time the risk of drought and surface water flooding may increase, requiring a change in focus for future research. The change in the frequency of drought risk could be assessed using the same model architecture as the one presented here albeit with an emphasis on simulating groundwater at low flow levels. In addition, higher temporal resolution hydrological modelling should adopt a similar ensemble scenario methodology to assess the impact on future pluvial and fluvial flood risk in permeable catchments such as the Pang/Lambourn.

References

Adams, B., Bloomfield, J.P., Gallagher, A.J., Jackson, C.R., Rutter, H.K., and Williams, A.T., 2010, An early warning system for groundwater flooding in the Chalk: Quarterly Journal of Engineering and Hydrogeology, v. 43, p. 185-193.

Adams B., P.D.W., Bloomfield J.P., 2003, The LOCAR hydrogeological infrastructure for the Pang/Lambourn catchment: Keyworth, Nottingham, British Geological Survey.

Alcolea, A., Carrera, J., and Medina, A., 2006, Pilot points method incorporating prior information for solving the groundwater flow inverse problem: Advances in Water Resources, v. 29, p. 1678-1689.

Allen, D.J., Brewerton, L.J., Coleby, L.M., Gibbs, B.R., Lewis, M.A., Macdonald, A.M., Wagstaff, S.J., and Williams, A.T., 2007, Physical properties of major aquifers in England and Wales.

Arnell, N.W., 1996, The effects of climate change due to global warming on river flows in Great Britain: Journal of Hydrology, v. 183, p. 397-424.

Avery, B.W., 1980, Soil classification for England and Wales (higher categories). Soil survey technical monograph No. 14. Harpenden.

Banks, D., Davies, C., and Davies, W., 1995, The Chalk as a karstic aquifer: evidence from a tracer test at Stanford Dingley, Berkshire, UK.: Quarterly Journal of Engineering Geology, v. 28, p. 31-38.

Barker, J.A., 1993, Modelling groundwater flow and transport in the Chalk. The hydrogeology of the Chalk of North-West Europe: Oxford, Clarendon, p. 59-66.

Batelaan, O., and De Smedt, F., 2001, WetSpass: A flexible, GIS based, distributed recharge methodology for regional groundwater modelling: IAHS-AISH Publication, p. 11-18.

Batelaan, O., and De Smedt, F., 2007, GIS-based recharge estimation by coupling surface-subsurface water balances: Journal of Hydrology, v. 337, p. 337-355.

Bell, J.P., 1987, Neutron Probe Practice, Institute of Hydrology.

Berkshire Unitary Authorities Joint Strategic Planning Unit, 2005, Berkshire Structure Plan: 2001-2016.

Bloomfield, J.P., Gaus, I., and Wade, S.D., 2003, A method for investigating the potential impacts of climate- change scenarios on annual minimum groundwater levels: Journal of The Chartered Institution of Water and Environmental Management, v. 17, p. 86-91.

Bloomfield, J.P., and McKenzie, A., 2005, Avoiding wet feet, Surveyor, p. 13-14.

Box, G.E.P., and Jenkins, G.M., 1976, Time series analysis, Forecasting and Control: San Francisco, Holden-Day.

Bradford, R.B., 2002a, Controls on the discharge of Chalk streams of the Berkshire Downs, UK: Science of the Total Environment, v. 282-283, p. 65-80.

Bradford, R.B., 2002b, Volume-duration growth curves for flood estimation in permeable catchments: Hydrology and Earth System Sciences, v. 6, p. 939-947.

Bradford, R.B., and Croker, K.M., 2007, Application of head- flow responses to groundwater floods in chalk catchments: Quarterly Journal of Engineering and Hydrogeology, v. 40, p. 67-74.

Bradford, R.B., Ragab, R., Crooks, S.M., Bouraoui, F., and Peters, E., 2002, Simplicity versus complexity in modelling groundwater recharge in Chalk catchments: Hydrology and Earth System Sciences, v. 6, p. 927-937.

Bravo, H., and Jiang, F., 2002, Using groundwater temperature data to constrain parameter estimation in a groundwater flow model of a wetland system: Water Resources Research, v. 38, p. 281-289.

Brenchley, P.J., and Rawson, P.F., 2006, The geology of England and Wales, Geological Society Publishing House.

Brouyere, S., Carabin, G., and Dassargues, A., 2004, Climate change impacts on groundwater resources: modelled deficits in a chalky aquifer, Geer basin, Belgium: Hydrogeology Journal, v. 12, p. 123-134.

Brown, J.D., and Damery, S.L., 2002, Managing flood risk in the UK: towards an integration of social and technical perspectives: Transactions of the Institute of British Geographers, v. 27, p. 412-426.

Buttle, J.M., 1994, Isotope hydrograph separations and rapid delivery of pre-event water from drainage basins: Progress in Physical Geography, v. 18, p. 16-41.

Calver, A., 1997, Recharge response functions: Hydrology and Earth System Sciences, v. 1, p. 47-53.

Chae, G.T., Yun, S.T., Kim, D.S., Kim, K.H., and Joo, Y., 2010, Time series analysis of three years of groundwater level data (Seoul, South Korea) to characterize urban groundwater recharge: Quarterly Journal of Engineering Geology and Hydrogeology, v. 43, p. 117-127.

Chatfield, C., 2003, The Analysis of time series. An introduction, CRC Press.

Chen, K., and Blong, R., 2003, Towards an integrated approach to natural hazards risk assessment using GIS: With reference to bushfires: Environmental Management, v. 31, p. 546-560.

Chow, V.T., Maidment, D.R., and Mays, L.W., 1988, Applied Hydrology: New York, McGraw-Hill.

Clausen, B., Young, A.R., and Gustard, A., 1994, Modelling the impact of groundwater abstraction on low river flows. , Flow regimes from international experimental and network data (FRIEND): proceedings of the Braunschweig conference, p. 77-85.

Cobby, D., Morris, S., Parkes, A., and Robinson, V., 2009, Groundwater flood risk management: advances towards meeting the requirements of the EU floods directive: Journal of Flood Risk Management, v. 2, p. 111-119.

Connorton, B.J., and Reed, R.N., 1978, A numerical model for the prediction of long term well yield in an un unconfined Chalk aquifer: Quarterly Journal of Engineering Geology, v. 11, p. 127-138.

Crook, N., Griffiths, J., Binley, A., Pates, J., and Young, A., 2004, Indentification and quantification of surface-groundwater interaction in the lowland Chalk catchments of the Pang and Lambourn: Hydrology: Science and Practice for the 21st Century, v. 2, p. 64-71.

Cross, G.A., Rushton, K.R., and Tomlinson, L.M., 1995, The East Kent Chalk aquifer during the 1988-92 drought: Journal of the Institute of Water and Environmental Management, v. 9, p. 37-48.

Darcy, H., 1856, Les fontaines publiques de la ville de Dijon: Paris, Victor Dalmont.

DEFRA, 2006a, Making space for water - Groundwater flooding records collation, monitoring and risk assessment - initial statement (Chalk aquifers)

DEFRA, 2006b, Making space for water - Groundwater flooding records collation, monitoring and risk assessment - initial statement (non- Chalk aquifers).

Delta-TDevices, 2004, User manual for the Profile Probe type pr2.

Dobney, K., Baker, C.J., Chapman, L., and Quinn, A.D., 2010, The future cost to the United Kingdom's railway network of heat-related delays and buckles caused by the predicted increase in high summer temperatures owing to climate change: Proceedings of the institution of Mechanical Engineers, v. 224, p. 25-34.

Doherty, J., 2003, Ground water model calibration using pilot points and regularization: Ground Water, v. 41, p. 170-177.

Dolman, A.J., and Nonhebel, S., 1988, Modelling forest water consumption in the Netherlands: Agricultural Water Management, v. 14, p. 413-422.

Downing, R.A., Davies, M.C., Pontin, J.M.A. and Young, C.P., 1972, Artificial recharge of the London Basin: Bulletin of the International Association of Hydrological Sciences, v. 17, p. 183-187.

Environment Agency, 1997, Groundwater quality in the London Basin: Major ion and general chemistry for the Chalk aquifer. Accessed December 2010: http://216.31.193.173/gwcl/Thames/Chalk-London-Basin/GW_QRepChalkLondon.html.

Fekete, A., 2009, Validation of a social vulnerability index in context to river-floods in Germany: Natural Hazards and Earth System Science, v. 9, p. 393-403.

Finch, J.W., 2000, Modelling the soil moisture deficits developed under grass and deciduous woodland: The implications for water resources: Journal of the Chartered Institution of Water and Environmental Management, v. 14, p. 371-376.

Finch, J.W., 2001, Estimating change in direct groundwater recharge using a spatially distributed soil water balance model: Quarterly Journal of Engineering Geology and Hydrogeology, v. 34, p. 71-83.

Finch, J.W., Bradford, R.B., and Hudson, J.A., 2004, The Spatial distribution of groundwater flooding in a chalk catchment in southern England: Hydrological Processes, v. 18, p. 959- 971.

Flerchinger, G.N., Cooley, K.R., and Ralston, D.R., 1992, Groundwater response to snowmelt in a mountainous watershed: Journal of Hydrology, v. 133, p. 293-300.

Foster, S.S.D., 1975, The Chalk groundwater tritium anomaly- a possible explanation: Journal of Hydrology, v. 25, p. 159-165.

Fowler, H.J., Kilsby, C.G., and Stunell, J., 2007, Modelling the impacts of projected future climate change on water resources in north-west England: Hydrology and Earth System Sciences, v. 11, p. 1115-1126.

Fuller, K., 2003, Going to ground, Surveyor, p. 12-14.

Gardener, C.M.K., Cooper, J.D., Wellings, S.R., Bell, J.P., Hodnett, M.G., Boyle, S.A., and Howard, M.J., 1990, Hydrology of the unsaturated zone of the Chalk of SE England, Chalk: London, Thomas Telford, p. 611-618.

Grapes, T.R., Bradley, C., and Petts, G.E., 2005, Dynamics of river-aquifer interactions along a chalk stream: The River Lambourn, UK: Hydrological Processes, v. 19, p. 2035-2053.

Grapes, T.R., Bradley, C., and Petts, G.E., 2006, Hydrodynamics of floodplain wetlands in a chalk catchment: The River Lambourn, UK: Journal of Hydrology, v. 320, p. 324-341.

Great Britain, 2010, Flood and Water Management Act 2010: Elizabeth II. Chapter 29: London: The Stationery Office.

Green, C., Wilson, T., Masterson, T., and Boothby, N., 2006, An assessment of the additional flood losses associated with groundwater flooding: a report to Hampshire County Council and Winchester City Council, Flood Hazard Research Centre, Middlesex University.

Griffiths, J., Binley, A., Crook, N., Nutter, J., Young, A., and Fletcher, S., 2006, Streamflow generation in the Pang and Lambourn catchments, Berkshire, UK: Journal of Hydrology, v. 330, p. 71-83.

Griffiths, J., Nutter, J., Binley, A., Crook, N., Young, A., and Pates, J., 2007, Variability of dissolved CO2 in the Pang and Lambourn Chalk rivers: Hydrology and Earth System Sciences, v. 11, p. 328-339.

Grindley, J., 1967, The estimation of soil moisture deficits: Meteorology Magazine, v. 96, p. 97-108.

Grindley, J., 1969, The calculation of actual evaporation and soil moisture deficits over specified catchment areas: Hydrological Memorandum 28, Meteorological Office, Bracknall, UK.

Haque, C.E., Dominey-Howes, D., Karanci, N., Papadopoulos, G., and Yalciner, A., 2006, The need for an integrative scientific and societal approach to natural hazards: Natural Hazards, v. 39, p. 155-157.

Harbaugh, A.W., Banta, E.R., Hill, M.C., and McDonald, M.G., 2000, Modflow-2000, The U.S. Geological Survey modular groundwater-water model- user guide to modularization concepts and the ground-water flow process U.S.G.S.

Haria, A.H., Hodnett, M.G., and Johnson, A.C., 2003, Mechanisms of groundwater recharge and pesticide penetration to a Chalk aquifer in southern England: Journal of Hydrology, v. 275, p. 27-41.

Hassan, M., and Gregory, P.J., 2002, Dynamics of water movement on Chalkland: Journal of Hydrology, v. 257, p. 27-41.

Headworth, H.G., 1972, The analysis of natural groundwater level fluctuations in the Chalk of Hampshire: Journal of the Institution of Water Engineers, v. 26, p. 107-124.

Healy, R.W., and Cook, P.G., 2002, Using groundwater levels to estimate recharge: Hydrogeology Journal, v. 10, p. 91-109.

Heathcote, J.A., Lewis, R.T., and Soley, R.W.N., 2004, Rainfall routing to runoff and recharge for regional groundwater resource models: Quarterly Journal of Engineering Geology and Hydrogeology, v. 37, p. 113-130.

Herrera-Pantoja, M., and Hiscock, K.M., 2008, The effects of climate change on potential groundwater recharge in Great Britain: Hydrological Processes, v. 22, p. 73-86.

Hill, M.C., 1990, Solving groundwater flow problems by conjugate gradient methods and the strongly implicit procedure: Water Resources Research, v. 26, p. 1961-169.

Hill, M.C., 2007, Effective groundwater model calibration: with analysis of data, sensitivities, predictions and uncertainty: Hoboken, John Wiley & Sons Inc.

Hiscock, K., 2005, Hydrogeology: Principles and Practice: Oxford, Blackwell.

Holman, I.P., 2006, Climate change impacts on groundwater recharge-uncertainty, shortcomings, and the way forward?: Hydrogeology Journal, v. 14, p. 637-647.

Holman, I.P., Nicholls, R.J., Berry, P.M., Harrison, P.A., Audsley, E., Shackley, S., and Rounsevell, M.D.A., 2005a, A regional, multi-sectoral and integrated assessment of the impacts of climate and socio-economic change in the UK: Part II. Results: Climatic Change, v. 71, p. 43-73.

Holman, I.P., Rounsevell, M.D.A., Shackley, S., Harrison, P.A., Nicholls, R.J., Berry, P.M., and Audsley, E., 2005b, A regional, multi-sectoral and

integrated assessment of the impacts of climate and socio-economic change in the UK: Part I. Methodology: Climatic Change, v. 71, p. 9-41.

Holman, I.P., Tascone, D., and Hess, T.M., 2009, A comparison of stochastic and deterministic downscaling methods for modelling potential groundwater recharge under climate change in East Anglia, UK: implications for groundwater resource management: Hydrogeology Journal, v. 17, p. 1629-1641.

Howard, K.W.F., and Lloyd, J.W., 1979, The sensitivity of parameters in the Penman evaporation equations and direct recharge balance: Journal of Hydrology, v. 41, p. 329-344.

Hudson, J.A., Gilman, K., and Calder, I.R., 1997, Land use and water issues in the uplands with reference to the Plynlimon study: Hydrology and Earth System Sciences, v. 1, p. 389-397.

Hughson, H., Huntley, D., and Razack, M., 1996, Cokriging limited transmissivity data using widely sampled specific capacity from pump tests in an alluvial aquifer: Groundwater, v. 34, p. 12-18.

Hulme, M., and Jenkins, G.J., 1998, Climate change scenarios for the United Kingdom: scientific report. UKCIP technical report No. 1: Norwich, Climate Research Centre, p. 80.

Hulme, M., Jenkins, G.J., Lu, X., Turnpenney, J.R., Mitchell, T.D., Jones, R.G., Lowe, J., Murphey, J.M., hassell, D., Boorman, P., MacDonald, R., and Hill, S., 2002, Climate change scenarios for the United Kingdom: The UKCIP02 scientific report: Norwich, Tyndall Centre for Climate Change Research, School of Environmental Sciences, UEA, p. 120.

IPCC, 2000, Special report on emissions scenarios. 2000. Special report of the Intergovernmental Panel on Climate Change, Cambridge University Press.

IPCC, 2007, Climate Change 2007. The physical science basis, summary for policymakers. Contribution of working group I to the fourth assessment report of the intergovernmental panel on climate change. IPCC secretariat Switzerland.

Ireson, A.M., Mathias, S.A., Wheater, H.S., Butler, A.P., and Finch, J., 2009, A model for flow in the chalk unsaturated zone incorporating progressive weathering: Journal of Hydrology, v. 365, p. 244-260.

Ireson, A.M., Wheater, H.S., Butler, A.P., Mathias, S.A., Finch, J., and Cooper, J.D., 2006, Hydrological processes in the Chalk unsaturated zone - Insights from an intensive field monitoring programme: Journal of Hydrology, v. 330, p. 29-43.

Jackson, B.M., Wheater, H.S., Wade, A.J., Butterfield, D., Mathias, S.A., Ireson, A.M., Butler, A.P., McIntyre, N.R., and Whitehead, P.G., 2007, Catchment-scale modelling of flow and nutrient transport in the Chalk unsaturated zone: Ecological Modelling, v. 209, p. 41-52.

Jackson, C.R., Chettham, M., and Guha, P., 2006, Groundwater and climate change research scoping study: Nottingham, BGS.

Jackson, D., and Rushton, K.R., 1987, Assessment of recharge components for a chalk aquifer unit: Journal of Hydrology, v. 92, p. 1-15.

Jacobs, 2004, Strategy for flood and coastal erosion risk management: Groundwater flooding scoping study (LDS 23). Final Report, Volumes 1 and 2. May 2004. Available at http://www.louistalboys.com/stonehenge/downloads/gw1.pdf

Jacobs, 2006, Making Space for Water: Groundwater flooding records collation, monitoring and risk assessment (HA5). Final Report. Environment Agency.

Jacobs, 2008, West Berkshire Strategic Flood Risk Assessment (SFRA).

Jenkins, G.J., Murphy, J.M., Sexton, D.M., Lowe, J., Jones, P., and Kilsby, C.G., 2009, UK climate projections: Briefing report: Exeter, UK, Met Office.

Jenks, G.F., 1967, The data model concept in statistical mapping: International Yearbook of Cartography, v. 7, p. 186-190.

Jessel, B., and Jacobs, J., 2005, Land use scenario development and stakeholder involvement as tools for watershed management within the Havel River Basin: Limnologica, v. 35, p. 220-233.

Jones, H.K., and Cooper, J.D., 1998, Water transport through the unsaturated zone of the Middle Chalk: a case study from the Fleam Dyke lysimter, *in* Robins, N.S., ed., Groundwater pollution, aquifer recharge and vulnerability: Geological Society special publication, p. 117-128.

Jyrkama, M.I., and Sykes, J.F., 2007, The impact of climate change on spatially varying groundwater recharge in the grand river watershed (Ontario): Journal of Hydrology, v. 338, p. 237-250.

Kay, A.L., Davies, H.N., Bell, V.A., and Jones, R.G., 2008, Comparison of uncertainty sources for climate chnage impacts: flood frequency in England: Climatic Change, v. 92, p. 41-63.

Kelly, B., 2003, Missouri river alluvial groundwater flow model: Missouri, USGS.

Kilsby, C.G., Jones, P.D., Burton, A., Ford, A.C., Fowler, H.J., Harpham, C., James, P., Smith, A., and Harpham, C., 2007, A daily weather generator for use in climate change studies: Environmental Modelling and Software, p. 1-15.

Kitanidis, P.K., 1999, Introduction to geostatistics: applications to hydrogeology, Cambridge University Press.

Korkmaz, S., Ledoux, E., and Önder, H., 2009, Application of the coupled model to the Somme river basin: Journal of Hydrology, v. 366, p. 21-34.

Kreibich, H., Thieken, A.H., Grunenberg, H., Ullrich, K., and Sommer, T., 2009, Extent, perception and mitigation of damage due to high groundwater levels in the city of Dresden, Germany: Natural Hazards and Earth System Sciences, v. 9, p. 1247-1258.

Kruskal, W.H., and Wallis, W.A., 1952, Use of ranks in one-criterion variance analysis: Journal of American Statistical Association, v. 47, p. 583-621.

Krysanova, V., Kundzewicz, Z.W., Pinskwar, I., Habeck, A., and Hatterman, F., 2006, Regional socio- economic and environmental changes and their impacts on water resources on example of Odra and Elbe basins: Water Resources Management, v. 20, p. 607-641.

Law, F., 1956, The effect of afforestation upon the yield of water catchment areas: Journal of The British Waterworks Association, v. 38, p. 484-494.

Lee, J.Y., and Lee, K.K., 2000, Use of hydrologic time series data for identification of recharge mechanism in a fractured bedrock aquifer system: Journal of Hydrology, v. 229, p. 190-201.

Lee, L.J.E., Lawrence, D.S.L., and Price, M., 2006, Analysis of water-level response to rainfall and implications for recharge pathways in the Chalk aquifer, SE England: Journal of Hydrology, v. 330, p. 604-620.

Lehman, A., and Rode, M., 2000, Long-term behaviour and cross-correlation water quality analysis of the river Elbe, Germany: Water Resources, v. 35, p. 2153-2160.

Lerner, D.N., 1990, Groundwater recharge: A guide to understanding and estimating natural recharge: Hannover, Verlag Heinz Heise.

Lim, K.J., Engel, B.A., Tang, Z., Choi, J., Kim, K., Muthukrishnan, S., and Tripathy, D., 2005, Automated web GIS based hydrogrpah analysis tool, WHAT: Journal of the American Water Resources Association, v. 41, p. 1407-1416.

Ljung, G.M., and Box, G.E.P., 1978, On a measure of lack of fit in time series models: Biometrika, v. 65, p. 297-303.

Loaiciga, H.A., 2003, Climate change and ground water: Annals of the Association of American Geographers, v. 93, p. 30-41.

Loke, M.H., 2010, Tutorial: 2-D and 3-D Electrical Imaging Surveys.

Macdonald, A.M., Brewerton, L.J., and Allen, D.J., 1998, Evidence for rapid groundwater flow and karst-type behaviour in the Chalk of southern England: Groundwater pollution, aquifer recharge and vulnerability. Geological Society Special Publications, p. 95-106.

Mann, M.E., Zhang, Z., Hughes, M.K., Bradley, R.S., Miller, S.K., Rutherford, S., and Fenbiao, N., 2008, Proxy-based reconstructions of hemispheric and global surface temperature variations over the past two millennia: Proceedings of the National Academy of Science of the United States of America, v. 105, p. 13252-13257.

McDonald, M.G., and Harbaugh, A.W., 1988, A modular three-dimensional finite-difference groundwater flow model, USGS techniques of water-resources investigations, Volume Book 6.

Moiwo Juana, P., 2006, Impact of land-use patterns on distributed groundwater recharge and discharge: Chinese Geographical Science, v. 16, p. 229-235.

Mondal, N.C., 2004, A new approach to delineate the groundwater recharge zone in hard rock terrain: Current Science, v. 87, p. 658-662.

Monteith, J.L., 1965, Evaporation and environment, *in* Fogg, G.E., ed., The state and movement of water in living organisms: New York, Academic Press Inc., p. 205-234.

Moon, S.K., Woo, N.C., and Lee, K.S., 2004, Statistical analysis of hydrographs and water-table fluctuation to estimate groundwater recharge: Journal of Hydrology, v. 168, p. 73-89.

Morel, E.H., 1980, The use of a numerical model in the management of the Chalk aquifer in the upper Thames basin: Quarterly Journal of Engineering Geology, v. 13, p. 153-165.

Morris, S.E., Simpson, R., and Cobby, D., 2005, Groundwater flooding in England - A neglected risk, Flood and Coastal Management Conference.

Morris, S.E., Cobby, D., and Parkes, A., 2007, Towards groundwater flood risk mapping: Quarterly Journal of Engineering and Hydrogeology, v. 40, p. 203-211.

Mul, M.L., Savenije, H.H.G., Luxemburg, W.M.J., and Weng, P., 2003, Groundwater Induced floods, Somme river (March 2001): Geophysical Research Abstracts, v. 5, p. 01412.

Najib, K., Jourde, H., and Pistre, S., 2007, A methodology for extreme groundwater surge predetermination in carbonate aquifers: Groundwater flood frequency analysis: Journal of Hydrology, v. 352, p. 1-15.

Oakes, D.B., 1981, A numerical model of a stream aquifer system subject to delayed rainfall recharge: Transactions of the Geological Society of South Africa, v. 84, p. 135-144.

Oakes, D.B., and Pontin, J.M.A., 1976, Mathematical modelling of a Chalk aquifer, Water Research Centre.

ONS, 2001a, 2001 census: Digitised Boundary Data (England and Wales). ESRC/JISC Census Programme Census Geography Data Unit (UKBORDERS).

ONS, 2001b, Office for National Statistics, 2001 Census: Standard Area Statistics (England and Wales). ESRC/JISC Census Programme, Census Dissemination Unit, Mimas (University of Manchester).

Owen, M., 1981, Thames groundwater scheme. Case studies in groundwater resource evaluation, Clarendon Press.

Owen, M., Connorton, B.J., and Greenfield, B.J., 1982, Discussion on 'The use of a numerical model in the management of the Chalk aquifer in the Upper Thames Basin' by E. H. Morel: Quarterly Journal of Engineering Geology and Hydrogeology, v. 15, p. 57-61.

Owen, M., and Robinson, V.K., 1978, Characteristics and yield in fissured Chalk., *in* Engineers, I.o.C., ed., Thames Groundwater Scheme, p. 33-49.

Paul, M.J., 2006, Impact of land-use patterns on distributed groundwater recharge and discharge - A case study of western Jilin, China: Chinese Geographical Science, v. 16, p. 229-235.

Penman, H.L., 1949a, The dependence of transpiration on weather and soil conditions: Journal of Soil Science, v. 1, p. 74-89.

Penman, H.L., 1949b, Natural evaporation from open water, bare soil and grass: Proceedings of the Royal Society, v. 193, p. 120-145.

Pilgrim, D.H., and Cordery, I., 1992, Flood runoff, *in* Maidment, D.R., ed., Handbook of hydrology: New York, McGraw-Hill.

Pinault, J.L., Amraoui, N., and Golaz, C., 2005, Groundwater-induced flooding in macropore-dominated hydrological system in the context of climate changes: Water Resources Research, v. 41, p. -.

Price, M., 1976, Chalk pore-size measurements and their significance: Water Services, v. 80, p. 596-600.

Price, M., 1982, A study of integranular and fissure permeability in Chalk and Permian aquifers, using double-packer injection testing: Journal of Hydrology, v. 54, p. 401-423.

Price, M., 2000, Mechanisms of water storage and flow in the unsaturated zone of the Chalk aquifer: Journal of Hydrology, v. 233, p. 54-71.

Prudhomme, C., Jakob, D., and Svensson, C., 2003, Uncertainty and climate change impact on the flood regime of small UK catchments: Journal of Hydrology, v. 277, p. 1-23.

Ragab, R., Finch, J., and Harding, R., 1997, Estimation of groundwater recharge to chalk and sandstone aquifers using simple soil models: Journal of Hydrology, v. 190, p. 19-41.

Renard, P., 2007, Stochastic hydrogeology: what professionals really need?: Ground Water, v. 45, p. 531-541.

Reynard, N.S., Prudhomme, C., and Crooks, S.M., 2001, The flood characteristics of large U.K. rivers: Potential effects of changing climate and land use: Climatic Change, v. 48, p. 343-359.

Richards, L.A., 1931, Capillary conduction of liquids through porous mediums: Physics, v. 1, p. 318-333.

Richardson, C.W., 1981, Stochastic simulation of daily precipitation, temperature and solar radiation: Water Resources Research, v. 17, p. 182-190.

Roberts, J., 1983, Forest Transpiration: a conservative hydrological process?: Journal of Hydrology, v. 66, p. 133-141.

Robinson, M.A., and Reay, W.G., 2002, Groundwater flow analysis of a Mid-Atlantic outer coastal plain watershed, Virginia, USA: Ground Water, p. 123-131.

Robinson, V.K., 1976, The hydrogeological model of the Kennet Chalk aquifer: Reading, Thames Water Authority.

Robson, A.J., and Faulkner, D.S., 1999, Adjusting for permeable catchments, Flood estimation handbook. Vol 3, statistical procedures for flood frequency estimation: Wallingford, Institute of hydrology.

Rounsevell, M.D.A., Evans, S.P., and Bullock, P., 1999, Climate change and agricultural soils: Impacts and adaptation: Climatic Change, v. 43, p. 683-709.

Rushton, K., 2003, Groundwater Hydrology. Conceptual and computational models: Chichester, Wiley.

Rushton, K.R., Connorton, B.J., and Tomlinson, L.M., 1989, Estimation of the groundwater resources of the Berkshire Dowsn supported by mathemetical modelling: Quarterly Journal of Engineering Geology, v. 22, p. 329-341.

Rushton, K.R., Eilers, V.H.M., and Carter, R.C., 2006, Improved soil moisture balance methodology for recharge estimation: Journal of Hydrology, v. 318, p. 379-399.

Rushton, K.R., and Ward, C., 1979, The estimation of ground water recharge: Journal of Hydrology, v. 41, p. 345-361.

Rygel, L., O'Sullivan, D., and Yarnal, B., 2006, A method for constructing a social vulnerability index: An application to hurricane storm surges in a developed country: Mitigation and Adaptation Strategies for Global Change, v. 11, p. 741-764.

Sasaki, Y., 1992, Resolution of resistivity tomography inferred from numerical simulation: Geophysical Prospecting, v. 40, p. 453-464.

Scanlon, B.R., Healy, R.W., and Cook, P.G., 2002, Choosing appropriate techniques for quantifying groundwater recharge: Hydrogeology Journal, v. 10, p. 18-39.

Scibek, J., and Allen, D.M., 2005, Modeled climate change impacts in the Abbortsford-Sumas aquifer, central Fraser Lowland of BC, Canada and Washington State, US, 2005 Puget Sound Georgia Basin Research Conference.

Scibek, J., and Allen, D.M., 2006, Modeled impacts of predicted climate change on recharge and groundwater levels: Water Resources Research, v. 42.

Scibek, J., Allen, D.M., Cannon, A.J., and Whitfield, P.H., 2007, Groundwater-surface water interaction under scenarios of climate change using a high-resolution transient groundwater model: Journal of Hydrology, v. 333, p. 165-181.

Shackley, S., and Deanwood, R., 2003, Constructing social futures for climate-change impacts and response studies: Building qualitative and quantitative scenarios with the participation of stakeholders: Climate Research, v. 24, p. 71-90.

Shaw, E.M., 1994, Hydrology in practice: Oxford, Routledge.

Shepard, D., 1968, A two-dimensional interpolation function for irregularly-spaced data, Proceedings of the 1968 23rd ACM National Conference.

Slater, L., Binley, A., Zaidmam, M.D., and West, L.J., 1997, Investigation of Vadose Zone Mechanisms in Unsaturated Chalk using Cross-Borehole ERT, Proc. 3rd Meeting of the Environmental and Engineering Geophysics Society: Aarhus, p. 17-20.

Smedema, L.K., and Rycroft, D.W., 1988, Land Drainage: London, B.T. Batsford.

Smith, D.B., Wearn, P.L., Richards, H.J., and Rowe, P.C., 1970, Water movement in the unsaturated zone of high and low permeability strata by measuring natural tritium, *in* IAEA, ed., Isotope Hydrology: Vienna, p. 259-270.

Smith, K., 2003, Environmental hazards: Assessing risk and reducing disaster: London, Routledge.

Smith, K., and Ward, R., 1998, Floods: Physical processes and human impacts: London, Wiley.

South East England Regional Assembly, 2006, A clear vision for the South East: The South East Plan.

Tapsell, S.M., Penning-Rowsell, E.C., Tunstall, S.M., and Wilson, T.L., 2002, Vulnerability to flooding: health and social dimensions: Philosophical Transactions of the Royal Society A: Mathematical, Physical and Engineering Sciences, v. 360, p. 1511-1525.

Thompson, N., Barrie, I.A., and Ayles, M., 1981, The Meteorological Office rainfall and evaporation calculation system: MORECS: Memorandum 45, The Meteorological Office, UK.

Townsend, P., Phillimore, P., and Beattie, A., 1988, Health and deprivation: inequality and the North: London, Croom Helm.

UKCIP, 2001, Socio- economic scenarios for climate change impact assessment: a guide to their use in the UK climate impacts programme: Oxford.

USDA-NRCS, 1972, National Engineering Handbook. Vol. Hydrology Section 4.

USGS, 2006, Groundwater flooding n glacial terrain of southern Puget Sound, Washington, Volume 2006.

Vandewiele, G.L., Xu, C.Y., and Ni Lar, W., 1992, Methodology and comparative study of monthly water balance models in Belgium, China and Burma: Journal of Hydrology, v. 134, p. 315-347.

Webber, A., Fohrer, N., and Moller, D., 2001, Long-term land use changes in a mesoscale watershed due to socio-economic factors - effetcs on landscape structrue and functions: Ecological Modelling, v. 140, p. 125-140.

Wellings, S.R., 1984, Recharge of the Chalk aquifer at a site in Hampshire, England, 1. Water balance and unsaturated flow: Journal of Hydrology, v. 69, p. 259-273.

WestBerkshireCouncil, 2007, West Berkshire District Profile.

WH (Waterloo Hydrogeologic), 2000, Visual MODFLOW user's manual: Ontario.

Wheater, C.P., and Cook, P., A., 2005, Using statistics to understand the environment: London, Routledge.

Wheater, H., and Peach, D., 2004, Developing Interdisciplinary science for integrated catchment management: the UK Lowland Catchment research (LOCAR) programme. : Water Resources Development, v. 20, p. 369- 385.

Whitehead, P.G., Johnes, P.J., and Butterfield, D., 2002, Steady state and dynamic modelling of nitrogen in the River Kennet: impacts of land use change since the 1930s: The Science of The Total Environment, v. 282, p. 417-434.

Wilby, R.L., Whitehead, P.G., Wade, A.J., Butterfield, D., Davis, R.J., and Watts, G., 2006, Integrated modelling of climate change impacts on water resources and quality in a lowland catchment: River Kennet, UK: Journal of Hydrology, v. 330, p. 204-220.

Wilks, D.S., and Wilby, R.L., 1999, The weather generation game: a review of stochastic weather models: Progress in Physical Geography, v. 23, p. 329-357.

Woldeamlak, S.T., Batelaan, O., and De Smedt, F., 2004, Effects of climate change on the groundwater systems of the Grote Nete catchment, Belgium, International conference on finite element models, MODFLOW and more: solving groundwater problems: Czech Republic.

Yamaguchi, D.K., 1986, Interpretation of cross correlation between tree-ring series: Tree Ring Bulletin, v. 46, p. 47-54.

Younger, P.L., 2007, Groundwater in the environment: An introduction: Oxford, Blackwell.

Younger, P.L., Teutsch, G., Custodio, E., Elliot, T., Manzano, M., and Sauter, M., 2002, Assessments of the sensitivity to climate chnage of flow and natural water quality in four major carbonate aquifers of Europe, *in* Hiscock, K.M., Rivett, M.O., and Davidson, R.M., eds., Sustainable Groundwater Development: Bath, The geological society publishing house, p. 325-344.

Yusoff, I., Hiscock, K.M., and Conway, D., 2002, Simulation of the impacts of climate change on groundwater resources in eastern England: Geological Society Special Publication, p. 325-344.

Zaidman, M., MIddleton, R.T., West, L.J., and Binley, A., 1999, Geophysical investigation of unsaturated zone transport in the Chalk in Yorkshire: Quarterly Journal of Engineering Geology, v. 32, p. 185-198.

Zhang, H., and Hiscock, K., 2010, Modelling the impact of forest cover on groundwater resources: a case study of the Sherwood Sandstone aquifer in the East Midlands, UK: Journal of Hydrology, v. In press.

Zhou, W., 2007, Drainage and flooding in karst terrains: Environmental Geology, v. 51, p. 963-973.

Appendices

1 Appendix 1

1.1 Monthly root constant (*C*) and wilting point (*D*) values for the Penan-Grindley method in the UK (values in mm). From Hiscock (2005) and Lerner (1990). Crop types are: 1, cereals, Sept. harvest; 2, cereals, Aug. harvest; 3, cereals, July harvest; 4, potatoes, Sept. harvest; 5, potatoes, May harvest; 6, vegetables, May harvest; 7, vegetables, July harvest; 8, vegetables, Aug. harvest; 9, vegetables, Oct. harvest; 10, bare fallow; 11, temporary grass; 12, permanent grass; 13, rough grazing; 14, woodland.

		Crop Type												
	Month	***1***	***2***	***3***	***4***	***5***	***6***	***7***	***8***	***9***	***10***	***11***	***12***	***13***	***14***
C	Jan & Feb	25	25	25	25	25	25	25	25	25	25	56	76	13	203
D		25	25	25	25	25	25	25	25	25	25	102	127	51	254
C	Mar	56	56	56	25	25	56	25	25	25	25	56	76	13	203
D		102	102	102	25	25	102	25	25	25	25	102	127	51	254
C	Apr	76	76	76	76	56	56	56	25	25	25	56	76	13	203
D		127	127	127	102	102	102	102	25	25	25	56	76	13	254
C	May	97	97	97	56	56	56	56	56	25	25	56	76	13	203
D		152	152	152	102	102	102	102	102	25	25	102	127	51	254
C	Jun & Jul	140	140	140	76	76	25	56	56	56	25	56	76	13	203
D		203	203	203	127	127	25	102	102	102	25	102	127	51	254
C	Aug	140	140	25	97	97	25	25	56	56	25	56	76	13	203
D		203	203	25	152	152	25	25	102	102	25	102	127	51	254
C	Sept	140	25	25	97	25	25	25	25	56	25	56	76	13	203
D		203	25	25	152	25	25	25	25	102	25	102	127	51	254
C	Oct	25	25	25	97	25	25	25	25	56	25	56	76	13	203
D		25	25	25	152	25	25	25	25	102	25	102	127	51	254
C	Nov & Dec	25	25	25	25	25	25	25	25	25	25	56	76	13	203
D		25	25	25	25	25	25	25	25	25	25	102	127	51	254

1.2 Sample syntax to allow rainfall time series to be applied to summer/winter interception parameter raster datasets in ArcGIS™ command line.

GP tool	Rain	LU	New raster name		Command line code	Month
Times_sa	78	SumInt	D:\WetSp\Int\b5\	1	Times_sa 78 SumInt D:\WetSp\Int\b5\1	Apr
Times_sa	43.2	SumInt	D:\WetSp\Int\b5\	2	Times_sa 43.2 SumInt D:\WetSp\Int\b5\2	May
Times_sa	25.3	SumInt	D:\WetSp\Int\b5\	3	Times_sa 25.3 SumInt D:\WetSp\Int\b5\3	Jun
Times_sa	58.8	SumInt	D:\WetSp\Int\b5\	4	Times_sa 58.8 SumInt D:\WetSp\Int\b5\4	Jul
Times_sa	82.3	SumInt	D:\WetSp\Int\b5\	5	Times_sa 82.3 SumInt D:\WetSp\Int\b5\5	Aug
Times_sa	78.1	SumInt	D:\WetSp\Int\b5\	6	Times_sa 78.1 SumInt D:\WetSp\Int\b5\6	Sep
Times_sa	43.2	WinInt	D:\WetSp\Int\b5\	7	Times_sa 43.2 WinInt D:\WetSp\Int\b5\7	Oct
....	....	....	....	....	....	....

1.3 Selection of runoff vegetation IDs in relation to lands use categories

GIS-DIRT land use category	Veg category	Veg ID
Deciduous woodland	Forest	3
Coniferous woodland	Forest	3
Meadow/ref grass	Grass	2
Agriculture	Crop	1
Open built-up	Grass	2

1.4 Soils of the Pang/Lambourn according to the soil survey of England and Wales (Avery, 1980), corresponding texture and soil ID

Soil association	Geology	Site characteristics	WetSpass texture	Soil ID
Coombe 1	Chalky Drift and chalk	Well drained calcareous fine silty soils, deep in valley bottoms, shallow to chalk or valley sides in places. Slight risk of water erosion	silt	6
Charity 2	Flinty and chalky drift over chalk	well drained flinty fine silty soils in valley bottoms. Calcareous fine silty soils over chalk or chalk rubble on valley sides, sometimes shallow	silt	6
Carstens	Plateau drift and clay-with-flints	well drained fine silty over clayey, clayey and fine silty soils, often very flinty	silty clay	11
Hornbeam 2	Plateau drift	Deep fine loamy over clayey soils with slowly permeable subsoils and slight seasonal waterlogging. Some well drained fine loamy and fine silty over clayey and clayey sols. Some soils very flinty	silty clay loam	8
Upton 1	Chalk	Shallow and well drained Calcareous silty soils over chalk. Mainly on moderately steep, sometimes very steep land. Deeper fine silty calcareous soils in coombes and dry valleys	silt	6
Andover 1	Chalk	Shallow well drained calcareous silty soils over chalk on slopes and crests. Deep calcareous and non-calcareous fine-silty soils in valley bottoms. Striped soil patterns locally.	silt	6
Icknield	Chalk	Shallow, mostly humose, well drained calcareous soils over chalk on steep slopes and hill tops. Deeper flinty calcareous silty soils in small coombes and valleys	silty loam	4
Frilford	Mesozoic and tertiary sands	Deep well drained sandy and coarse loamy soils. Some ferruginous sandy and some coarse loamy soils affected by groundwater. Risk of water erosion	sandy clay	10
Frome	Chalky and gravelly river alluvium	Shallow calcareous and non-calcareous loamy soils over flint gravel affected by groundwater. Small areas of peat. Risk of flooding	loam	5
wickham 3	Drift over Mesozoic and Tertiary	Slowly permeable seasonally waterlogged fine loam over clayey and coarse loamy over clayey soils, and similar more permeable soils with slight waterlogging.	sandy clay loam	7

	clay and loam	Some deep coarse loamy soils affected by groundwater. Landslips with irregular terrain locally		
Sonning 1	Plateau gravel and river terrace drift	Well drained flinty coarse loamy and sandy soils, mainly over gravel. Some coarse loamy over clayey soils with slowly permeable subsoils and slight seasonal waterlogging	sandy clay loam	7
Southampton	Plateau gravel and river terrace drift	Well drained very acid, very flinty sandy soils with bleached subsurface horizon. Some very acid sandy over clayey soils with slowly permeable subsoils and slight seasonal waterlogging	sandy clay	10
Sonning 2	Plateau drift and clay-with-flints	Well drained flinty coarse loamy and gravelly soils. Associated with slowly permeable seasonally waterlogged fine loamy over clayey soils, and coarse loamy over clayey soils with slowly permeable subsoils and slight seasonal waterlogging	sandy clay loam	7
Batcombe	Plateau drift and clay-with-flints	Fine silty over clayey and fine loamy over clayey soils with slowly permeable subsoils and slight seasonal water logging. Some well drained clayey sol over chalk. Variably flinty.	silty clay loam	8
Wantage 1	Chalk	Well drained calcareous silty soils, in places shallow over argillaceous chalk	silt	6
Block	Chalky Drift and chalk	Moderately permeable calcareous loamy soils over chalky gravel variably affected by groundwater	NA	
Harwell	Cretaceous and Jurassic sandstone, siltstone and clay	Well drained loamy soils over sandstone and some similar soils with slight seasonal waterlogging. Shallow stony soils locally. Some slowly permeable seasonally waterlogged fine loamy or fine silty over clayey soils mainly on scarp slopes. Risk of water erosion	NA	
Frilsham	Drift over chalk	Well drained mainly fine loamy soils over chalk, some calcareous. Shallow calcareous fine loamy and fine silty in places	silty clay loam	8
Hucklesbrook	River terrace drift	Well drained coarse loamy and some sandy soil, commonly over gravel. Some similar permeable soils affected by groundwater. Usually on flat land	sandy loam	3
Newmarket 2	Chalk and Chalky drift	Shallow well drained calcareous coarse loamy and sandy soils over chalk rubble associated with well drained deeper coarse loamy and sandy soils often in an intricate pattern. Slight risk of water erosion	sandy loam	3
Unsurveyed			impermeable/clay	12
Wickham 4	Drift over tertiary clay	slowly permeable seasonally waterlogged fine loamy over clayey and fine silty over clayey soils associated with similar clayey soils, often with brown subsoils	silty clay loam	8
Coombe 2	Chalky Drift and chalk	Well drained calcareous fine silty soils over chalk or chalk rubble. Shallow soils in places especially on brows and steeper slopes	silt	6
Thames	River Alluvium	Stoneless mainly calcareous clayey soils affected by groundwater. Flat land. Risk of	clay	12

		flooding		
Sutton 2	River terrace gravel	well drained fine and coarse loamy soils usually over gravel with a calcareous matrix	sandy loam	3
Bursledon	Eocene and Jurassic loam and clay	Deep fine loamy soils with slowly permeable subsoils and slight seasonal waterlogging associated with deep coarse loamy soils variably affected by groundwater. Some slowly permeable seasonally waterlogged loamy over clayey soils. Landslips and associated irregular terrain locally	clay loam	9
Hamble 2	Aeolian silty drift	Deep stoneless well drained silty soils and similar soils affected by groundwater; over gravel locally. Usually flat locally	silt	6
Hurst	River terrace gravel	coarse and fine loamy permeable soils mainly over gravel variably affected by groundwater	silty loam	4

1.5 (a) CEH 2000 land use and classifications in the Pang/Lambourn and equivalent Penman-Grindley nomenclature and ID. (b) Monthly *C* and *D* values associated with each ID.

(a)

CEH classification	Penman-Grindley (PG) classification	PG ID
broadleaved/mixed woodland	woodland	14
coniferous woodland	woodland	14
improved grassland	permanent grass	12
neutral grass	permanent grass	12
set-aside grass	permanent grass	12
calcareous grass	permanent grass	12
arable cereals	cereals	1,2,3
arable horticulture	potatoes/Vegetables	4,5,6,7,8,9
suburban/rural development	bare fallow	10

(b)

	Month											
	Jan		Feb		Mar		Apr		May		Jun	
PG ID	***C***	***D***	***C***	***D***	***C***	***D***	***C***	***D***	***C***	***D***	***C***	***D***
14	203	254	203	254	203	254	203	254	203	254	203	254
12	76	127	76	127	76	127	76	127	76	127	76	127
1,2,3	25	25	25	25	56	102	76	127	97	152	140	203
4,5,6,7,8,9	25	25	25	25	22	30	49	76	51	106	58	98
10	25	25	25	25	25	25	25	25	25	25	25	25

	Month cont.....										
Jul		Aug		Sep		Oct		Nov		Dec	
D	***C***	***D***	***C***	***D***	***C***	***D***	***C***	***D***	***C***	***D***
254	203	254	203	254	203	254	203	254	203	254
127	76	127	76	127	76	127	76	127	76	127
203	102	144	63	220	25	25	25	25	25	25
98	59	93	42	59	42	59	25	25	25	25
25	25	25	25	25	25	25	25	25	25	25

1.6 Monthly rainfall and *Pet* used in recharge calculations from 1978-2006 Location of flow gauge at Shaw, catchment-wide rain gauges and extent of MORECS sq 159.

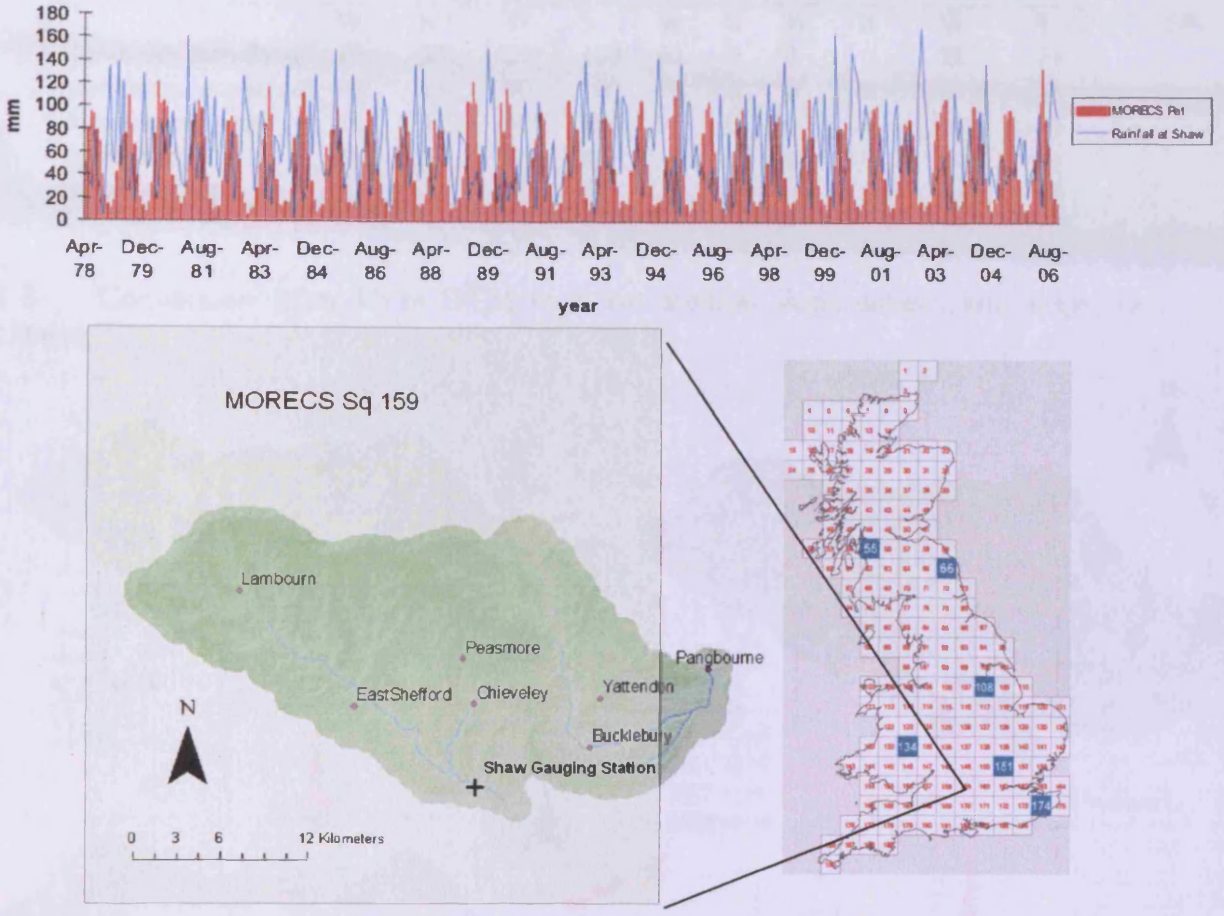

1.7 (a) CEH land use, equivalent GIS-DIRT category and associated interception value expressed as a percentage of rainfall.(b) Interception parameters as a function of the proportion vegetation cover for each land use category in the Pang/Lambourn. % effective rainfall represents the proportion of rainfall that reaches the ground surface (S, summer; W, winter)

(a)

CEH 2000 Land use	GIS-DIRT Equivalent Land use	Winter Interception (% rainfall)	Summer Interception (% rainfall)
broadleaved/ mixed woodland	deciduous woodland	10	25
coniferous woodland	coniferous woodland	45	45
improved grassland	meadow/ref grass	10	10
neutral grass	meadow/ref grass	10	10
set-aside grass	meadow/ref grass	10	10
calcareous grass	meadow/ref grass	10	10
arable cereals	agriculture	0	15
arable horticulture	agriculture	0	15
suburban/rural development	open built-up	10	10

(b)

GIS-DIRT land use category	Interception (% Rainfall)		% Vegetation		% Bare		% Impervious		% Effective Rainfall	
	W	S	W	S	W	S	W	S	W	S
deciduous woodland	10	25	20	100	80	0	0	0	98	75
coniferous woodland	45	45	90	100	10	0	0	0	59.5	55
meadow/ref grass	10	10	100	100	0	0	0	0	90	90
agriculture	0	15	0	80	100	20	0	0	100	88
open built-up	10	10	60	60	10	10	30	30	94	94

1.8 Conversion from 10 m DTM to 1 km median slope dataset and slope ID classes

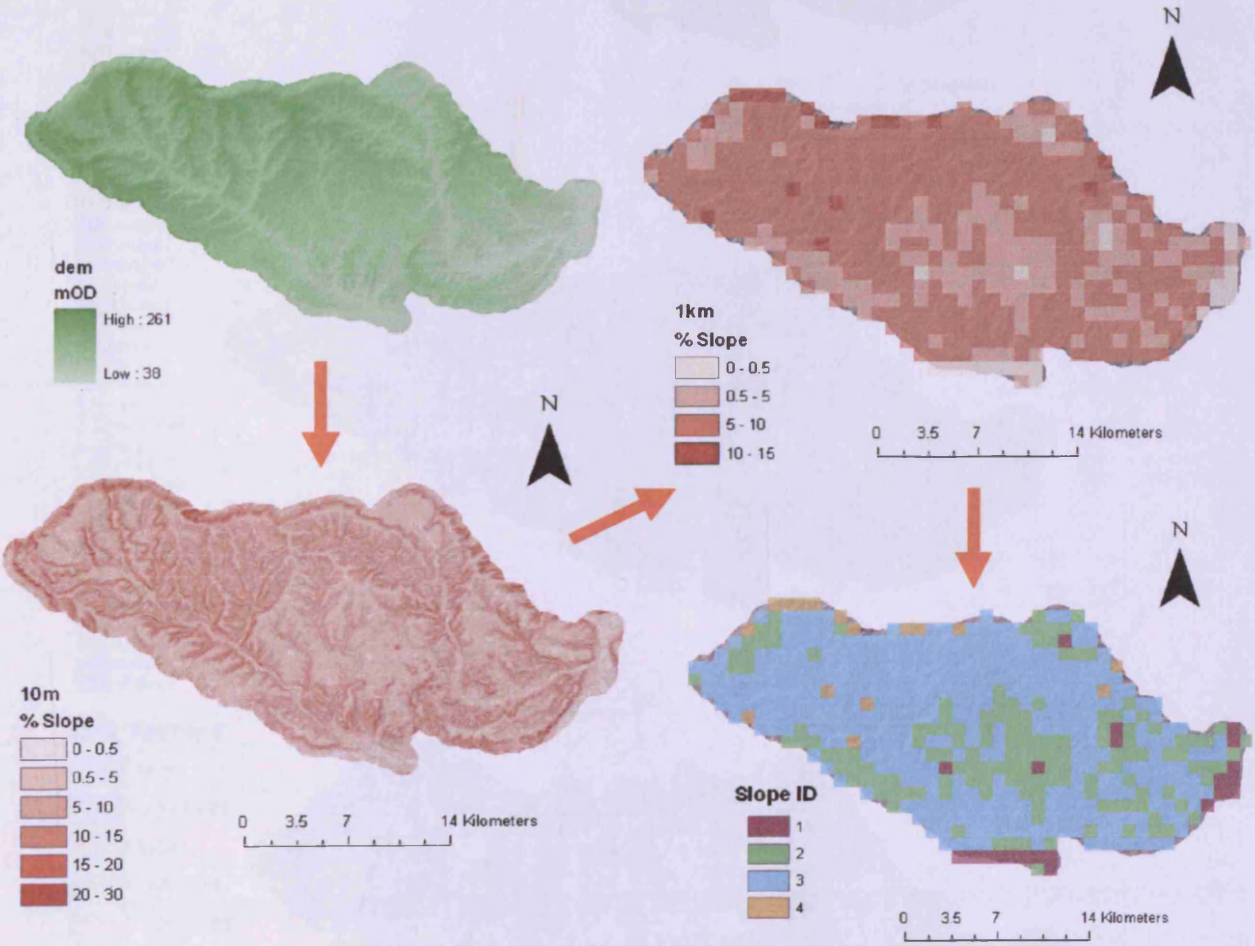

1.9 Conversion from digitised soil map to distributed 1 km soil texture from which an ID is established.

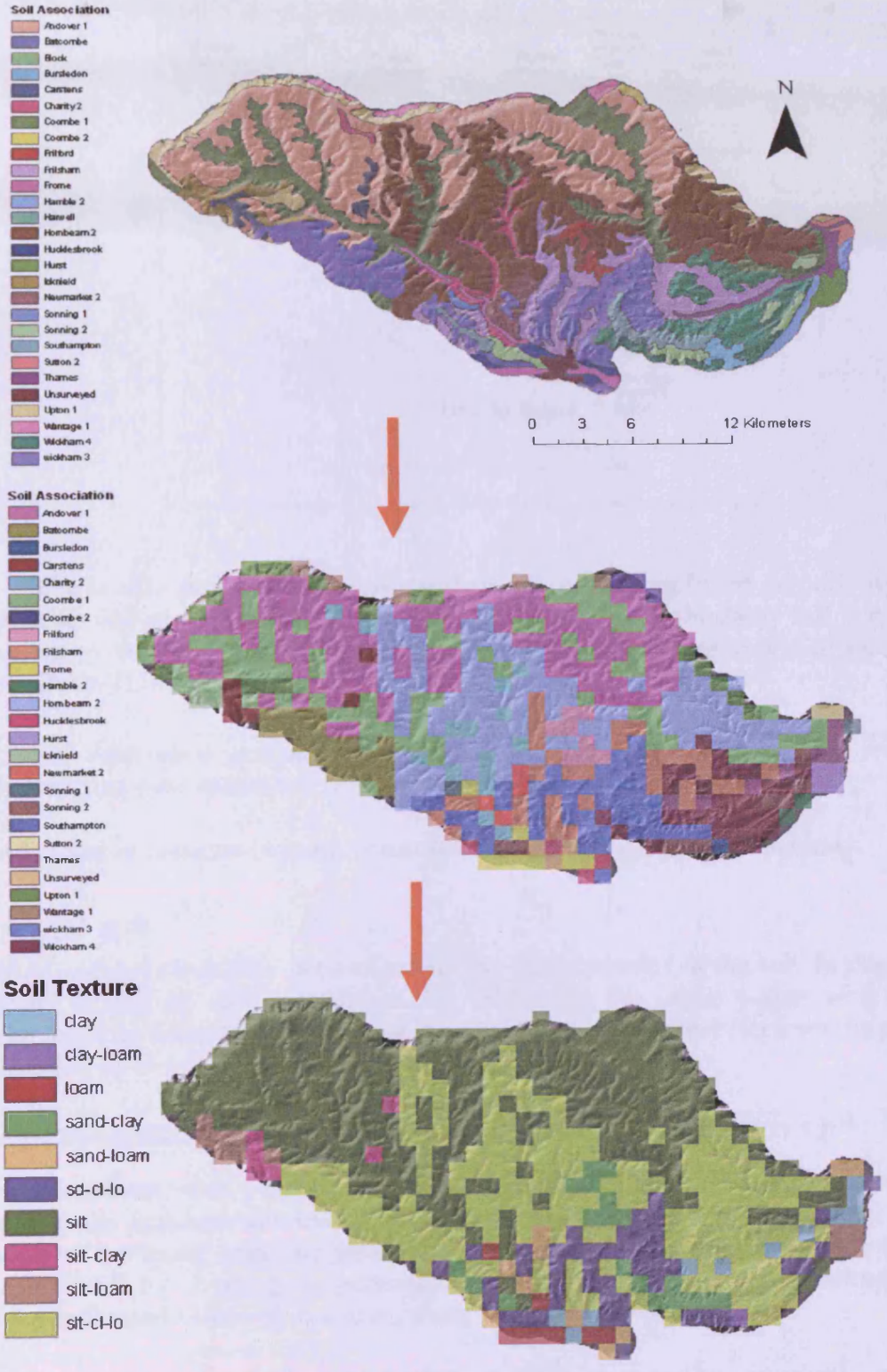

1.10 The distribution of CEH administered profile probes and neutron probes access sites at Frilsham in the Pang catchment.

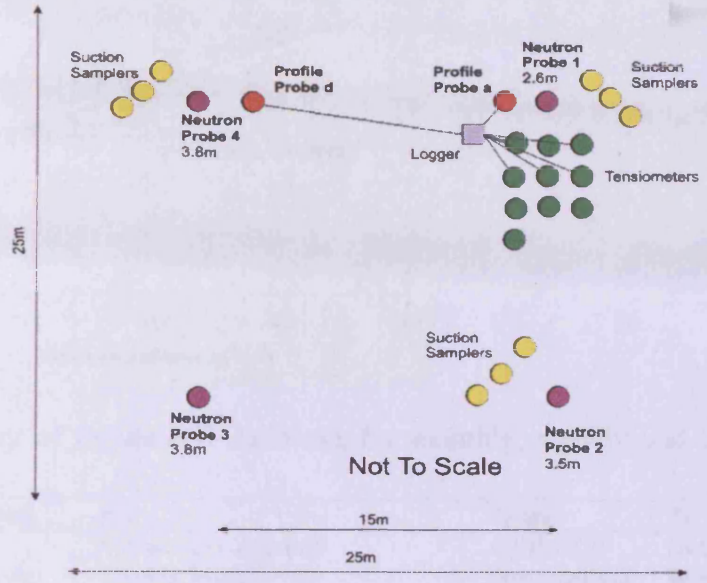

1.11 The profile probe detects soil moisture by responding to the permittivity (ε') of the damp soil or more accurately to the refractive index of the damp soil, which is equivalent to $\sqrt{\varepsilon}$. As a result, the performance of the profile probe is split into two stages (Delta-TDevices, 2004):

1. Soil calibration: soil moisture (θ) determines $\sqrt{\varepsilon}$
2. Profile probe response: $\sqrt{\varepsilon}$ determines voltage output (Volts)

The relationship between (θ) and $\sqrt{\varepsilon}$ can be summed up by a simple equation,

$$\sqrt{\varepsilon} = a_o + a_1\theta$$

where a_o and a_1 are usually determined by the characteristics of the soil. In this case however, a_o and a_1 were determined by calibrating the probe output with local neutron probe soil moisture recordings. Firstly, the voltage output (V) from the probe is converted to $\sqrt{\varepsilon}$ using a polynomial relationship:

$$\sqrt{\varepsilon} = 1.125 - 5.53V + 67.17V^2 - 234.42V^3 + 413.46V^4 - 356.68V^5 + 121.53V^6$$

The plot between $\sqrt{\varepsilon}$ at profile probe a and moisture content, θ [m^3m^{-3}] at neutron probe 1 at the Frilsham site over a period of several years can be seen below. The equation of the linear trendline yields the value of a_o and a_1. Therefore, a_o is 0.891 and a_1 is 3.214. By combing the polynomial relationship between $\sqrt{\varepsilon}$ and Voltage (V) with the calibrated values of a_o and a_1, water content (θ) becomes

$$\theta = \frac{\left[1.125 - 5.53V + 67.17V^2 - 234.42V^3 + 413.46V^4 - 356.68V^5 + 121.53V^6\right] - a_0}{a_1} \; m^3m^{-3}$$

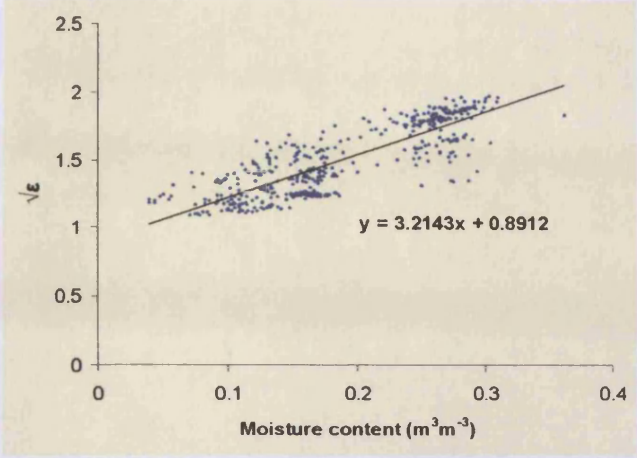

1.12 Summary of inputs and durations for monthly, weekly and daily GIS-DIRT simulations

Time step	*Rainfall*	*Pet*	*From*	*To*
Monthly	Shaw	Morecs 159 monthly	April 1978	December 2006
Weekly	Chieveley	Weekly Morecs 159	Week ending 06/04/1999	Week ending 22/03/2005
Daily	Chieveley	Weekly Morecs 159 (monthly after week ending 03/05/2005)	1/04/1999	26/02/2007

1.13 (a) Soil moisture content (mm) at each horizon and Field Capacity values at profile probe a, Frilsham between 2002 and 2007. (b) Resulting daily *SMD* at probe a, Frilsham.

(a)

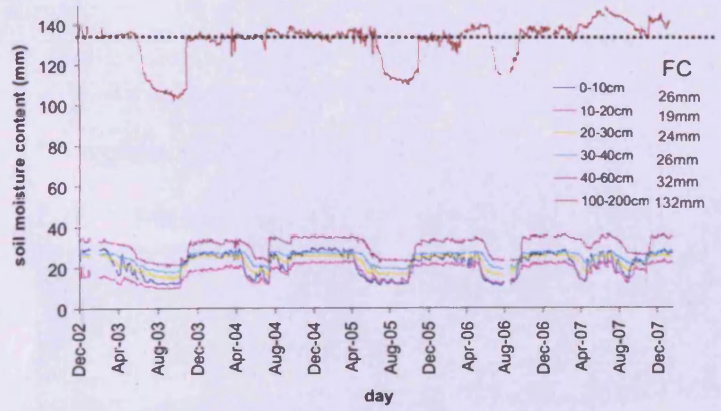

(b)

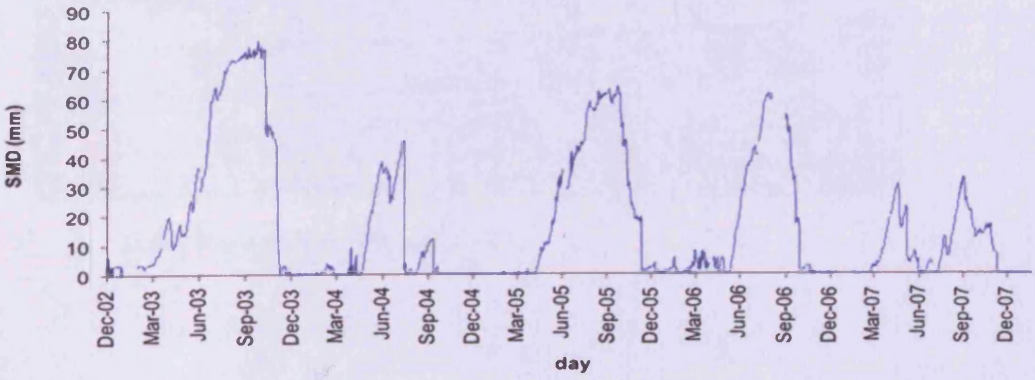

1.14 The impact of *SMD* calibration at Bechewood and Frilsham on modelled recharge (a) and Spearman's rank correlation (b) for a-h calibration conditions at Frilsham and Beche Farm

(a)

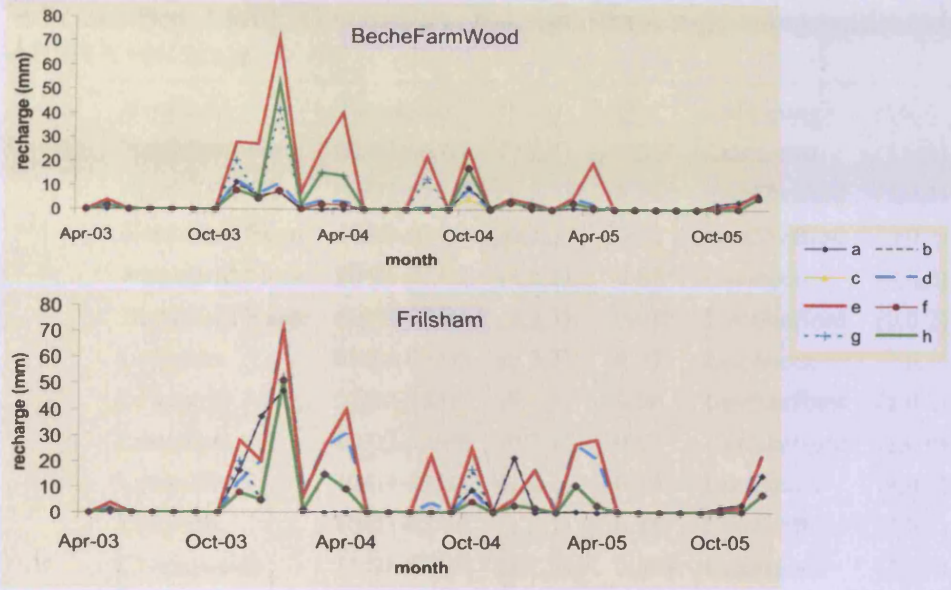

(b)

Calibration condition	*Frilsham*	*Beche Farm Wood*
a	0.62**	0.72**
b	0.62**	0.72**
c	0.72**	0.82**
d	0.86**	0.88**
e	0.85**	0.75**
f	0.72**	0.84**
g	0.71**	0.71**
h	0.72**	0.67**

** significant P<0.01

1.15 Mean monthly modelled *SMD* from between April 1978 and December 2006.

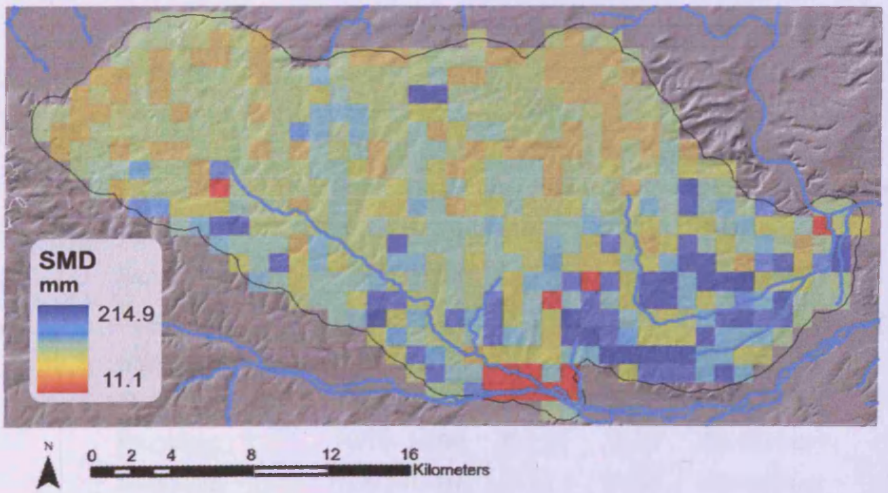

2 Appendix 2

2.1 Order of ARIMA model components (p,d,q) for borehole and rainfall time series in the Pang/Lambourn covering varying periods between 2000 and 2005. * indicates Box-Ljung, Q statistic is not significant suggesting autocorrelation amongst ARIMA residuals.

Borehole	*Timeseries*	*p,d,q*	*Q*	*Rain gauge*	*p,d,q*	*Q*
Northfield Farm	02/03-06/05	(2,2,7)	0.03*	Lambourn	(1,0,1)	0.89
Northfield Farm	08/02-12/05	(2,2,7)	0.24	EastShefford	(1,0,1)	0.69
Northfield Farm	10/02-03/03	(0,2,0)	0.78	EastShefford	(0,0,2)	0.58
Northfield Farm	10/03-03/04	(4,2,3)	0.02*	Lambourn	(0,0,2)	0.85
Northfield Farm	10/03-03/04	(4,2,3)	0.02*	EastShefford	(0,0,2)	0.78
Longacre	02/03-06/05	(0,2,3)	0.07	Lambourn	(1,0,1)	0.89
Longacre	03/02-12/05	(0,2,4)	0.90	EastShefford	(1,0,1)	0.73
Longacre	10/02-02/03	(0,2,1)	0.97	EastShefford	(1,0,0)	0.42
Longacre	10/03-03/04	(1,2,1)	0.14	Lambourn	(0,0,2)	0.85
Longacre	10/03-03/04	(1,2,1)	0.14	EastShefford	(0,0,2)	0.78
Chapelwood	11/01-08/05	(2,2,5)	0.508	Peasemore	(2,0,2)	0.70
Chapelwood	10/02-03/03	(1,2,0)	0.421	Peasemore	(0,0,2)	0.38
Chapelwood	10/03-03/04	(0,2,7)	0.01*	Peasemore	(2,0,0)	0.90
Chapelwood	10/04-03/05	(2,2,0)	0.135	Peasemore	(0,0,0)	0.62
Chapelwood	10/02-12/02	(0,2,0)	0.01*	Peasemore	(1,0,0)	0.66
Chapelwood	01/03-03/03	(1,2,0)	0.751	Peasemore	(0,0,2)	0.08
Hodcott	08/01-08/05	(0,2,7)	0.31	Peasemore	(2,0,2)	0.65
Hodcott	10/02-03/03	(0,0,2)	0.90	Peasemore	(0,2,1)	0.38
Hodcott	10/03-03/04	(0,2,1)	0.87	Peasemore	(0,0,2)	0.38
Hodcott	10/02-12/02	(2,2,0)	0.08	Peasemore	(2,0,0)	0.90
Hodcott	01/03-03/03	(0,2,1)	1.00	Peasemore	(0,0,2)	0.08
Hodcott	11/02-07/05	(1,2,3)	0.89	WestIlsley	(1,0,0)	0.76
Saltbox	03/02-06/05	(1,2,13)	0.04*	Peasemore	(2,0,0)	0.70
Saltbox	10/02-03/03	(0,2,13)	0.30	Peasemore	(0,0,2)	0.38
Saltbox	10/03-03/04	(0,2,1)	0.95	Peasemore	(2,0,0)	0.90
Saltbox	10/02-12/02	(0,2,0)	0.38	Peasemore	(1,0,0)	0.66
Saltbox	01/03-03/03	(0,2,0)	0.69	Peasemore	(0,0,2)	0.08
Saltbox	11/02-06/05	(0,2,13)	0.12	WestIlsely	(2,0,0)	0.84
Beenham	10/99-08/04	(1,1,13)	0.18	Bucklebury	(2,0,2)	0.08
Beenham	10/00-03/01	(0,1,1)	0.51	Bucklebury	(0,0,0)	0.25
Beenham	10/01-03/02	(0,1,0)	0.83	Bucklebury	(0,0,1)	0.61
Beenham	10/02-03/03	(0,1,13)	0.20	Bucklebury	(0,0,2)	0.14
Beenham	10/00-12/00	(0,1,0)	0.30	Bucklebury	(0,0,0)	0.66
Beenham	01/01-03/01	(0,1,1,)	0.36	Bucklebury	(0,0,0)	0.96
Newbury	06/01-08/04	(0,1,6)	0.00*	Bucklebury	(1,0,1)	0.19
Newbury	10/01-03/02	(0,1,0)	0.35	Bucklebury	(0,0,1)	0.61
Newbury	10/02-03/03	(1,1,0)	0.67	Bucklebury	(0,0,2)	0.14

Newbury	10/02-12/02	(1,1,0)	0.87	Bucklebury	(0,0,1)	0.28
Newbury	01/03-03/03	(0,1,1)	0.46	Bucklebury	(0,0,2)	0.12

2.2 (A) CCF plot between Hodcott borehole hydrograph and West Ilsley rain gauge at hourly intervals. (B) Table of significant hourly lags between Hodcott and WestIlsley over different time periods. Mean doeth to groundwater table was 16.3m between 2002 and 2005 and 10m between 2002 and 2003. (C) Hourly lags at Hodcott according to equivalent day. (D), (E) and (F) as above but using Saltbox borehole hydrograph

(A)

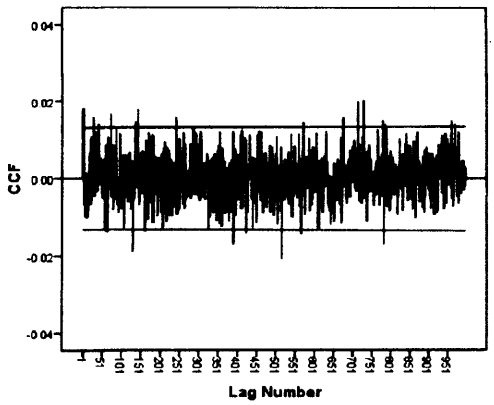

(B)

Time period			
11/2002- 07/2005		10/2002- 03/2003	
1	571	28	281
28	676	41	322
41	714	150	393
73	729	171	453
137	779	174	676
143	786	203	729
242	962	242	945
286	971		960

(C)

Time period			
11/2002- 07/2005		10/2002- 03/2003	
<1	28	2	12
1	29	6	13
3	30	7	16
10	32	7	19
34	34	8	28
		10	30
			39

(D)

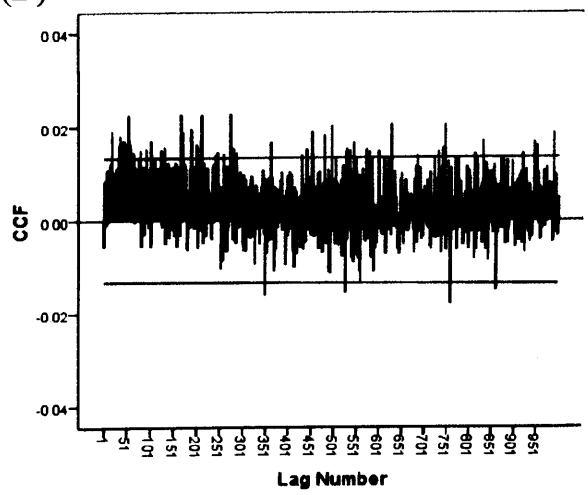

(E)

Time period					
11/2002-06/2005				11/2002-02/2003	
19	93	281	583	18	139
33	103	287	599	20	152
35	105	362	611	33	219
36	106	430	620	44	264
41	125	441	627	53	273
42	132	452	685	55	430
43	167	454	722	56	500
46	170	480	731	67	574
49	190	496	741	74	685
55	191	505	745	77	689
57	201	527	768	86	745
58	211	529	811	91	802
59	213	536	830	111	817
65	242	544	870	114	818
76	247	548	875	127	947
81	259	572	919	132	
	275	578	944	135	
			950		
			988		

(F)

Time period				
11/2002-06/2005			11/2002-02/2003	
<1	15	30	<1	24
1	17	31	1	29
2	18	32	2	31
3	20	34	3	33
4	21	36	4	34
5	22	37	5	34
6	23	38	6	39
7	24	39	9	
8	25	50	11	
10	26	41	18	
11	28		21	

3 Appendix 3

3.1 (i) Formations and members of the Chalk southern province. Those found in the Pang/Lambourn at highlighted in colour and bold. (ii) Geological maps detailing the spatial distribution of member outcrops making up the Upper (A), Middle (B) and Lower Chalk (C). Palaeogene (south east of the domain), Greensand and others are also shown (D).

Formation Name	Member
Upper Chalk	Portsdown Chalk
	Spetsbury Chalk
	Tarrant Chalk
	Newhaven Chalk
	Seaford Chalk
	Lewes Nodular Chalk
Middle Chalk	**New Pit Chalk**
	Holywell Nodular Chalk
Lower Chalk	**Zig Zag Chalk**
	West Melbury Marely Chalk

(i)

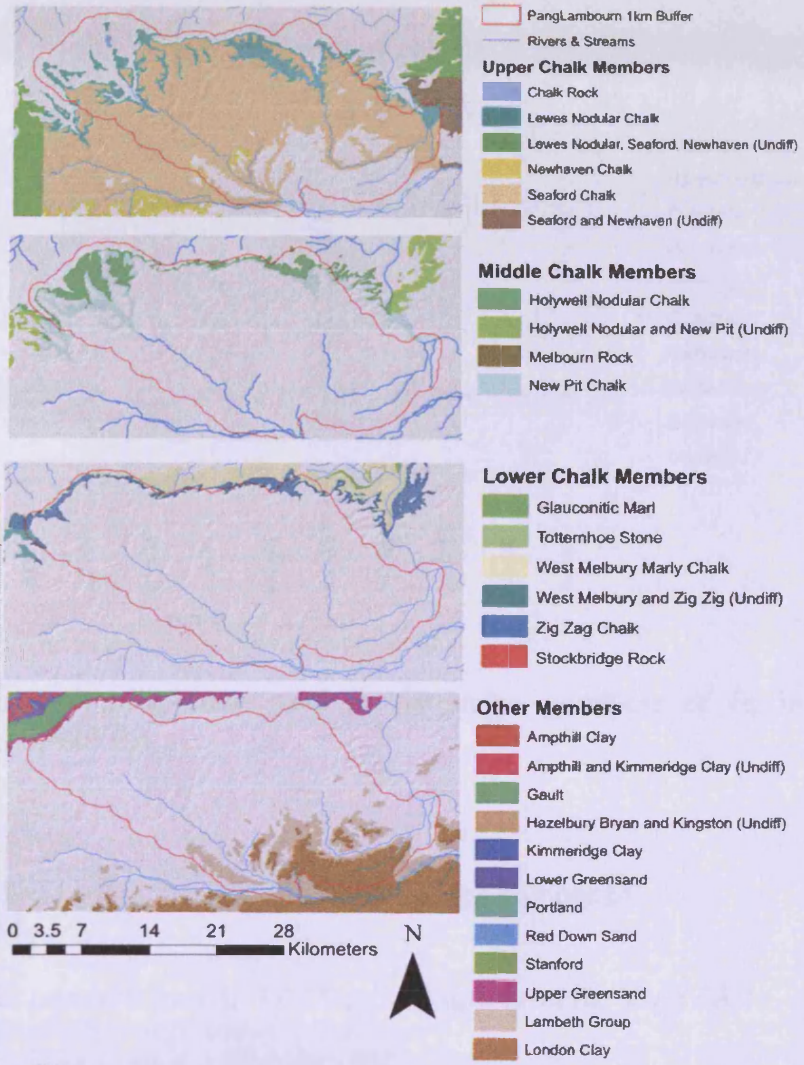

(ii)

3.2 Kriging fits a mathematical spatial autocorrelation function to all data points within a specified radius. A continuous prediction surface can then be plotted using the resulting model. In this case, ordinary kriging using a spherical semivariogram was used. A variable search radius of 12 input points is used to control the final model prediction surface. The kriging method predicts for a location S_o, a value $\hat{Z}$,

$$\hat{Z}(S_o) = \sum_{i=1}^{N} \lambda_i Z(S_i),$$

where $Z(S_i)$ is the measured value at the $_i$th location, λ_i is an unknown weight value at the $_i$th location and N is the number of measured values. In ordinary kriging, the weight λ_i depends on a fitted model to the measured points, the distance to the

prediction location and the spatial relationships among the measured values around the prediction location. As a comparison, in inverse Distance Weighted (IDW) interpolation methods, λ_i depends solely on the distance to the prediction location.

3.3 Sample borehole hydrographs representing distinct hydrogeological regions within the Pang/Lambourn catchment between 1980 and 2006.

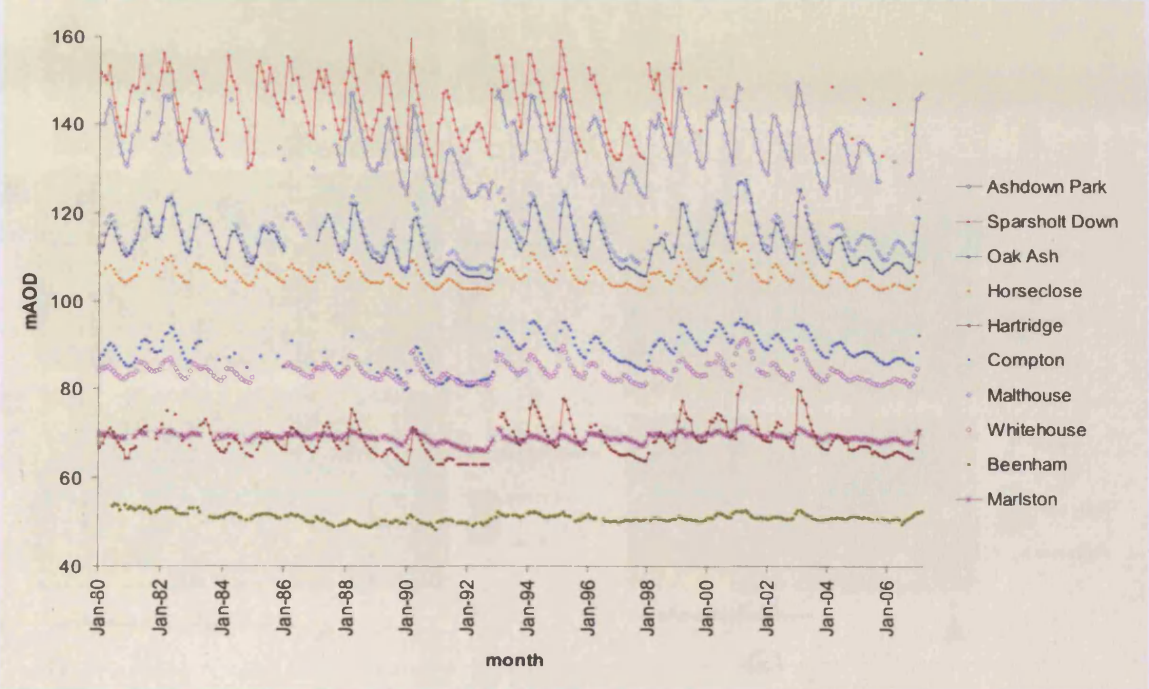

3.4 Root Mean Square (RMS) error used to determine goodness of fit in groundwater modelling is given by,

$$RMS = \sqrt{\frac{\Sigma(f(x_i) - y_i)^2}{n}}$$

where x is the modelled head value, y is observed and n is the number of observations/stress periods.

3.5 Recharge zones imported from GIS-DIRT as they appear in the VMF GUI.

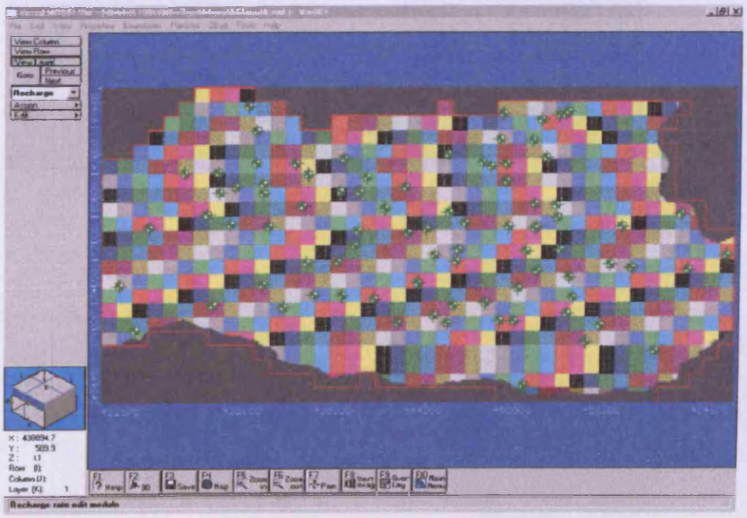

3.6 (i) Depth of vadose zone from the top of the Chalk (A), distance from valleys (B) and C aquifer thickness used in Cokriging process. (ii) Distributed *K* (A) and *Ss* (B) as a product of co-kriging observations with depth of vadose zone, aquifer thickness and distance from valleys.

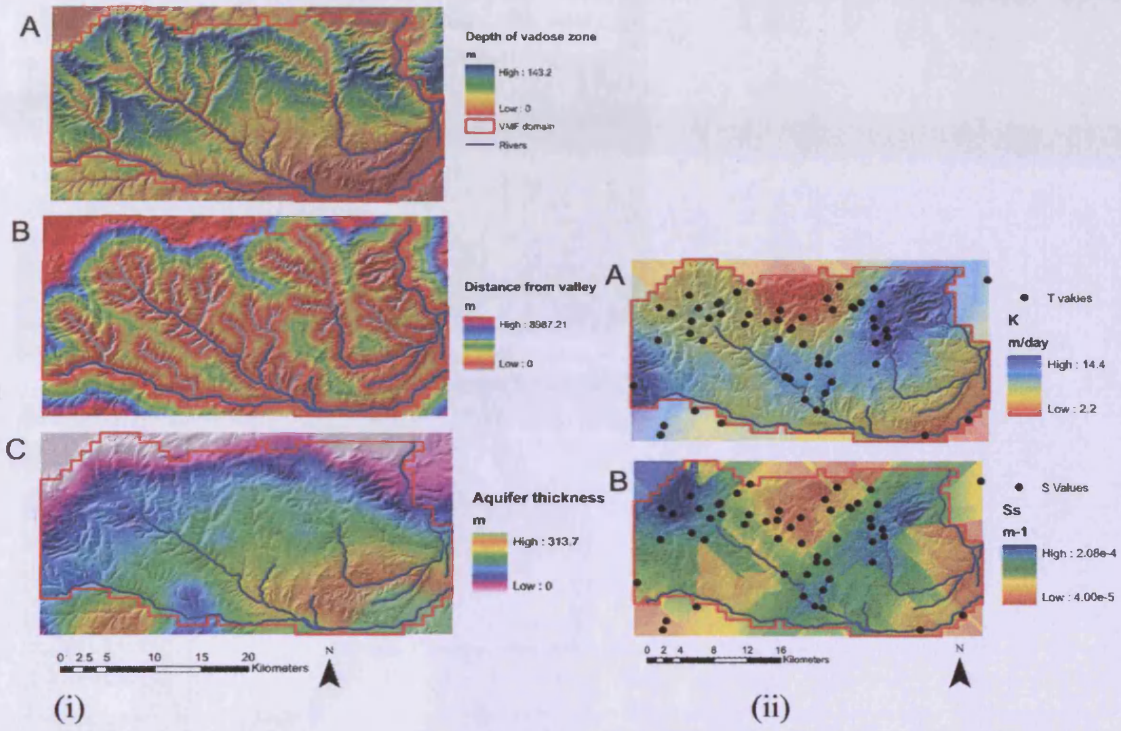

3.7 Three-dimensional structure of the VMF model and *K* zones used for calibration

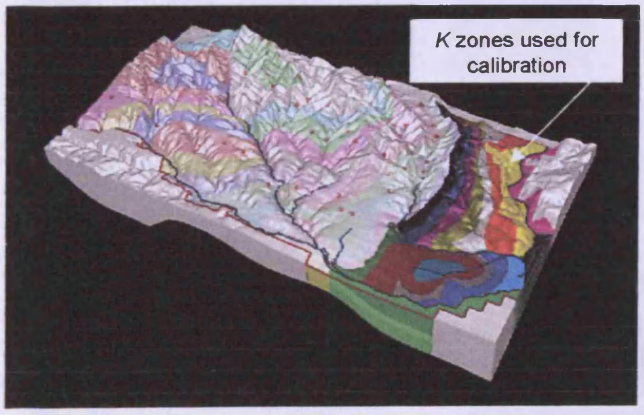

3.8 Calibration of the VMF model in steady state. (A) Modelled groundwater levels and graduated residuals. (B) Plot of modelled and observed groundwater levels across the domain and all 3 layers.

(A)

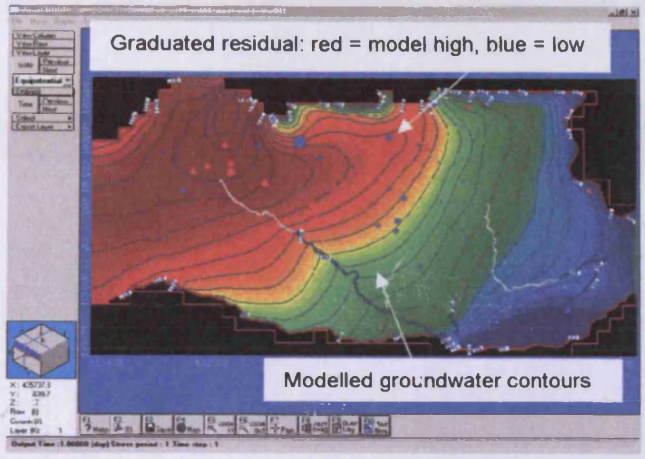

(B)

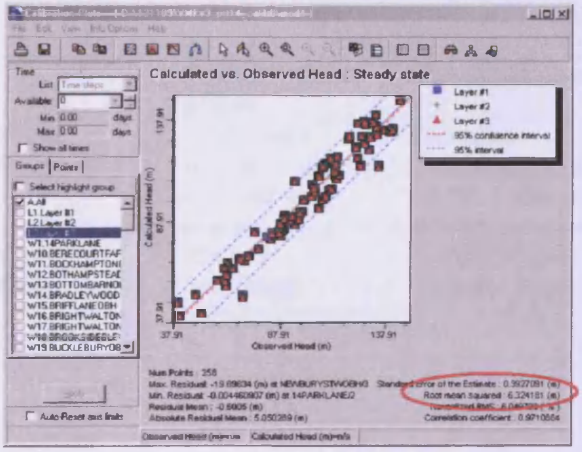

3.9 (i) Distributed *T* values for layers 1-3 in Visual MODFLOW. (ii) Distributed *S* values for layer 1-3 in Visual MODFLOW.

(i) (ii)

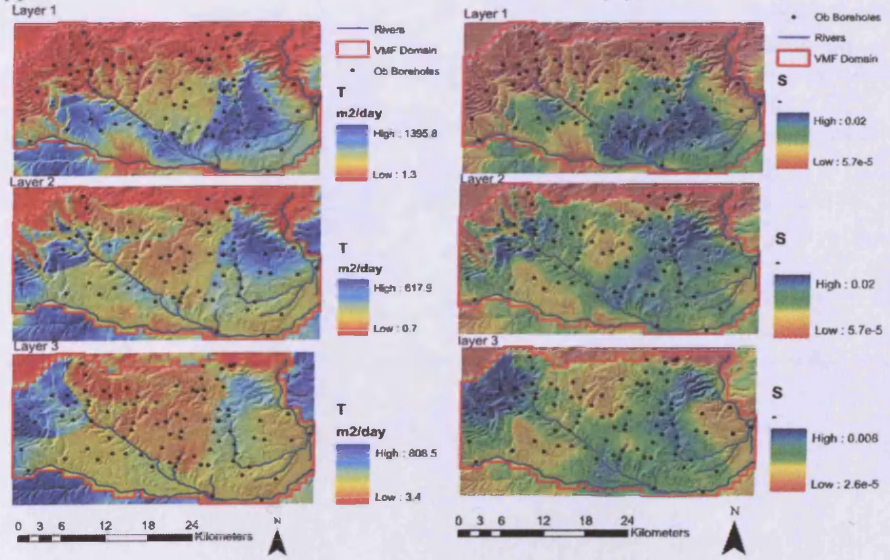

4 Appendix 4

4.1 UKCIP Socio-economic scenarios (UKCIP, 2001) as function of future values and governance (A) and the core characteristics of each in terms of social/political values, economic development, construction and agriculture (B).

(A)

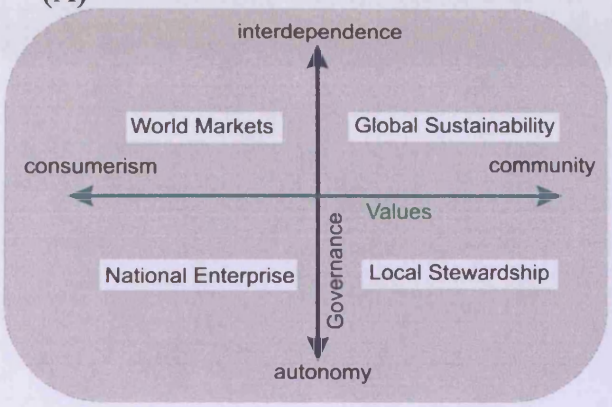

(B)

	Social/Political Values	*Economic development*	*Construction*	*Agriculture*
World Markets	Importance placed on person material well-being	Increased globalisation/integration of EU. Increased economic development	Increased demand for smaller households	Increasingly concentrated. Liberalisation of world trade
National Enterprise	Private consumption with little regard for environmental protection	Economic protectionism – decrease in growth	Lack of investment – low growth in housing	Subsidies remain. Intensification – high inputs of pesticides and fertilisers
Global Sustainability	Internationalist focus with focus on maintenance of social and environmental equality	Average growth. International co-operation and regulation reduces tension between profit and social justice	Average – Most new housing is met by dense low-rise development mainly on existing urban land	Slow down in productivity and production. Areas used to support nature conservation
Local Stewardship	Community orientated. Conservation of resources a major objective	Slow. Small scale, local production and trade encouraged	Low growth	Heavily subsidised to protect food security, landscapes and reduce environmental impact

4.2 EARWIG GUI

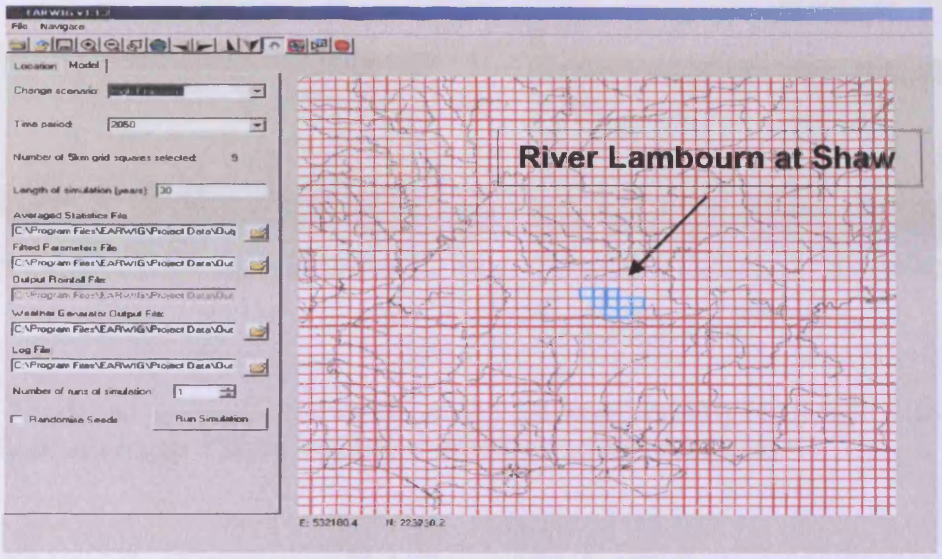

4.3 Mean annual distributed recharge over 10 years from 1978 to 1988 for a baseline scenario (A) in comparison to a h2020 scenario (B). In both cases the land use distribution remains the same.

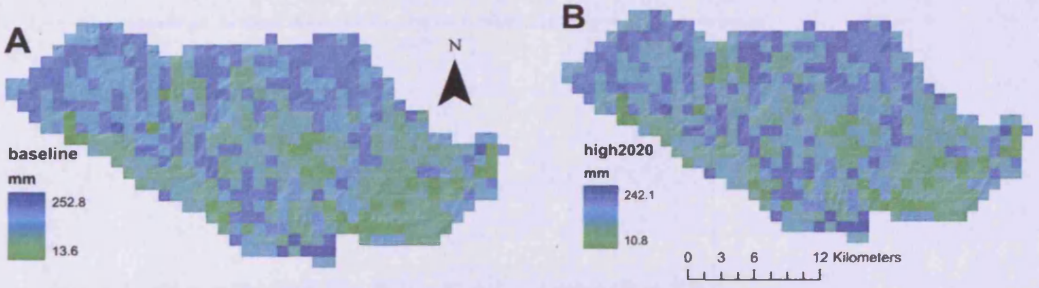

4.4 Summary statistics for representative boreholes across climate change scenarios. ** t test significant, P<0.05.

	mean GW level % change			extreme GW level % change				
				low		high		
scenario	min	mean	max	min	max	max	min	t test
h2020	-2.0	-0.8	1.0	-0.4	2.3	-0.4	-8.9	4.3**
h2050	-4.5	-3.1	-1.5	-1.8	-0.2	-3.9	-11.3	17.9**
h2080	-5.8	-4.8	-3.7	-5.0	-0.9	-6.8	-11.7	27.9**
l2020	-1.6	-0.6	0.1	-2.6	2.5	-5.7	-8.0	3.4**
l2050	-4.6	-2.9	-1.9	-1.5	1.3	-8.5	-9.8	17.0**
l2080	-3.8	-2.8	-2.0	-2.0	2.2	-7.3	-8.8	16.7**
h2020	-1.3	-0.4	0.8	-0.2	1.9	-0.4	-6.7	3.7**
h2050	-3.1	-2.1	-1.0	-1.5	-0.2	-3.1	-8.3	18.2**
h2080	-4.1	-3.4	-2.5	-4.3	-0.8	-5.6	-8.9	29.1**
l2020	-1.1	-0.4	0.1	-2.1	1.9	-4.1	-5.9	3.1**
l2050	-3.2	-1.9	-1.2	-1.2	1.2	-6.1	-7.4	17.1**
l2080	-2.6	-1.9	-1.3	-1.6	1.8	-5.7	-6.8	16.9**

	mean GW level % change			extreme GW level % change				
				low		high		
scenario	min	mean	max	min	max	max	min	t test
h2020	-0.6	-0.2	0.5	0.0	0.7	-0.4	-3.5	3.1**
h2050	-1.4	-1.0	-0.4	-0.4	0.0	-1.7	-4.5	18.8**
h2080	-1.8	-1.5	-1.2	-1.2	-0.1	-3.2	-5.0	30.1**
l2020	-0.5	-0.2	0.1	-0.6	0.9	-2.0	-3.2	3.0**
l2050	-1.5	-0.9	-0.6	-0.3	0.4	-3.1	-4.2	17.9**
l2080	-1.2	-0.9	-0.6	-0.4	0.6	-3.1	-3.8	18.0**
h2020	-1.8	-0.8	0.8	0.0	3.0	-0.9	-6.9	5.7**
h2050	-4.1	-2.9	-1.4	-1.3	0.1	-3.8	-9.7	21.7**
h2080	-5.3	-4.3	-3.3	-4.3	-0.3	-6.3	-10.7	32.9**
l2020	-1.6	-0.6	0.0	-2.4	3.0	-4.1	-6.6	4.6**
l2050	-4.3	-2.6	-1.7	-1.1	1.9	-6.3	-8.8	20.5**
l2080	-3.5	-2.6	-1.8	-1.4	2.9	-6.3	-7.1	20.3**

	mean GW level % change			extreme GW level % change				
				low		high		
scenario	min	mean	max	min	max	max	min	t test
h2020	-0.9	-0.3	0.5	0.1	1.6	0.0	-1.9	4.6**
h2050	-2.1	-1.4	-0.7	-0.7	0.2	-0.7	-3.0	22.7**
h2080	-2.7	-2.2	-1.7	-2.2	0.0	-1.8	-3.7	35.6
l2020	-0.7	-0.3	0.0	-1.2	1.7	-0.9	-1.6	4.8**
l2050	-2.2	-1.3	-0.8	-0.7	1.0	-1.6	-2.5	21.2**
l2080	-1.7	-1.3	-0.9	-0.7	1.5	-1.6	-2.2	21.2**
h2020	-1.3	-0.5	0.6	0.0	1.9	-0.6	-5.7	5.2**
h2050	-2.9	-2.0	-1.0	-0.9	0.1	-3.0	-7.7	20.6**
h2080	-3.7	-3.1	-2.3	-3.0	-0.3	-5.2	-8.4	31.7**
l2020	-1.1	-0.5	0.0	-1.7	2.0	-3.6	-5.4	4.6**
l2050	-3.0	-1.9	-1.2	-0.8	1.2	-5.4	-6.9	19.5**
l2080	-2.4	-1.8	-1.3	-1.0	1.9	-5.3	-6.1	19.3**
h2020	-0.6	-0.2	0.2	0.0	0.5	-0.5	-3.4	4.6**
h2050	-1.1	-0.8	-0.5	-0.4	0.0	-1.6	-4.0	16.6**
h2080	-1.5	-1.2	-1.0	-1.2	-0.1	-2.4	-4.5	25.8**
l2020	-0.4	-0.2	-0.1	-0.6	0.7	-1.8	-2.7	4.5**
l2050	-1.2	-0.8	-0.5	-0.4	0.3	-3.0	-3.5	15.8**
l2080	-1.0	-0.8	-0.6	-0.4	0.5	-2.4	-3.2	15.8**

Malthouse
Oak Ash
Whitehouse
Compton
Marlston
Hartridge
Beenham

4.5 Mean groundwater levels for (A) the h2020 and (B) luh2020 climate/land use change scenario.

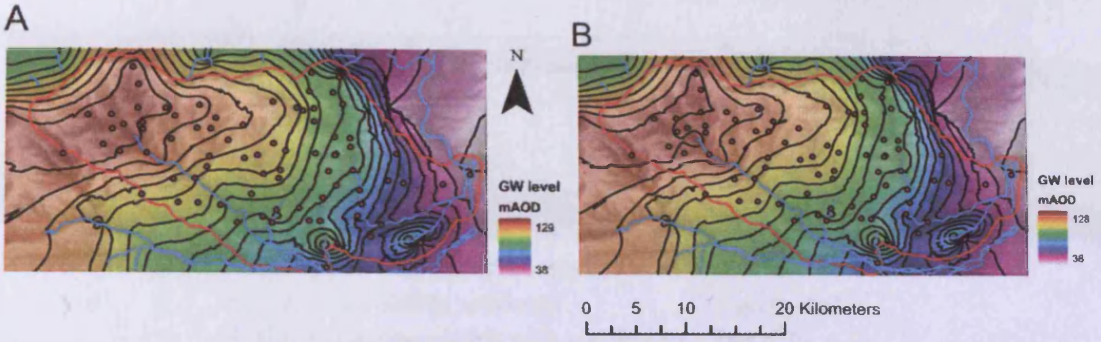

4.6 Modelled groundwater levels at (A) Hodcott and (B) Northfield farm using monthly or aggregated daily input in comparison to observed values.

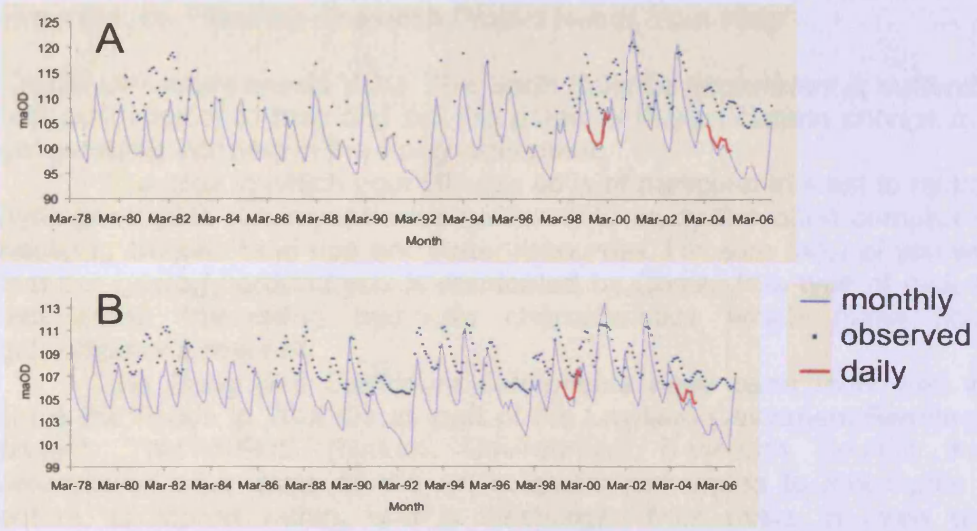

5 Appendix 5

5.1 CASWEB codes for Social Groundwater Flood Vulnerability Index variables:

- Unemployed residents aged 16-74 ***CS0210046***
- Economically active aged 16-74 ***CS0210010***
- Over 1 and up to 1.5 persons per room ***CS0520013***
- Over 1.5 persons per room ***CS0520017***
- All Households ***CS0520001***
- No Cars or vans in household ***KS0170002***
- Renting home ***KS0180005, KS0180006, KS0180007, KS0180008***
- Households suffering from limiting long-term illness ***KS0082***
- Single parent households with dependent children ***KS02011***
- Residents aged 75 and over ***KS00215, KS00216, KS00217***
- Households with basements ***KS0199***

5.2 Transformations used to minimise skew and kurtosis in raw percentages (U_n, O_v, N_c, N_h, S_i, S_p, E_r, B_h) for all census OAs in the Pang/Lambourn

	Indicator	*Transformation*
U_n	Unemployment	Square root
O_v	Overcrowding	Square root
N_c	Non-car ownership	Log10 (x + 1)
N_h	Non-home ownership	Log10 (x + 1)
S_i	Proportion of long term sick	Log10
S_p	Proportion of single parent households	Square root
E_r	Proportion of elderly residents	Square root
B_h	Percentage of households with a basement	Log10 (x + 1)

5.3 Article published in local 'Compilations' magazine to encourage participation in online survey (Appendix 5.4)

Groundwater Flooding Research Project Needs Your Help

Cardiff University needs YOU. The Earth Science department is currently running a research project to help find out the potential impact climate change may have on groundwater flooding in the Pang catchment.

The area in which your villages lie is of particular interest to hydrologists and hydrogeologists like myself who are keen to study the often complex relationship between climate, land use and water resources. I'm sure most of you will be aware that the geology around you is dominated by Chalk. This type of rock in particular has some interesting hydraulic characteristics which make flooding from groundwater a real risk.

The Pang and Lambourn catchments have been monitored very closely since the floods in 2000/01 as part of the Lowland Catchment Research (LOCAR) project. This NERC (Natural Environment Research Council) funded £5m programme uses state of the art scientific techniques to investigate how water enters, is stored within, and is discharged from rivers in three groundwater-dominated catchments, the Frome/Piddle in Dorset, the Tern in Shropshire and the Pang/Lambourn.

This project has provided a wealth of data that can be used to develop computer simulations of the processes happening in the catchment. These models can then be used to predict what might happen when changes take place in the climate or land use of the area. It's early in the proceedings at the moment but any results will be published and available for all.

As part of the project we are very interested to hear about people's experiences of groundwater flooding during the 2000/01 flood and at other times. To help with this, we have set up an online survey which can be accessed from the web address at the end of the article. It's not the catchiest URL, but it works! Alternatively you can contact us by email, phone, post or via the parish councillor, Kathy Howells (578507) who has kindly offered her assistance.

We are looking for details about when, where, how and how badly groundwater flooding has affected the local community. This can then give us an idea of the impact a change in the climate might have in terms of economic cost as well as disruption to people's lives.

Look forward to hearing from you all

Ben Rabb

5.4 Online survey to quantify the impact of groundwater flooding on households in Compton and East Ilsley.

www.surveygalaxy.com/surPublishes.asp?k=E6FYF6L7ATRW

Survey 5252 (Preview) Groundwater flooding in compton & east ilsley

Groundwater flooding in Compton and East Ilsley

Welcome!

This is a short survey to find out about the experiences people have had with flooding from groundwater in Compt East Ilsley.

The survey is part of a research project at Cardiff University which is aiming to quantify the impact future changes climate and landuse may have on the risk of groundwater flooding in areas of Chalk geology.

The information will help us understand the social and economic costs of high groundwater in the past. This will help us better manage the risk of flooding in the future.

CARDIFF UNIVERSITY
PRIFYSGOL CAERDYDD

The information in this survey will only be used for academic purposes

Many will remember the floods in 2000/2001

How many years have you lived in Compton/ East Ilsley?

-- Select Answer --

What type of property do you own/ live in?

-- Select Answer --

Has your property been flooded by groundwater in the past?

This can be from a spring or intermittent stream / lake that does not flow all the time - including the Pang) and usually during winter

- Yes
- No
- Not Sure

How much do you estimate groundwater flooding to have cost in damage to your property since you ha in the area? (including costs covered by insurance companies)

-- Select Answer --

Has your property been affected by other types of flooding?

This can be storm drains overflowing, surface runoff during intense storms - usually during the summer months

- Yes
- No
- Not Sure

Please describe the nature of any flooding from groundwater in and around your property

Give an indication of where you think the water came from (e.g. River Pang, directly from below into cellar etc.), dates, depth and duration of flood

Have you done anything to alleviate groundwater flooding yourself?

This could include pumps or drainage ditches etc.

If willing please enter your postcode

It would be useful to pin point areas where groundwater repeatedly causes problems (for academic purposes only)

Has groundwater flooding impacted on other areas of your life (not just property damage)

	Yes	No	Not Sure
Health/ stress			
Insurance blight			
Ability to travel			
General standard of living			

Any other comments?

Thanks for taking the time to fill out the survey.
Feedback and results will be available through the parish magazine 'Compilations'

- Yes
- No
- Not Sure

Please describe the nature of any flooding from groundwater in and around your property

Give an indication of where you think the water came from (e.g. River Pang, directly from below into cellar etc.), dates, depth and duration of flood

Have you done anything to alleviate groundwater flooding yourself?

This could include pumps or drainage ditches etc.

If willing please enter your postcode

It would be useful to pin point areas where groundwater repeatedly causes problems (for academic purposes only)

Has groundwater flooding impacted on other areas of your life (not just property damage)

	Yes	No	Not Sure
Health/ stress			
Insurance blight			
Ability to travel			
General standard of living			

Any other comments?

Thanks for taking the time to fill out the survey.
Feedback and results will be available through the parish magazine 'Compilations'

5.5 Areal view of particle tracking back from the 2000-2001 flood zone delineated by a local resident.

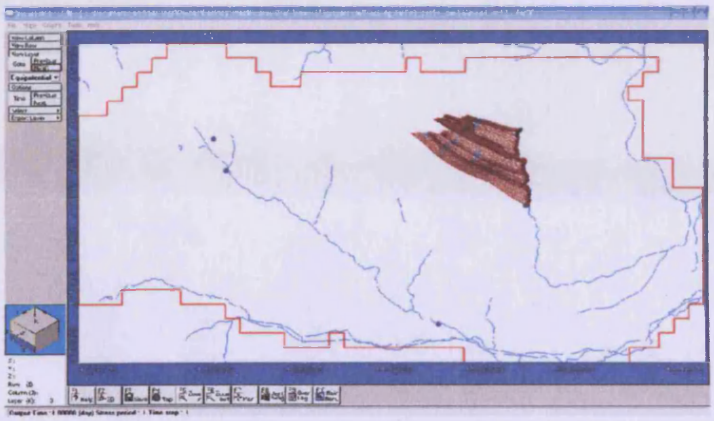

5.6 Equivalent land use 1 km 2000 and 25 m 1990 nomenclature used in the development of recharge potential rankings where needed.

Land use 1990	*Land use 2000*
Bracken	Grass
Continuous urban	Suburban/rural
Inland bare earth	Suburban/rural
Unclassified	Grass